A Computer Model of *In Vitro* Cellular Response to Radiation

Morgiane Richard

Submitted for the Degree of
Doctor of Philosophy
from the
University of Surrey

Surrey Centre for Ion Beam Applications,
Faculty of Engineering and Physical Sciences
University of Surrey
Guildford, Surrey GU2 7XH, U.K.

March 2008

Abstract

It is believed that irradiation interacts with biological tissues to break or modify the DNA, which is the molecule contained in the nuclei of cells that carries all the relevant information for the organism. As such, radiation is dangerous for individuals; however, its properties can also be used in medicine, e.g. in cancer treatments. Nevertheless, the exact mechanisms of cellular response to radiation are not fully understood yet, especially for low doses (below 50 cGy), where non-targeted effects, i.e. that do not involve only the interactions radiation-DNA, are taking place. In order to deepen the knowledge of those non-targeted effects, a computer model of a population of cells irradiated *in vitro* was written, taking into account the phenomena in the low dose domain.

As a start, two non-targeted effects were studied, the bystander effect and the low dose hyper-radiosensitivity. The program was written in C++ and the technique of the cellular automaton was used. The clonogenic assay was reproduced; cells were seeded in a dish and if the colony they formed after a given period of time was bigger than 50 cells, the seeded cells were assumed to have survived. The direct effect of radiation was calculated by the traditional linear quadratic model and in addition cells were subjected to the bystander effect.

Some simulations were run in the case of two cell lines, the hamster cell line V79 and the glioma cell line T98G. The results show that the bystander effect is unlikely to be limited to one period of the cell cycle, but that the low dose hyper-radiosensitivity and the bystander effect could be the same phenomenon. This work also suggests that the bystander effect may be significant after low doses of conventional radiotherapy. Such a model represents a very useful tool for solving problems that at the moment cannot be investigated experimentally.

Acknowledgments

Just as the Belgium comics character Lucky Luke, an episode of my life has finished, and like him I can go away singing "I'm a poor lonesome cow-boy and a long far way from home"! Many people have contributed to my adventure, and here are a few I would like to thank:

- Georges Kass, without whom I would not have started this PhD;
- Norman and Karen Kirkby, Roger Webb, without whom I would not have finished this PhD;
- My parents and brothers, who have supported me, in both French and English meanings, throughout my long education;
- Lionel, who is still decided to take me as his wife;
- Montse and Himat for the M&M's house - this one was love, friendship, joy and understanding flavoured;
- Yuko, for Friday night Guinness pints and Saturday night dinners, at the early days of our PhDs;

- Liliana, for the afternoon tea times, and chats about life, boyfriends, supervisor and occasionally, scientific issues;

- Many others: Kevin Prise, Mick Woodcock and Giuseppe Schettino for the scientific advice, Raj and Marie-Laure for the moral support, Giselle, Joshua, Guillermo, Alicia, Graham and the Oxfam team and St John's homegroup... who have made my life easier in one way or another.

My PhD project was funded by Marie Curie Research Training Network (project CELLION), which provided me the living costs and the funding to go to many conferences and have access to useful training and materials.

Contents

Glossary

apoptosis : programmed cell death during which cells go through a series of events leading to a change in their morphology.

adaptive response (AR) : mechanism by which cells become more resistant to an ionizing agent after priming with a small dose of either the same or a different ionizing agent.

astrocyte : star-shaped glial cell in the brain.

adenosine triphosphate (ATP) : cellular energy.

bystander effect (BE) : mechanism by which cells that are not irradiated but are in the neighbourhood of irradiated cells show irradiation-type effects.

broadbeam : particle beam which is not focused.

bystander signal (BS) : the bystander effect is believed to be due to a signal emitted by irradiated cells affecting neighbours.

carcinoma : malignant tumour derived from the epithelium.

cyclin-dependent kinases (CDK) : proteins involved in cell cycle controls.

cell cycle : series of biochemical events between the birth of a cell and its division.

checkpoint : molecular control that forces cells to stop cycling when it would be unsafe to.

chromosome aberration : abnormalities in number or structure of chromosomes.

clonogenic assay : technique for studying the response of cells to a specific agent. Cells are seeded in a dish, treated and their capability of producing a colony of a given size is tested.

deoxyribonucleic acid (DNA) : molecule carying the genetic information.

epithelium : tissue made of one or more layer of cells which covers most of the external and internal surfaces of the body and its organs. Cells of the epithelium are epithelial cells.

fibroblast : cell which maintains the structure of the body, that is important in connective tissues (e.g. blood, cartilage, bone, marrow) and in healing.

gene expression : process of converting a gene into a protein.

genomic instability (GI) : mechanism by which the progeny of an irradiated cell shows irradiation-type effects.

gap junction inter-cellular communication (GJIC) : junction that connects the cytoplasm of adjacent cells.

glioma : tumour cells and tumour derived from glial cell lines.

low dose hyper-radiosensitivity (HRS) : enhanced sensitivity of some cell lines to very low doses of radiation.

irradiated cell conditioned medium (ICCM) : culture medium in which cells have been irradiated.

inverse dose rate effect (IDRE) : mechanism by which at very low dose rate, the toxicity of radiation increases when the dose rate is decreased.

interphase : set of events between two divisions of a cell.

increased radio-resistance (IRR) : mechanism by which cells showing HRS become increasingly resistant to radiation in an intermediate dose range.

keratinocyte : major cell constituting the epidermis.

linear energy transfer (LET) : average energy deposited per unit length of radiation track (keV/μm).

malignant : cancerous.

microbeam : focused particle beam, the dimensions of which are of the order of the μm.

micronucleus : abnormal small cell nucleus.

mitosis : cell division, M phase of the cell cycle, including the different steps of division prophase, metaphase, anaphase and telophase.

mutation : change in the genetic material.

nitric oxide : gas that has a wide range of functions in the body, and amongst others takes part in the transport of oxygen to the organs.

nucleotide : fundamental building block of the deoxyribonucleic acid (DNA); it consists of a base, a deoxyribose sugar and a phosphate group.

ribonucleic acid (RNA) : molecule involved in the transcription of proteins.

reactive oxygen species (ROS) : small molecule by-product of the metabolism of oxygen, including oxygen ions, free radicals and peroxide.

transformation : process by which a cell becomes malignant.

Nomenclature

α : parameter of the linear quadratic equation (Gy^{-1}).

β : parameter of the linear quadratic equation (Gy^{-2}).

τ : life time of the bystander signal (min).

chem_neighbours : concentration of nutrient at the sites of the neighbouring cells (mole/m2).

lattice : matrix describing the concentration of nutrient present in the dish (-).

m : maximum number of cells sitting in one element of the matrix lattice (-).

n_{irrad} : number of cells irradiated (-).

neighbours : set of neighbouring cells (-).

p_f : proliferation factor (-).

population : matrix describing the cells living in the dish (-).

r : rate of consumption of nutrient by cells (mol/cell/min).

BS_resis : Boolean tracing whether a G2 cell has passed the bystander effect checkpoint (-).

Cell_Init : number of cells initially seeded in the dish (-).

d : dose of radiation (Gy).

$\mathbf{D_B(Q)}$: proportion of G2 cells killed by the bystander signal for a given quantity of signal Q (-).

d_l : parameter of the equation of probability of producing a bystander signal (models 1 and 2) (Gy).

d_m : parameter of the equation of probability of producing a bystander signal (model 1 only) (Gy).

D_{max} : maximum proportion of G2 cells killed by the bystander signal (-).

K : saturation constant of the glucose consumption of cells (mol/cell/min).

K_S : glucose concentration at which the rate of consumption is half K (mol/l).

LX : number of lists of lists of the matrix lattice (-).

LY : number of elements in the lists of the matrix lattice (-).

P_E : plating efficiency (-).

Q_0 : initial quantity of bystander signal in the medium (-).

Q_B : quantity of signal at which 63% of bystander cells are killed (-).

Q(t) : quantity of bystander signal at time t (-).

S_F : survival fraction (-).

S_{max} : parameter of the equation of probability of entering the S phase (mol/cell).

Chapter 1

Introduction

The World Health Organization (WHO) reports that 13% of the world deaths are due to cancer (World Health Organization website, Factsheet 297). The WHO definition of cancer is as follows:

> Cancer is a generic term for a group of more than 100 diseases that can affect any part of the body. Other terms used are malignant tumours and neoplasms. One defining feature of cancer is the rapid creation of abnormal cells which grow beyond their usual boundaries, and which can invade adjoining parts of the body and spread to other organs, a process referred to as metastasis. Metastases are the major cause of death from cancer.

The main cancers responsible for cancer-induced deaths are the lung, stomach, liver, colon and breast cancers. According to the WHO, a healthy style of living would help reduce the rate of cancers (eating healthy, practising sport and not smoking). There are different ways of curing or controlling the spread of a cancer, and the main ones are: surgery, radiotherapy and chemotherapy. Chemotherapy uses drugs, and radiotherapy uses radiation. The National Cancer Institute of the U.S. (National Cancer Institute website, Factsheet) records that about half of the patients receive a radiotherapy treatment, either alone or in combination with other types of treatment.

Radiotherapy can be external (the tumour is targeted by an external beam), or internal (a radioactive substance is absorbed or placed next to the tumour). In external radiotherapy, the radiation type most commonly used is X-ray radiation, although the benefit of using protons

has been shown in Europe and in the U.S.A.. The main interest of protons or ions of high linear energy transfer (LET, average energy deposited locally) is that they deposit all their energy at the end of their track in the region of the Bragg peak, and the sparing of surrounding healthy tissues is therefore easier than with X-rays. However, proton therapy is not used very much yet in the United Kingdom. In spite of its benefit in medicine, radiation is not safe, and actually it may lead to cancer development itself (Health Protection Agency website, Ionising Radiation Damage and Cancer; World Health Organization website, Programmes and Projects). This is the paradox of radiation and consequently, its use needs care.

The estimation of radiation effects at low (below 1 Gy) and very low (below 50 cGy) doses is difficult; they are usually extrapolated from the data coming from the study of the survivors of the atomic bombs in Japan and the Chernobyl accident (Health Protection Agency website, The Estimation of Cancer Risk at Low Doses). These data concern very high doses of radiation, but the basic assumption is that radiation effects are linear with dose, because the main action of radiation is to break the DNA molecule contained in the cells nuclei. However, in the past two decades, technological advances allowed for an accurate and direct study of low dose effects; they are not linear as previously assumed. It has been discovered that radiation does not only target the DNA and some phenomena, named the non-targeted effects, involve more than just the nuclei of the irradiated cells. It seems that other substructures of the cells, and also cells in the neighbourhood or from the progeny of irradiated cells may be affected.

The exact relevance of the non-targeted effects for cancer risk and radiotherapy is still in dispute (Little, 2006; Mothersill and Seymour, 2004a; Prise *et al.*, 2003). They have not been clearly demonstrated *in vivo* yet, but if so, a review of the current approach taken for risk assessment and radiotherapy planning might be needed. Indeed, during radiotherapy, the healthy tissues surrounding the tumour will be exposed to low dose margins. This is known as the biological penumbra (Mothersill *et al.*, 2004b). Moreover, since the beginning of the 20^{th} century, the number of doses has been increased, while the energy of a single dose has been decreased; this is the fractionation of treatment, and one well-known plan is the continuous hyperfractionated accelerated radiation therapy (CHART, Hall and Giaccia, 2006, Chapter 22). Human bodies are also exposed to daily background radiation, such as radon, coming from the earth or buildings in granite (Health Protection Agency website, Radon), which can cause lung cancer. Space research is also concerned with biological problems due to low doses, since astronauts are

continuously exposed when they are in mission (NASA website).

All the non-targeted effects share striking similarities, and it may be that all the non-targeted effects are related to each other. Nevertheless this has not been shown experimentally, and it is still not known whether they are all different manifestations of the same set of events.

Radiation physics and biology use mathematical and computer models extensively, in order to understand and predict the effects of radiation on cells. Because of the non-targeted effects recently shown, new models are necessary to describe the low dose domain. Some models have been proposed for some non-targeted effects, but they focus on one particular effect only. A comprehensive model, including all non-targeted effects, is needed; such a model could then be used in models of tumours and their response to radiotherapeutic treatments, as well as in the calculation of radiation risks.

1.1 Aims and Objectives

The work presented in this thesis is part of a Marie Curie Research Training Network programme, the Cellion project [1], on the study of cellular response to targeted single ions. The aims here are to set up a model of tumour and tissue response to radiation, which would take into account all the newly discovered non-targeted effects, and their relation with the cell cycle and nutrients conditions. This model could then be used for improving radiotherapy treatment planning. Another aim is to investigate the dependency of the low dose response on radiation type and in particular to investigate the effects of protons.

To reach these aims, a set of intermediate objectives were defined for the course of this doctorate. It was proposed, as a first step, to create a computer model of a culture of cells being irradiated *in vitro*:

- The modelling of cell interactions and the diffusion of components will be implemented.
- The clonogenic assay is to be reproduced.
- The cell cycle will be described, as well as the change in sensitivity to radiation with cell phase.

[1] http://cellion.ifj.edu.pl/, August 2007

- Two non-targeted effects will be included: the bystander effect (i.e. not only irradiated cells but also cells in their neighbourhood and their progeny suffer from irradiation effects) and the low dose hyper-radiosensitivity (i.e. the surviving probability of cells to doses of radiation lower than 1 Gy is less than expected by the linear assumption). Those two effects have been mainly studied independently; although a single study has concluded that they are mutually exclusive, some data show that both effects co-exist in some cell lines.

- The experimental characteristics of the bystander effect as they appear to be from the experimental studies will be implemented in the model.

- It will be tested whether the low dose hyper-radiosensitivity can be seen when only assuming a bystander effect mechanism.

- Due to technological limitations, it is not possible to directly measure the bystander effect after irradiation with X-rays of the type used in radiotherapy. Hence, the model will be used to predict the bystander effect after this type of radiation has been applied.

- The model will address the question of the variability of the bystander effect with cell cycle.

- Could the bystander effect be limited to a particular period of the cell cycle?

- Could the low dose hyper-radiosensitivity be the same as the bystander effect?

1.2 Overview of the Dissertation

The model that has been written is described fully in Chapters 3 and 4. It has been applied on the study of two particular cell lines, the hamster lung cell line V79 and the glioma cell line T98G, because they have been studied for both the bystander effect and the low dose hyper-radiosensitivity. The results of the simulations run in both cases are also shown in Chapter 4. The predictions of the model are compared to experimental data obtained from the Gray Cancer Institute, Oxford University, UK. Two types of populations are studied: populations of cells synchronised at particular times of the cell cycle, and populations of asynchronous cells,

randomly distributed throughout the cell cycle. Figures and tables are presented after Chapter 6.

A discussion of the work is presented in Chapter 5. Some possible improvements and developments are also proposed. The report ends with an overall conclusion and a series of recommendations for future work.

A literature review of the background in radiation biology can be found in Chapter 2. It starts with some basic cellular biology; this is followed by the classic radiobiological theory. Finally, the current knowledge on the non-targeted effects, and especially the low dose hyper-radiosensitivity and the bystander effect is reviewed, along with their existing mathematical models.

Chapter 2

Literature Survey

2.1 Background in Biology

Radiation biology studies start in the laboratories with experiments on cultured cells - those are called *in vitro* experiments. The cell is a small structured element that composes any living organism; yet, the cell has been revealed to be a very complex entity, and its mechanisms have not been entirely unraveled. This work focuses on the radiation effects on eukaryotic cells, and this section gives a brief description of their properties.

2.1.1 Basic Structure of the Eukaryotic Cell

The different activities of eukaryotic cells are run by specific units called organelles:

- the nucleus: it contains the deoxyribonucleic acid (DNA), which is the genetic information of the cell and the ribonucleic acid (RNA), which are molecules involved in the production of proteins. The replication of the DNA before cell division and the synthesis of the RNA take place in the nucleus.

- the mitochondria: organelles where organic compounds are converted into adenosine triphosphate (ATP), i.e. cellular energy. It is unusual in that it possesses its own DNA.

- the endoplasmic reticulum and the Golgi apparatus: they are responsible for the sorting and transport of synthesized proteins.

- the cytoskeleton: it maintains the shape of the cell.
- others, such as lysosomes, endosomes, peroxisomes...

Those organelles, with the exception of the nucleus are part of the cytoplasm, with the cytosol, a water-like substance that fills the cell. The cell is contained within its plasma membrane, which is a semi-permeable lipid bi-layer (Figure 2.1).

There are many different types of cells with different properties and functions; for instance, a cell in the skin does not have the same function or properties as a neurone. Those cells that have specific activities are said to be differentiated; this means they have acquired a type. During differentiation, the cell may, amongst other characteristics, change size, shape and they lose their proliferation capabilities. A cell that is not differentiated is a stem cell; stem cells maintain their number by continuously dividing, but they can also differentiate. Tumours are believed to originate from the abnormal proliferation of one or a group of differentiated cells (World Health Organization website, Factsheet 297); however, there is a growing evidence that stem cells may become cancerous as well (Travis, 2004).

In culture as well as *in vivo*, normal cells growth depends on 2 factors: they are anchorage-dependent, i.e., cells need to attach to a solid surface to grow and contact-inhibited, i.e. cells stop growing as soon as they touch each other. Transformed cells (e.g. cells that have become malignant) may loose either one or both of these characteristics.

2.1.2 The Eukaryotic Cell Cycle

Cell division is the process by which a cell gives rise to a colony of cells, which is part of the process by which a fertilized egg gives an animal. Cell division is only a short period of the cell cycle. The cell cycle is usually described in two parts: the M phase, which is the division process itself, and the interphase, which is the time between two divisions.

2.1.2.1 The Order of the Cell Cycle

The interphase is the time when the cell meets the requirements necessary to carry out a division. One aim is to keep the genetic information, the DNA, intact and to pass on an exact copy to

the two daughters. After division, the cell enters a first gap phase, G1, during which the DNA forms chromosomes of one double helix. In the next phase, called S for synthesis, each of these chromosomes is duplicated and becomes a pair of sister chromatids, which should be identical and which will be distributed to the daughters. The completion of the synthesis of DNA leads to the last step of the interphase, the second gap G2, after which the M phase can happen.

In nature, eukaryotic cells cycle at very different speeds: a typical human cell cycle is of the order of 24 hours, while a rodent cell cycle time is about 12 hours. Mitosis is a very short time in the cell cycle: on average 30 minutes out of 24 hours in human cells (Murray and Hunt, 1993, Chapter 1). The difference between cell cycle durations is believed to be mainly due to the G1 phase: for instance in human, G1 takes on average 12 hours, while it takes on average 3 hours in Chinese hamster cells (Hall and Giaccia (2006, Chapter 4) and Pathak (1977)).

It is very important that the order of the different phases of the cycle should be respected; the cell needs to make sure, for instance, that the DNA is synthesized once, and only once, or that it does not divide twice successively. This is achieved by two families of proteins, the cyclin-dependent kinases (CDK), and their activators the cyclins (Figure 2.2). The association of specific CDKs with specific cyclins is necessary for the onset of the different phases. While the level of the CDK proteins remains constant during the cell cycle, the level of cyclins varies, which makes possible the activation of some CDKs at some point of the cell cycle; the activity of the CDKs can also be reduced by cell cycle inhibitory proteins (CDK inhibitors: Nurse, 2000; Vermeulen *et al.*, 2003). The CDKs proteins are upstream of a complicated network of many other proteins, working at the activation or inhibition of the events of the cell cycle.

To study the different properties of the phases of the cell cycle, some techniques have been used to produce synchronised populations of cells. Usually, cells are asynchronous, i.e. they are randomly distributed throughout the cell cycle (Murray and Hunt, 1993, Chapter 1). Synchronisation can be induced by growing cells in specific conditions (such as starvation, confluence or using drugs) that stop cells in a known point in the cell cycle. Synchronisation can otherwise be achieved by selecting cells, for instance according to their DNA content. In this latter case, the DNA is dyed and the fluorescence is measured by flow cytometry: cells with the highest DNA content are G2 and M cells and cells with the lowest DNA content are G1 cells.

2.1.2.2 The G1 phase and the Restriction Point

As mentioned previously, it is believed that differences in cell cycle times arise mainly from different lengths of the G1 phase. Pardee (1974) first demonstrated that cells grown in a medium with different types of nutrient-deficiencies were all stopped at one point in G1; from this came the idea of the existence of a restriction point in G1: cells in G1 make the irreversible decision that the nutrient conditions are sufficient for cycling and dividing.

Actually, nutrients provide cells with growth factors, whose availability is checked in the G1 phase; in the absence of which cells stop the progression to the S phase and enter a reversible quiescent phase named G0 (Murray and Hunt, 1993, Chapter 3, Chapter 6). If the nutrients conditions become normal, cells can re-enter the cell cycle. In this view point, it is cell growth, i.e. mass accumulation, that regulates cell division (Neufeld and Edgar, 1998).

It has been proposed that the G1 phase be divided in two steps, processed either successively or in parallel, with distinct objectives (Jones and Kazlauskas, 2001; Murray *et al.*, 1991), such as mass accumulation or synthesis of specific proteins necessary for DNA replication.

2.1.2.3 The Checkpoints: Control of the Cell Cycle

The restriction point introduced above functions to control cell growth in response to nutrient conditions: it makes sure the cell can safely synthesize the DNA and divide. There are other controls in the cell cycle, essentially checking the integrity of the DNA and the completion of its replication (Hartwell and Weinert, 1989; Sancar *et al.*, 2004; Vermeulen *et al.*, 2003). Three DNA-damage induced checkpoints are reviewed by Vermeulen *et al.* (2003) and Sancar *et al.* (2004): a checkpoint at the transition G1/S, an intra-S checkpoint and a checkpoint preventing the entry to mitosis, if damage occurs during the G2 phase. Four types of proteins are involved in these checkpoints: the sensors of the DNA damage, the mediators and transducers of the signal and finally the effectors that stop the cell cycle (Figure 2.3). Some of the proteins taking part in the checkpoint mechanisms have been identified, although their exact role has not always been clarified (Zhou and Elledge, 2000).

2.1.3 Cell Cycle Modelling

It is believed that cancer is linked to cell cycle deregulation (Vermeulen *et al.*, 2003). However, the network of proteins involved in the cell cycle is complicated, and it is difficult to unravel the interactions and connections between different events; for this purpose, modelling may be a useful tool (Fuss *et al.*, 2005). Different levels can be adopted when one models the cell cycle: from the cell level down to the gene level. Ordinary differential equations are often used to describe the progress of cells through the cell cycle, in different ways.

Tyson and Novak (2001) presented a model that works at the molecular level; it included 2 checkpoints: the restriction point in the G1 phase when cells are committed irreversibly to division, called Start, and a second restriction point in G2 after the DNA had been replicated, named Finish. These points were controlled by different proteins and their concentration was derived with time. Basse *et al.* (2003, 2004) wrote equations for the time evolution of DNA content in each phase, with the idea that the DNA content of cells doubled between G1 and G2, and this content was evenly distributed between the 2 daughters at mitosis; no checkpoint was introduced in this model. Considering a number of possible fates of a cell in a given phase at a given time, Faraday *et al.* (2001) used in their model a function of the number of cells with time in each phase. The restriction point was included at the transition G1/S: cells in G1 had a probability to enter S which depended on the total quantity of glutamine consumed since the start of the G1 phase.

Some simplified cell cycle models, involving no checkpoint and assuming constant phase duration were used in some tumour models (Dionysiou *et al.*, 2004, 2006; Duchting *et al.*, 1995; Duchting and Vogelsaenger, 1985); these works focused on tumour growth and tumour response to therapy. Some tumour models of tumour interaction with the environment included the quiescent state (Alarcon *et al.*, 2004; Antipas *et al.*, 2004). In the model by Antipas *et al.* (2004), the quiescence was defined by a range of pH: cells became proliferative again if the concentration in ions H^+ rose above the upper value of the range, and cells died if the concentration decreased below the lower limit. Different approaches were taken for the cell division: in the model by Kansal *et al.* (2000), cells died if there was no space in the neighbourhood, while in the model by Borkenstein *et al.* (2004), cells could push the neighbours in random directions when they divided. The direction of division could also depend on the distribution of nutrients surrounding

the cells: cells divided preferably where there is most nutrients (Antipas *et al.*, 2004).

2.2 Classic Radiation Biology

The cell is a very small component of the organism — on average 12 μm in diameter — but it contains the essential information for the organism to live: the DNA. The DNA is a helix formed of two long strands of nucleotides; a nucleotide is a block consisting in a phosphate group and a sugar plus a base, either pyrimidine or purine (Figure 2.4). The pyrimidine bases are the cytosine (C) and the thymine (T), while the purine bases are the adenine (A) and the guanine (G). The DNA is stabilized by bonds between bases (bonds A-T or C-G).

DNA mutations (i.e. change in the DNA structure) lead to the synthesis of modified proteins, or to no synthesis at all, and loss of their functionality. Mutations may arise naturally, during the replication process, or, to a much higher extend, due to external agents, such as drugs or radiation. The following section introduces what is known about how ionizing radiation interacts with the DNA, and how the cell may respond to it.

2.2.1 Ionizing Radiation and DNA

Cells may be exposed to radiation of different qualities: electromagnetic radiation such as X-rays or γ-rays or particulate radiation, either charged (protons, α-particles, electrons and carbons) or uncharged (neutrons).

When matter is traversed by a radiation track, its atoms get excited or ionized, i.e. their electronic structure is changed, and secondary particles are ejected. In the case of a cell, these processes can modify the DNA (Figure 2.4 and Hall and Giaccia, 2006, Chapter 1):

- either directly: they interact with the DNA itself; these interactions cannot be prevented and are predominant after particulate radiation.
- or indirectly: the particles interact with the water molecules and produce free radicals that interact with the DNA; these interactions can be prevented by scavengers of free radicals and are predominant after X- and γ-rays.

Electromagnetic radiation is sparsely ionizing, while particle radiation is densely ionizing (Goodhead *et al.*, 1993). Particles have different linear energy transfer (LET), i.e. the average energy they deposit locally varies and therefore have different biological effects. For this reason, the relative biological effect (RBE) of a given particle of radiation is defined as the ratio of doses d required for equal biological effects after 250 kVp X-rays and the radiation in question:

$$RBE = \frac{d(250\,kVp\,Xrays)}{d(radiation)} \tag{2.1}$$

The higher the LET of the radiation, the higher the RBE — up to 100 keV/μm; above this, the RBE decreases because the distance between ionizing events is smaller than the dimensions of the DNA, and therefore, the energy is wasted (Figure 2.5 and Hall and Giaccia, 2006, Chapter 7).

Amongst all agents, ionizing radiation produces the widest range of DNA damage (Goodhead, 1994). Different types of damage may result (see Figure 2.6): base damage, cross-links (i.e. some genetic material is exchanged, either intra- or inter-chromosomes, or between the DNA and some proteins), single-strand break (SSB), or double-strand break (DSB). Track structure analysis allows for the study of the relative importance of different types of damage after radiation of different LET (Nikjoo *et al.*, 1998). DSBs have long been considered to be the principal break leading to cell death (Chadwick and Leenhout, 1973; Goodhead, 1994), while SSBs are regarded as being negligible, although they are produced in high numbers. However, some evidence has been gathered that even DSBs alone are probably not responsible for any significant effect, but rather more complex damage, such as clusters of different types of damage (Goodhead, 1994; Goodhead *et al.*, 1993), is required to cause cell death.

This damage is sensed by the cells. This triggers checkpoints and cell cycle arrest (Wilson, 2004), and the cell may try to repair the DNA. In base excision repair (BER) and nucleotide excision repair (NER), the damaged bases (or nucleotides) are removed and new bases (or nucleotides) are synthesized and inserted (Sancar *et al.*, 2004). Three mechanisms of DSB repair are known: non-homologous end joining (NHEJ), homologous repair (HR) and single strand annealing (SSA). In NHEJ, the damaged area is removed and the resulting DNA strands are joined; therefore, this is an error-prone repair mechanism. In HR and SSA, the sister chromatid is used to re-synthesize the damaged area; this repair is potentially error-free. The damage is

quite often a cluster of close breaks of different types. It may be that the damage is converted by successive repairs to a simpler type of damage (for instance SSB: Zhou and Elledge, 2000).

Because the repair itself may not be error-free, or may not be possible, cells may die after radiation. Hall and Giaccia (2006, Chapter 3) distinguish two types of cell death: loss of cell functionality for differentiated cells or loss of the ability to reproduce for proliferative cells. However, the cells may survive but show DNA mutations (Goodhead *et al.*, 1993).

Several parameters may affect the response of cells to radiation. Cells irradiated at different stages of the cell cycle show different survival fractions, usually cells in the M phase are the most sensitive cells to radiation and cells in late-S phase are the most resistant (Wilson, 2004). Cells are usually more resistant if they are hypoxic, which causes a problem when treating tumours, whose core is usually hypoxic (Steel, 2002, Chapter 15). The dose rate is also an important issue: when it decreases, cells have more time to repair the sub-lethal damage and the overall surviving fraction increases with total dose. In addition, there is time for cells to move from sensitive to resistant part of the cell cycle. These problems have been summarized in the expression "the 4-Rs of radiobiology" (Hall and Giaccia, 2006, Chapter 5):

- Repair: repair proteins are activated for an immediate repair of sub-lethal damage;
- Reassortment and synchronisation: cells progress through the cell cycle or sensitive cells are killed, leaving resistant cells only;
- Repopulation: cells divide and therefore their number increase, leading to a rise of the surviving fraction;
- Re-oxygenation: radiation kills the aerobic cells, leaving only the hypoxic cells, a proportion of which may re-oxygenate between fractions.

2.2.2 The Clonogenic Assay

As mentioned earlier, one of the outcomes of cellular radiation is death. It is not easy to measure cell death due to radiation, as it may not happen at the time of exposure, but the cell may also divide a number of times before dying (Hall and Giaccia, 2006, Chapter 3). Therefore,

biologists usually study the survival fraction of an irradiated population as follows (Hall and Giaccia, 2006, Chapter 3):

1. Two dishes are prepared containing nutrient medium, one to be irradiated and one to be used as a control (not irradiated); a known number of cells is seeded in each of the dishes (i.e. injected in the dish). Cells will naturally attach to the bottom of the dish.

2. The irradiation takes place when the cells have attached to the dish (this can take a couple of hours); after the irradiation process, the dishes are placed in an incubator and cells are left long enough (usually about a week) to develop into colonies.

3. After period of time which depends on the cell cycle length of the cell line studied, the dishes are revisited: any colony counting more than 50 cells (Puck and Marcus, 1955) is said to be viable and is supposed to come from a cell that survived radiation. The plating efficiency is calculated by the ratio of surviving to seeded cells:

$$P_E = \frac{N(surviving)}{N(seeded)} \tag{2.2}$$

4. The surviving fraction in the irradiated dish is the ratio of its plating efficiency over the plating efficiency in the control dish:

$$S_F = \frac{P_E(d)}{P_E(0)} \tag{2.3}$$

The number of cells initially seeded in the dish is chosen so that in any dish there will be around a 100 viable colonies at the end of the experiment. Therefore, more cells are seeded in dishes that will receive a bigger radiation dose; an estimation of the surviving fraction is used to determine the number of initial cells to be seeded. The choice of the number 50 as a discriminant between viable and non-viable colonies is arbitrary (Puck and Marcus, 1955) and the value of the plating efficiency for both control and irradiated dishes depends on the cut-off number chosen. As a consequence, it is essential to work with the values of the surviving fraction rather than the plating efficiencies, since the former ones are expected to be independent of the number 50. However, it could be that some cells are greatly delayed at radiation-induced checkpoints, and survive but produce colonies of say 45 cells; then these cells would be counted as dead, although they are not (Bartkowiak *et al.*, 2001; Enns *et al.*, 2004). It has been proposed that

the proliferation of single cells, using flow cytometry techniques, rather than the formation of colonies should be measured (Bartkowiak *et al.*, 2001; Enns *et al.*, 2004). Moreover, the experimental errors may be reduced in these conditions, due to the high numbers of cells involved. Nevertheless, Schettino *et al.* (2001) led some clonogenic assays on a hamster cell line and showed that most colonies contained between 75 cells and 85 cells, and that the proportion of those colonies decreased with dose. Therefore, Equation 2.3 is appropriate to measure the change in proliferation of cells occurring after radiation. Although the clonogenic assay is extensively used and allows for comparison of results between experiments that all used the assay, it may be necessary to establish a new protocol for the measurement of radiation-induced death.

Even in dishes that receive no radiation at all, the plating efficiency is not 100%, because cells are not growing in their natural environment, and also probably because of seeding and counting uncertainties (Hall and Giaccia, 2006, Chapter 3). Calculating the surviving fraction according to Equation 2.3 rather than with Equation 2.2 is also a way of eliminating those errors.

The survival fraction is usually plotted against dose on a semi-logarithmic scale. For sparsely ionizing radiation (X- and γ-rays), the survival fraction gradient increases with increasing dose in the lower dose range, therefore, the curve describes a shoulder at intermediate doses; at higher doses, the gradient becomes constant. For densely ionizing radiation, such as α particles, the curve is just a straight line, which is usually represented by a simple exponential function at any dose (see Figure 2.7 and Hall and Giaccia (2006, Chapter 3)).

2.2.3 Modelling Survival of Cells to Radiation

In order to explain the survival curves obtained after clonogenic assays, two theories were built: the lesion interactions theory and the enzyme saturation theory (Figure 2.8 and Steel, 2002, Chapter 7).

The enzyme saturation model states that the rate of repair of the damaged DNA depends on the availability of the repair enzymes. When there is little damage, enzymes are unsaturated and therefore the repair is quick; as the amount of damage increases, the velocity of repair decreases. The maximum velocity is reached in cases where there is so much damage that the enzyme is completely saturated. This explains the shoulder in the survival curves at low doses, and the linear shape at higher doses (Steel, 2002, Chapter 7).

In the lesion interactions point of view (Steel, 2002, Chapter 7), additional lesions arise after high doses of radiation due to interactions between sublesions, or accumulation of sublesions that the cell cannot repair; this is the reason why there is a shoulder in the curves at low doses. If it is considered that death is due to one hit in one critical target in the cell, then, applying Poisson statistics for calculating the probability P of hit with dose, the survival is modelled by:

$$P(0\,\text{hit}) = S_F = \exp(-\frac{d}{d_0}) \tag{2.4}$$

In Equation 2.4, d_0 is the dose that gives an average of one hit per target. Yet, this equation cannot render the shouldered curve seen after sparsely ionizing radiation; instead, the multi-target single hit inactivation equation, based on the idea that a number n of critical targets must be inactivated to lead to cell death, can be used:

$$\begin{aligned} P(\text{1 or more hits}) &= 1 - P(0\,\text{hit}) \\ P(\text{specific target inactivated}) &= 1 - exp(-\frac{d}{d_0}) \\ P(\text{n targets inactivated}) &= (1 - exp(-\frac{d}{d_0}))^n \\ S_F &= 1 - (1 - exp(-\frac{d}{d_0}))^n \end{aligned} \tag{2.5}$$

This equation, though, is still not completely satisfactory since it predicts a flat curve at low doses. A combination of the single and multi-target theories gave rise to a more accurate model (Steel, 2002, Chapter 7):

$$S_F = \exp(-\frac{d}{d_1}) \times (1 - [1 - exp(-d(\frac{1}{d_0} - \frac{1}{d_1}))]^n) \tag{2.6}$$

The lethal-potentially lethal damage model (LPL model) considers two types of lesions: the non-repairable lethal lesions, which occur with the probability η_L and the repairable, potentially lethal lesions, which occur with the probability η_{PL}. The potentially lethal lesion may be successfully repaired at rate ε_{PL}, but there may be interactions between those lesions, and as a consequence misrepair, at the rate ε_{2PL}. The lethal events are responsible for a linear component of the survival curve and the misrepair of potentially lethal lesions are responsible for a quadratic component. This model is in good agreement with dose-rate data, and predicts that the number of misrepaired potentially lethal lesions decreases with dose rate (Figure 2.8 and Steel, 2002, Chapter 7).

The linear quadratic model (LQ model), introduced by Chadwick and Leenhout (1973) is the most widely used model. It assumes that DSBs lead to cell death; those double strand breaks can come from either a single track breaking the two strands of the DNA or from two independent tracks breaking the two opposite strands. Using Poisson statistics for the probability of hit, the survival to a dose d is given by:

$$S_F = \exp(-\alpha d - \beta d^2) \tag{2.7}$$

In Equation 2.7, the term $\exp(-\alpha d)$ accounts for single track events, while the term $\exp(-\beta d^2)$ accounts for double track events. The dose $\mathrm{d} = \frac{\alpha}{\beta}$ is the dose at which both contributions to cell death are equal.

Despite the common use of the linear quadratic model in radiobiology, the other models described in this section cannot be disregarded (Hall and Giaccia, 2006, Chapter 3); none of these models gives a definitively better fit than the others to the experimental data, which have in any case great uncertainties. The advantage of the LQ model is that it has only two parameters to fit, α and β.

2.3 Non-Targeted Effects of Radiation

In the previous section, the implicit assumption is made that the effects of radiation all originate from the deposition of energy by the particles in the nucleus of the cells, where their DNA is. For this reason, radiation effects were long thought to be linear with dose, i.e. the lower the dose, the lower the effect (Mothersill *et al.*, 2006). Because no data were available in the low dose domain (below 1 Gy), those were extrapolated from the data at high dose gathered from the study of the survivors of the atomic bombs in Japan and the accident in Chernobyl (Huang *et al.*, 2007).

Yet, when it was possible to directly measure the effects of low doses *in vitro*, results showed a non-linear behaviour.

2.3.1 Limitations of the Classic Radiation Theory

A set of phenomena, called the non-targeted effects, have been discovered recently which challenges the idea that the only critical effect of ionizing radiation in the cell is the DNA damage and that less incident energy means less death, fewer DNA breaks and fewer mutations (Morgan, 2003; Mothersill *et al.*, 2006; Prise *et al.*, 2005). Those effects are:

- Adaptive response (AR): a small priming dose may render cells more radio-resistant to a subsequent challenging dose (Wolff, 1996).
- Bystander effect (BE): cells in the neighbourhood of irradiated cells may suffer radiation-type effects even when they have not been traversed by any track (Morgan, 2003).
- Genomic instability (GI): cell death and DNA mutation may appear generations after the irradiation took place, even though the irradiated mother cell survived and showed no effect (Morgan, 2003).
- Inverse dose rate effect (IDRE): there is a dose-rate domain for which decreasing the dose rate leads to an increase in radiation effect, where it would be expected to decrease (Vilenchik and Knudson, 2000).
- Low dose hyper-radiosensitivity (HRS): there is a dose range in which the smaller the dose the higher the killing efficiency (Joiner *et al.*, 2001).

It has been shown that these phenomena appear after low doses of radiation, but the full mechanisms underlying each of them are not clearly understood yet. Their similarities and possible connections have been studied (Huang *et al.*, 2007; Kadhim *et al.*, 2004; Mitchell *et al.*, 2002; Mothersill *et al.*, 2002; Mothersill and Seymour, 2004b; Skov, 1999), but no unified explanation, enclosing all the non-targeted effects has been found yet.

Non-targeted effects, if proven *in vivo* as well, have potential implications for radiation risk assessment and radiotherapy (Mothersill *et al.*, 2004b; Prise *et al.*, 2003). As a consequence, understanding them is essential. The rest of this section reviews in details the current knowledge of two non-targeted effects specifically: HRS and BE.

2.3.2 Low Dose Hyper-Radiosensitivity

The survival curve of some cell lines cannot be described by the LQ model (see Equation 2.7) because at very low doses (below 0.3-0.5 Gy), the radiosensitivity is higher than predicted by the coefficient α; this has been named HRS (see figure 2.9). This hyper-radiosensitivity (HRS) is followed by an increase in radio-resistance up to 1 Gy; this has been called increased radio-resistance (IRR). Above 1 Gy, the survival curve fits the LQ model (Marples and Joiner, 1993; Mothersill *et al.*, 1995; Skarsgard *et al.*, 1996; Wouters *et al.*, 1996). The phenomenon was first detected in non-mammalian systems (algae and yeast); it was then possible to observe it in both mammalian (in hamster cells: Marples and Joiner, 1993, 1995; Marples and Skov, 1996) and human cells (Mothersill *et al.*, 1995; Short *et al.*, 1999a,b; Skarsgard *et al.*, 1996).

2.3.2.1 Experimental Techniques

The description of HRS had been made possible because new methodologies were set up for the measurement of plating efficiency. Indeed, usually, in the clonogenic assay, cells that are seeded come from an aliquot of a cell suspension whose average concentration in cells is measured by a manual or automatic cell counter. From this, a certain volume of the solution is added to the flask that contains on average the number of desired cells. When flasks of cells are irradiated at high doses (above 1 Gy) and the cell killing is high, this uncertainty does not have a big impact. However, at low doses, the killing proportion is expected to be very small, and thus the difference in cell numbers between irradiated flasks and control flask should be small as well. In these conditions, working with average cell numbers is not appropriate.

Two new methods have been used to solve this problem:

1. The dynamic microscope image processing scanner (DMIPS: Marples and Joiner, 1993; Short *et al.*, 1999a,b) scans the flasks and recognises the cells via image processing software, which allows the exact number of cells and their position in the dish to be known. Cells are then incubated for a period of time theoretically necessary to let them grow in colonies of more than 50 cells; after this, the DMIPS scans again the flasks and counts the number of viable colonies.

2. The fluorescence-activated cell sorter (FACS) detects cells thanks to their scattering properties; two protocols have been tested with the FACS (Wouters *et al.*, 1996). A known number of cells is selected by the FACS either before or after irradiation, and then seeded in flasks. After the incubation period, cells are stained and the number of colonies with more than 50 cells is recorded. This second method is preferred for some cell lines which grow in non-discrete colonies that cannot be detected automatically.

2.3.2.2 Possible Mechanisms of the HRS

It was suggested that HRS-IRR could be explained either by the existence of a very sensitive sub-population of cells, or by the existence of a threshold dose for triggering repair processes; recently the role of a checkpoint in G2 phase has been discussed.

If there were a sensitive sub-population, the hyper sensitive domain would reflect the killing of these sensitive cells, and the increased radio-resistance would result from the decrease in the average sensitivity of the population due to the fact that only more resistance cells are still alive (Skarsgard *et al.*, 1994). However, it is unlikely to be the only reason for HRS, since modelling work has shown that the sensitivity of the sub-population would have to be unrealistically big (Wouters *et al.*, 1996). No difference for dose above 1 Gy was found between the survival of human tumour cells that have been primed with a small dose of radiation (0.3 Gy) and the survival of cells receiving the dose without priming (Wouters and Skarsgard, 1997). It is argued, that if there were a sensitive sub-population, though, it would be killed by the priming dose and the survival of the primed cells would therefore be higher than the survival of the population of un-primed cells. Nevertheless, HRS has proved to be dependent on the position in the cell cycle in two human glioblastoma cell lines (Short *et al.*, 2003); HRS is strongest in the G2-M phase of the cell cycle. The HRS in the other phases of the cell cycle (G1 and S) is less evident.

Indirect evidence of repair processes being triggered above a certain dose is found in the results of split dose experiments (Marples and Joiner, 1995; Marples and Skov, 1996; Mitchell and Joiner, 2002; Wouters *et al.*, 1996). A priming dose of either low or high LET radiation (Marples and Joiner, 1995) can eliminate HRS. However, too low a priming dose does not affect the HRS response, which could mean that cellular mechanisms of response to radiation are not switched on when the insult is too small. Non-repaired DSBs have been raised has a possible cause of

HRS (Joiner *et al.*, 2001), but the study of a variety of mammalian cell lines (rat and human) has shown that proteins involved in DSBs repair are active even after very low doses of radiation (Short *et al.*, 2005; Wykes *et al.*, 2006). Nonetheless, it should be pointed out that those studies were led on asynchronous populations, which does not eliminate the possibility that lack of damage recognition may be specific to one cell cycle phase or sub-phase.

A second G2-checkpoint has been discovered in 2002 in addition to the one previously known (see Section 2.1 and Sancar *et al.*, 2004); this checkpoint is not triggered at very low doses of radiation (Xu *et al.*, 2002). Marples *et al.* (2003) therefore proposed that HRS is due only to cells in G2 phase: damaged cells in G2 would fail to arrest and would enter mitosis with damaged DNA.

Looking at the activation of apoptosis-related proteins, Enns *et al.* (2004) showed that HRS is caused by apoptotic death. They also demonstrated that HRS happens during the first cell cycle after radiation.

HRS is also seen after high-LET radiation (Bohrnsen *et al.*, 2002; Marples and Skov, 1996; Schettino *et al.*, 2001; Tsoulou *et al.*, 2001) but then IRR seems not to happen (Marples *et al.*, 1996). Although Marples and Skov (1996) found that HRS was independent of LET in hamster cells using π-mesons, Tsoulou *et al.* (2001), using helium, found an increase in HRS with increasing LET. As a consequence, the effect of LET on HRS and IRR remains unclear.

It has been asked whether the adaptive response and HRS-IRR could be the same phenomenon, since the elimination of HRS by priming doses suggests that the mechanisms underlying these two non-targeted effects are similar. It has also been shown that both the elimination of HRS and the adaptive response can be inhibited by a common chemical agent (cycloheximide, Joiner *et al.*, 2001). However, differences have been noticed for some priming agents such as neutron (Skov, 1999), and Wouters and Skarsgard (1997) showed in a human tumour cell line that no protection was afforded against HRS by the priming dose if the challenging dose is above 1 Gy, while the adaptive response is triggered in these conditions.

Finally, there is some early evidence on human tumour cell lines that the inverse dose rate effect is seen in cell lines showing HRS-IRR (Mitchell *et al.*, 2002); IDRE may actually be another consequence of the hyper-radiosensitivity at low doses.

2.3.2.3 Modelling HRS-IRR

For testing the theory of a sub-population of high sensitivity, Wouters *et al.* (1996) uses a combination of two exponentials. If a population of cells consists in a resistant and a sensitive sub-population, and if f is the proportion of sensitive cells, then the surviving fraction is (see Figure 2.9):

$$S_F = f \times \exp(-\alpha_s d) + (1 - f) \times \exp((-\alpha_r - \beta d)d) \tag{2.8}$$

The parameter α_s applies to the sensitive cells and is larger than its corresponding parameter for resistant cells α_r. The survival of the sensitive population was modelled by the authors by a single-hit single-target model (no β parameter, see Equation 2.4) because first there were not many experimental data at low doses, so the fewer parameters to fit the better, and second because the single-hit single-target model is appropriate to describe a high killing at low doses. At high doses, the influence of the term $f.\exp(-\alpha_s d)$ is negligible and only the second term applies; at low doses, the response of the whole population is a mixture of the response of the two populations. However, the model predicts for human tumour cells that the sensitive population should be 50 to 700 times more sensitive than the resistant population, to obtain a good fit to the initial slope of the experimental data. The authors argue that there is no phase of the cells cycle where the sensitivity is so high, and if so, under continuous low-dose-rate irradiation, as cell cycle into this particular phase, they would all be killed; the possibility that this sub-population would be characterised by genetic factors rather than by a cell cycle position is unlikely since the predicted sensitivity is also greater than the sensitivity of known repair-deficient cell lines. Nevertheless, the authors did underline that this did not rule out the existence of an extremely sensitive population, but only set doubts. Although this model predicted the HRS with accuracy, the IRR could be reproduced (Wouters *et al.*, 1996).

The "accumulated damage induced radio-resistance model" assumes that at any dose there are two sub-populations, a sensitive and a resistant one for which resistance has been triggered. Cells belong to either of the populations, according to the level of a given type of DNA damage they have accumulated (Wouters *et al.*, 1996). The equation is the same as 2.8, but the definition of the parameter f is as follows:

$$f = \sum_{n=0}^{c-1} \frac{(ad)^n \exp(-ad)}{n!}$$

In Equation 2.9, a is the average number of damage events per Gray (so this determines the type of DNA damage) and c the number of these damage events required to trigger radio-resistance. Two situations are tested in Wouters *et al.* (1996). In the first case, the critical damage is assumed to be DSB ($a = 20$) and the number of those DSBs necessary to trigger radio-resistance is allowed to vary for different cell lines. In the second case, the number of critical damage events is fixed to 1 ($c = 1$) and values of a are fitted for the different cell lines; the type of damage is then less common than DSBs ($5 < a < 12$), but the fit is better for these later conditions. This model is the only one that allows for a qualitative investigation of radiation effects (via the parameters a and c), as well as quantitative (via the dose of radiation).

With the variable-α or induced repair model, it is assumed that the cellular sensitivity evolves from a sensitive state to a resistant one as a continuous function of dose (Wouters *et al.*, 1996):

$$S_F = \exp((-\alpha(d) - \beta d)d) \tag{2.9}$$

$$\alpha(d) = \alpha_r + (\alpha_s - \alpha_r) \times \exp(-\frac{d}{d_c})$$

In Equation 2.9, the parameter d_c describes how quickly the curve changes from low to high dose response. At low doses ($d << d_c$), $\alpha(d)$ has a value very close to α_s, until $d \approx d_c$, when $\alpha(d_c) = 0.63\alpha_r + 0.37\alpha_s$. At high doses, ($d >> d_c$), $\alpha(d)$ has a value close to α_r (Short *et al.*, 1999a,b). This model has been widely used for the analysis of experimental data of HRS. These three last models are shown on Figure 2.9, along with the LQ model.

Finally, a new model has recently been proposed (Marples *et al.*, 2003), called the 3-components induced repair model. The first two components are the response of G1 and S phase modelled by two linear quadratic models, and the third component is the response of G2 cells modelled according to Equation 2.9. Therefore, only G2 cells are supposed to show HRS.

2.3.3 Bystander Effect

When cells are irradiated in a dish, or when non-irradiated cells are cultured in filtered medium from irradiated cells, more cells than expected manifest effects of radiation; this has been termed

the bystander effect (Morgan, 2003). This demonstrates that the biological consequences of radiation spread beyond the physical interactions of the radiation track with the cells (Mothersill and Seymour, 2004a). The following analogy has been made: if a lecturer throws oranges at their students, the oranges may target some students, and not touch them, but the targeted students may rise and agitate their arms, thus injuring their neighbours, who did not receive any direct hit from the oranges: the number of injured students during the course of the experiment does not correspond to the number of oranges thrown or to their trajectories (Mothersill and Seymour, 2004a).

2.3.3.1 Measuring the Bystander Effect

Very different protocols are used to demonstrate the bystander effect *in vitro*; Morgan (2003) thinks of the results of those experiments as being different categories of bystander effect. A first method consists in irradiating cells with low fluences of high LET radiation; a second method puts non-irradiated cells in contact with medium in which cells have been irradiated. In the third approach, a microbeam, i.e. a focused beam of micrometer dimensions, is used to select cells to be irradiated.

When cells are irradiated at low fluence at a known average number of particles, the probability of receiving one or more particles can be calculated by using Poisson statistics:

$$\begin{aligned} P(\text{n hits}) &= \frac{\exp(-\bar{N}) \times \bar{N}^n}{n!} \\ P(\text{one or more particles}) &= 1 - P(0\text{ hit}) \\ P(\text{one or more particles}) &= 1 - \exp(-\bar{N}) \end{aligned} \tag{2.10}$$

In Equation 2.10, $\bar{N}$ is the average number of particles per unit area; the probability of receiving one or more particles corresponds to the proportion of cells being hit. It is possible to predict the extent of a given endpoint (e.g. clonogenic death, mutation, micronuclei) assuming a linear relationship between the number of cells hit and the intensity of the endpoint. The results have been compared to experimental results by Azzam *et al.* (2001, 2002) and Little *et al.* (2005a, 2002).

The study of the toxicity of the medium in which cells have been irradiated for non-irradiated cells is another way of characterizing the bystander effect (irradiated cell conditioned medium

(ICCM): Mothersill and Seymour, 1997, 2001, 1998). Some cells which are seeded and irradiated, may be incubated for different periods of time. Their medium is then filtered and added to non-irradiated cells, which are left in contact with this conditioned medium for various times as well. There are variants to this protocol: a closed dish with two Mylar sides facing each other on which it is possible to seed cells is used (Zhou *et al.*, 2002a). The distance between the two faces is long enough so that all α particles targeting one face are absorbed before being able to reach the second face. In the second variant, the transwell technique is used (Yang *et al.*, 2005); irradiated cells are seeded in large wells, while non-irradiated cells are seeded in a smaller permeable insert which is added after irradiation.

Finally, a more direct observation of the bystander effect can be achieved via microbeam irradiation. Microbeams, contrary to broadbeams, produce a focused beam of dimensions that are small enough to target only a single cell, and even a given area of the cell (nucleus, cytoplasm). A finite proportion of cells in a dish is irradiated with a known number of particles or known dose. So far, irradiation with helium particles (Burdak-Rothkamm *et al.*, 2006; Shao *et al.*, 2005; Zhou *et al.*, 2004), soft carbon X-rays (Schettino *et al.*, 2005), carbon and uranium particles (Fournier *et al.*, 2007) have been used. Again the effect for a given endpoint is estimated from the proportion of irradiated cells and compared to the experimental measurements.

As seen in Section 2.2, there is a diversity of consequences to cell irradiation, from cell cycle checkpoints to cell death. The bystander effect has been identified in terms of many of these endpoints:

1. gene expression (Azzam *et al.*, 2001, 2002; Fournier *et al.*, 2007);
2. apoptosis (Belyakov *et al.*, 2005; Mothersill *et al.*, 2006);
3. micronuclei formation (Burdak-Rothkamm *et al.*, 2006; Prise *et al.*, 1998; Shao *et al.*, 2005, 2003a, 2004);
4. gene mutation (Zhou *et al.*, 2004, 2000, 2002b);
5. chromosome aberration (Little *et al.*, 2005a);
6. transformation (Sawant *et al.*, 2001a,b);

7. survival fraction (Sawant *et al.*, 2001b; Schettino *et al.*, 2005, 2003);

8. genomic instability (Huang *et al.*, 2007; Moore *et al.*, 2006);

9. or enhanced proliferation (Gerashchenko and Howell, 2003).

The above studies were carried out in very different conditions and have sometimes led to contradictory conclusions, although some general characteristics are starting to appear, as will be presented in the following section. There is a need to find a protocol that would be used by all laboratories, with an agreement on the technical settings and the cell systems used. Unless this is achieved, it is difficult to draw clear and general conclusions on the mechanisms of the bystander effect.

2.3.3.2 Possible Mechanisms of the Bystander Effect

A feature that has been seen in many experiments is the presence and the saturation of the bystander effect for high doses (Ballarini *et al.*, 2002; Morgan, 2003; Prise *et al.*, 2003). This has been proved in terms of:

1. survival fraction: between 5 cGy and 5 Gy for human keratinocytes in γ-rays ICCM experiments (Mothersill and Seymour, 1997, 1998; Seymour and Mothersill, 2000) and between 3 cGy and 3 Gy for hamster lung cells in C_k-X-rays microbeam experiments (Schettino *et al.*, 2005) (see Figure 2.10). Schettino *et al.* (2005) suggested that at doses below 0.3 Gy, the bystander effect in the hamster cell line was linear with irradiation dose.

2. micronuclei formation: for 1 or more α particle(s) for human glioblastoma (Shao *et al.*, 2003a) and between 5 and 15 α particles in human fibroblasts (Prise *et al.*, 1998) using a microbeam.

However, a few experimental results disagree with this idea:

1. Huang *et al.* (2007) noticed a slight increase in the bystander genomic instability in a human carcinoma cell line between 5 and 10 cGy;

2. also, there was an increase in the bystander cell killing and transformation frequency in mouse cells after α particles microbeam irradiation (Sawant *et al.*, 2001a,b);

3. on the contrary, Shao *et al.* (2003a), comparing the survival of cells incubated with an inhibitor of the BE with control culture, showed that when all human glioblastoma of a population are irradiated with α particles, the bystander effect disappears at doses higher than 5 particles per cell. This actually contradicts the idea that there is any bystander effect at high doses.

Seymour and Mothersill (2000) predicted in human keratinocytes harvested in ICCM that at doses below 0.5 Gy, cells were killed predominantly by the bystander effect, but for doses up to 5 Gy, the killing resulted from both direct and bystander effects. Schettino *et al.* (2003), comparing the survival fraction of dishes where all cells are irradiated, with dishes where one cell is irradiated, draws a similar conclusion: for hamster cells, below 0.2 Gy of soft C_k X-rays, the bystander effect is the main killing pathway. The sensitivity of cells to the bystander effect may depend on whether they have been irradiated (which is the case in the experiment by Shao *et al.* (2003a)) or only exposed to the bystander effect (which is the case in the experiments by Schettino *et al.* (2003) and Seymour and Mothersill (2000)).

There may be a saturation of the bystander effect with the number of irradiated cells as well; several microbeam experiments report that when the number of targeted cells increases, the extent of the bystander effect does not change significantly (Morgan, 2003). For instance, there is no significant difference of mutation induction in bystander human-hamster hybrid cells when 10% or 20% of the cells are irradiated with α particles (Zhou *et al.*, 2004, 2000, 2002b); in glioblastoma, the induction of micronuclei in the bystander population does not increase when more than 20% of the population is irradiated (Shao *et al.*, 2003a). Irradiation of a single cell can lead to a detectable bystander effect (Schettino *et al.*, 2005; Shao *et al.*, 2005); because of this saturation with both dose and number of irradiated cells, the bystander effect is sometimes described as an "all or nothing" phenomenon. Its consequences are fully triggered as soon as the effect is switched on. Yet, the situation seems to be different in ICCM experiments, where an increase in the cell density of the donor flasks leads to an increase in bystander cell killing for keratinocytes (Mothersill and Seymour, 1997).

The bystander effect is believed to be due to a signal released by irradiated cells (the bystander signal (BS), Mothersill and Seymour, 2001) but no protein has been definitely identified yet (Little, 2006). There is accumulating evidence that reactive oxygen species (ROS) are involved (Ballarini *et al.*, 2002; Morgan, 2003; Prise *et al.*, 2003). The role of ROS is essential for the bystander up-regulation of cell cycle related proteins, in human fibroblasts irradiated with low fluence of α-particles at less than 10 cGy (Azzam *et al.*, 2002). It is also required for the bystander micronuclei formation after α-particles microbeam irradiation in fibroblasts (Shao *et al.*, 2005) and in astrocytes (Burdak-Rothkamm *et al.*, 2006). The bystander induction of gene mutation in human-hamster hybrid cells, though, does not require ROS (Zhou *et al.*, 2004, 2000, 2002b). In human glioblastoma, nitric oxide (NO) may also play a critical role in the bystander effect (Burdak-Rothkamm *et al.*, 2006; Shao *et al.*, 2005, 2003a).

Because the action of the bystander effect spreads at least 1mm far from its source (Belyakov *et al.*, 2005; Fournier *et al.*, 2007; Prise *et al.*, 2003; Schettino *et al.*, 2003), and because ROS and NO are very short-lived molecules which cannot travel that far, they must create more persistant secondary messengers of the bystander effect (Burdak-Rothkamm *et al.*, 2006; Moore *et al.*, 2006; Shao *et al.*, 2005). A possible molecule is the tumour growth factor TNF-β, which is induced by both NO and ROS (Burdak-Rothkamm *et al.*, 2006; Iyer and Lehnert, 2000). ROS and NO can induce DNA DSBs which have been seen in bystander cells and been proposed as being the critical damage leading to the bystander effect (Burdak-Rothkamm *et al.*, 2006; Kashino *et al.*, 2004; Little *et al.*, 2002). However, calculations show that there is no correlation between the bystander cell killing and formation of complex DSBs in hamster cells after microbeam C_k X-rays irradiation (Schettino *et al.*, 2005); also the bystander effect is seen after cytoplasmic irradiation (Shao *et al.*, 2004), which does not suggest that DSBs could trigger the bystander effect.

The communication of the BS from emitting cells to neighbours is a controversial issue. The studies of the bystander effect via ICCM show that the signal must be a protein that is soluble and transmissible through the medium (Iyer and Lehnert, 2000; Mothersill and Seymour, 1997, 1998); microbeam irradiation experiments on non-confluent cell populations also suggest that the signal can diffuse in the media and does not require cell-cell contact (Prise *et al.*, 1998; Shao *et al.*, 2003a). On the other hand, the bystander effect in some cell lines and for some endpoints requires that junctions connecting cytoplasms, gap junction inter-cellular communication

(GJIC), be active. GJIC is crucial in the bystander up-regulation of cell-cycle related proteins in fibroblasts after low fluence of α particles (Azzam *et al.*, 2001, 2002) and in the bystander mutation induction after α particles microbeam irradiation of human-hamster hybrid cells (Zhou *et al.*, 2004, 2000, 2002b). The activity of GJIC has also been visualized in fibroblasts after X-rays and carbon irradiation (Fournier *et al.*, 2007).

A more likely possibility is that different pathways work for different endpoints. Moore *et al.* (2006) shows that cell-cell communication is necessary for bystander genomic instability but not bystander killing in lymphoblastoids after X-rays. Zhou *et al.* (2002a) suggests that in human-hamster hybrid cells, the bystander killing is mediated via a soluble factor, while the bystander mutation induction is transmitted via GJIC. On the other hand, it has been suggested that both the GJIC and the medium transfer may play a role, and this would explain the difference in intensity of BE found by at the Gray Cancer Institute and at Columbia University in V79 cells (Mitchell *et al.*, 2004). For fibroblasts harvested in γ-rays ICCM, blocking the GJIC triggers an increase in the bystander cell killing (Mothersill and Seymour, 1998); according to Ballarini *et al.* (2002), this could be explained if the signal spread by both GJIC and medium diffusion: blocking the GJIC would render the medium more toxic because all the signal would be released and no signal would be communicated to neighbours.

The ICCM studies allow for the time-characterization of the bystander signal, but again quite different conclusions are drawn by different laboratories. The medium of irradiated human fibroblasts or keratinocytes is already toxic 30 minutes after irradiation (Lehnert and Goodwin, 1997; Mothersill and Seymour, 1997), whereas the medium of human-hamster hybrid cells is not toxic 20 minutes after the irradiation (Suzuki *et al.*, 2004). The action of the signal produced by human keratinocytes seems to be transient, as there is no difference in survival fraction of recipient cells exposed to the ICCM for 30 minutes or for 24 hours (Mothersill and Seymour, 1998). The medium of human-hamster hybrid cells and hamster cells, on the contrary, becomes more toxic with time (Kashino *et al.*, 2004; Suzuki *et al.*, 2004), and the bystander signal was active at least 48 hours after irradiation in these cell lines. An early study on human keratinocytes (Mothersill and Seymour, 1997) using the medium transfer methods showed that a bystander effect could be seen in recipient cells harvested in conditioned medium left up to 60 hours after irradiation in the donor flask. Therefore the conclusion was that the bystander signal was still present and efficient 60 hours after its production, i.e. about 2.5 cell

cycles, considering that the average human cell cycle is 24 hours. The question is still: if the bystander signal stayed active for 60 hours, most donor cells would have been killed by the signal, even if the signal only affects cells in a particular phase of the cell cycle. This question was not addressed by the authors.

It seems that not all cells can generate a bystander signal (Belyakov *et al.*, 2005; Mothersill and Seymour, 1997; Mothersill *et al.*, 2002), even though they may be sensitive to a signal produced by the irradiation of a different cell line. Indeed, several experiments using co-culture showed that the bystander effect is possible between different cell lines (Belyakov *et al.*, 2005; Burdak-Rothkamm *et al.*, 2006; Mothersill *et al.*, 2006; Shao *et al.*, 2005), which suggests that it may be observed at the tissue level (Mothersill and Seymour, 2004a). Furthermore, the maximum response of recipient cells vary with the type of cell line of donor cells (Mothersill *et al.*, 2004a; Shao *et al.*, 2005, 2003a); this suggest that that the saturation in the bystander effect is not due to a sub-population that would be sensitive to the signal.

Not only has the bystander effect been noticed from nucleus to nucleus, but also from cytoplasm to nucleus. Shao *et al.* (2004) showed that irradiating glioblastoma in the cytoplasm led to micronuclei formation in both bystander and irradiated cells. The intensity of the bystander effect is similar to the one after nucleus traversal, and it is again independent of the number of α particles and proportion of cells targeted in the population. The results also suggest that the signal is mediated via the membrane. This study is critical as it proves that there is no need of any nucleus DNA damage to produce a lethal effect, and because cytoplasmic irradiation is not lethal, there is no need to kill the irradiated cell to produce a signal which may be harmful to the rest of the population. The cell membrane might increase permeability during the bystander effect, but this has not been addressed experimentally yet.

The effect of ionizing density has not been examined widely yet. Shao *et al.* (2002, 2001) detected a variation in bystander enhanced plating efficiency and bystander micronuclei formation with radiation LET in human salivary gland cells, although the dependency between bystander effect intensity and radiation LET is not clear. In contrast, Fournier *et al.* (2007) and Shao *et al.* (2003b) found a similar intensity of up-regulation of cell cycle proteins and micronuclei formation respectively in bystander fibroblasts, and concluded that the extent of the bystander effect did not vary with LET; yet, Fournier *et al.* (2007) noticed that different types of signalling seem

to be involved for different doses of different radiation LET. Since the two first studies were led on a human salivary gland cell line and the two other experiments on human fibroblasts, it could be that the dependency of the bystander effect with LET is different in different cell systems. In any case, the fact that a bystander effect can be induced by heavy ion irradiation, which produces complex DNA damage (see Section 2.2), suggests that cells can produce the signal even when they are greatly injured.

The dependency of bystander effect with cell cycle phase also needs further investigation. Mothersill *et al.* (2004b) reports that G2 cells may be either the cells emitting the signal or the cells susceptible to be affected by it. However, early results show that in fibroblasts and glioblastoma, bystander micronuclei are mostly induced in cells in S phase (Burdak-Rothkamm *et al.*, 2006).

In conclusion, there are still many controversies and ideas to be clarified concerning the bystander effect. In some cell lines, the bystander effect is expressed in terms of some endpoints but not in terms of others. This is the case of a carcinoma which does not show bystander cell killing but shows bystander genomic instability (Huang *et al.*, 2007). Also, no bystander cell killing is detectable in a human glioblastoma using the ICCM method (Mothersill *et al.*, 2002), contrary to bystander micronuclei formation, which is shown using microbeam α particles irradiation and ICCM (Burdak-Rothkamm *et al.*, 2006; Shao *et al.*, 2005, 2003a). In addition, there may well be different mechanisms responsible for these different endpoints (Zhou *et al.*, 2002a). This supports the idea from Morgan (2003) that there are several, rather than 1, bystander effects. Table 2.1 summarises the cell lines studied in the different publications cited in this literature review; it is indicated for each cell line whether the BE has been studied, using which protocol and measuring which endpoint, as well as whether the HRS has been studied. The very different conditions of experimentation, for both methodology and cell systems, make conclusions difficult, and caution should be taken. However, no laboratory tried to reproduce the experiment of others, and only the Center for Radiological Research at Columbia University started exploring a single cell line using different protocols and looking at different endpoints (Zhou *et al.*, 2004, 2000, 2002a,b). Unless this is generalised, it will be difficult to know whether all these experiments relate to the same phenomenon.

2.3.3.3 BE and Other Non-Targeted Effects

The bystander effect is sometimes measured in terms of genomic instability (Huang *et al.*, 2007; Moore *et al.*, 2006) and early studies raise their similarities (Mothersill and Seymour, 2001). Indeed, the two phenomena share common features, although Little (2006) points out that they concern different cells (bystander cells present at the time of exposure versus progeny of cells irradiated). They can be detected for the same endpoints, such as cell killing, micronuclei formation, transformation, chromosome re-arrangement. Also, the same type of mutation is seen in bystander cells and in the unstable progeny of irradiated cells. Finally, up-regulation of ROS happens in the two cases (Little, 2006; Morgan, 2003). The bystander signal might be responsible for the genomic instability in the progeny of either irradiated or non-irradiated cells (Mothersill and Seymour, 2001; Mothersill *et al.*, 2006). An interesting finding is that cells harvested in the medium of non-irradiated but unstable parent cells show increased cell killing or genomic instability (Huang *et al.*, 2007; Morgan, 2003), even though these cell lines do not show the bystander effect by ICCM. This has been called the death-inducing effect; this questions the origin and spread of genomic instability.

Priming cells decreases the bystander effect. So far, priming doses of X-rays have been used 6 and 4 hours respectively before α particles microbeam irradiation of mouse and human-hamster hybrid cells (Sawant *et al.*, 2001b; Zhou *et al.*, 2004, 2002b). A small dose of γ-rays before transferring ICCM on human keratinocytes also diminishes the bystander cell killing. These results therefore suggest that adaptive response and bystander effect may be triggered partly by the same mechanisms.

Only one study has been carried out so far on the relationship between BE and HRS (Mothersill *et al.*, 2002), using the classic clonogenic assay and the ICCM method, on a variety of human cell lines. The tendency would be that cells show either HRS or BE, but both phenomena are mutually exclusive. However, it is worth noting that this study finds no bystander cell killing in a human glioblastoma which yet shows bystander micronuclei formation after α particles irradiation (Burdak-Rothkamm *et al.*, 2006; Shao *et al.*, 2005, 2003a, 2004); also HRS has been detected in hamster cells (Schettino *et al.*, 2001; Tsoulou *et al.*, 2001), as well as the bystander effect for survival (Schettino *et al.*, 2005, 2003). Again, those experiments used different protocols, and looked at different endpoints, and therefore, conclusions are difficult.

2.3.3.4 Modelling Survival

The bystander effect, as well as HRS, modifies the traditional LQ equation used in radiobiology. New models have been derived for high LET microbeam and high LET broadbeam irradiation.

In microbeam experiments where targeted cells receive an exact number of particles N, the probability of survival for those cells to N independent hits is:

$$S_N = s^N \tag{2.11}$$

s : Probability of surviving one hit

If p is the proportion of cells being targeted, then (Brenner *et al.*, 2001; Nikjoo and Khvostunov, 2003):

$$S_F = p \times s^N + (1-p) \times S_B \tag{2.12}$$

S_B : survival fraction of bystander cells to the signal

In case of broadbeam irradiation with an average particle number $\bar{N}$, Poisson statistics apply, and the proportion of cells surviving a direct hit can be determined as follows:

$$\text{Probability receiving N hits: } P_N = \exp(-\bar{N}) \times \frac{\bar{N}^N}{N!}$$

$$\text{Probability surviving N hits: } S_N = s^N \times \exp(-\bar{N}) \times \frac{\bar{N}^N}{N!}$$

$$\text{Probability surviving broadbeam: } S_F = \exp(-\bar{N}) \times \sum_{N=0}^{N=\infty} \frac{(s\bar{N})^N}{N!}$$

$$S_F = \exp(-(1-s)\bar{N}) \tag{2.13}$$

The proportion of cells not directly hit that die because of the bystander signal should be subtracted from this (Brenner *et al.*, 2001; Nikjoo and Khvostunov, 2003):

$$S_F = \exp(-(1-s)\bar{N}) - \exp(-\bar{N}) \times (1-S_B) \tag{2.14}$$

(2.15)

In his model, Brenner *et al.* (2001) assumes that, in the case of broadbeam radiation, there is no bystander effect and S_B is 1. An implicit assumption in these models is that only cells that

have not been traversed by a track are sensitive to the signal, but not cells that have survived a particle traversal. According to Nikjoo and Khvostunov (2003), the surviving probability to the signal does not depend on dose but depends on the quantity of signal emitted. The BAD model of Brenner *et al.* (2001) assumes that S_B, in the case of microbeam radiation, decreases with dose but is independent of the quantity of signal in the medium. The two models predict that at low doses (up to two α particles), the bystander component is important, but contrary to the model of Brenner *et al.* (2001), the model of Nikjoo and Khvostunov (2003) assumes that the contribution of the bystander effect is also non-negligible at high doses.

The statistical model of Little *et al.* (2005b) considers a 3 dimensional lattice containing the cells; the experimental situation in which cells are seeded on a 2D dish being a particular case of the 3D situation. Cells can be in 4 different states:

- alive;
- affected by the signal and non-signalling;
- affected by the signal and signalling;
- dead.

A cell can die for spontaneous or radiation-induced reasons; it can become signalling if it was previously alive non-affected for spontaneous, radiation-induced or bystander effect reasons. The cell can stop signalling because of spontaneous or bystander effect reasons; finally the cell can become alive and non-affected if it was previously signalling for spontaneous or radiation-induced reasons. Therefore, secondary messengers are possible in this model which introduces the idea that cells may not emit the signal continuously and that the bystander action depends on the spatial position of the cells and the diffusivity of the signal; however, the signal cannot kill cells, and death occurs only after a spontaneous or a radiation event. The model predicts the saturation of the bystander effect with dose, but a disadvantage of such a model is its complexity which makes interpretations not straightforward. Moreover, quantitative studies are not possible, and the intensity of different endpoints (such as cell death, micronuclei formation) cannot be predicted.

2.3.4 Implication of Non-Targeted Effects for Cancer

A question that arises from the discovery of the non-targeted effects is if and how radiotherapy and radiation risk assessment should be changed, in case they were confirmed to play a role *in vivo* as well (Little, 2006; Mothersill *et al.*, 2004b).

If cells die of HRS at low doses because of a radio-protective mechanism preventing any risk of mutation propagation, then the risk of cancer at low doses is less than what is expected from the linear no-threshold model. Nevertheless, this assumption needs to be confirmed by the evidence that there is no HRS in terms of mutation, or that cells hyper-sensitive to mutation are the ones killed (Joiner *et al.*, 2001). So far, HRS has only been studied for the survival fraction endpoint, even if some calculations on a human fibroblast show that HRS in G2 cells may be responsible for the change in transformation frequency in asynchronous cells (Redpath *et al.*, 2003).

Radiotherapy treatments are designed to minimize the effects on normal tissues. Treatment fractionation (i.e. splitting the total dose to be given in small subsequent doses) has proved to spare the healthy tissues surrounding the tumour (Mothersill *et al.*, 2004b). If tumour cells are very sensitive to small doses of radiation, and many tumour cell lines show HRS, it may be interesting to plan an ultra-fractionated treatment (e.g.: 3 fractions of 0.5 Gy a day, Harney *et al.* (2004a,b)) rather than the conventional fractionated treatment (e.g.: 1 fraction of 1.5 Gy a day, Harney *et al.* (2004a,b)). However, because it has been shown that HRS may be eliminated by priming doses, the ultra-fractionated treatment has to be designed carefully. As an example, no hyper-radiosensitivity could be seen in rodent cell lines (Smith *et al.*, 1999) when irradiated with fractionated doses at 3 hours interval. On the other hand, Short *et al.* (2001) demonstrated that an increased cell killing was obtained using an ultra-fractionated regime on human glioblastoma cell lines showing HRS. The difference in results may come from the fact that in the first study the adaptive mechanisms eliminating HRS were triggered, but not in the second. Yet, the results *in vivo* are quite contradictory. Conventional treatments appear to be more efficient than ultra-fractionated treatments for curing glioblastoma tumours implanted in mice (Krause *et al.*, 2003, 2005). HRS is seen in normal human skin, but ultra-fractionated irradiation does not lead to increase cell death compared with conventional irradiation; however, it seems that ultra-fractionated irradiation is a better cure for skin tumours (Harney *et al.*, 2004a,b). In conclusion, no evidence of a clear advantage in the use of HRS properties in radiotherapy has been given

so far, and further investigation is needed. The advantage may depend critically on individual characteristics. In addition, there is some evidence that there may be no benefit in fractionating the radiation dose for bystander cells, as the bystander signal (or signals) does not seem to be less toxic in these conditions (Mothersill *et al.*, 2004b).

The bystander effect has not been proved directly to happen *in vitro* either; however, some phenomena, observed for a long time in radiotherapy and that could not be explained, may be the result of bystander signalling in the organism (Mothersill and Seymour, 2001). The observation of radiation-type effects in a non-irradiated part of the body after irradiation of another part has been termed the abscopal effect; a positional or contralateral effect happens when the irradiation of a precise part of an organ leads to effects in a different non-irradiated part of this organ. Furthermore, the question has been raised as to whether the bystander effect is responsible for secondary cancers and metastasis development (Prise *et al.*, 2003).

It is not clear whether the bystander effect is beneficial or detrimental. On the one hand, because there is a bystander cell killing, it may well be a protective mechanism to avoid the reproduction of any cell potentially carrying mutations, similar to the HRS. On the other hand, several studies have reported a bystander induction of genetic mutation, genomic instability and enhanced cell proliferation; from this point of view, the bystander effect would be genotoxic. Therefore, the balance between those two aspects needs to be determined (Ballarini *et al.*, 2002; Little, 2006; Prise *et al.*, 2003).

In radiotherapy, the bystander cell killing could possibly be used in two ways: either inhibiting it to limit the risk to normal cells death, or by enhancing it and achieving complete tumour death, while treating only a few tumour cells. This has started being developed in gene therapy (Prise *et al.*, 2003).

In any case, the non-targeted effects, if of relevance *in vivo* as well, would bring uncertainty in radiotherapy and risk assessment. Mothersill and Seymour (2004a) proposes that dose should not be the only criteria in estimating the effects of low doses of radiation, but that the genetic background, environment and signalling network should also be accounted for. Non-linearity is likely and the evidence is growing that energy deposition in the nucleus is not required for cells to be affected (Mothersill *et al.*, 2006).

2.4 Concluding Comments

The objectives of this review have been to show the shift radiobiology and radiobiologists are going through at present. While for many years, it was thought that radiation energy deposition in the nucleus meant radiation effect and reciprocally, recent evidence has been found to challenge this. The cellular response to radiation, at least *in vitro*, appears to be much more complex and involves more factors.

The existence of non-targeted effects in systems *in vitro* have been proved in different cell types and for different radiobiological markers. However, because these effects would mean that response to exposure involves the cell network, rather than the individual cell, studies in 3-D systems, such as in Belyakov *et al.* (2005), or in *ex vitro* systems such as spheroids (Bishayee *et al.*, 1999), should be developed. The relevance of these phenomena *in vivo* also needs to be demonstrated clearly.

Besides, so far, experimental protocols use radiation of high LET but there is not many data concerning radiation such as γ- or X-rays, which are widely used in medical applications. Therefore, there is a need for building microbeams for low LET irradiation of the energies of interest (Little, 2006). Nevertheless, in the hope of increasing the proportion of high LET radiotherapies, the knowledge of non-targeted effects in the context of heavy particles radiation is still useful.

Many similarities are seen between the non-targeted effects; it is tempting to think that they are all manifestations of a common mechanism. The rest of this report describes a first attempt to find this potential underlying mechanism. The initial focus is on HRS and BE.

Chapter 3

Theory and Model Implementation

3.1 Introduction

The following chapter details the assumptions and implementation of the preliminary model of in vitro cell response to radiation that was developed during the course of this project. This model focuses on two non-targeted effects: the low dose hyper-radiosensitivity (HRS) and the bystander effect (BE).

A simple model of HRS is described in details in Appendix A, based on the assumption that HRS is due to repair mechanisms not triggered below a given dose of radiation. The results confirmed the idea that the sensitivity of cells to low doses of radiation is not linear. However, two main limitations of this model were:

i. the survival probability of a single cell is discontinuous at the dose switching on the repair processes, which is biologically unrealistic and,

ii. it is not possible to explain other non-targeted effects with such a model.

Yet, it is plausible that all non-targeted effects are related: as seen in Section 2.3, several studies have been carried out on the relationship between HRS and adaptive response, and between BE and adaptive response or genomic instability.

This chapter describes a first attempt at a new theory that could explain the response of cells to ionizing radiation, taking into account non-targeted effects. At this stage, it accounts only for the bystander effect and low dose hyper-radiosensitivity.

On the one hand, the hyper-sensitive region of cell lines showing HRS was always found below 1 Gy; this hyper-radiosensitivity could be followed by an increased radio-resistance at higher doses. On the other hand, the bystander effect saturates at doses below 1 Gy. The following scenario was consequently proposed: cells in the dish that were traversed by a track of ionizing radiation released a signal. This signal targeted the neighbouring cells and triggered some processes that led to their death. The curve of the survival fraction of the population with dose would have a HRS-like shape (see Figure 3.2). The model below was based on these assumptions. The general definition of the model is given in Section 3.2; the following sections detail the different aspects of the model: the nutrient availability (Section 3.3), the division of cells and growth of colonies (Section 3.4), and finally the radiation effects (Section 3.5).

3.2 General Description of the Model

In the model, cells are considered to be in a dish containing 5 ml of medium (Marples and Joiner, 1995; Marples and Skov, 1996) and the nutrient is in excess so that cells never starve (see Section 3.3). In this first version of the model, the dish is square, although cells are usually harvested in rectangular dishes. The edges of the dish are the fixed impermeable boundaries for both the nutrient and the cells; this means that the nutrient cannot diffuse outside the dish and cells cannot move outside the dish.

The population of cells is modelled by a cellular automaton. The nodes of the cellular automaton are either biological cells, the status of which is defined by their age (total number of cell cycles undergone), their position in the cell cycle (phase) and their nutrient consumption, or empty spaces of the dish that can potentially be filled by a newly-born cell. Nodes are arranged in a square grid and their neighbourhood consists of the 8 cells in the vertical, horizontal and diagonal directions (see Figure 3.1). The progression of cells through the cell cycle depends on their previous status: a cell starts a new phase of the cell cycle only if it has completed the previous phase (see Section 3.4). At division, the fate of the cell also depends on the status of

its neighbours: the cell divides into an empty neighbouring node, and if there is none, it may push the existing neighbouring cells (see Section 3.4).

A simulation consists in setting the quantity of nutrient in the dish and seeding cells (first block in the diagram of Appendix D). All or some cells are irradiated, and have a probability of surviving the radiation and of emitting a signal (second block in the diagram of Appenidx D). Cells are let to form colonies for a period of time which depends on their average cell cycle length (blocks 3 to 6 in the diagram of Appendix D). Finally, the number of viable colonies that have formed is counted (see Section 3.5 and last block in the diagram of Appendix D). The cells are originally seeded at random positions within the boundaries of the dish, and are tracked by a colony number which their progeny inherits; this helps counting the number of viable colonies.

The following sections describe in details the theory and implementation of the nutrient consumption, cell growth and cell response to irradiation.

3.3 Nutrient Availability and Consumption

3.3.1 Theory and Assumptions

The diffusion of nutrients in the dish was considered instantaneous. The rate of consumption of nutrient can be modelled by a Michaelis-Menten equation (Burrows *et al.*, 2004):

$$r(t) = \frac{\mathrm{K} \times Q(t)}{\mathrm{K}_S + Q(t)} \text{ mol/min/cell} \qquad (3.1)$$

$$Q(t) : \text{quantity of nutrient at time t (mol)}$$

In Equation 3.1, K (mol/min/cell) is the maximum rate of consumption by cells, K_S (mol) is the saturation constant and corresponds to the quantity of nutrient at half the maximum rate of consumption. It was assumed that K and K_S were constant throughout the cell cycle.

Burrows *et al.* (2004) measured a concentration of glucose in the medium of 5.5 mM; in these conditions, since the volume of medium was 5 ml, the initial number of moles of glucose in the dish was Q(t=0) = 5 ml $\times$ 5.5 mM = 27.5 μmol. In the absence of data on the rate of consumption of nutrient of V79 cells or T98G cells in culture, the two cell lines studied

here, these were approximated by the data for rodent glioblastoma and human fibroblasts (Burrows *et al.*, 2004). The values of the parameters K and K_S in Equation 3.1 were respectively 6.4×10^{-6} nmol/cell/min and 5.25 μmol for the rodent glioblastoma and respectively 16.6×10^{-4} nmol/cell/min and 44.5 μmol for the human fibroblast. This gave approximately the consumption rate of 5×10^{-6} nmol/cell/min for both cell lines at the concentration of glucose of 5 mM. It was assumed that the rate of consumption was constant; this is justified if the quantity of nutrient Q(t) remains high compared to the parameter K_S. Therefore, this was a crude approximation for the T98G cell line.

3.3.2 Implementation of Nutrient Availability

Because the nutrient was assumed homogenous on the dish, it could have been computed by a single number representing the quantity available at any time on the dish. However, in order to facilitate further developments of the model in which the distribution of the nutrient may not be homogeneous (e.g. in case of a tissue or spheroid), it was decided to mesh the dish and compute the quantities of nutrient available at the different nodes.

The code was written in C++, an object oriented language, under the UNIX environment; a flow chart of the program can be found on Appendix D. The code of the program is available on a CD at the end of the dissertation. A class CA was defined that contained two matrices, one for the description of the nutrient distribution and one for the description of cell growth, the dimensions of the dish and the initial number of cells seeded (See Figure 3.3). The nutrient matrix (class vector in C++ language, used with two dimensions) was called *lattice* and the cell matrix was a list called *population*. The details of the matrix *population* are presented in the following sections. The program was run for a number of time iterations chosen, and one iteration represented one minute. This was short compared to the duration of any cell cycle phase (see Section 2.1), and long enough to enable the simulation of harvest periods in a reasonable time. A set of simulations were run with a time step of 2 minutes instead of 1 minute and gave the same results for Q(t), showing that results are independent of the time step chosen.

The elements of *lattice* were objects of the class Chemical, which contained a number representing an amount of nutrients and a pair of coordinates, which are the different nodes of the

meshed dish, see above; in the matrix, the Chemical object (i, j) represented the amount of nutrient at the position (i, j) in the dish. After each time step, the new total amount of nutrient, decreased by the amount consumed by cells, was calculated; the value of each element of *lattice* was set to the new total divided by the number of elements (see Figure 3.4).

For reasons of computer memory capacities, the space scale of *lattice* was m times smaller than the one of *population*. The number m was set to 10, i.e., the distribution of nutrients was divided into squared areas of the size of 100 cells. Because in the present study, the nutrients were always in excess and the diffusion was instantaneous, using two different space scales did not pose a problem. The number of C++ vectors and number of nodes in each C++ vector of *lattice* were chosen to be equal to LX=LY=100, so there were 10^4 nodes in the matrix, each representing an area of 0.25 mm^2.

3.4 Cell Cycle and Growth of Colonies

3.4.1 Cell Cycle Rules

In the model, the cell cycle was divided into mitosis (M), gap 1 (G1), synthesis (S), and gap 2 (G2). Throughout their cycle, it was assumed that cells consumed nutrients at the same rate. Although many checkpoints exist throughout the cell cycle, only one was introduced in the model, at the G1/S transition (see Faraday *et al.* (2001) and Figure 3.5). The G1 phase consisted of a first sub-phase called G1a, the duration of which was fixed and that any cell completed when entering the G1 phase, and a subsequent sub-phase called G1b, the duration of which depended on the quantity of absorbed nutrients. The probability of transition to the S phase depended on the total amount of nutrients consumed since the last M phase. For subsequent phase transitions, the nutrient consumption was not taken into account. This was in agreement with the theory of the restriction point (Pardee, 1974). The duration of the other phases (S, G2 and M) of the cell cycle was fixed and identical for all cells and all cell cycles. The probability p to pass the G1/S checkpoint was described by the following equation (Faraday *et al.*, 2001):

$$p = 2 \times \frac{r\delta t}{\mathrm{S}_{max} - rt} \times (1 - \frac{r\delta t}{\mathrm{S}_{max} - rt}) \tag{3.2}$$

In Equation 3.2, r was the rate of consumption of nutrients, t the time spent in G1b and S_{max} (mol/cell) a parameter depending on the cell line that was to be fitted, and δt the time step in the simulations. S_{max} represents the maximum quantity of nutrient a cell may accumulate in G1 phase, and the probability of starting the S phase depended on the total nutrient uptake by the cell at time t.

If $a = \frac{S_{max}}{r\delta t}$ and $\delta t = \frac{1}{b}$ minute then:

$$\begin{aligned} p &= 2 \times \frac{1}{a - bt} \times (1 - \frac{1}{a - bt}) \\ \frac{dp}{dt} &= 2 \times \frac{b}{(a - bt)^2} \times (-1 + \frac{2}{a - bt}) \\ \text{so: } \frac{dp}{dt} &= 0 \Leftrightarrow t = \frac{a - 2}{b} \end{aligned}$$

Therefore, the probability of a cell leaving G1b increased up to the time $t = (\frac{S_{max}}{r\delta t} - 2)\delta t$. For times greater than $t = (\frac{S_{max}}{r\delta t} - 1)\delta t$, the probability defined by Equation 3.2 became negative, and cells never jumped to the S phase. This checkpoint existed in the code, but since in the conditions studied S_{max} was large compared to $r\delta t$ throughout the entire simulation, cells never failed the checkpoint.

Some cells may, for different reasons, stop proliferating and enter a quiescent state, sometimes called the G0 phase in the literature (see Section 2.1). In this model, cells could become quiescent when the nutrient availability became too low. Only cells in G1 could become quiescent, since the nutrients did not influence the other phases of the cell cycle. It was assumed that cells would cycle as long as the amount of nutrients stayed above a minimum value, but that cells would become quiescent as soon as the amount of nutrients fell below this minimum value. It was also assumed that quiescent cells would die if the amount of nutrients fell below a second lower minimum, but that they could become proliferative again if the amount of nutrients rose above the first minimum (Alarcon *et al.*, 2004; Antipas *et al.*, 2004).

When a cell had reached the end of mitosis, it attempted division. The probability that the cell gave two viable daughters was:

$$p = \frac{p_f}{2} \tag{3.3}$$

In Equation 3.3, the parameter p_f was the proliferation factor and accounted for the fact that not all cells produced exactly 2 viable daughters. If only one viable cell resulted from the division

process, then it sat at the node where the mother cell had been. Otherwise, one daughter was where the mother cell had been, and the other was placed in a neighbouring node. Different events were possible:

- If there was only one space in the neigbourhood of the mother cell, the new daughter was there;
- If there were several spaces free, the new daughter was where there was the most nutrients (Antipas *et al.*, 2004); in the use of the model presented in this thesis, the nutrient was uniform, and cells choose randomly a direction of division. The influence of nutrient distribution would be critical for modelling the case of tumours.
- If there was no space, the new cell pushed the existing cells away in random directions on the dish (Borkenstein *et al.*, 2004).

At the start of the simulation, 2000 cells were seeded that could be either synchronised in a phase or distributed throughout the cell cycle. In any case, the age of a cell in its phase at the start of the simulation was random (i.e. cells did not all start the beginning of the phase at the start of the simulation). However, they were all assumed to start at age zero, i.e. without having completed any cell cycle yet. Each time a cell completed a cell cycle, its age was increased by one. This accounted for the time that cells may take to disappear physically, after the process has started.

When cells died, they did not disappear immediately; they remained physically present for a period of time, although they did not consume nutrients (Borkenstein *et al.*, 2004). In the absence of experimental data, this time was assumed to be four hours, i.e. of the order of a cell cycle phase.

3.4.2 Cellular Automaton for Cell Colonies

The growth of the population of cells was modelled by a cellular automaton. The elements of this cellular automaton were the cells, the status of which was characterised by their position in the cell cycle, their age and the amount of nutrients they absorbed since last division.

The evolution of a cell depended on its state, because it changed phase only if it had completed the phase it was in. At the G1/S transition, the cell had a probability of starting the S phase which depended on the rate of consumption of nutrients; nevertheless, the rate was constant (see Section 3.3), therefore it did not influence the transition: all cells had the same probability of passing the checkpoint, at any time in the simulation. The position of any cell on the dish depended on the position of other cells and their division, as a random re-arrangement of cells could result from the division of a cell in the dish.

The evolution with time of the number of cells in populations of T98G was measured for synchronised and asynchronous populations in a series of simulations (Figure 3.6). The curve of cell number for the asynchronous population was fitted using the Microsoft Excel tool to an exponential:

$$\begin{aligned} n(cells) &= 1564.7\exp(1.572t) \qquad (3.4)\\ \text{correlation factor} &= 0.9982\\ (n(cells), t) &: \text{(number of cells, time(min))} \end{aligned}$$

Therefore, the growth of the asynchronous population could be modelled by the exponential growth of a population of cells of initially 1565 cells of doubling time of 26.5 hours. The shape of the curves for the synchronised populations was in agreement with the shape of curves for synchronised populations for mouse-mouse hybridoma (Faraday *et al.*, 2001): periods of time when the cell number was constant alternating with periods of time when the cell number doubled. The time needed to double the cell number increased, as populations lost their synchronisation; however, the de-synchronisation was expected to be faster (Faraday *et al.* (2001) and Murray and Hunt (1993, Chapter 1)). This is probably due first to the fact that the G1/S checkpoint did not work because of the constant excess in nutrients, and second to the fact that no other checkpoint have been introduced in the cell cycle.

3.4.3 Implementation of Cell Growth

The coordinates of each cell on the dish was stored in the class Node (see Figure 3.7). The class Node contained two integers representing the abscissa and ordinate of the cell on the dish. Some characteristics of the cell do not depend on its position in the cell cycle: its status (either

proliferative or quiescent), its total age (number of cell cycles undergone by the cell) and the amount of nutrients it has absorbed since last division; these characteristics were stored in the class Cell, which derived from the class Node.

The phase in which the cell was at any time of the simulation, as well as the duration of this phase, the time the cell has spent in the phase and the rate of nutrient consumption were defined in the class Phase, which derived from the class Cell. The class Phase also stored the number of the colony the cell belonged to; this artificial parameter was added to facilitate determining the number of cells per colony at the end of the simulation, and the survival fraction after irradiation (see Section 2.2). Daughters belonged to the same colony as their mother cell and inherited the colony number of their mother cell. Colonies could physically merge if the original cells were close, but the model would still be able to distinguish cells belonging to the two colonies. This differs from the experimental situation, where the biologist cannot distinguish with certainty when colonies have merged, although the size of the colony and its shape may indicate whether it is a single big colony or 2 colonies that have merged.

Because cells divide and their division depends on the position of the other cells of the population, it was necessary to compute the population in such a way that the growth of the population was computed easily and that the neighbourhing nodes could be detected easily. For this reason, the objects of class Phase were stored in the list of lists *population*; in C++ language lists can grow and shrink dynamically unlike vectors. The list of lists initially contained as many elements as there were cells seeded on the dish; as the cells divided and new cells were born, the list increased its number of elements. Therefore, at any time, the list contained exactly as many elements as there were cells on the dish, but did not contain the empty nodes of the dish; this helps reducing the computational effort. Each list of the list stored cells with a given abscissa on the dish (see Figure 3.1); this allowed to search easily whether the neighbouring nodes in vertical directions were empty or not. However, the list does not contain the empty nodes of the dish, but only the cell; therefore, it could consist of cells that were not physically adjacent (see Figure 3.1):

$$\begin{aligned} \forall i \in [0, M], \qquad & \forall j \in [0, N_i], \\ abs.population[i][j] &= abs.population[i][j+1] \\ &= abs.population[i][j-1] \end{aligned} \tag{3.5}$$

In Equation 3.5, M corresponded to the number of lists and N_i the number of nodes of the list i; $abs.population[i][j]$ represented the abscissa of the node (i, j). The index i did not have to be equal to the value of the abscissa; the number M represented the number of different abscissa that had been generated by the model. Similarly, j and the ordinate of the cell did not have to be equal, and N_i was the number of cells with abscissa i. The different lists represented the cells at different abscissa in the dish (the different "lines of cells" in the dish); again, the different lines of cells may not be adjacent (see Figure 3.1). For this reason, searching whether the cell has cell neighbours means searching whether the elements with adjacent coordinates exist in the list of lists (see below).

Cells with the same abscissa were elements of the same list; similarly, the lists were not ordered with increasing abscissa. The lists were sorted with increasing abscissa only after the irradiation of the dish, which happened just after the initial 2-D list was created; this was because the irradiation process is such that the first element of the list of lists is irradiated in single cell irradiation experiment (see Appendix B and Appendix C), and thus this permits a random cell to be irradiated rather than the one at the top right corner of the dish. For each of the subsequent time steps, cells cycled, possibly changed phase or died, absorbed nutrients, checked the surrounding level of nutrients, divided and could push neighbouring cells. At the end of each time loop, because new lists may have been created at division time, the lists were re-sorted with increasing abscissa.This facilitated the search for neighbouring cells at division.

For cells entering the G1b phase, at any time step, the program generated a random number γ in the interval $[0, 1]$, and compared it to the value of p in Equation 3.2:

- If $\gamma < p$, the cell entered S.
- Else, the cell stayed in G1b for the next time step.
- If the cell age had exceeded the maximum age allowed in G1b, it died.

The algorithm for generating random numbers was the function "ran0" suggested by Press *et al.* (1988, Chapter 7). For cells attempting division, it was first determined whether there was a node free of cells in the neighbourhood, i.e. it was determined whether one of the following nodes did not already exist in the list: $(abs - 1, ord - 1)$, $(abs - 1, ord)$, $(abs - 1, ord + 1)$,

$(abs, ord-1)$, $(abs, ord+1)$, $(abs+1, ord-1)$, $(abs+1, ord)$, $(abs+1, ord+1)$ (see Figure 3.1 and Figure 3.8). In the matrix, the distance to the neighbours on the diagonals is longer than the distance to the neighbours in the horizontal and vertical; therefore, there should be a higher probability that cells divide in the horizontal or vertical directions. No such difference was introduced in the model because cells do not diffuse; they only move by displacement due to the birth of new cells, and the exact spatial distribution of cells is not an issue.

Because in C++ lists do not support the indexation, the search process for neighbouring cells was not straightforward. If abs and ord were respectively the abscissa and ordinate of the cell about to divide (stored in the class Node), the following steps took place (see Figure 3.8):

1. The list *population* was screened to check whether the lists with elements of abscissa abs-1 and abs+1 existed;

2. If L, L-1 and L+1 were the lists of object Phase of abscissa abs, abs-1 and abs+1 respectively, L, L-1 and L+1 were screened (if they existed) to check the presence of objects Phase of ordinate ord, ord-1 or ord+1 (except the cell itself);

3. If some coordinates were found that did not already exist, they were stored in a vector *neighbours*, and the concentrations of nutrient at those nodes were stored in a vector *chem_neighbours*.

4. If *neighbours* was not empty, the node with the highest nutrient was chosen;

5. If *neighbours* was empty, the cell chose a neighbourhing node to divide into, and the cell already present was pushed away. This latter cell chose in turn a random node in its neighbourhood and pushed the cell present, if there was one. The process was done recursively until an empty node was found.

The matrix *population* could contain m times as many nodes as the matrix *lattice*, i.e, the maximum number of lists and the maximum number of cell nodes in each list were $m \times$LX=$m \times$LY. The number m was set to 10 (see Section 3.3); therefore the cellular automaton could contain at most 10^6 cells in total. It was shown in Section 3.3 that in case where cells cycled at the fastest rate, the total number of cells could exceed 10^6 cells; if this had happened, it would have been possible to increase the parameter m during the simulation and re-calculate accordingly the nodes of each of the cells.

3.5 Direct Effects and Bystander Effects of Radiation

3.5.1 Direct Effects of Radiation

When cells were irradiated, their probability of surviving the dose was calculated by the linear quadratic equation (LQ, see Section 2.2):

$$S_F = \exp(-\alpha d - \beta d^2) \tag{3.6}$$

In Equation 3.6, the parameters α and β depended on the radiation type, the cell line and the phase of the irradiated cell.

There were three equations for each of the two cell lines studied (V79 and T98G), for cells in G1, or in S or in G2. Cells in M phase followed the same trend as cells in G2 phase (Short *et al.*, 2003).

The coefficients α and β for these six equations were determined by minimising the sum of the errors squared between the simulation results and the experimental data from the Gray Cancer Institute, Oxford University, UK (for V79: M. Woodcock, personal communication and for T98G: Short *et al.* (2003)). The following definition of the sum of the errors squared was used:

$$\begin{aligned} \Phi &= \sum_{i=0}^{i=N} (S_{Fexp}(i) - S_{Fmodel}(i))^2 \\ N &= \text{number of experimental measures} \end{aligned} \tag{3.7}$$

3.5.2 Release of the Signal

In the microbeam experiments described in Schettino *et al.* (2005, 2003), a single random cell was irradiated in a dish of asynchronous V79 cells; a subsequent increased cell killing was always detected in the rest of the population. As a consequence, it was sensible to assume that any irradiated cell, regardless of the point at which it was in the cell cycle, was capable of producing a bystander signal.

The induction of a bystander effect was also studied after cytoplasmic irradiation; an unexpected increase in the yield of micronuclei was detected in the non-irradiated population (Shao *et al.*,

2004). Because the chance of killing the cell by cytoplasmic irradiation is much less than in the case of irradiation in the nucleus, it was concluded that the signal could be produced by a cell that was not dying of direct hit. In addition, medium transfer experiments showed that the bystander effect appeared already 30 minutes after irradiation (Burdak-Rothkamm *et al.*, 2006; Moore *et al.*, 2006; Morgan, 2003), while the cell may die after only a few hours or days. For these reasons, the fate of the irradiated cells and the production of the bystander signal were considered independent.

There is much less experimental evidence about how cells that have been irradiated can release the signal, and how much they release. The probability of release of the signal by irradiated cells was (Schettino *et al.*, 2005):

$$p(d) = 1 - \exp(-\frac{d}{d_l}) \tag{3.8}$$

$$d \ll d_l, \quad p(d) \approx \frac{d}{d_l}$$

In Equation 3.8, d_l was a parameter that could depend on the cell line and radiation type. The probability of releasing a signal increased with dose and was nearly linear with slope $\frac{1}{d_l}$ at low doses; for d=d_l, the probability is 0.63.

However, this equation would not allow for the increased radio-resistance in some cell lines in the dose domain following the dose domain of HRS. Therefore another equation was tried for describing the release of the BS:

$$p(d) = \exp(-\frac{d}{d_m}) \times (1 - \exp(-\frac{d}{d_l})) \tag{3.9}$$

In Equation 3.9, d_l and d_m were parameters that depended on the cell line and irradiation type. The number of emitting cells increased up to a maximum, and then decreased with increasing dose, while in the first release mode (Equation 3.8), the probability of releasing the signal continuously increased with dose (see Figure 3.9). The term d_m represents the possibility that the cell has been too damaged to produce a bystander signal.

The diffusivity of the signal was not considered in this model; the only criterion that was taken into account was whether a bystander signal had been released or not. It was assumed that there was no space limitation to the bystander effect (Belyakov *et al.*, 2005; Schettino *et al.*, 2005).

Also, no other sources of the signal but the emitters at the time of irradiation were considered in this model.

3.5.3 Life Time of the Signal

Neither the life time of the bystander signal, nor the evolution of its concentration with time in the medium, is known, although in some experiments the bystander effect has been shown to last at least 60 hours (see Section 2.3.3 and Mothersill and Seymour, 1997). Reactive oxygen species (ROS) and nitric oxides (NO) are possibly involved in the bystander signalling, but they are unlikely to be the only elements (see Section 2.3.3). Therefore, it was chosen to describe the decay of the quantity of signal by an exponential decay, which is the simplest model of the evolution of a chemical with time:

$$Q(t) = Q_0 \times \exp(-\frac{t}{\tau}) \tag{3.10}$$

In Equation 3.10, Q_0 is the amount of signal initially present in the dish, and $\frac{\tau}{\ln(2)}$ is the half-life of the signal.

3.5.4 Toxicity of the Bystander Signal

Many endpoints have been used in studies of the bystander effect, including micronuclei formation, gene mutation and genomic instability, transformation, cell proliferation and survival; only survival was included in this model. Two main features of the bystander effect were retained:

- It was shown that the bystander effect saturated for small doses of radiation (from 3 to 5 cGy) (Mothersill and Seymour, 1997, 1998; Prise *et al.*, 1998; Schettino *et al.*, 2005; Shao *et al.*, 2003a);
- It was also shown that a small number of emitters of the bystander signal was enough to trigger a full effect (Schettino *et al.*, 2005; Shao *et al.*, 2004; Zhou *et al.*, 2004).

The following equation was assumed for the response of bystander cells to the signal (see Figure 3.10):

$$\mathrm{D}_B(Q) = \mathrm{D}_{max} \times (1 - \exp(-\frac{Q(t)}{\mathrm{Q}_B})) \tag{3.11}$$

In Equation 3.11, D_B(Q) represented the fraction of cells dying because of the BE when the medium contained the amount c(t) of bystander signal; D_{max} was the maximum fraction of cells that may be killed by bystander effect, and Q_B is the amount of signal at which the fraction of death is 63% of this maximum. The parameters Q_B and D_{max} were assumed to depend on the cell line and radiation type. The response of cells to the bystander signal was assumed to be independent of the dose possibly received.

The additional assumption was made that only cells in G2 phase could be killed by the bystander signal; this was because HRS has been shown to be the strongest in the G2 phase of the cell cycle (Short *et al.*, 2003). The response of cells to the signal was similar to a checkpoint; it was tested only once whether a cell in G2 phase was killed by the BS: if not, it was then considered resistant to it for the rest of the current G2 phase.

To quantify the goodness of fit of the model to the experimental data, and to run the sensitivity analysis, the chi-square value was used, with the following definition (Press *et al.*, 1988, Chapter 14):

$$\chi^2 = \sum_{i=0}^{i=N} \left(\frac{S_{Fexp}(d_i) - S_{Fmodel}(d_i)}{\sigma_i} \right)^2 \tag{3.12}$$

N : Number of experimental measures

σ_i : experimental standard error on measurement i

3.5.5 Implementation of Radiation Effects

The irradiation of the dish took place once at the beginning of the simulation, just after the cells were seeded, i.e. the 2-D list was created. The user chose the number n_{irrad} of cells that were to be irradiated; the n_{irrad} first cells generated by the program (which were positioned randomly in the dish) were considered irradiated and their probability of survival $\mathrm{S}_F(d)$ was calculated according to Equation 3.6: a random number γ was computed in the interval [0, 1]:

- If $\gamma < S_F(d)$, the cell survived;
- Else, it died.

The was computed only at the time of irradiation but not at any subsequent time. Cells with the same abscissa on the dish were stored in the same lists (see Section 3.4), and lists stored in *population* are irradiated subsequently, therefore biological cells were irradiated in lines on the dish. However, in the experimental situations, cells are also being irradiated in subsequent lines on the dish (Schettino *et al.*, 2003).

To compute the production of bystander signal, a random number between 0 and 1 was also generated and compared to the result of Equation 3.8 or Equation 3.9. In the absence of any experimental data on the quantity of signal a single cell could release, this was arbitrarily set to 1, and the total amount of signal (Q_0, see Equation 3.10) was equated to the number of emitting cells. This means that there was no variation in the quantity of signal emitted by individuals, but the initial quantity of signal in the dish could change. At each time step, the new amount of signal was calculated according to Equation 3.10.

After the irradiation took place, the program was run for a number of time steps that depended on the cell cycle length of the cell line studied, and corresponded to the incubation period used in biological experiments (see Section 2.2). The proportion of G2 cells being killed by the signal, $D_B(Q)$ was calculated according to Equation 3.11. When the signal was emitted, or when cells entered in G2 phase and the signal was present in the medium, a random number γ was generated in the interval $[0, 1]$ and compared to the result of the Equation 3.11:

- If $\gamma < D_B(Q)$, the cell died;
- If $\gamma > D_B(Q)$, the cell remained alive and was not to be killed by the signal until at least the next G2 phase. A Boolean BS_resis was set to 1 to indicate that the cell had passed the checkpoint; BS_resis was reset to 0 at division for daughter cells.

At the end of the simulation, the number of cells in the colonies was counted and when there were more than 50 cells, colonies were considered viable. The plating efficiency was defined as the ratio of the number of viable colonies over the number of seeded cells:

$$P_E = \frac{N_{colonies}}{N_{seeded}}$$

$N_{colonies}$ and N_{seeded} are the number of colonies containing more than 50 cells and the number of cells initially seeded, respectively. The survival fraction was calculated as the ratio on the plating efficiency of irradiated dish PE_d over the plating efficiency in the control dish PE_c

$$S_F = \frac{P_{Ed}}{P_{Ec}}$$

3.6 Concluding Comments

This chapter described the model that was written during this project. Cells were assumed to be seeded in a dish containing medium with nutrients in excess; cells cycled and divided in the dish to form colonies. The cell cycle included the four phases: G1, S, G2 and M phases. Only one checkpoint was included at the G1/S transition, but this was driven by nutrients, and was actually not necessary since the amount of nutrients was assumed to remain constant throughout the simulations. At division, cells could push neighbours in random directions, in order to make space for new-born cells. The nutrient distribution and the growth of cell colonies were modelled by two parallel cellular automata.

Cells that were directly irradiated had a probability of surviving that was calculated by the linear quadratic equation; the radiosensitivity depended on both the cell line and the position in the cell cycle at the time of radiation. In addition, it was assumed that irradiated cells could release a bystander signal. Two modes of signal production were proposed: in the first mode, the probability of emitting a signal decreased at high doses, contrary to the second mode. Only primary sources of the signal were considered, i.e. only cells irradiated could release the signal and no subsequent source was assumed; the amount of signal was also assumed to decrease with time, with a first order kinetics. Neighbouring cells, as well as progeny of cells were assumed to be sensitive to the signal when they reached the G2 phase; the sensitivity to the signal increased with the amount of signal present in the medium.

The model was applied to the simulation of the survival of two cell lines, the hamster cell line V79 and the human brain tumour cell line T98G. In the next chapter, the values of the param-

eters specific to those cell lines are determined, and the results of the simulation presented. A sensitivity analysis of the model is also presented in detail.

Chapter 4

Applications of the Theory

Within the studies reviewed in Chapter 2, fibroblasts, carcinoma and glioma cell lines are the most widely studied human cell lines for either their BE and HRS characteristics (see Table 2.1). Carcinoma and glioma cell lines have been mostly studied for their HRS properties and fibroblasts for their BE properties. The glioma cell line T98G has been studied both for the HRS and the BE, using two different protocols (Mothersill *et al.*, 2002; Shao *et al.*, 2003a), and the variability of HRS with cell cycle position has also been measured for this cell line (Short *et al.*, 2003). The hamster lung fibroblast cell line V79 has also been extensively characterised for both its HRS and its BE; moreover, it is the only cell line on which single cell experiments have been carried out (i.e., only one cell is irradiated within the population: Schettino *et al.*, 2005), and for which an equation for the probability of emitting the bystander signal has been proposed. In addition, the data for those two cell lines were available from the Gray Cancer Institute, University of Oxford.

In this chapter, the application of the model to first the V79 cell line, and then the T98G cell line is presented. The response of synchronised populations as well as asynchronous populations is studied. The third section presents the sensitivity analysis of the model in the particular case of V79 cells. A complement to the results on the V79 cell line can be found in Appendix B and Appendix C, in which the response of the cell line to C_K X-rays and 3.2 MeV protons is also described.

4.1 Study of the Hamster Lung Cell V79

This section describes the results of simulations of the response of V79; two models of the bystander signal were used (see Section 3.5). The values of the parameters of the model particular to the cell line are given in the section, but the full explanation of the model is in Chapter 3. Simulations were compared to experimental data from the Gray Cancer Institute (M. Woodcock, personal communication).

4.1.1 Cell Cycle of the V79 Hamster Cell Line

The phase data (average length of each phase) and the average distribution of cells around the cell cycle in asynchronous population were determined from a personal communication, M. Woodcock. In asynchronous populations, the distribution of cells is on average as follows:

- 59% of cells in G1 (G1: 30 minutes)
- 17% of cells in S (S: 300 minutes)
- 24% of cells in G2/M (G2: 90 minutes and M: 60 minutes)

Therefore, when the model was applied to asynchronous populations, seeded cells were distributed in the cell cycle according to those proportions; within each phase, the age of cells was uniformly distributed.

There were three remaining parameters, i.e. S_{max}, the length of G1b for the G1/S checkpoint, and the proliferation factor. It was attempted to determine them by fitting them, using the size distribution of colonies of V79 after 3 days culture (Schettino *et al.*, 2001). However, no good fit could be obtained, and it was decided to take the value of $S_{max} = 18 \times 10^{-4}$ nmol/cell and length of G1b=600 minutes for mouse cells from Faraday *et al.* (2001). This meant that the probability that cells entered the S phase increased up to $p_{max} = 0.49$, which happened at $t_{max} = 355$ minutes after the start of G1b (see Figure 4.1 and Equation 3.2). After t_{max}, the probability decreased and for times greater than 356 minutes, the result of Equation 3.2 was negative and cells still in G1 had no probability to jump to S. Because the rate of consumption

of glucose was assumed constant, decreasing S_{max} decreased the maximum time cells surviving the G1/S checkpoint could spend in G1b (see Section 3.4, Equation 3.2 and Figure 4.1).

The proliferation factor was fixed to 1.7; this gave an average plating efficiency of 0.85, which was consistent with experimental data (personal communication from M. Woodcock and G. Schettino).

The size distribution of colonies in these conditions is shown on Figure 4.2. A high proportion of colonies have less than 5 cells; this is a major difference with the experimental distribution of colony size (Schettino *et al.*, 2001). It is due to the fact that at start of the simulation, cells are given a random age between 0 and the maximum phase length. Therefore, cells in G1b that are older than 356 minutes at the start of simulation all die. In reality, the length of G1b should have been set to 356 minutes, or cells originally seeded in G1a phase only. This simplification in the program causes a low plating efficiency for asynchronous and G1 synchronised populations. However, for colony sizes between 15 and 55 cells, the simulations and the experimental data are similar; for higher colony sizes, the experimental proportion of colonies is significantly higher than the simulations: this is probably due to the high number of colonies of less than 5 cells predicted by the simulations that decreases the overall number of colonies of more than 50 cells.

It is to be noted that the biological parameters clearly represent a weakness of the model, as they are parameters difficult to obtain experimentally, especially the parameters for consumption of nutrient and the parameters of the G1/S checkpoint. Therefore, it is important to determine the sensitivity of the model to those parameters (see Section 4.3). However in the situations studied, the nutrients are in excess and no cell dies of starvation at the G1/S checkpoint; in fact, only cells in the G1b phase at the start of the simulation may die in G1b, because the probability for cells in G1b to start the S phase is 1. Secondly, the plating efficiency of cells would be equally affected at any dose of irradiation by a change of proliferation factor or G1/S checkpoint parameters and little difference would be expected in the value of the survival fraction. The time spent in G1b phase may have an influence, though, as it modifies the length of a phase in which cells are not sensitive to the bystander signal.

4.1.2 Irradiation

All cells seeded in the dish were irradiated with increasing doses of 250 kVp X-rays, between 0 and 5 Gy. The LQ equations used for the response to a direct hit were (see Figures 4.4 to 4.7 and Table 4.3, see Section 3.5 for the definition of Φ):

$$\begin{aligned} S_{FG1} &= \exp(-0.301d + 0.004d^2) \text{ with least squares of } \Phi = 1.32 \times 10^{-2} \\ S_{FS} &= \exp(-0.097d - 0.036d^2) \text{ with least squares of } \Phi = 1.05 \times 10^{-3} \\ S_{FG2/M} &= \exp(-0.102d - 0.052d^2) \text{ with least squares of } \Phi = 6.25 \times 10^{-3} \end{aligned} \tag{4.1}$$

The parameter β was not well determined in case of the G1 population, as the search for the minimum Φ gave a negative value for the parameter, which is non-probable.

All parameters concerning the bystander signal (life time, emission, killing properties) were fitted (see Table 4.4). A bystander signal was emitted by the irradiated cells with a probability given either by the Equation 3.9, with the parameters d_m and d_l having the values 1 and 0.12 respectively (Model 1 on Table 4.4 and on Figure 4.3):

$$p(d) = \exp(-d) \times (1 - \exp(-\frac{d}{0.12})) \tag{4.2}$$

Or by the Equation 3.8, with $d_l = 0.2$ (Model 2 on Table 4.4 and on Figure 4.3):

$$p(d) = (1 - \exp(-\frac{d}{0.2})) \tag{4.3}$$

In Model 1, the decay in the amount of signal after it has been released was modelled by: (Model 1, Table 4.4 and Figure 4.3):

$$Q(t) = \mathrm{Q_0} \times \exp(-\frac{t \times \ln(2)}{30}) \tag{4.4}$$

This means that at time t=30 minutes, the quantity of signal in the medium is half the quantity at the time of irradiation. In Model 2, the half life of the signal was more than 10 times smaller (Model 2, Table 4.4 and Figure 4.3):

$$Q(t) = \mathrm{Q_0} \times \exp(-\frac{t \times \ln(2)}{0.25}) \tag{4.5}$$

The proportion of cells in G2 phase killed by the bystander signal was calculated by the Equation 3.11, and the parameters Q_B and D_{max} were either set to 6000 units and to 1 unit respectively (Model 1, Table 4.4 and Figure 4.3):

$$D_B(Q) = 1 - \exp(-\frac{Q}{6000}) \tag{4.6}$$

In Model 2, the parameters were set to Q_B=1 and D_{max}=0.1 (Model 2, Table 4.4 and Figure 4.3):

$$D_B(Q) = 0.1 \times (1 - \exp(-\frac{Q}{1})) \tag{4.7}$$

After irradiation, the program was run for 4320 iterations = 3 days (Schettino *et al.*, 2001). At the end of the simulation, the number of cells in each colony was counted and surviving colonies were the ones of at least 50 cells (see Section 2.2 and Section 3.5).

4.1.3 Survival Curves

Survival curves for the LQ model and the 2 cellular automaton models were produced and compared with experimental data (Figures 4.4 to 4.7). The response of populations of cells synchronised in G1, S or G2, as well as the response of asynchronous populations was simulated. The parameters of the model were chosen in order to get a good fit to all data sets. The goodness of fit was quantified by the χ^2 and the Φ values, whose definitions are given in Section 3.5.

4.1.3.1 The LQ model

Table 4.3 gives a summary of the parameters of the LQ equations for the V79 cell line. The values of the parameters, α and β, are different for the different populations, which is in agreement with the observation that the radiosensitivity varies throughout the cell cycle. Furthermore, α is highest for the G1 population, indicating that G1 cells are the most sensitive to single hit events, while β is highest for the G2 population, indicating that G2 cells are the most sensitive to multiple hits events.

When only data at high doses are considered, the χ^2 values are of the same order for all synchronised populations (see Table 4.5). The χ^2 is highest for the S population, but this is probably

due to the experimental standard errors that are the smallest for this data set, which increases the value of χ^2 (see Equation 3.12). This does not mean that the model gives values greatly different from the experimental data, and actually the sum of errors squared is smaller for the S population than for the G1 and G2 populations (see Table 4.3). The smallest χ^2 and Φ are obtained with the asynchronous population. These results further support the LQ equation as an accurate model of the high dose survival.

When the entire data range is taken into account, the values of χ^2 increase (see Table 4.5), with the highest value for the S population (χ^2=30.4, about 7.5 times the value of low dose fit). Again, this may be due in part to the small experimental standard errors; this is also probably due to the fact that the survival fractions for doses lower than 0.5 Gy are all 1 (i.e. no cell killing is detected). This constant response at doses below 0.5 Gy is not predicted by the LQ equation, and should be better reproduced by a multi-target model (see Equation 2.5). The χ^2 for the asynchronous population increases highly (χ^2 =15.1, about 750 times the value for the low dose fit). This suggests that although the LQ model can reproduce the high dose data, it is inadequate for reproducing the low dose data. The LQ model clearly overestimates the survival of asynchronous populations to doses below 0.5 Gy (see Figure 4.7). No such clear conclusions can be drawn for the G1 and G2 populations. The χ^2 values are increased but the tendency of the low dose survival is not obvious, and the experimental standard errors are high (see Figures 4.4 and 4.6).

4.1.3.2 Model 1

A series of 4 independent simulations were run and the χ^2 values were calculated. The average value of χ^2 is shown in Table 4.5. The value of χ^2 obtained for the fit to the G1 population is higher than with the LQ model, but not significantly; this is because the model is such that there is little influence of the bystander effect when cells are irradiated in the G1 phase, since cells emit the signal but are not sensitive to it before reaching G2 phase. The χ^2 for the S population is more than doubled, because of the slight hyper-radiosensitivity predicted at doses below 0.5 Gy, due to cells in the late S phase, which enter the G2 phase soon after irradiation. For the G2 population, the value of χ^2 is nearly 10 times higher than the value for the LQ model: the simulated curve shows a hyper-radiosensitivity at low doses, but not the experimental data,

although some points lie below the LQ curve. On the contrary, the χ^2 for the asynchronous population is less than half the value of χ^2 for the LQ model and the model can reproduce the HRS shape at low doses described by the experimental data (see Table 4.5 and Figure 4.7). It could be argued that since the cellular automaton models have many more parameters than the LQ equations, the values of χ^2 should be smaller. However, it must be remembered that while the minimum sum of errors squared has been searched for the LQ equations, it has not been done for the cellular automaton models. This study is a first indication of the trend of the model.

What might be a problem here is that the model generates initially pure synchronised populations, while the experimental populations obtained are enriched in cells belonging to one particular phase, but are not perfectly synchronised (Marples and Joiner, 1993; Short *et al.*, 2003). To test how much the composition of the population influenced the bystander effect at low doses, enriched populations were generated, according to the measurements of Marples and Joiner (1993):

- G1-enriched population: 90% of G1 cells, 9% of S cells and 1% of G2/M cells
- S-enriched population: 17% of G1 cells, 71% of S cells and 12% of G2/M cells
- G2-enriched population: 5% of G1 cells, 5% of S cells and 90% of G2/M cells

There were no data for the composition of a G2-enriched population; a composition inverse to the one of a G1-enriched population was generated (i.e. there were as many G2 cells in the G2-enriched population as G1 cells in the G1 enriched population), on the basis that G1 and G2 cells are fairly easy to distinguish according to their DNA content and S cells are the most problematic cells (Short *et al.*, 2003). The χ^2 values calculated on the low dose domain ($d < 1$ Gy) were compared; at higher doses, the LQ equations used should be fitted to the experimental measures and therefore already account for any variation in the composition of the populations. The χ^2 of the G1 enriched and G2 enriched populations are not significantly different from the synchronised populations ($2.15 \pm 65\%$ versus $1.44 \pm 46\%$ for the G1 cells and $16.09 \pm 19\%$ versus $23.95 \pm 31\%$ for the G2 cells). However, the χ^2 value of the S enriched population is much higher than the value for the S synchronised population ($83.00 \pm 15\%$ versus $64.76 \pm 11\%$). This may be due to the presence of G1 and G2 cells that are more sensitive to radiation

than S cells, and therefore decreases the survival to direct irradiation; in addition, the presence of G2 cells at the time of radiation increases the sensitivity to the bystander signal.

4.1.3.3 Model 2

The second model was adapted from the assumptions made by Schettino *et al.* (2005) on the mechanisms of the bystander effect. The χ^2 values for the G1 and asynchronous populations are not significantly different from the ones obtained with Model 1 (see Table 4.5). The χ^2 is much smaller for the S and G2 populations (about half of the value for Model 1). This is because the life time of the bystander signal is much shorter and as a consequence, its action is much reduced. This model gives a better fit to the experimental data than Model 1, but the life time of the signal does not agree with the experimental suggestions that it is of the order of an hour (Kevin Prise, private communication).

In conclusion, with the parameters chosen here, Model 2 better reproduces the experimental data than Model 1. It should be stressed that the response of synchronised populations is best simulated by the LQ equation, whereas the cellular automaton models give the best fit to the response of the asynchronous population. This suggests that for this cell line, HRS is only seen in the asynchronous population, or that it is very small in synchronised populations. It could either be that HRS is the result of interactions between cells in different phases of the cell cycle, or that cells have a different response (direct or indirect) to radiation when they have been synchronised or when they are asynchronous. It was originally proposed that only cells irradiated in a certain phase (G1 or S) could release the bystander effect and cells in G2 phase could be killed. However, the bystander effect is always seen when a single cell is randomly irradiated in a dish of V79, which supports the idea that any cell can release the bystander signal, regardless its phase (Schettino *et al.*, 2005). A series of experiments also supports the idea that the bystander effect saturates at higher doses, but does not disappear (see Chapter 2). Model 2 agrees with this assumption, while Model 1 does not (see Equation 3.8), since it assumes that the release of the signal decreases at high doses. However, the life time of the signal in Model 2 has to decrease significantly, otherwise the predicted sensitivity of G2 cells is much higher than the one measured. It could also be that the bystander effect is less strong in G2 phase, but is seen in other phases as well; for instance, G1 cells could be sensitive to the bystander

signal (G. Schettino, personal communication). It may otherwise be, of course, that the fundamental assumption of the model that BE and HRS are two manifestations of one mechanism, is wrong. These may be two unrelated phenomena, in spite of a few similarities. Nevertheless, the question remains to be answered of how data on synchronised and asynchronous data could be considered consistent.

4.2 Study of a Human Glioblastoma

The response of a human glioblastoma (T98G) to 250 kVp X-rays was then simulated. T98G is a tumour cell line, which has been widely studied for both its very marked hyper-radiosensitivity (Short *et al.*, 1999a, 2005, 1999b), and its bystander response (Shao *et al.*, 2005, 2003a, 2004). It is also one of the two cell lines for which the variability of HRS with cell cycle phase has been demonstrated (Short *et al.*, 2003).

Simulations were compared to experimental data from the Gray Cancer Institute (Short *et al.*, 2003, and personal communication, M. Woodcock).

4.2.1 Cell Cycle of the T98G Cell Line

The lengths of the different phases of the cell cycle were taken from Short *et al.* (2003) and the distribution in the phases for asynchronous populations were the estimation of M. Woodcock (personal communication):

- 75% of G1 cells (G1: 320 minutes)
- 17% of S cells (S: 768 minutes)
- 8% of G2/M cells (G2: 132 minutes and M: 60 minutes)

The same values as for V79 cells were taken for the proliferation factor, the length of G1b and S_{max}. This is a crude approximation, however no experimental values were found for fitting these parameters (see Table 4.2). The average colony size distribution of the T98G cell line is similar to the one of the V79 cell line, with a high number of colonies with less than 5 cells, but the maximum is for slightly bigger colonies (Figure 4.2).

4.2.2 Irradiation

The same doses of irradiation were studied, and the best LQ fit to survival data for doses above 1 Gy, obtained by least squares maximum likelihood estimation, were (see Table 4.3):

$$S_{FG1} = \exp(-0.041d - 0.036d^2) \text{ with least squares of } \Phi = 6.75 \times 10^{-3}$$
$$S_{FS} = \exp(-0.056d - 0.040d^2) \text{ with least squares of } \Phi = 7.47 \times 10^{-3}$$
$$S_{FG2} = \exp(-0.261d + 0.010d^2) \text{ with least squares of } \Phi = 2.44 \times 10^{-3}$$

The parameter β for the G2 population is very small negative, which shows that it is not been well determined.

In the case of T98G, only one model was simulated. This was because there was a strong increased radio-resistance in G2 populations (Short *et al.*, 2003), and some simulations run with Model 2 as defined in Section 4.1 showed that it could not reproduce the IRR. The probability of release of the bystander signal was computed by Equation 3.9, with $d_l = 0.25$ and $d_m = 0.31$:

$$p(d) = \exp(-\frac{d}{0.31}) \times (1 - \exp(-\frac{d}{0.25})) \tag{4.8}$$

The life time of the signal τ was fitted to be $\frac{150}{\ln(2)}$ (Equation 3.10):

$$Q(t) = \mathrm{Q}_0 \times \exp(-\frac{t \times \ln(2)}{150}) \tag{4.9}$$

Cells in G2 phase were being killed by the bystander signal with a probability of (Equation 3.11):

$$\mathrm{D}_B(Q) = 1 - \exp(-\frac{Q}{1000}) \tag{4.10}$$

Although the emission of the signal by T98G cells was confined to a window of doses narrower than the emission by V79 cells, the life time of the signal was longer for T98G and the maximum proportion of G2 cells killed by the signal was higher. These differences accounted for the strong HRS that is seen in G2 synchronised T98G, while the HRS in G2 synchronised V79 cells is not evident. The life time of the signal was chosen in agreement with the ICCM experiments, showing that the signal is still effective after 24 to 48 hours after irradiation (Suzuki *et al.*, 2004). In the case of V79, the life time of the signal had to be decreased since otherwise the radiosensitivity would be much more than experimentally measured.

The cell cycle of T98G is much longer than the cell cycle of V79 (23 hours against 8 hours on average); therefore T98G cells are cultivated for a longer period. The program was run for 11520 time iterations = 8 days before colonies were counted (Short *et al.*, 1999b).

4.2.3 Survival Curves

The fit of the models to the experimental data was measured by the sum of errors squared Φ and the chi-square value χ^2 (see Equations 3.7 and 3.12).

The parameter α of the LQ equation is the highest for the G2 population, suggesting that G2 cells are the most sensitive to single hit events. Furthermore, the ratio $\frac{\alpha}{\beta}$ is also the biggest for the G2 population (-26), while in comparison, this ratio is close to 1 for the G1 and S populations (respectively 1.1 and 1.4). This would mean that in the G1 and S populations, single and multiple hit events make similar contributions to the biological effect of radiation, contrary to G2 cells, for which the single hit events are predominant (see Table 4.3).

The χ^2 for the fit of the LQ model to the high dose data are of the same order (10^{-1}, see Table 4.6) for all the populations, and are the smallest values within all models. This confirms again that the LQ model is an appropriate model of the high dose response. The fit is the best for the G2 cells ($\chi^2 = 6.0 \times 10^{-1}$).

When the low dose data is taken into account in the calculation of the χ^2 of the LQ model, those increase significantly (2 times for the asynchronous population, 18 times, 3 times and 15 times for the G1, S and G2 populations respectively). The fit to the G1 cells becomes the worse fit ($\chi^2 = 12.7$, see Table 4.6). Compared to the V79 cell line, the fit to the G1 and G2 synchronised populations is worst (the χ^2 is about 6 times higher than for the V79 cell line), whereas the χ^2 values are smaller for the S synchronised and asynchronous populations (about 10 times less than for the V79 cell line). In this latter case, the difference can be explained by the bigger experimental standard error in the experimental data for T98G than in the experimental data for V79.

Compared to the linear quadratic equation, the cellular automaton model (Model CA) can reproduce the experimental data of the G1 and G2 populations slightly better, but the χ^2 is increased in case of the S population. This is because Model CA predicts some HRS at low doses in the S

population, which is not detected in the experimental data (see Figure 4.10). On the contrary, in the G1 population, Model CA actually predicts no HRS at all, while some experimental points for doses below 0.5 Gy lie below the linear quadratic curve. Looking at the experimental data, it could be argued that G1 T98G cells are hypersensitive (Figure 4.9). For the G2 population, the strong HRS is well reproduced by Model CA, but at 0.3 Gy, the measured sensitivity is very close to the value of the linear quadratic model, whereas the sensitivity simulated at 0.3 Gy is much higher (Figure 4.11). For the asynchronous population, there are fewer experimental data points at low doses; they all lie below the LQ curve, but the experimental standard errors are big, and the differences between the LQ values and the experimental values are not significant. The χ^2 obtained with Model CA is slightly bigger than the one obtained with the LQ model.

Compared to Model 1 in the case of the V79 cell line, the χ^2 values for Model CA are smaller for the asynchronous S and G2 populations, but bigger for the G1 population.

4.3 Sensitivity Analysis

The sensitivity of the model to the different parameters was studied in the case of the V79 cells. To this purpose, chosen parameters were varied by + and - 5% and the χ^2 values were calculated and compared (see Equation 3.12).

4.3.1 Standard Deviation in the Model

The variability in the results of the simulations was checked on Model 1, by running a series of 5 simulations for each dose point, for the 4 types of populations. This tests whether the model in robust.

The standard deviations on the model are shown on Figures 4.13 to 4.16. For all data points and all populations, the standard deviation was never more than 7.4%. Therefore, the differences arising between simulations are very small and in every case much smaller than the experimental standard deviation.

4.3.2 Sensitivity Analysis of Model 1

The sensitivity of the model to its parameters was studied for the case of an asynchronous population. At the start of each simulation, the sequence of random numbers generated throughout the program was seeded with the same seed, so that the sensitivity to a single parameter was clearly seen. The parameters studied were varied by + and - 5% of their values. The χ^2 values for the modified models were compared to the χ^2 values on Model 1. The following parameters were tested: Q_B, τ, d_l and d_m, and the values α and β of the LQ equations. The sensitivity of the model to the length of the phases and the parameter S_{max} was also studied. A summary of all the χ^2 values can be found on the Table 4.7. The parameters LX and LY related to the size of the dish and the parameter m related to the maximum number of cells on the dish (see Table 4.1) were not investigated because the focus was made on the parameters related to the radiosensitivity, which would not be influenced by those parameters. When the initial amount of nutrient was changed of 5%, the predicted survival fraction did not change.

Model 1 is most sensitive to the parameters related to the cell cycle: the value of S_{max}, and the length of the G1, G2 and M phases. This is because the effect of the bystander signal depends on the cell cycle distribution of the population, since it kills cells in G2 phase only. Changing the length of the different phases changes the time during which cells are or not sensitive to the signal. Model 1 is almost completely insensitive to the length of the S phase, though. Cells in S phase play a role as emitters of the signal if there are irradiated, and as they cycle towards G2 phase, they become sensitive to the signal; therefore, they contribute to both the production of the signal and its overall toxicity.

From Table 4.7 it can also be seen that some parameters have a non-linear effect. τ is the most non-linear parameter, with the length of the M phase, S_{max} and the parameter β for the LQ equation in phase G2. Overall, Model 1 is not very sensitive to the parameters of the LQ equations. It is also more sensitive to the parameters of the response to the bystander signal and its life time (Q_B and τ) than to the parameters of its emission (d_l and d_m). What matters is how long the signal is present in the medium and how many cells can be killed by the signal, and the way it is produced matters less.

To check whether setting the length of G1b to $tmax$ makes any difference, the χ^2 was calculated after fixing the length of G1b to 357 minutes. It is surprising to observe that the fit is improved;

in fact, when G1b=357 minutes, the surviving fraction of the population decreases. The reason may be that lowering G1b increases the number of cells surviving initially the G1/S checkpoints; therefore, while the plating efficiency is increased in control dishes, more cells may release the BS and more cells may be killed by bystander effect in irradiated dishes. First, the parameter Q_0 in Equation 4.4 increases, and the signal remains present in the medium for longer. Second, the concentration, c(t), of signal increases and the number of cells killed by bystander effect as predicted by Equation 4.6 increases. Moreover, Model 1 is also sensitive to changes in the rate of consumption, which affects the probability of passing the G1/S checkpoint (increasing or decreasing the rate of 5% results in a change in χ^2 of 2 and 16% respectively). Similarly, some simulations were run to test the sensitivity of the model to the initial number of cells and to the proliferation factor. Increasing or decreasing the initial number of cells of 5% led to a change in χ^2 of 24 or 4% respectively; a 5% increase or decrease in the proliferation factor led to a change in χ^2 of 35 or 9% respectively. The reasons for this sensitivity are probably the same than the sensitivity to the length of G1b.

4.3.3 Sensitivity Analysis of Model 2

For Model 2, the sensitivity to 3 further parameters was tested: Q_B, τ and d_l. The model shows no sensitivity to the parameter d_l; this is because Equation 4.7 predicts no difference in the response of bystander cells whether 1 or more cells release a signal (see Figure 4.3). Since 2000 cells are irradiated, there will be always at least 1 cell emitting the signal, and the bystander effect will be always triggered. A decrease of 5% in Q_B leads to a change of 24% in the value of the χ^2 and an increase of 5% in τ a change of 2% in the value of χ^2.

For the parameters of the bystander effect to be significant in the dose range [0,0.2] Gy, the response of cells to the signal must be dependent on the concentration of signal at least at low concentration, and the half life of the signal must be greater than $\frac{0.25}{\ln(2)}$. Otherwise, there is no dose dependency of the bystander effect at low or high doses and the signal disappears too quickly. However, in case the life time of the signal is increased, since the probability of both emitting and responding to the signal saturates quickly, the bystander effect contributes significantly to the death of G2 cells, at least at low doses. Therefore, the direct effect must be smaller than the one predicted by the LQ model used at low doses. A possibility would be to

use the multi-target model instead, which predicts a very low response to direct irradiation at low doses (see Section 2.2 and Appendix C).

It must be pointed out that this statistical analysis is only an indication of which parameters are sensitive in the two models. No search for minimum χ^2 has been made. Surprisingly, Model 1 is more sensitive to the parameters related to the cell cycle, and less sensitive to the parameters related to the bystander effect. Under the conditions presented here, Model 2 shows little sensitivity to its BE parameters and this is because the response to the BS is independent of the signal concentration, and therefore of dose, and because the life time of the signal is too short; this is the reason why the sensitivity to other parameters (phase durations and parameters of the LQ equation) was not investigated. This does not mean that Model 2 is invalid, but it needs more investigation to determine the parameters.

4.4 Concluding Comments

The model has been used to simulate the response of two cell lines, V79 and T98G, to 250 kVp X-rays. The direct effects of radiation hits were modelled by a linear quadratic equation which depended on the cell cycle position of the irradiated cell; those cells released a signal that affected cells in the G2 phase of the cell cycle.

Two different sets of assumptions on the production and response to the bystander signal were used to simulate the response of synchronised and asynchronous V79 cells. The sensitivity analysis revealed that the durations of the cell cycle phase are critical parameters to be determined with care, as well as the parameters describing the response to the signal and its life time, more than the parameters describing the production of signal.

One set of assumptions was used to model to response of synchronised and asynchronous T98G cells to radiation. The life time of the signal emitted by T98G cells was longer than the life time of the signal by V79 cells, and the toxicity higher. Even though the model does not simulate the high dose data (dose $>$ 1 Gy) better than the LQ equation, it reproduces more faithfully the low dose data.

The next chapter discusses in detail the different aspects of the results from the models.

Chapter 5

Discussion

The preceding chapters describe a computer program that has been written to simulate the irradiation of cells in culture dishes and their response to different doses, measured in terms of clonogenic properties. It has been used to test the idea that the bystander effect (BE) could be responsible for the hyper-radiosensitivity at low doses seen in some cell lines. The program was run for two particular cell lines, V79 and T98G, widely studied for their BE and HRS properties.

Such a program is a good complement to the *in vitro* study of non-targeted effects; it offers new perspectives that are not possible in the laboratory. It allows for the confirmation or refutation of assumptions drawn from the different experiments reported so far; in this study, the focus has been on the bystander effect and low dose hyper-radiosensitivity. This chapter will discuss the capabilities of the model, as well as the results obtained in this project.

5.1 A Novel Approach to the Study of Non-Targeted Effects

5.1.1 Review of the Assumptions

At the start of the simulations, a known number of cells are seeded in a dish and irradiated with a given dose of 250 kVp X-rays; the effect is observed on the treated dish, as compared to the control dish that did not receive any radiation. When the program was written, and as it is described in Chapters 3 and 4, it includes a number of parameters to describe the nutrient diffusion that were of no use in the main conditions in which the program was run.

An attempt has been made to describe the consumption of nutrients by cells. For this, 3 parameters are needed: K, K_S and the concentration C(t) of nutrients in the dish, at the place where the cell is located and at the time the cell consumes (see Equation 3.1). However, at least K and K_S are difficult to determine and cannot be found easily in the literature. In this study, the parameters have been approximated by the parameters for a rat glioblastoma for the V79 cell line and by the parameters for a human fibroblast for T98G; the distribution of nutrients was assumed uniform and the rate of consumption was assumed constant. The latter assumption is valid for V79 since the value of K_S is much lower than the initial amount of nutrients Czero (see Section 3.3); therefore a change in Czero does not lead to a big change in the rate of consumption. This assumption should be revisited for T98G cells, because the value of K_S is much bigger than Czero; consequently even a small change in Czero may lead to a significant change in the rate of consumption. Since the anaerobic or starvation situation is not explored here, it may be reasonable not to model the consumption of nutrients by cells.

The proportion of cells in each phase of the cell cycle at the start of simulation in case of an asynchronous population is fixed to the estimations of M. Woodcock (personnal communication) by flow cytometry. Yet, it is likely that all asynchronous populations do not have exactly the same composition; therefore, it would be better to set those proportions as average values, and to add some variations amongst different populations.

In addition, the model of the cell cycle is such that only the length of the G1 phase varies for the different individuals; for other phases, the same phase is always the same length. It is known, though, that there are checkpoints throughout the S phase and between the S and the G2 phases as well (see Section 2.1) and that there are changes to phase length induced by radiation damage; as a consequence, cells will spend more or less time in these phases as well, depending on their individual characteristics. Again, the length of the different phases could be used as average values of phase length. The checkpoint at the G1/S transition could also be simplified in a similar way. The equation used here has been taken from Faraday *et al.* (2001), who studied the batch and continuous cultivation and analyzed the glucose consumption (see Equation 3.2). Because here, the nutrients are not an issue, such a model is not required. Moreover, the checkpoint model uses 2 parameters that have been determined only for the cell line of interest in Faraday *et al.* (2001), Smax and length of G1b, which forces avoidable approximations to be made.

The proliferation factor has been chosen equal to 1.7. This accounts for any reason why even non-treated dishes *in vitro* do not give a plating efficiency of 1. This value could probably be determined with more accuracy by collecting the experimental plating efficiencies of a series of control dishes.

5.1.2 Possibilities of the Model

To our knowledge, this model is unique at the time of writing. Most models of the bystander effect and low dose hyper-radiosensitivity described in Section 2.3.2 and Section 2.3.3 are only equations fitted to the average experimental data on populations of cells (Brenner *et al.*, 2001; Marples *et al.*, 2003; Nikjoo and Khvostunov, 2003; Wouters *et al.*, 1996). The novelty here is that the behaviour of the entire population is built from the behaviour of individuals. This is of importance, though, since at least some non-targeted effects are believed to be the consequence of interactions between individuals; it is therefore essential to go further than the study of the average effects of radiation to understand the non-targeted effects.

Furthermore, contrary to laboratory experiments, the program is not dependent on the material resources such as biological cell line, radiation type or radiation instrument (broad or focused beam) that is available. Any type of radiation treatment can be tried on any cell line, as long as the radiation process and the cell cycle parameters of the cell line are known.

The program has been applied to measure the survival fraction of cells. However, it could easily be modified so that it models other endpoints. Some equations for the mutation frequency are introduced in Brenner *et al.* (2001); Nikjoo and Khvostunov (2003), or for the micronuclei formation (Shao *et al.*, 2003a), that could be included in the model to calulate other endpoints.

As explained in Section 2.3.3, the study of the bystander effect has led to contradictory conclusions, because experimental situations are never exactly identical. This limitation is avoided by the program, for which the conditions are known and set. Therefore, the model may help clarify some uncertainties that could not be solved so far, such as the dose dependency of the bystander effect, the dependency on radiation LET, or the intensity of the bystander effect with varying numbers of irradiated cells. Also, the bystander effect has been widely studied after microbeam irradiation with ions or soft X-rays, or after γ-rays irradiated cells medium transfer,

but only a few studies have been found on the bystander effect after conventional X-rays ICCM exposure, of the type used in radiotherapy (Fournier *et al.*, 2007; Huang *et al.*, 2007; Moore *et al.*, 2006; Yang *et al.*, 2005). As a consequence, the question remains of the significance of the bystander effect in a population of cells that has been directly irradiated, partly or in totality, with radiotherapeutic X-rays, although some groups have assumed that there is no bystander effect after broadbeam irradiation (Brenner *et al.*, 2001).

5.2 A Study of the Bystander Effect

One of the aims of the project was to gain deeper insight into the mechanisms underlying the bystander effect. Some assumptions in the model are made, based on some of the results of the radiobiological experiments and will be reviewed in this section.

5.2.1 Emission of the Bystander Signal

The idea that the bystander effect is due to a signal, either released in the medium or transmitted via cell to cell communication channels, is widespread (Little, 2006; Mothersill and Seymour, 2001). This idea has also been adopted in the model. At this stage of development, the question of the diffusivity of this signal is not addressed: if the signal does diffuse in the medium, how fast it diffuses and how far.

It has been assumed that the release of the signal is independent of the fate of the cell being hit; this is in agreement with the observation of a bystander effect after cytoplasmic irradiation, while this is much less toxic than nuclear irradiation (Shao *et al.*, 2004), as well as after carbon or uranium radiation (Fournier *et al.*, 2007), which, on the contrary, is very toxic. No direct experiment has been designed yet, though, to determine the relationship between the fate of the emitting cell and the quality and quantity of signal emitted. It seems very possible that the cell might produce different molecules, at different intensities in the two cases.

In case of the V79 cell line, Model 1 and Model 2 use two different functions for the release of the signal with dose of radiation (see Figure 4.3 and Equations 4.2 and 4.3). In Model 1, the probability of releasing the signal increases linearly with dose up to a certain dose, after

which the probability decreases and tends to 0. The biological rationale underlying this is that when a cell is being hit with a small dose, it is not badly damaged and its machinery is still capable of synthesizing and sending an alert; as the dose becomes higher, though, the state of the cell becomes worse and it cannot produce anything. Some experiments in Shao *et al.* (2003a) suggest that indeed the bystander effect may not be seen at high doses. However, the theory is in contradiction with the experiments of heavy ion irradiation which is believed to induce complex damage in the cell (see Section 2.2), but still leads to a bystander effect (Fournier *et al.*, 2007; Zhou *et al.*, 2004); this is also in contradiction with the experiments at high doses of Sawant *et al.* (2001a,b), Mitchell *et al.* (2004) or Mothersill and Seymour (1998). The function used in Model 2 agrees with the assumption that the bystander effect is also present after high doses of radiation. In any case, the simulations obtained with the two models show that the bystander effect does not contribute significantly to the survival fraction of cells at higher doses, which is supported by some groups (Mothersill and Seymour, 2001; Schettino *et al.*, 2005).

As the models were built, only cells directly irradiated could release the signal; cells exposed to the signal could not themselves become sources if they were not already. However, it has been suggested that there are secondary sources of the signal (Schettino *et al.*, 2003), and that the progeny of emitting cells is also capable of emitting the signal (Mothersill *et al.*, 2004a). However, it is not known whether those cells emit the signal in the same manner than primary sources, and if they release the same signal.

5.2.2 Life Time of the Bystander Signal

No experiment directly measuring the time evolution of the concentration of bystander signal released in the medium has been reported yet. The reason for this is that there is no certainty about what the signal is, whether it is released in the medium rather than communicated to neighbouring cells via gap junctions, and whether there is 1 or a spectrum of signals.

In the models presented, only the bystander signal released in the medium is considered. It may well be that in reality, the signal is transmitted both ways (Mitchell *et al.*, 2004). However, in the experimental situation that the simulations have reproduced, cells are not in contact and the bystander effect must be due to a medium-diffusing signal (Schettino *et al.*, 2005, 2001), at least for the first generation of cells, although there may be gap junction communication between

cells of the progeny, once the colonies have started growing. The decay of the concentration of signal has been arbitrarily chosen to be first order (see Figure 4.3 and Equation 3.10).

With Model 1, because the emission of the signal decreases with increasing dose and the proportion of G2 cells being killed by the signal decreases with decreasing concentration, it was possible to use a longer half life than with Model 2. The half life used in Model 1 (30 minutes) is more likely than the half life used in Model 2: many ICCM experiments from different laboratories with different cells have shown a bystander effect when the medium was transferred after 30 minutes to 24 hours incubation (Burdak-Rothkamm *et al.*, 2006; Huang *et al.*, 2007; Kashino *et al.*, 2004; Lehnert and Goodwin, 1997; Mothersill *et al.*, 2006; Suzuki *et al.*, 2004). However, because the model 2 assumes that the bystander effect is an all or nothing phenomenon, when the life time of the signal is increased to 30 min, the model underpredicts the survival of cells irradiated in the S phase. If Model 2 is true, and if indeed the signal is long-lived, then either cells develop a resistance to the signal, at least for some time, or the bystander effect is continuous but very small, or both.

5.2.3 Response to the Bystander Signal

In the models, the resistance to the signal is computed once only in the G2 phase, at entrance of the G2 phase or at the time the signal is first emitted for cells present in G2 at the time of emission. Therefore, the probability is:

$$\partial \mathrm{D}_B(t,Q) = \frac{c(t)}{\tau}\mathrm{D}_{max} \times (1 - \exp(-\frac{Q(t)}{\mathrm{Q}_B}))\partial t \tag{5.1}$$

In Equation 5.1, ∂t is the integration step in the program, i.e. 1 minute. A different approach would be to compute the probability of surviving the signal at any time in G2 phase by the following equation:

$$\mathrm{D}_B(t,Q) = \int_{t_{G2}=0}^{t_{G2}=T_{G2}} \frac{\partial \mathrm{D}_B(t,Q)}{\partial t} dt \tag{5.2}$$

In Equation 5.2, t_{G2} is the time spent in G2 phase and T_{G2} the length of G2 phase. The latter method is probably more realistic on a biological point of view, especially for cells being in G2 phase already at the time of emission of the bystander signal; the former method is a little more efficient computationally since Equation 5.1 is calculated once for any cell, while Equation 5.2 would be calculated 150 times in case of V79 cells and 192 times in case of T98G cells.

In Model 2, the response to the signal is maximum as soon as there is one cell emitting the signal; this is in agreement with the idea that the bystander effect is an "all-or-nothing phenomenon" (Brenner *et al.*, 2001). The simulations and the sensitivity analysis on Model 2 show that in such case there is no possible modulation of the response of cells to low doses when they are broadbeam irradiated: their surviving probability is discontinuous when the dose tends to 0 Gy. This supports Mothersill and Seymour (2004a)'s suggestion that at low doses, for the bystander effects, dose has no influence, but rather environmental and genetic factors. However, it may be that when all cells are irradiated, their mechanisms of response to the bystander signal are switched off, and the direct effect only plays a role, although this contradicts the results of Shao *et al.* (2003a), who found a significant bystander effect at low doses when T98G cells are all irradiated. Otherwise, it may be that there is a dependency in the response of bystander cells at low concentrations of signal, or a modulation of quality or quantity of signal released at low doses, or both.

All simulations presented in this dissertation are based on the assumption that there is a bystander effect even when cells are all irradiated, and that cells do communicate in these conditions. This is not the point of view of Brenner *et al.* (2001) or Moore *et al.* (2006). In fact, although there are experimental suggestions that the emission of the bystander effect does not depend on the fate of the irradiated cells, only one experimental study was found giving early evidence that irradiated cells would be able to respond to the bystander signal: Shao *et al.* (2003a) detected a bystander effect after entire populations of T98G cells were irradiated. Mothersill and Seymour (1997) conducted some ICCM experiments leaving the irradiated cells incubating in their medium for varying period of times, but recorded the effects on the recipients cells only, and not on the donor cells.

It has been observed that any cell can emit the bystander signal (Schettino *et al.*, 2005), and also that G2 plays a particular role (Mothersill and Seymour, 2004b). There is also unpublished experimental data suggesting that not only G2 cells can respond to the signal but also G1 cells (G. Schettino, personal communication). However, Burdak-Rothkamm *et al.* (2006) shows that the bystander induction of γ-H_2AX foci is essentially seen in S phase; γ-H_2AX foci are known to be directly related to a site of DSB. This may not be contradictory, and it may just be that when cells are in S, they are given more opportunities to repair their DNA, either by homologous recombination or non-homologous end joining (Wilson, 2004); in other phases, cells may just

attempt repair less frequently and enter apoptosis, which would explain why the γ-H_2AX foci are not detected. This is especially likely for cells in G2 or M phase. In this case, bystander apoptosis or killing would be strongly detected in G1 and G2, while bystander γ-H_2AX foci would be strongly detected in S. In any case, the different endpoints used to study the bystander effect are cell cycle dependent, even after direct irradiation, and this complicates the study of the relationship between the cell cycle and the bystander effect.

It could also be that any cell responds to the bystander signal, but with different intensities according to their cell cycle position; cells could fail or pass a checkpoint and in the latter case gain resistance to the signal for the rest of the cell cycle. It has been shown that the transfer of ICCM is accompanied by a quick but transient increase in intra-cellular calcium (Lyng *et al.*, 2000); it could be that similarly, soon after irradiation or exposure to medium transfer, cells are sensitive to the signal, but quickly develop a defence mechanism, which is lost at the time of division. This is the same principle as the adaptive response, which is gained for a limited period of time and has been linked to the bystander effect for mouse cells (Sawant *et al.*, 2001b) and hamster-hybridoma cells (Zhou *et al.*, 2004).

If the progeny of cells are capable of both releasing the signal and responding to it, then they are also at risk. This would agree with some medium transfer experiments, showing that the progeny of cells that survived exposition to ICCM have a reduced plating efficiency (Mothersill *et al.*, 2004a; Seymour and Mothersill, 2000). Nevertheless, this would mean that at the time of radiation, cells pass or fail the checkpoint at the point of the cell cycle where they are; for those cells who survive and divide, the following checkpoints will be in G1 for the next cell cycles. This would create a sub-population of cells resistant to the bystander signal.

The question of the dependency of the bystander effect with LET has not been addressed in the previous chapters; an attempt has been made, which is described in Appendix C. The same assumptions concerning the mechanisms of the bystander effect (assumptions of Model 2) have been applied to the single cell and all cells irradiation with C_K X-rays, all cells irradiation with 3.2 MeV protons and broadbeam irradiation with 250 kVp X-rays. The results would support the possibility that the bystander effect is independent of the radiation LET, which is in agreement with some experimental studies from different laboratories (Fournier *et al.*, 2007; Shao *et al.*, 2003b) on a human fibroblast cell line, although Shao *et al.* (2002, 2001) detected a

dependency of the bystander effect on LET in a human salivary gland cell line.

In conclusion, this project tested some plausible mechanisms of the bystander effect. Many others can be proposed, which is the advantage of the modelling of experimental work; any parameter may be switched on or off and its consequences analyzed. The simulations revealed that there would be a need for studying the bystander effect in synchronised population, and its relation to cell cycle position. It seems non-trivial to reconstruct the response of an asynchronous population of a cell line from its phase responses. This work is also an early suggestion that there may be a bystander effect issued after broadbeam radiation of asynchronous cells, which is the situation in radiotherapy.

5.3 Relationship Between BE and HRS

Apart from studying the variability of the bystander effect with the cell cycle, and the relevance of the bystander effect after broadbeam irradiation, another objective of this modelling exercise was to understand whether BE and HRS would be related, and more specifically whether HRS could be due to BE. HRS has been shown in asynchronous populations of V79 (Marples and Joiner, 1993; Skarsgard *et al.*, 1994) and in synchronised and asynchronous populations of T98G (Short *et al.*, 1999a,b, 2003); the BE has also been shown in both cell lines in asynchronous populations, although for different endpoints, and only the BE in V79 has been studied in terms of bystander survival (Schettino *et al.*, 2005; Shao *et al.*, 2003a).

5.3.1 Hyper Sensitivity to Low Doses of Radiation

In both cell lines, the linear quadratic model overestimates the survival of the asynchronous populations at doses below 1 Gy; this is also apparent in G1 and G2 synchronised populations of T98G (see Figures 4.4 to 4.7 and Figures 4.9 to 4.12).

Both CA models can predict the hyper-radiosensitivity not present in the linear quadratic model. However, it is difficult to reconcile the data on synchronised populations with the data on asynchronous populations. For V79 cells, very little or no hyper-radiosensitivity is detected in synchronised populations while there is some in asynchronous populations; moreover, in both cell

lines, S synchronised populations are the most resistant while simulations of Model 1 show a hyper sensitivity due to S cells moving into G2 phase. This may be solved if cells are supposed to become resistant to the signal until the end of their cycle, once they have been exposed to the signal and survived it; an example of such a model is developed in Appendix C.

This is in contradiction to the only experimental work that has been carried out on the relationship between HRS and BE (Mothersill *et al.*, 2002). This paper argues that cells either show bystander effect or hyper-radiosensitivity; it is proposed that cells that would be hyper-sensitive would actually not be capable of releasing the toxic bystander signal and die themselves rather than the neighbours. Nevertheless, bystander-induced micronuclei formation, which is believed to be a lethal effect leading to cell death, has been demonstrated in T98G by Shao *et al.* (2003a, 2004), while no decrease of the plating efficiency was seen in T98G treated by ICCM (Mothersill *et al.*, 2002). It may be that the signal produced by T98G is very short lived and disappears during the medium transfer. The results of this work cannot confirm or refute those possibilities since a model at the molecular level would be needed. However, it shows that assuming only the bystander effect, the resulting survival is significantly decreased at low doses compared to the predictions of the LQ model.

5.3.2 Increased Radio-Resistance

As discussed in Section 5.2, Model 2 that computes the production of a bystander signal at any dose is more likely than Model 1, that computes a decrease in the probability of producing a signal at higher doses. The problem, though, with Model 2 is that no increased radio-resistance is possible. Therefore, there must be an additional independent mechanism responsible for the zero gradient seen in experimental data between about 0.5 and 1 Gy, in both cell lines. On the contrary, the induced radioresistance can be seen in the simulations of Mode1: this shows for the first time that the increased radio-resistance is a biologically realistic phenomenon.

In Appendix C, a multi-target model rather than a LQ model is used to calculate the direct effect of radiation. The multi-target curve has a zero gradient at zero dose, i.e. at low doses, there is little direct effect. In such case, cells are killed mainly by bystander effect and because this one saturates quickly, the survival of the population also shows a zero gradient for doses at which the bystander effect has saturated and the direct effect is not yet significant (see Figure C.2).

By adding a scavenger of nitric oxide in the cell culture, Shao *et al.* (2003a) measured in populations of T98G that were entirely irradiated a significant bystander induction of micronuclei at low doses, but no bystander effect at higher doses. This definitely demonstrates, at least in this cell line and with this endpoint, that the bystander effect disappears at high doses in populations entirely irradiated, even though it is significant when a small proportion of the population has been irradiated. It may be that compared to the direct effect, the bystander component is so small at high doses that it is hidden. It could be that cells respond differently to the bystander signal if they have been irradiated themselves, and their response to the signal would decrease as the received dose increases, because their properties of responding to environmental messages are modified. The response to the signal would then depend on the dose (either received by the emitter or by the receptor) as well as on the concentration of signal, and Equation 3.11 could be modified as follows:

$$\mathrm{D}_B(Q,d) = \mathrm{D}_{max} \times \exp(-\frac{d}{d_r}) \times (1 - \exp(-\frac{Q}{\mathrm{Q}_B})) \tag{5.3}$$

Equation 5.3 may predict an increased radio-resistance.

5.3.3 Cell Cycle Dependency

It is assumed that only cells in the G2 phase are sensitive to the bystander signal. It may be true that G2 cells have a predominant role in both the bystander effect and the low dose hyper-radiosensitivity; however, it seems untrue that G2 is the only phase involved. HRS has been seen in G1 synchronised T98G (Short *et al.*, 1999a, 2003), and bystander induction of γ-H2AX has been detected in S cells (Burdak-Rothkamm *et al.*, 2006); also there are unpublished data that bystander-induced killing occurs in G1 V79 to a lesser extend than G2 V79 (G. Schettino, personal communication). Therefore it would be more accurate and interesting to modify the model so that any cell can respond to the signal, G2 cells being the most sensitive and S cells being the least sensitive.

In addition, the hyper-radiosensitivity was first explained by the extreme sensitivity of a sub-population to radiation, and this idea was refuted by simulations showing that in such case, the sensitivity of this sub-population would be unrealistically high (Wouters and Skarsgard, 1997). It has been suggested that the bystander effect also would not be due to the response of

a sub-population (Mothersill *et al.*, 2004a). However, this is what the model implicitly says by assuming that only G2 cells respond to the signal and that they are responsible for the hyper-sensitivity of the cell lines. But, in fact, the simulations run on the phase data do support the conclusions of Wouters and Skarsgard (1997), by predicting a requirement for a sensitivity of G2 cells which is significantly higher than experimentally measured.

Actually, the equations derived in Chapter 3 can be fitted quite well to the asynchronous data only (see Figures 4.4 to 4.7). The problem arises when experimental data on synchronised populations are being modelled as well, and that an agreement between synchronised and asynchronous data is sought, in particular for the V79 cell line. In the case of the T98G cell line, Model 1 works well, except for G1 cells, but if G1 cells are also made responsive to the signal, the fitting of the G1 population may improve (see Figures 4.9 to 4.12). Comparison of χ^2 values in the case of V79 shows that while the cellular automata give a better fit than the LQ model for asynchronous populations, the LQ model gives a better fit for synchronised populations (see Section 4.1). The reason why the synchronised populations show no low dose hyper-radiosensitivity but the asynchronous populations do has not been found during the course of this project. It might be that an amplification process is happening only in asynchronous populations. Otherwise it might be that even though all cells can release a signal, the signals are phase-specific and very short-lived, and therefore, the effect would be more efficient in asynchronous populations when there are always cells in any phase of the cell cycle.

5.4 Concluding Comments

Several aspects of the work have been discussed in this chapter. The strengths as well as the weaknesses of the model have been underlined and explained. The cell cycle approach that has been taken could and should be improved, and the description of the nutrients availability simplified.

The breakthrough made with the model, though, is that it remains simple, fast and the assumptions concerning the bystander effect can be easily modified in order to study the effect and influence of particular parameters. It could also be adapted to take into account other non-targeted effects, such as an adaptive response or dose-rate effects. A particular set of simula-

tions has been presented in details in Chapters 3 and 4 for testing whether it is possible, with the same assumptions for the bystander effects, to predict the response of synchronised and asynchronous populations. It was possible to reproduce the hyper-radiosensitivity of the two cell lines V79 and T98G. Appendix C shows how the model can be used to test whether the same set of assumptions on the bystander effect can predict the response of cells to different types of radiation.

Possible future developments of the model, as well as recommendations for experimental works are proposed in the next chapter, after overall conclusions of the dissertation.

Chapter 6

Conclusions and Future Work

The past decade has shown that the mechanisms of response of cells to low doses of radiation are not linear, as it was assumed. A number of phenomena, called the non-targeted effects, have been described that take part in this response. The relevance of the non-targeted effects *in vivo* is not obvious, and the links that may be between some or all of them is not known, although they all share similarities.

From the experimental results, new theories have been proposed to explain radiation effects, taking into account the non-targeted effects. The objective of this project was to write a computer model which would allow for testing these theories. The model was applied to test the mechanisms of 2 particular phenomena: the bystander effect and the low dose hyper-radiosensitivity.

When some cells of a population are hit by radiation, their non-irradiated neighbours may also show radiation-type effects: this is the bystander effect (BE). There are 3 main experimental protocols used to study the bystander effect; cells may be irradiated by low fluence of high linear energy transfer (LET) particles (Little *et al.*, 2002), they may be harvested in filtered medium from irradiated cells (ICCM experiments: Mothersill and Seymour, 1997), or a microbeam can be used to select cells to be irradiated (Shao *et al.*, 2003a; Zhou *et al.*, 2000). Irradiated cells would release a signal (BS) that affects bystander cells; the experimental results suggest that the bystander effect is an all-or-nothing phenomenon, independent of the dose of radiation and the number of irradiated cells. It happens very soon after irradiation, and can last at least for 60 hours in some cases (Morgan, 2003; Prise *et al.*, 2005). The bystander effect has been shown in terms of a wide variety of endpoints, including survival fraction, gene mutation, micronuclei

induction; many different cells have also been studied. However, it could not be found in the literature a cell system which bystander effect has been investigated using the 3 protocols, or through several of the endpoints used so far.

Low dose hyper-radiosensitivity (HRS) was first detected in rat cells, and was later demonstrated in human cells, including cancer cells (Joiner *et al.*, 2001). The fraction of cells surviving radiation is usually modelled by a linear quadratic model, which is based on the idea that radiation effects are only due to the interactions between the radiation track and the nuclear DNA. However, at doses below 1 Gy, the number of cells surviving radiation as measured experimentally is significantly less than predicted by the linear quadratic model. It was first proposed that the low dose hyper-radiosensitivity could be due to a sensitive sub-population, but it was demonstrated that the sensitivity of this sub-population would then be unrealistically high (Wouters and Skarsgard, 1997); it has been confirmed in this work. It is now suggested that in this dose domain, repair processes are not triggered or are deficient, which renders cells more sensitive (Joiner *et al.*, 2001; Short *et al.*, 2005). Contrary to the bystander effect, the low dose hyper-radiosensitivity has been shown only in terms of survival fraction.

There is only one experimental study of the relationship between the bystander effect and the low dose hyper-radiosensitivity; Mothersill *et al.* (2002) concluded that they are two mutually exclusive characteristics. Yet, the two effects have been both shown in some cell lines, such as the hamster cell line V79 or the human brain cancer cell line T98G. Therefore, this was a first question that was addressed with the model; more precisely, it was tested whether the bystander effect could be responsible for the low dose hyper-radiosensitivity.

Secondly, the question of the possible variation of the bystander effect with cell cycle has not been addressed at all experimentally yet. This was a second point that was explored with the model.

Due to technological limitations, the bystander effect after the type of radiation used in radiotherapy, e.g. 250 kVp X-rays or cobalt-60 γ-rays, has been studied using the ICCM method only (Little, 2006). Moreover, the dependency of the bystander effect on radiation type is not clear. Therefore, it is difficult to predict its significance in situations such as radiotherapy treatments. To this purpose, the model was used to investigate the bystander effect after conventional X-rays, and its possible independence from radiation ionizing density.

6.1 Overall Conclusions

The model assumes that cells are seeded in a dish containing nutrients uniformly distributed at any time, and that cells consume at constant rate; nutrients are supposed to be always at a level at which cells are never starving. The cell cycle is described by the model and includes a checkpoint controlled by the absorption of nutrient at the G1/S transition; it also includes a G0 phase that cells enter in case of low level of nutrients. The length of the G1 phase is variable, while the other phases have a fixed length. At division, one daughter cell is located where the mother cell was and the second daughter cell is positioned in one of the 8 neighbouring nodes, and may displace in a random direction the cells already present.

When cells are irradiated, their probability of surviving is calculated by the linear quadratic equation, fitted to the experimental data points of synchronised populations for doses greater than 1 Gy. Therefore, the direct effect depends on the cell cycle phase. Irradiated cells release a bystander signal with a probability which varies with dose, and the proportion of cells killed by the signal depends on the number of cells that emitted the signal. The model assumes that cells are sensitive to the signal when they are in G2 phase only. The amount of signal initially emitted is supposed to decrease exponentially. However, the low dose hyper-radiosensitivity is not taken into account explicitly.

The solution technique of the cellular automaton was adopted, because it allows for solving easily the interactions between elements of the model, while keeping the overall program simple. The program is written in C++ language and reproduces the traditional clonogenic assay: cells are initially seeded in a dish at random positions and may be irradiated; after a period of incubation, colonies that are formed are revisited and the original cell is believed to have survived if its colony contains at least 50 cells.

Chapter 3 and Chapter 4 describe the model with these assumptions. Nevertheless the model is quite flexible and it is possible to test different situations. In Appendix C, different equations have been used to describe both the direct effect and the bystander effect. The objective of writing a model for testing different possible mechanisms of the non-targeted effects has been achieved; the approach taken in this model is novel, since the response of the populations is built from the response of the individuals and their interactions, within the population.

The results of simulations of the response of synchronised populations of cells as well as asynchronous populations are shown in Chapter 4, in the case of the two cell lines V79 and T98G. No complete agreement is found between the response of synchronised cells and the response of asynchronous cells; the sensitivity of G2 cells especially, as predicted by the model is significantly higher than experimentally measured (up to 16% at 1 Gy). This suggests that the assumption that the sensitivity to the bystander signal is limited to a single cell cycle phase is too simple and not correct, which is actually in agreement with early conclusions on the low dose hyper-radiosensitivity (Wouters *et al.*, 1996) and a conclusion on the bystander effect (Mothersill *et al.*, 2004a). The link between the experimental data on synchronised and asynchronous populations remains to be found.

However, the model predicts some hyper-radiosensitivity in the response of cells, although it includes no parameters for it. Therefore, this supports the idea that the non-linearity in the survival fraction at low doses may be due to the bystander effect, at least in asynchronous populations. Furthermore, the model has been run to study the bystander effect in population of cells directly irradiated with conventional 250 kVp X-rays, and the corresponding experiments have not been set up yet. According to these results, the response of asynchronous populations to this radiation type could be also a mixture of direct and bystander interactions.

The dependency of the bystander effect on radiation type has been studied and the results of some simulations are displayed in Appendix C. In these early studies, the same set of assumptions about the mechanisms of the bystander effect has been applied in every case, while only the equation of the direct effect varies with radiation quality. Under these conditions, it is possible to reproduce accurately the experimental data of survival fraction to 3 radiation types: 250 kVp X-rays, C_K X-rays and 3.2 MeV protons ($\Phi < 3.5 \times 10^{-3}$).

In conclusion, a model has been created which can be easily used to test assumptions about the bystander effect and its significance relative to the direct effect. It has been used for simulating the survival of synchronised and asynchronous populations of two cell lines, V79 and T98G. The particularities of this work are:

- the detailed description of the bystander effect and the bystander signal, which includes the simulation of the mode of release of the signal by irradiated cells, the time evolution of its concentration and the mode of response of neighbouring cells to the signal;

- the response of the population is built up from the response of its individuals and the inter-individual communication;

- the flexibility of the model allows for a wide variety of hypotheses on the mechanisms of non-targeted effects to be tested and, in the case of the bystander effect, the characteristics of the bystander signal;

- such a model can be easily extended to a three-dimensional model of tumours, and their response to radiation;

- for the first time, the relationship between the bystander effect and the cell cycle position of irradiated cells and the bystander effect in populations broadly irradiated with 250 kVp X-rays have been studied.

However, there are some limitations to the model as it is written now, and the following section develops some possible future work.

6.2 Recommendations for Future Work

The availability of nutrients has been modelled; this may not appear necessary for the applications of the model considered in this project. However, although the bystander effect has not been studied in conditions of hypoxia or reduced availability of nutrients, it may be important to investigate this. Indeed, in most tumours, the cells in the core are hypoxic, and hypoxic cells are known to be more resistant to radiation. The distribution of nutrients is also not uniform in tumours, and the model is constructed to describe this. However, the problem is that no detailed model of nutrient uptake by cells was found. Further investigation of the literature is therefore needed: more could probably be found in studies of spheroids or tumour models; otherwise, the consumption of glucose in cell culture could be measured experimentally. In parallel, the experiments that have been run to study the bystander effect with all types of protocols should be repeated when irradiated cells or bystander cells or both are grown in hypoxia or in nutrients-free medium. This would provide information on whether the production or response to the bystander signal or both requires the cells to have nutritional or oxygen supply.

A second weakness of the model is the description of the cell cycle. Only one checkpoint has been included, which is nutrient-controlled, at the G1/S transition. First, this means that except for the G1 phase, phases have exactly the same duration for all cells. Secondly, radiation-induced checkpoints and cell cycle delays have not been included, although they have been reported (Sancar *et al.*, 2004; Zhou and Elledge, 2000). The low dose hyper-radiosensitivity may be due to a checkpoint in G2 phase (Marples *et al.*, 2004), and even if there is no direct study on the relationship of the bystander effect with cell cycle, cell cycle-related proteins have been shown to be induced in bystander cells (Azzam *et al.*, 2001; Fournier *et al.*, 2007). It is necessary to develop a more precise description of the cell phase and phase transition, and dependency of phase duration on radiation.

In the literature, there is a strong opinion that the bystander effect is due to a signal; however, the characteristics of this signal are not known, although some assumptions have already been suggested (Little, 2006; Mothersill and Seymour, 2004a; Prise *et al.*, 2005). The possible diffusivity could easily have been implemented within the models. Other issues such as the quantitative aspects of the bystander signal, the existence of secondary sources of the signal should be investigated with the model. Nevertheless, it will be difficult to investigate these issues both theoretically and experimentally unless the nature of the signal is determined. Therefore, further experimental work is needed to identify the signal or possibly signals involved in the bystander effect. A solution may be the analysis of the composition of the medium of irradiated cells, to be compared with the composition of the medium of non-irradiated cells.

In this project, the focus was on the relationship between the bystander effect and the low dose hyper-radiosensitivity; the survival of cells to radiation was used as the endpoint. However, the bystander effect has been studied using many different endpoints, and it is likely that it actually depends on the endpoint used. Also, other non-targeted effects have been fully identified and the relation to each other and with the bystander effect and the low dose hyper-radiosensitivity has not been clarified yet. The model could be broadened to compute other endpoints and non-targeted effects. Cells response to radiation may be influenced by some genetic factors (Mothersill and Seymour, 2004a); in this case, it would have to be taken into account in the model as well. This would then produce a description of the cellular response to radiation that contains all effects known so far; many different hypotheses on the mechanisms of cellular response to radiation could then be tested.

The results of the model showed that there is no obvious correlation between the sensitivity of the synchronised populations and the sensitivity of asynchronous populations. There is only one published study on the relationship between cell cycle position and low dose hyper-radiosensitivity, and there is none regarding the relationship between cell cycle and bystander effect. The experiments on the relationship between HRS and cell cycle should be repeated with different cell lines, and some bystander effect experiments must be designed on synchronised populations as well. In microbeam and ICCM experiments, the irradiated and bystander populations could be synchronised both, or only one of them, or could be synchronised in different phases, to detect the possible interphase communications during the bystander effect.

In order to gain deeper understanding of the bystander effect after broadbeam irradiation and especially after 250 kVp X-rays irradiation, experiments such as the one led by Shao *et al.* (2003a) should be reproduced. They determined an inhibitor of the bystander effect by adding a scavenger of nitric oxides in culture of populations of glioblastoma T98G where a small proportion of cells were irradiated with alpha particles; then they added this inhibitor in the medium of populations that were entirely irradiated with alpha particles, and were able to measure the bystander effect in this latter situation. The effects of this inhibitor on the response of cells to 250 kVp irradiation could also be studied.

Contrary to the bystander effect, the low dose hyper-radiosensitivity has been studied exclusively in terms of survival fraction. To know whether this increased cell killing is beneficial, experiments should be set up to see whether the hyper-radiosensitivity in terms of cell killing is related to an hyper-radiosensitivity in terms of genetic mutation (Redpath *et al.*, 2003).

However, first and foremost, a series of experiments should be designed to measure the bystander effect on a given cell line, in terms of a given endpoint, using the different protocols. This would show whether the same phenomenon is measured with these different protocols. Then, fixing the cell systems and the protocols, comparison should be made between the measurements of different endpoints. This latter experiment has been done already (Huang *et al.*, 2007; Moore *et al.*, 2006; Shao *et al.*, 2001), but should be generalised. This is necessary to know whether the bystander effect is beneficial or detrimental (Little, 2006; Prise *et al.*, 2003).

Finally, it would be useful to develop a 3-D version of the model. This would be necessary for further studies of the non-targeted effects in tumours or tissues. If these effects are significant,

they should be taken into account in radiation risk assessment and treatment planning. Their mechanisms in three dimensional systems should then be investigated.

It should be remembered, though, that a model is never an exact copy of reality; there is always a compromise to make between accuracy, simplicity and computational load. Modelling provides a complementary view on the biological problem and helps discriminating between possible theories. It is hoped that the work presented in this report will be integrated in radiobiological studies in the future.

Figures

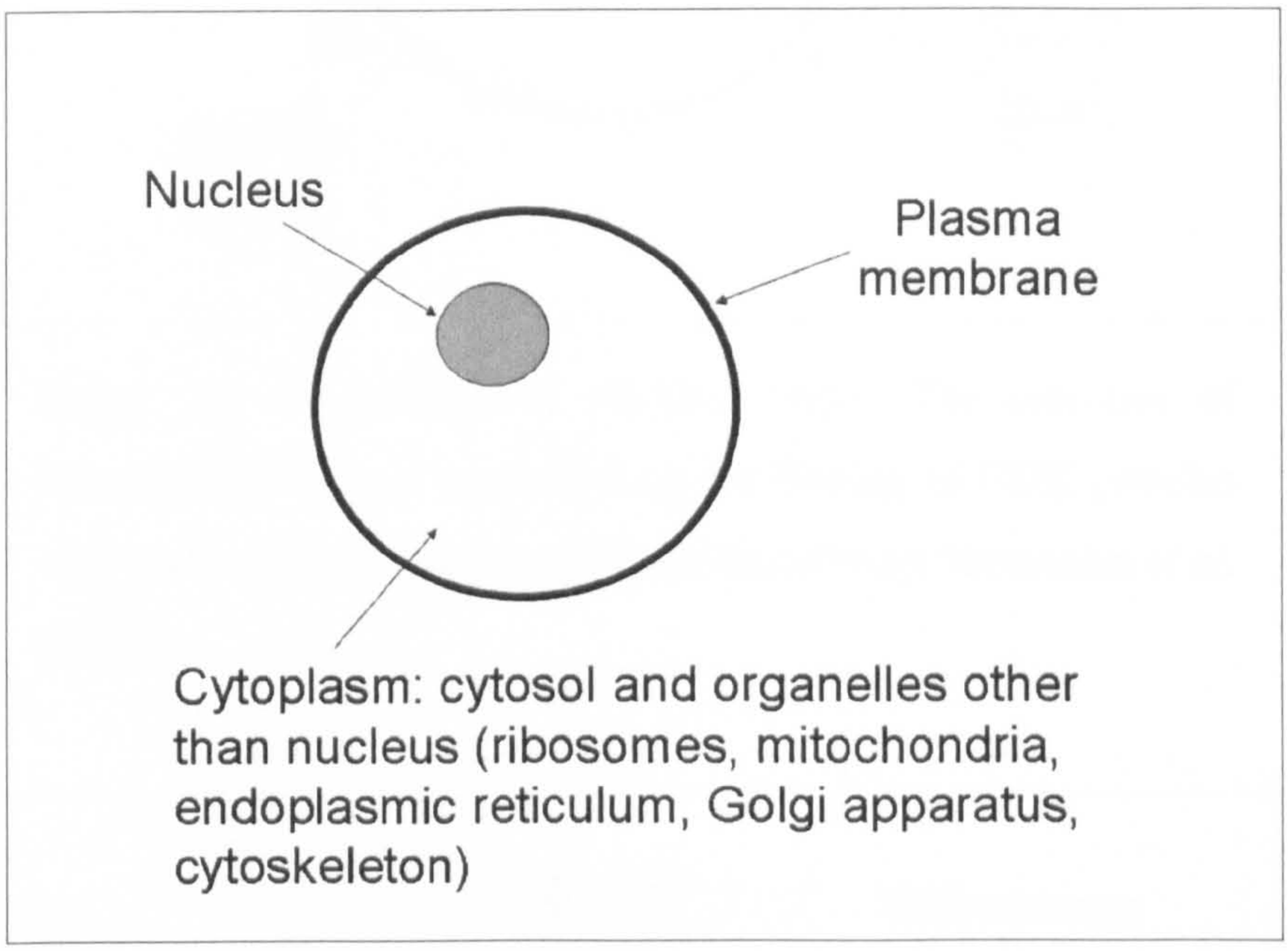

Figure 2.1: Structure of a Cell

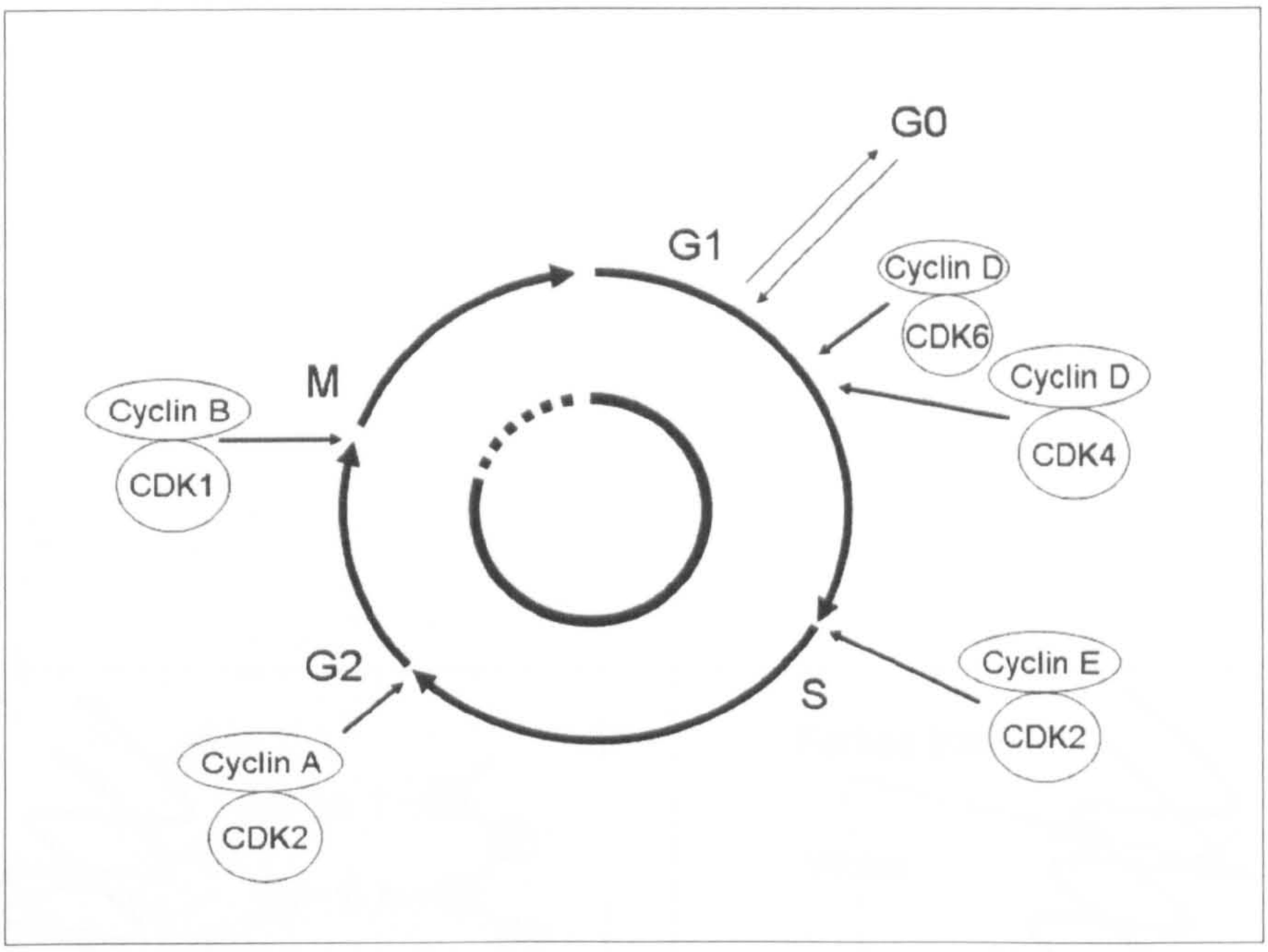

Figure 2.2: The Phases of the Cell Cycle: The execution of the different steps is controlled by the binding of CDK proteins with their activators (cyclins). Reproduced from Vermeulen *et al.* (2003)

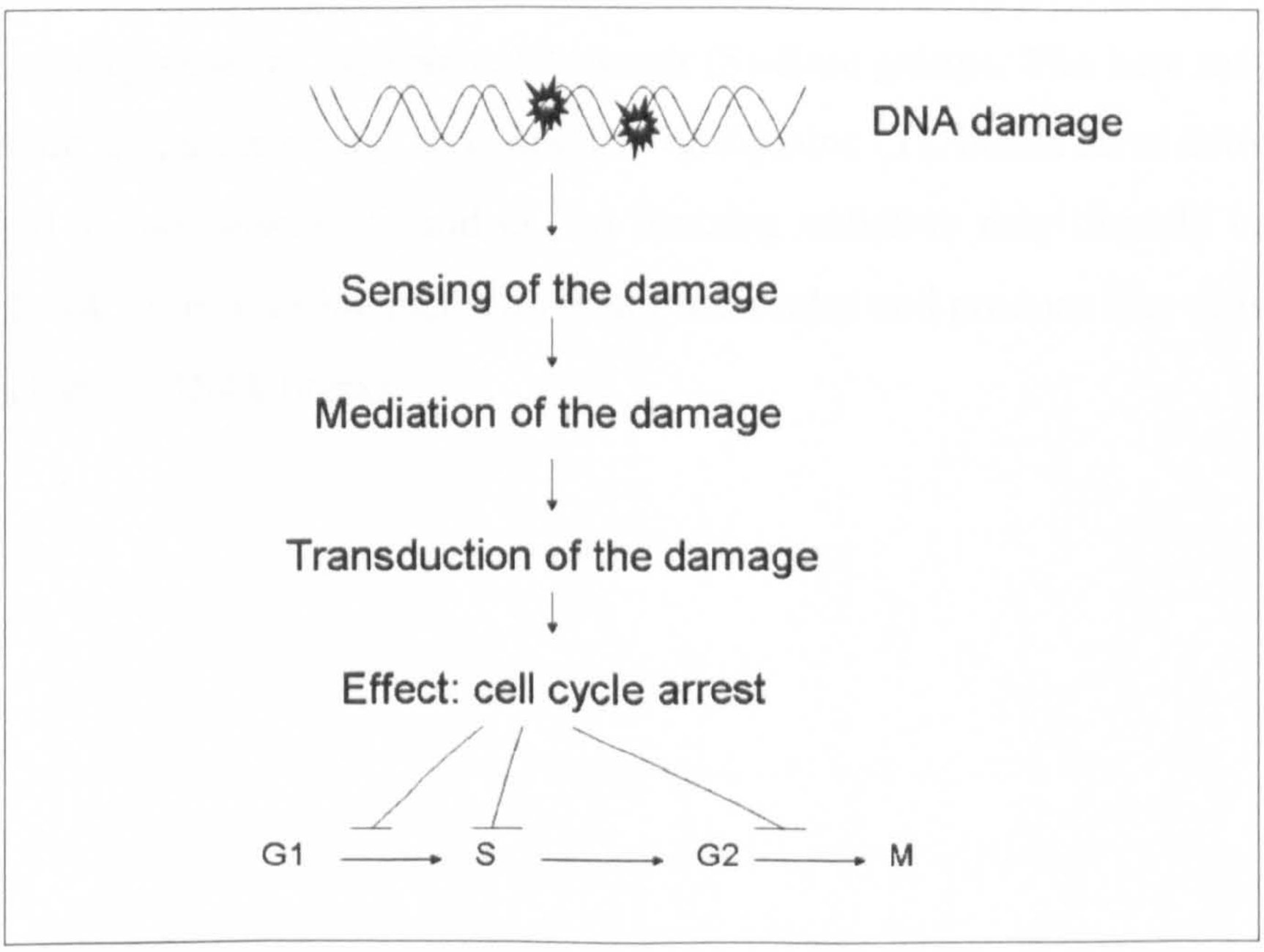

Figure 2.3: Steps of DNA Checkpoints (Sancar *et al.*, 2004).

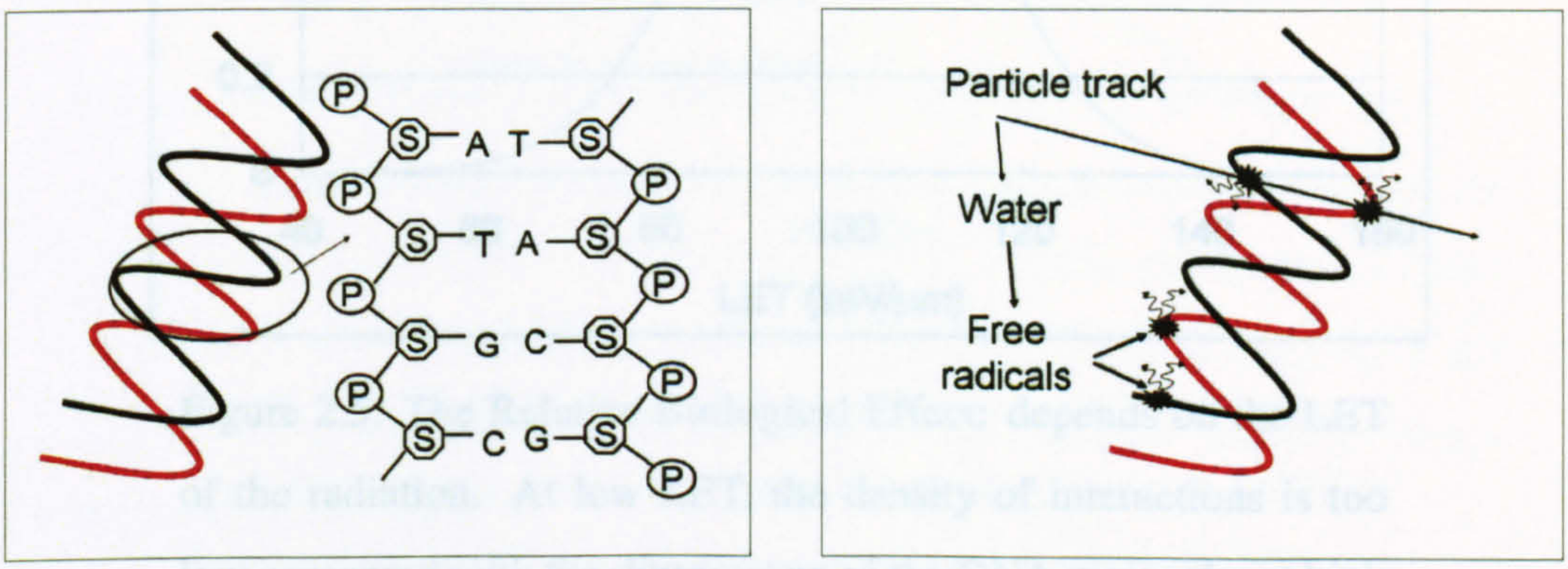

(a) (b)

Figure 2.4: The DNA Molecule: (a) The molecule consists in 2 long complementary series of Phosphate (P)-Sugar (S)-Base groups. The base may be adenine (A), guanine (G), cytosine (C) or thymine (T); bonds form between A and T and between C and G. (b) Ionizing radiation may directly break the DNA strands, or interact with water molecules and produce free radicals which cause DNA breaks.

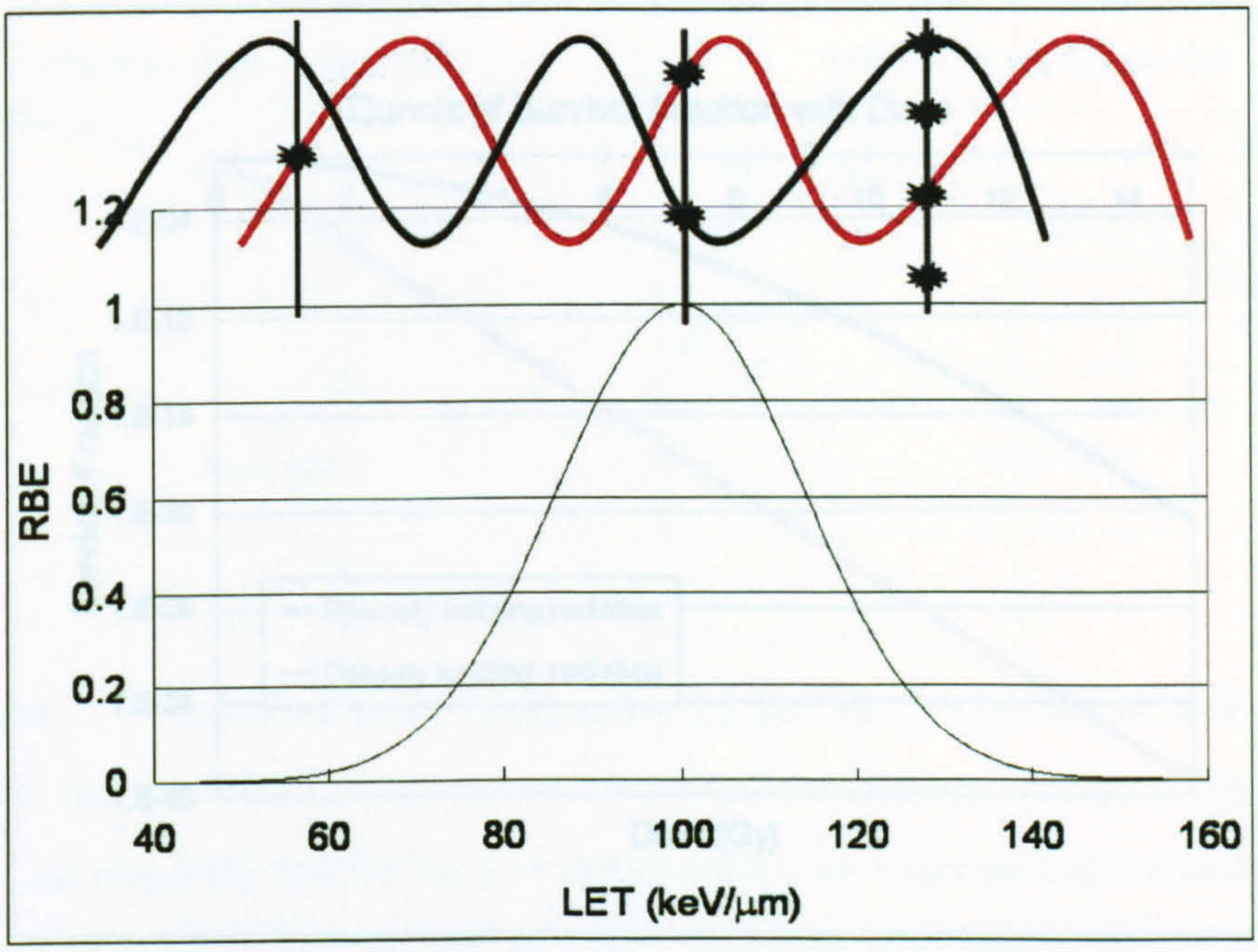

Figure 2.5: The Relative Biological Effect: depends on the LET of the radiation. At low LET, the density of interactions is too low compared with the dimensions of the DNA molecule; at high LET, the density of interactions is too high. The most efficient LET is about 100 kEV/μm, at which density of interactions and dimensions of DNA are the closest.

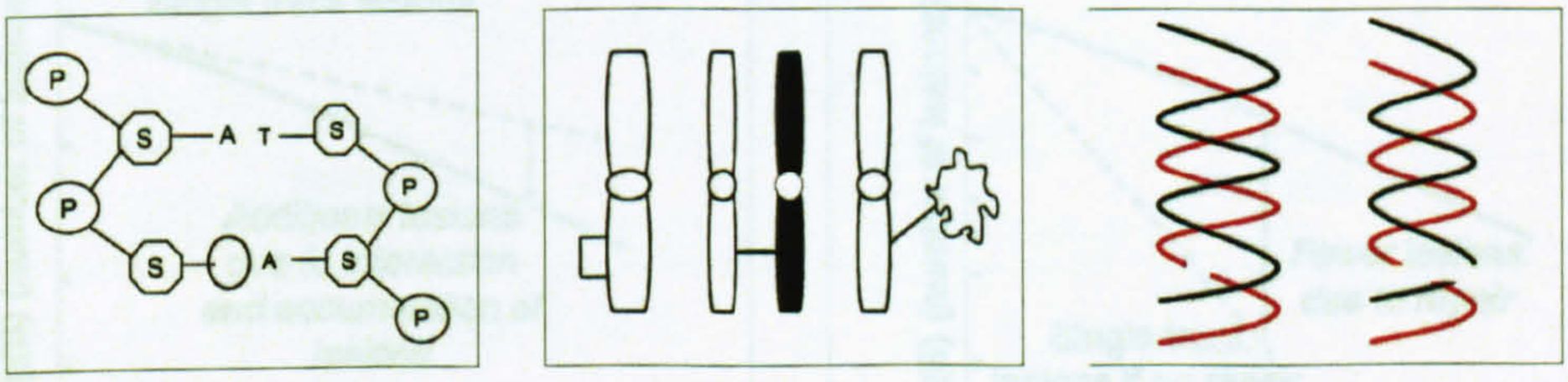

(a) (b) (c)

Figure 2.6: Possible DNA damage: (a) Base damage (b) From left to right: intra-chromosome cross-link, inter-chromosome cross-link and chromosome-protein cross-link (c) Single and double strand breaks.

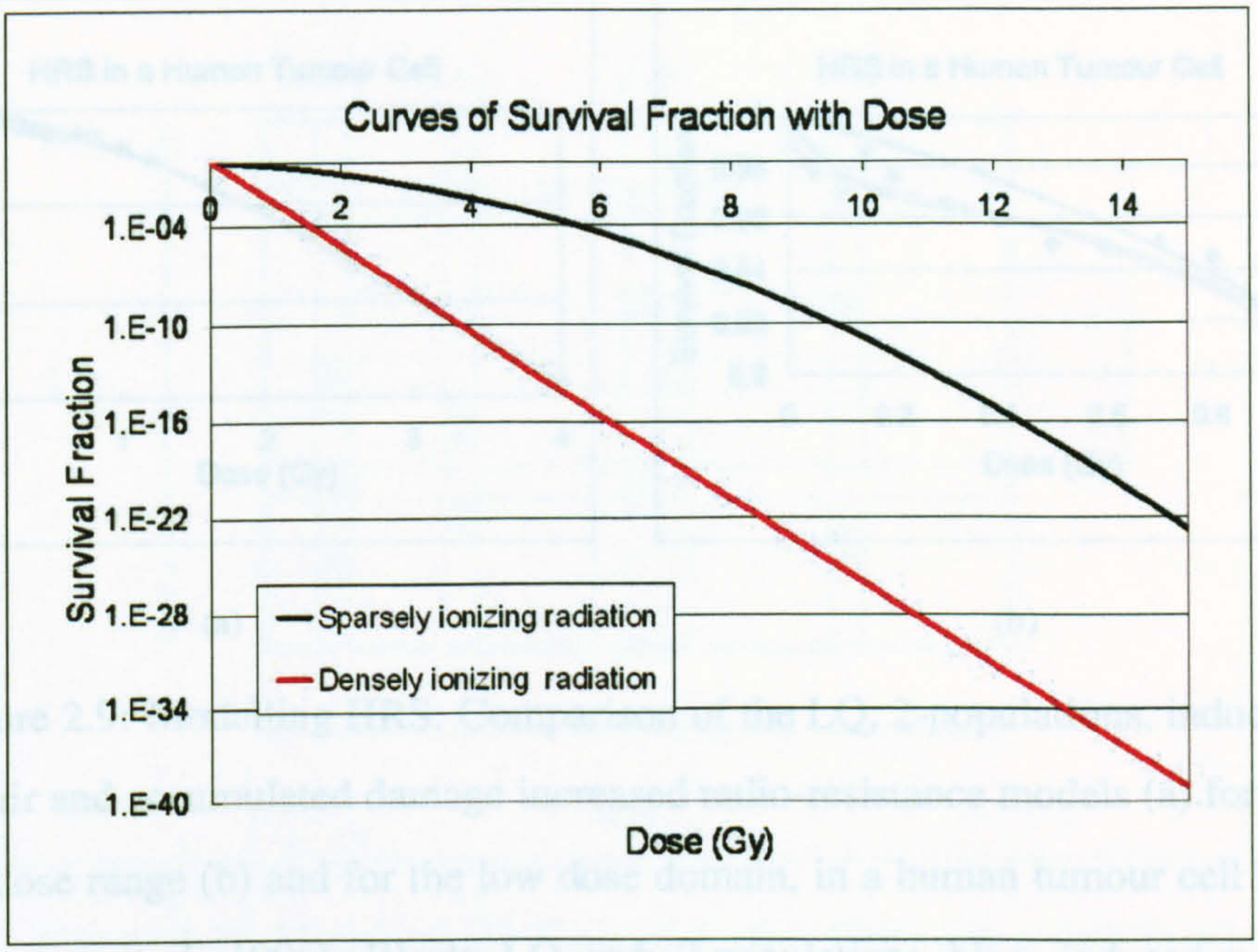

Figure 2.7: Shape of Survival Curves: The survival is plotted on a semi-logarithmic scale. The curve for densely ionizing radiation (e.g. α-particles) is straight, while the curves for sparsely ionizing radiation (e.g. X-rays) shows an increase in the steepness of the curve at higher doses.

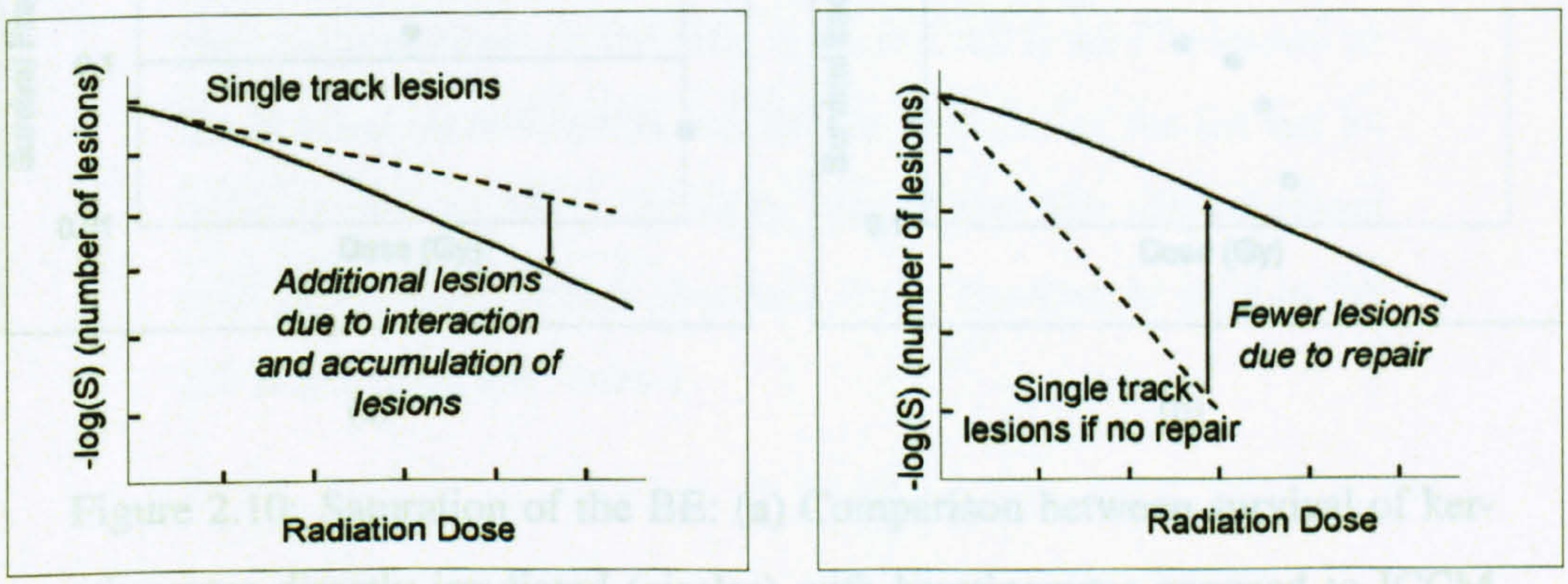

Figure 2.8: Cell Killing Models: (a) The lethal potentially lethal model (b) The repair saturation model. Reproduced from Steel (2002, Chapter 7).

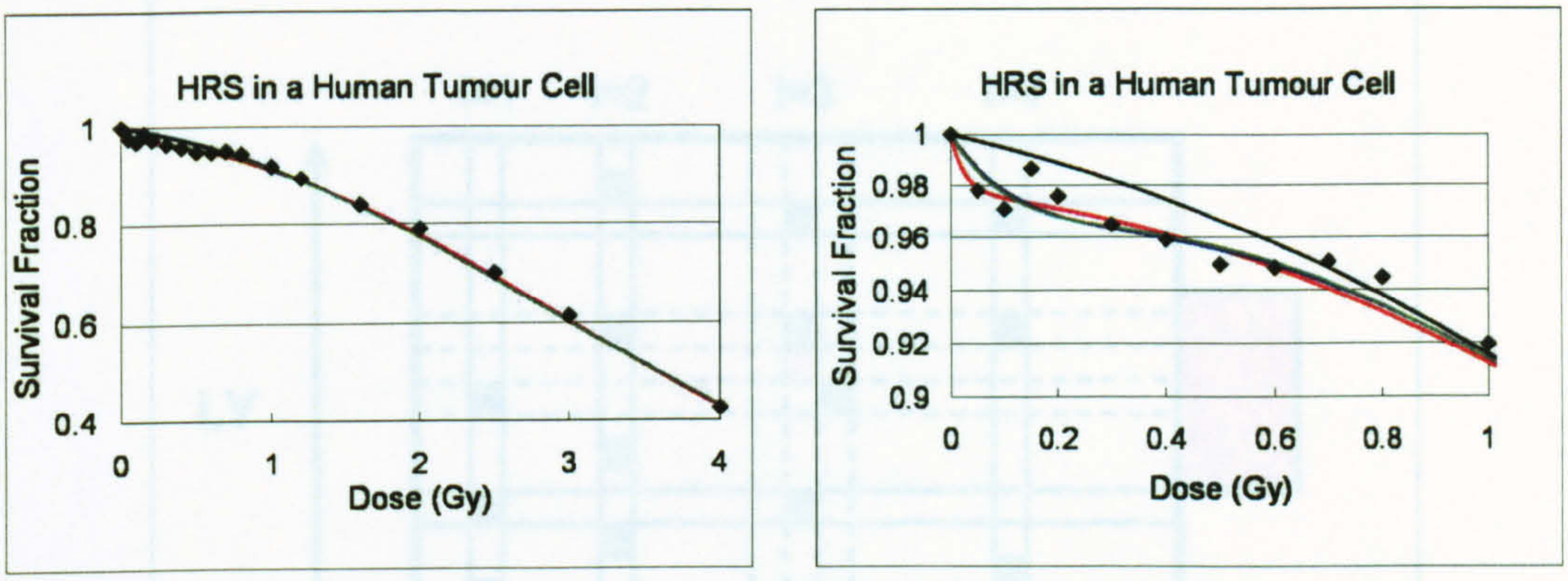

(a) (b)

Figure 2.9: Modelling HRS: Comparison of the LQ, 2-populations, induced-repair and accumulated damage increased radio-resistance models (a) for the all dose range (b) and for the low dose domain, in a human tumour cell line (Wouters *et al.*, 1996). Black: LQ, red: 2-populations, blue: induced-repair and green: accumulated damage increased radio-resistance. Black diamonds are experimental data.

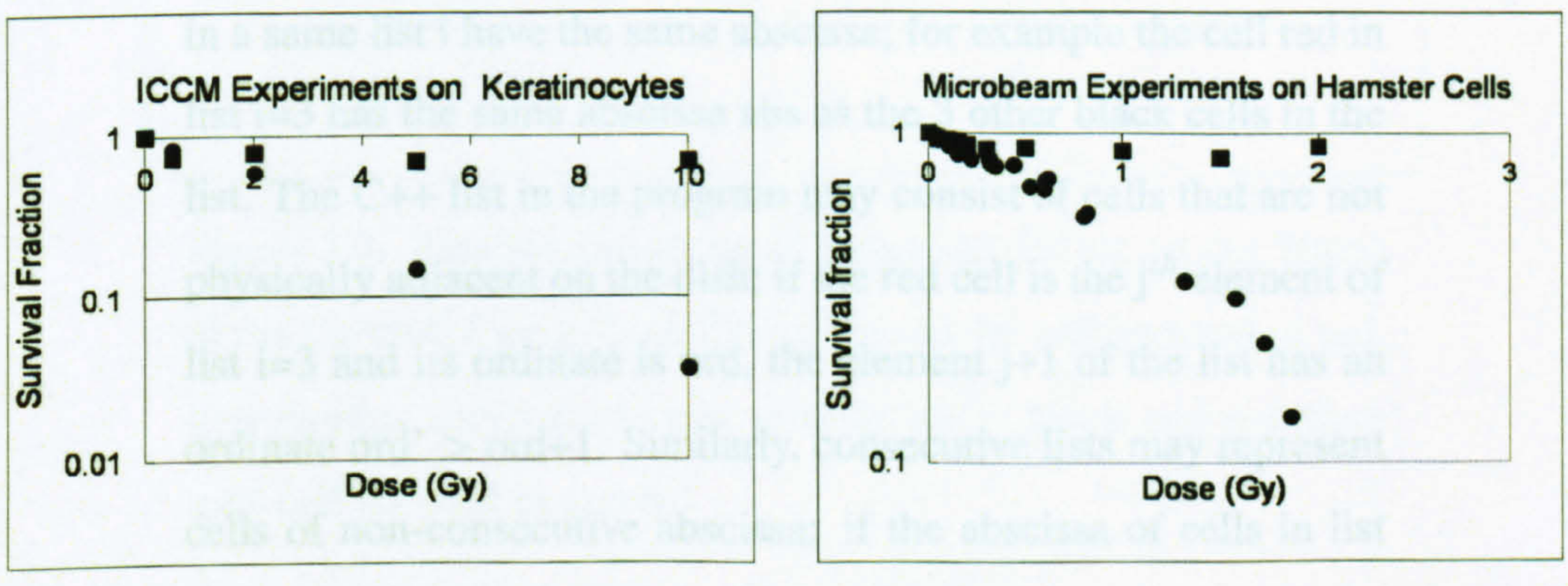

(a) (b)

Figure 2.10: Saturation of the BE: (a) Comparison between survival of keratinocytes directly irradiated (circles) with keratinocytes exposed to ICCM (squares) (Mothersill and Seymour, 1998). (b) Survival fraction in dishes where all hamster cells are C_k X-rays microbeam irradiated (circles) and in dishes where only one cell is irradiated (squares) (Schettino *et al.*, 2005).

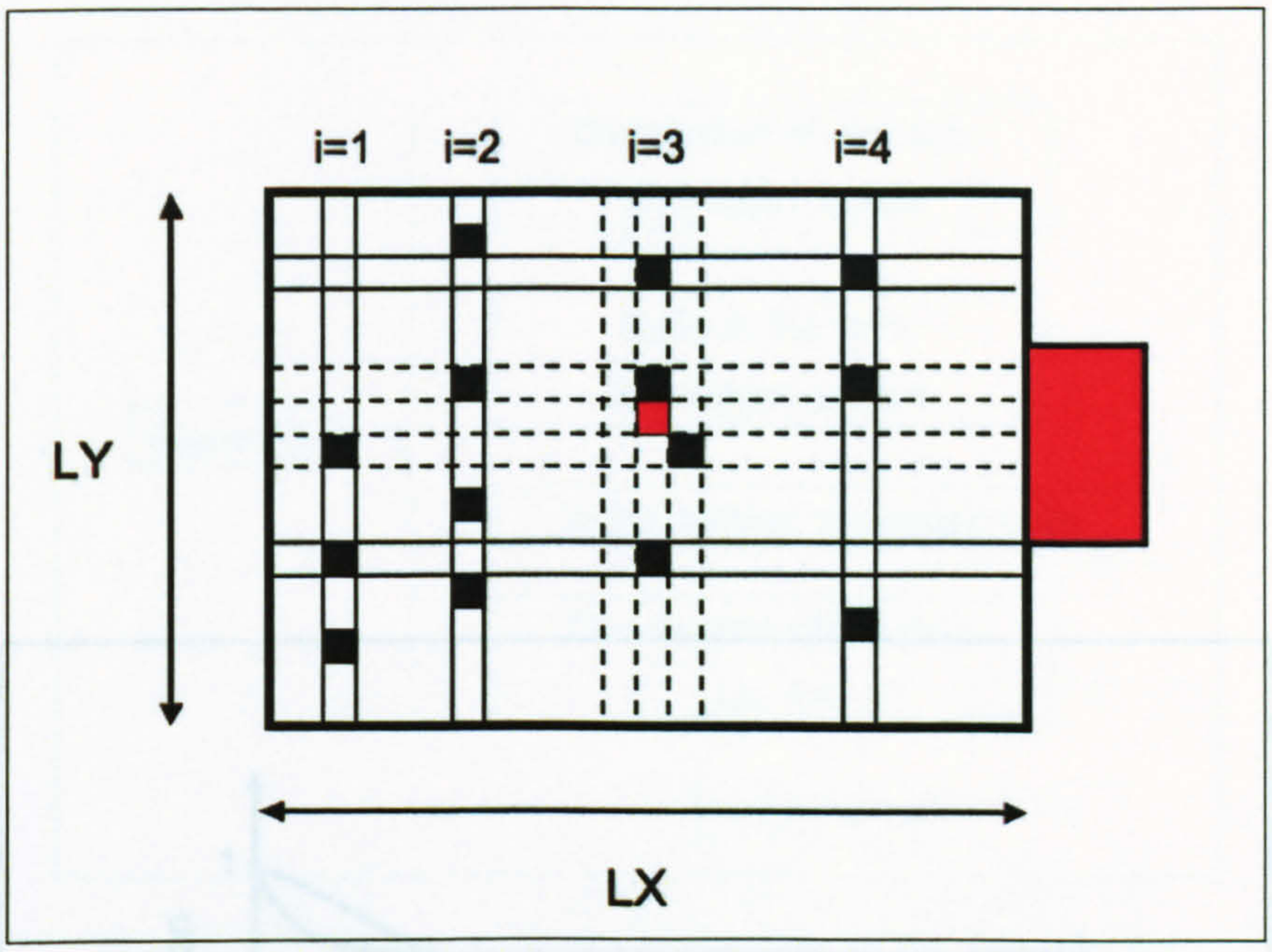

Figure 3.1: Model of the Dish of Cells: Cells are grown in a dish of dimensions LX=LY; the boundaries of the dish are fixed boundaries for the nutrient and the cells. Cells are squared and have 8 neighbours, in vertical, horizontal and diagonal directions. The population of cells is computed by lists in the program. Cells in a same list i have the same abscissa; for example the cell red in list i=3 has the same abscissa abs as the 3 other black cells in the list. The C++ list in the program may consist of cells that are not physically adjacent on the dish; if the red cell is the j^{th} element of list i=3 and its ordinate is ord, the element j+1 of the list has an ordinate ord' > ord+1. Similarly, consecutive lists may represent cells of non-consecutive abscissa: if the abscissa of cells in list i=2 is abs' then abs'<abs-1.

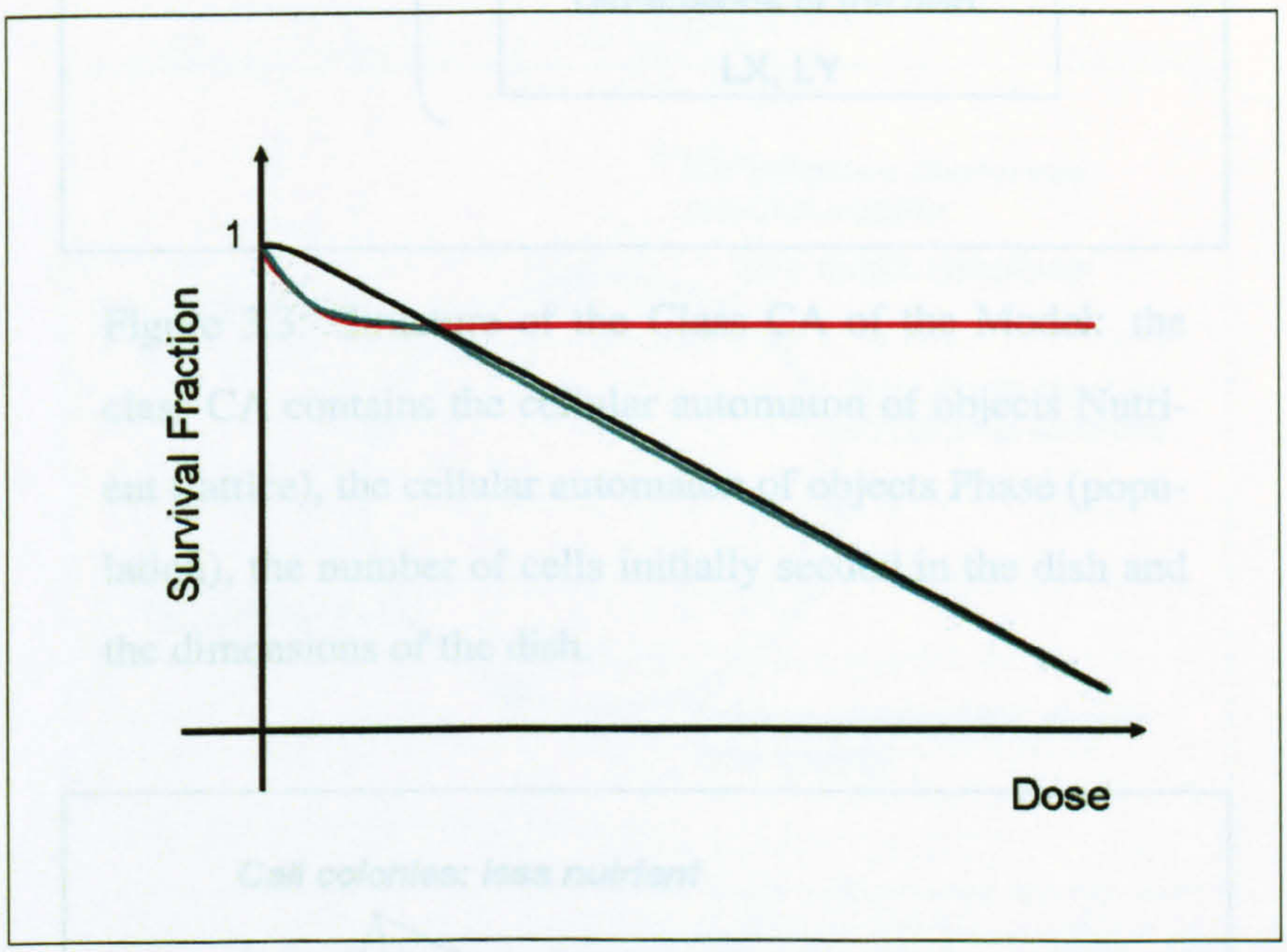

Figure 3.2: Possible Influence of Bystander Effect on the Shape of the Survival Curve: hypothetical bystander cell survival in red, hypothetical survival of cells directly hit in black and resulting total cell survival in green.

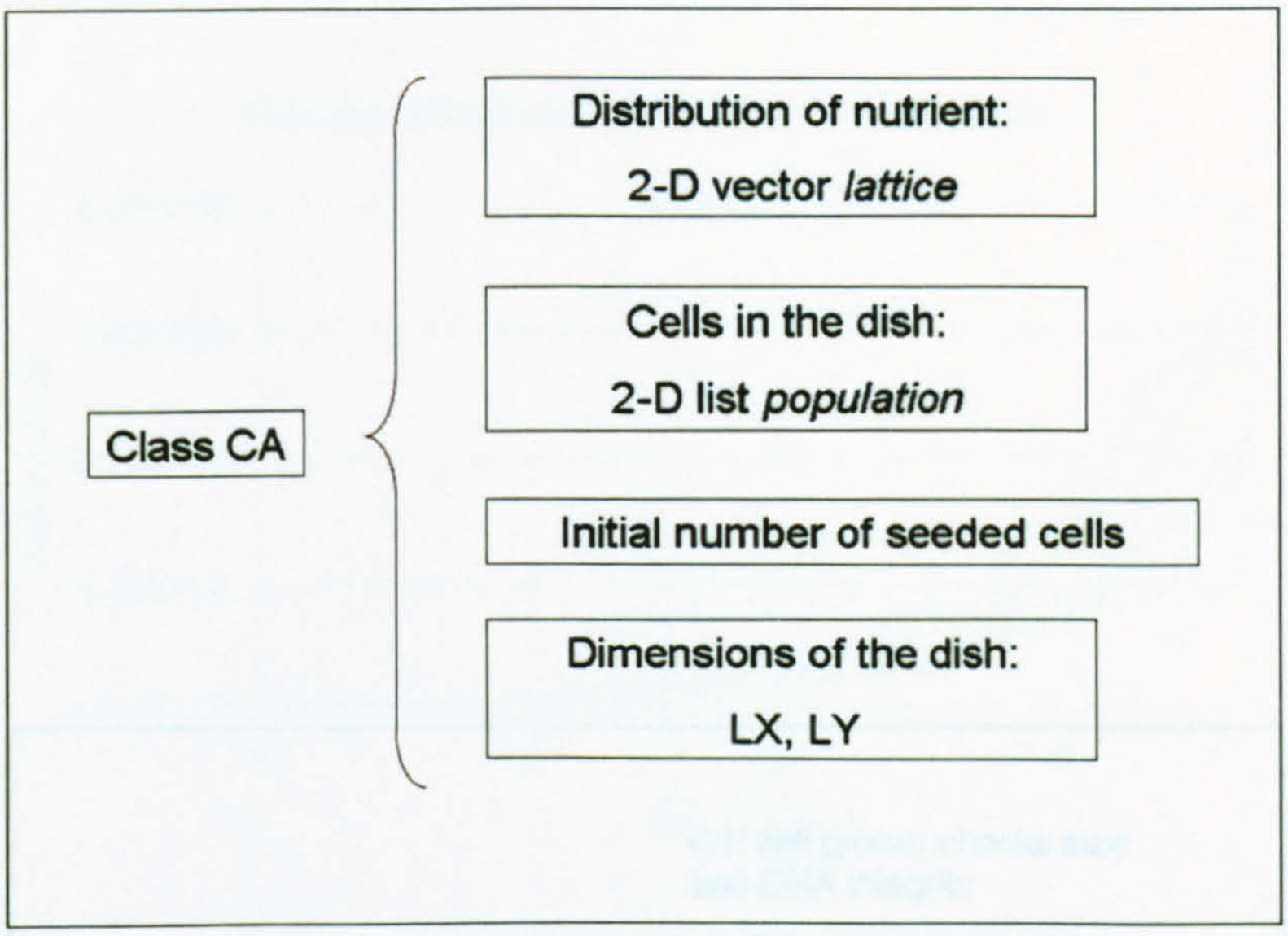

Figure 3.3: Structure of the Class CA of the Model: the class CA contains the cellular automaton of objects Nutrient (lattice), the cellular automaton of objects Phase (population), the number of cells initially seeded in the dish and the dimensions of the dish.

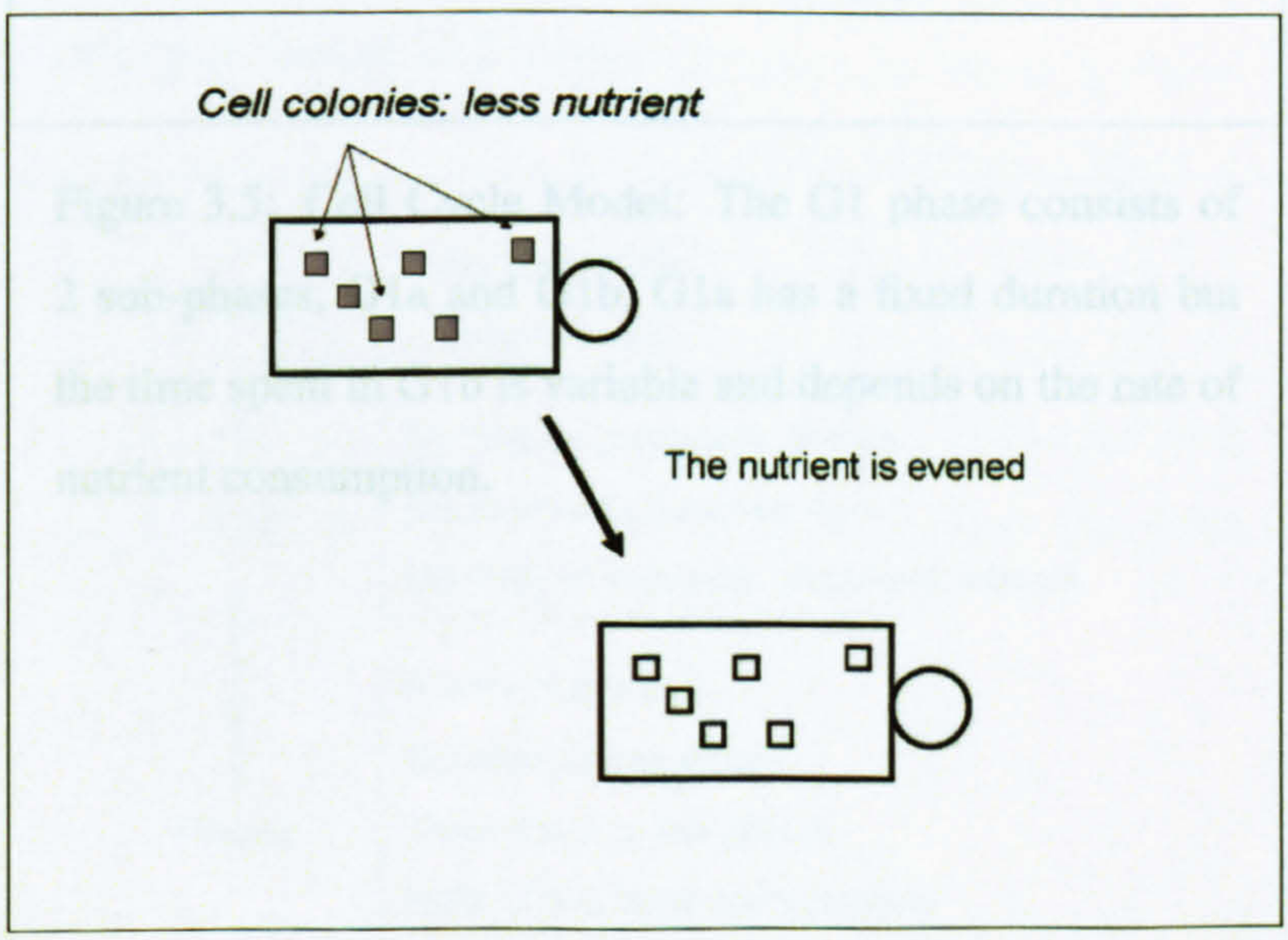

Figure 3.4: Nutrient Diffusion: At each time step, after the cell cycle rules have been applied, and cells have consumed the nutrient, the nutrient is redistributed evenly on the dish.

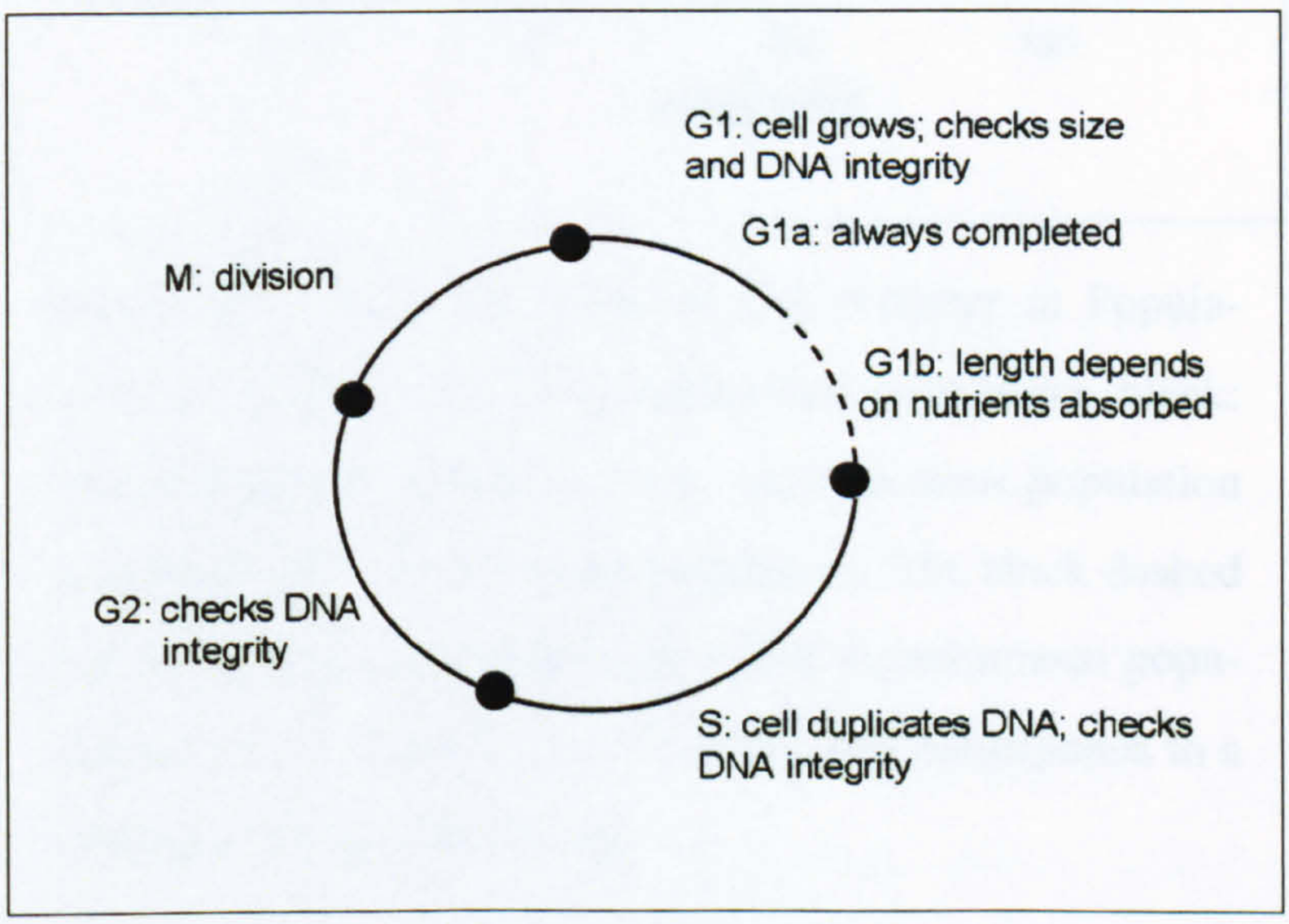

Figure 3.5: Cell Cycle Model: The G1 phase consists of 2 sub-phases, G1a and G1b, G1a has a fixed duration but the time spent in G1b is variable and depends on the rate of nutrient consumption.

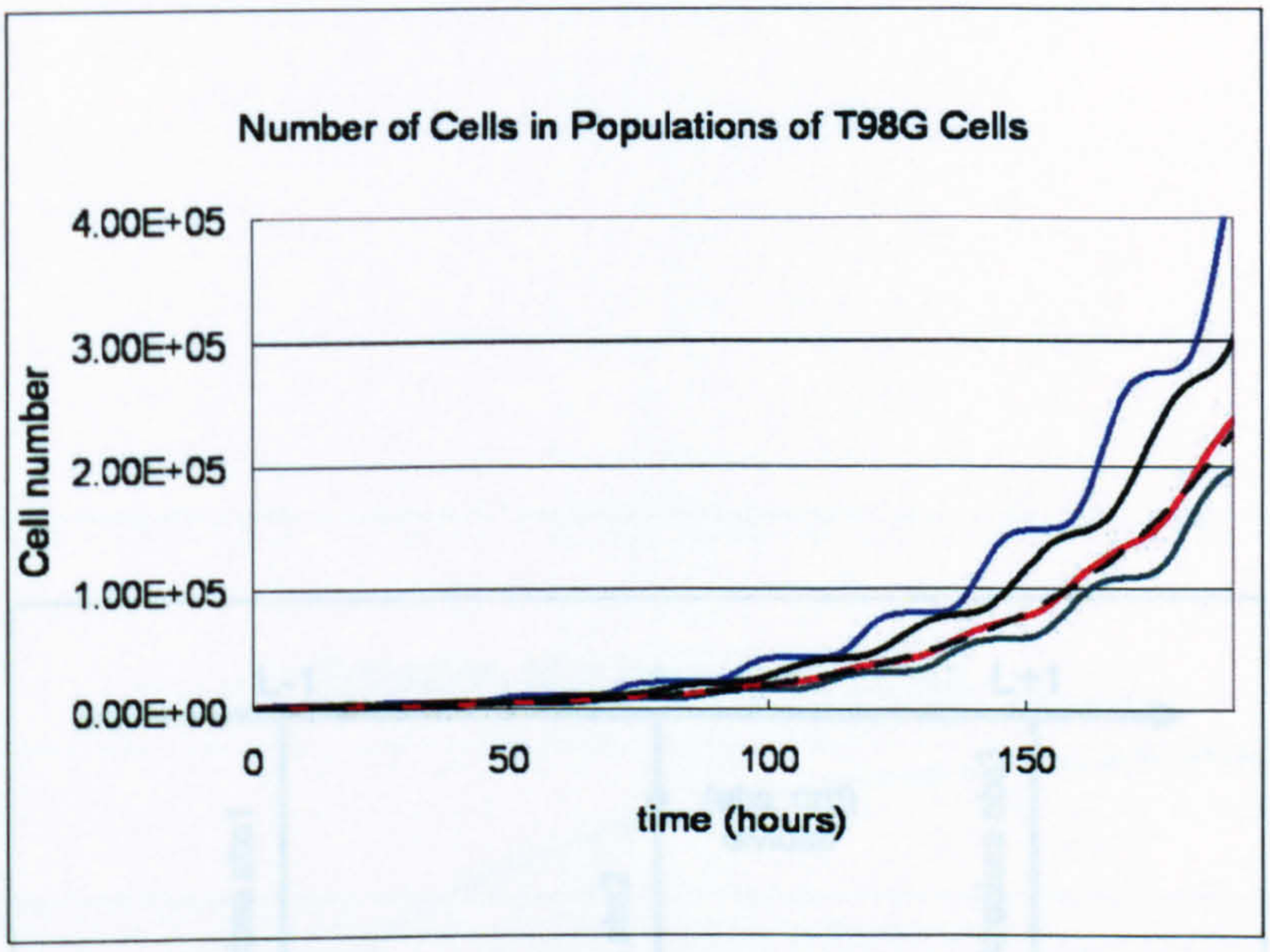

Figure 3.6: Time Evolution of Cell Number in Populations of T98G: blue: G2-synchronised population, black: S-synchronised population, red: asynchronous population and green: G1-synchronised population. The black dashed line is the Excel logarithmic fit to the asynchronous population: $n(t) = 1564.7 \times \exp(1.572t)$, this corresponds to a cell cycle time of 26.5 hours.

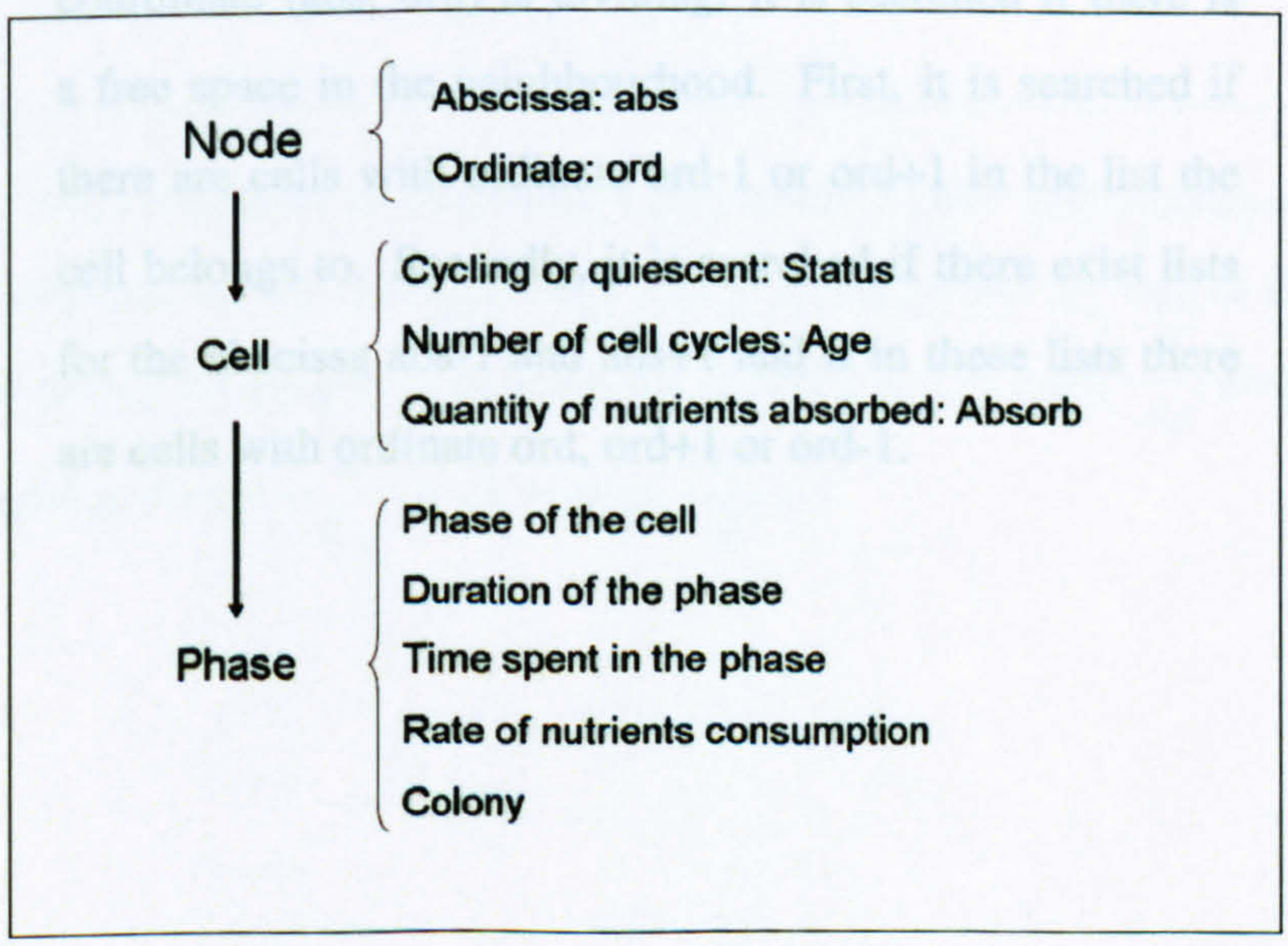

Figure 3.7: Class Derivation of Class Node.

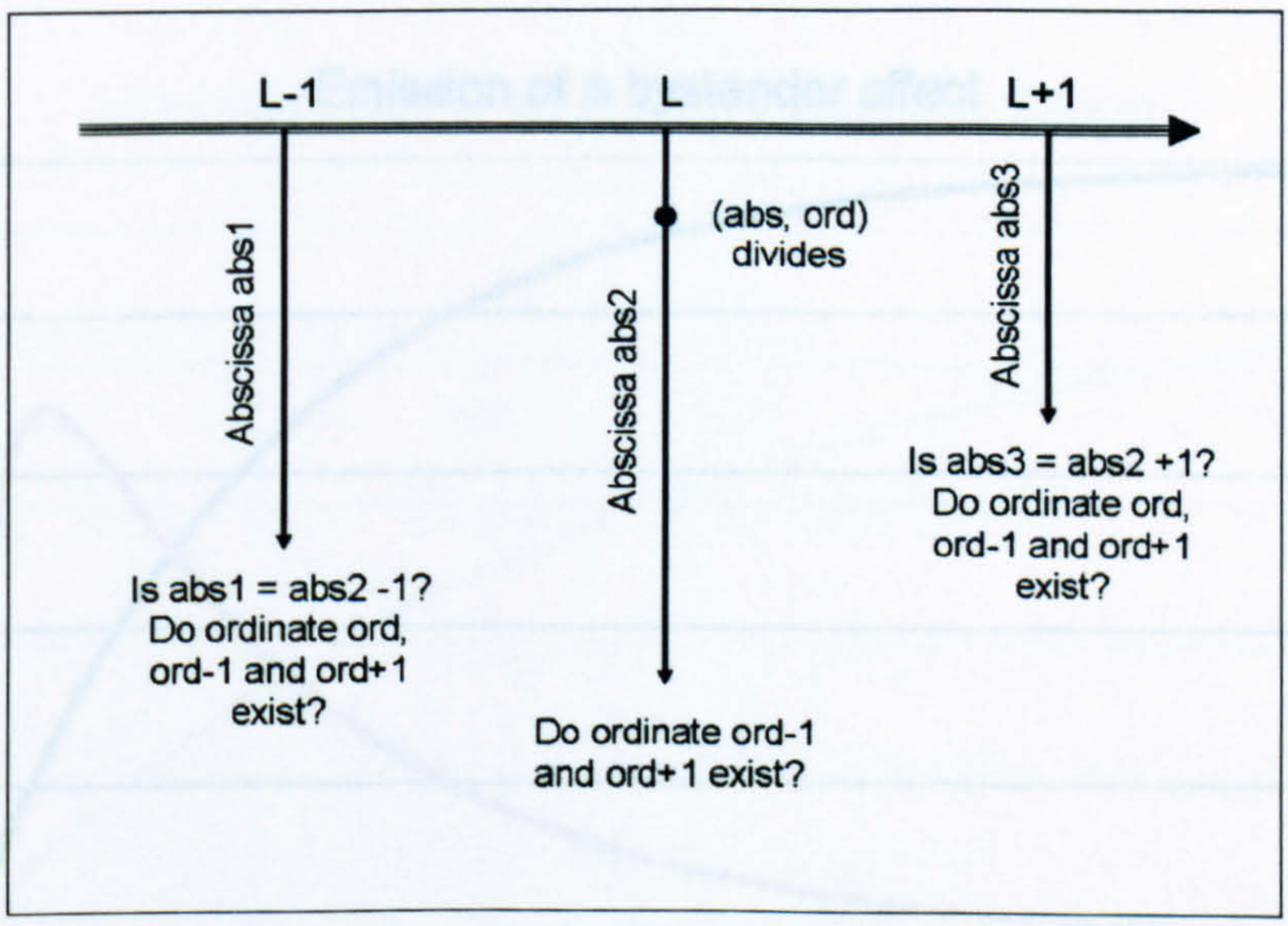

Figure 3.8: Computation of Cell Division: When a cell of coordinate (abs, ord) is dividing, it is searched if there is a free space in the neighbourhood. First, it is searched if there are cells with ordinate ord-1 or ord+1 in the list the cell belongs to. Secondly, it is searched if there exist lists for the abscissa abs-1 and abs+1 and if in these lists there are cells with ordinate ord, ord+1 or ord-1.

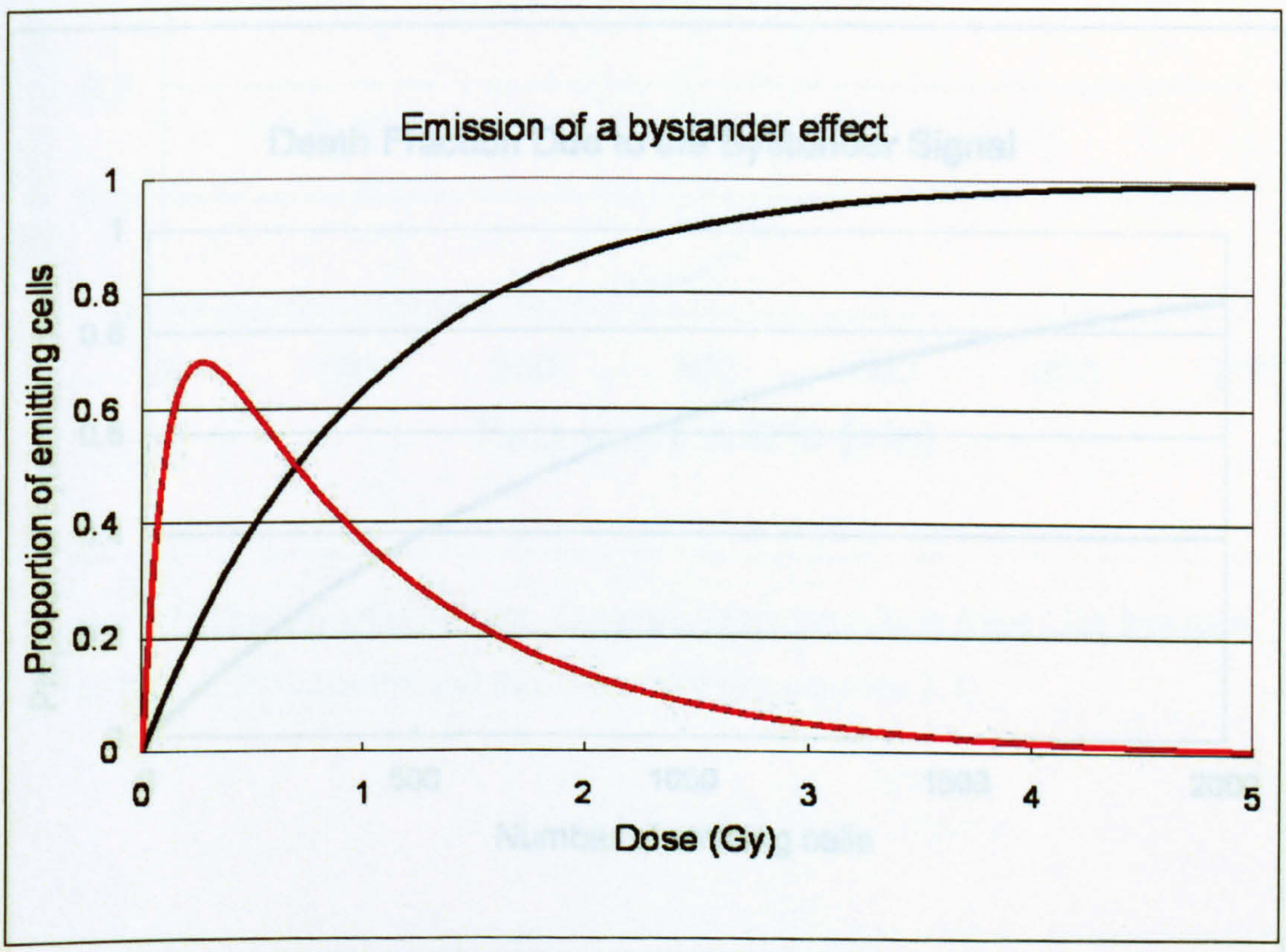

Figure 3.9: Probability of Releasing a Bystander Signal: The emission of the signal depends on the radiation dose and is characterised by one of the two models shown on the graph. In black the model $p = 1 - \exp(-\frac{d}{d_l})$ and in red the model $p = \exp(-\frac{d}{d_m}) \times (1 - \exp(-\frac{d}{d_l}))$.

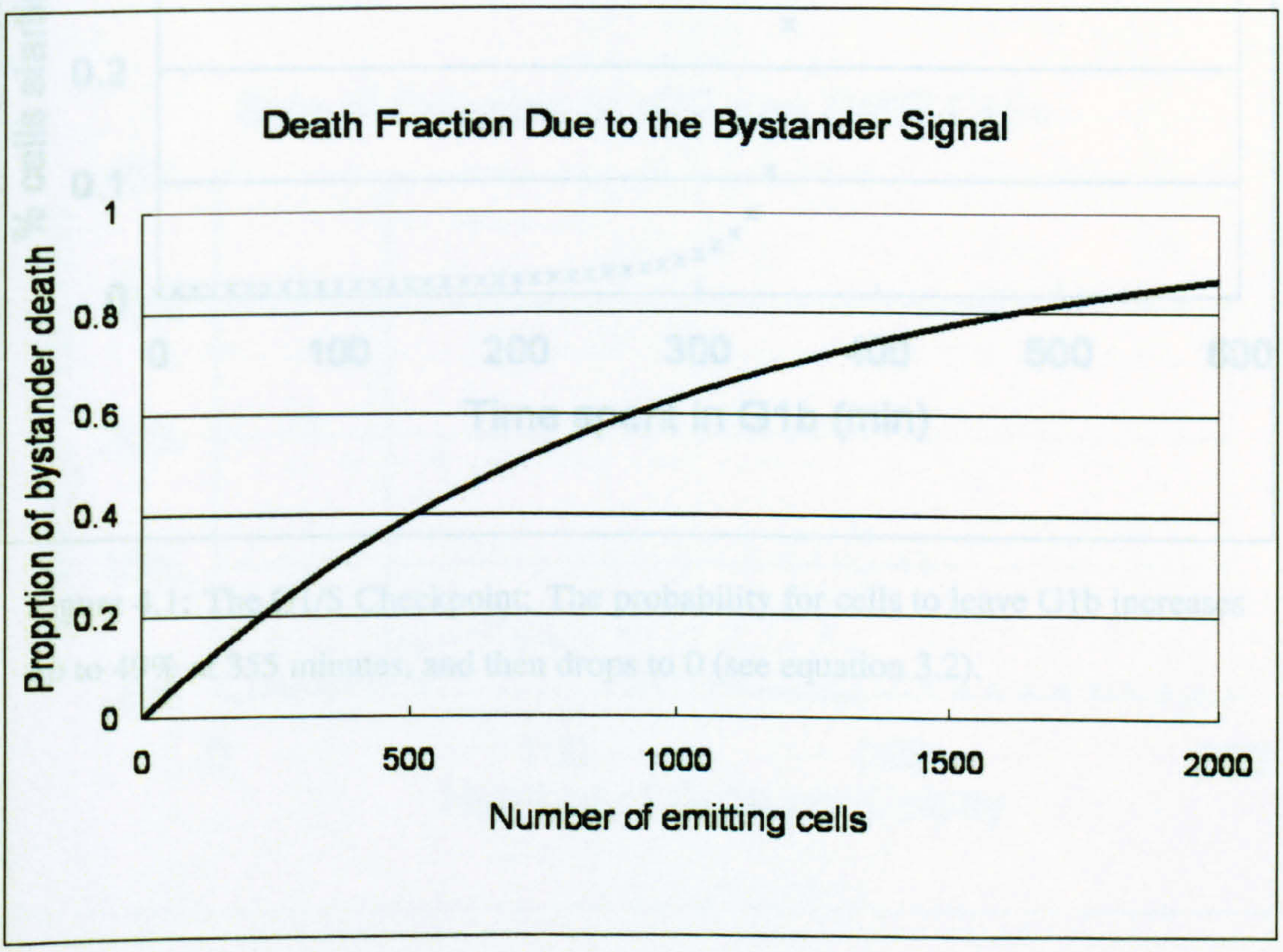

Figure 3.10: Killing Effect of the Bystander Signal: The proportion of bystander cells killed by the signal depends on the quantity of signal (i.e. in the model the number of initially emitting cells). The equation used is of the form

$$\mathrm{DF}_{BS}(c) = \mathrm{BS\_SF}_{max} \times (1 - \exp(-\frac{c(t)}{\mathrm{BS\_SF}})).$$

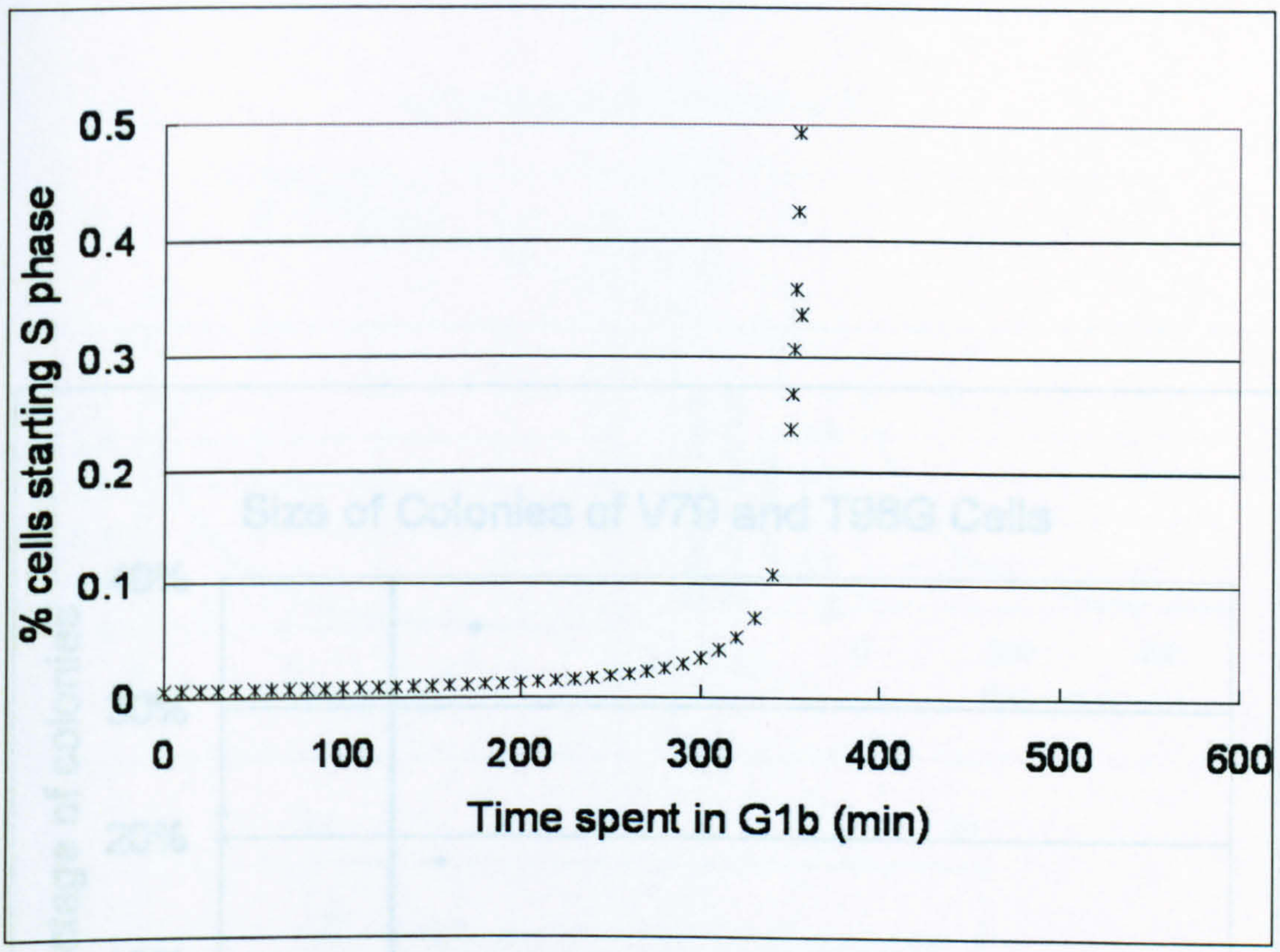

Figure 4.1: The G1/S Checkpoint: The probability for cells to leave G1b increases up to 49% at 355 minutes, and then drops to 0 (see equation 3.2).

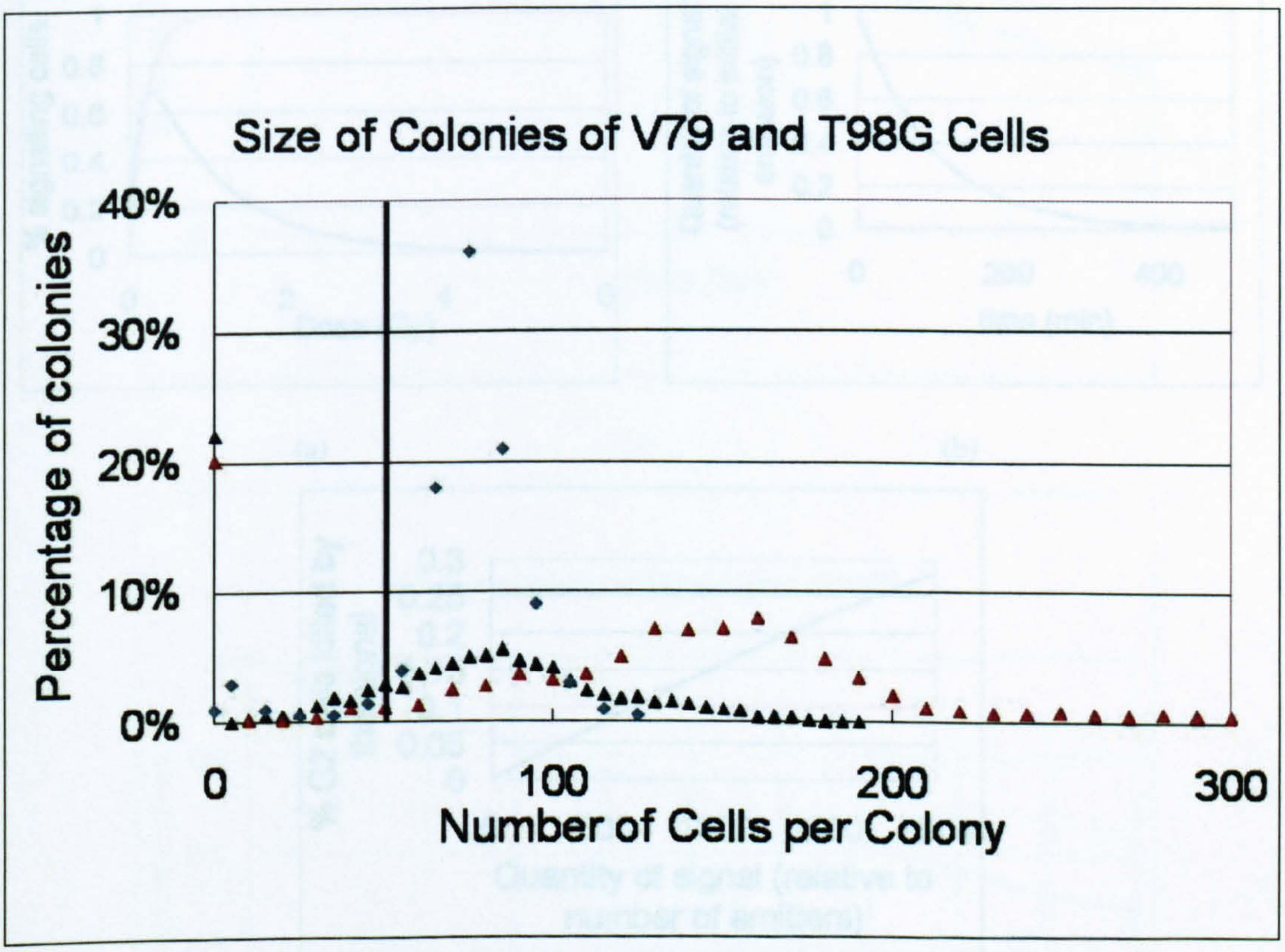

Figure 4.2: Size Distribution of Colonies of V79 Cells: The parameter S_{max} is 18 nmol/cell and the length of G1b is 600 minutes. Green diamonds are experimental data for V79 (Schettino *et al.*, 2001), black triangles are the results of the simulation for V79 and the brown triangles are the results of the simulation for T98G. The black vertical line shows the critical counting limit of 50 cells/colony.

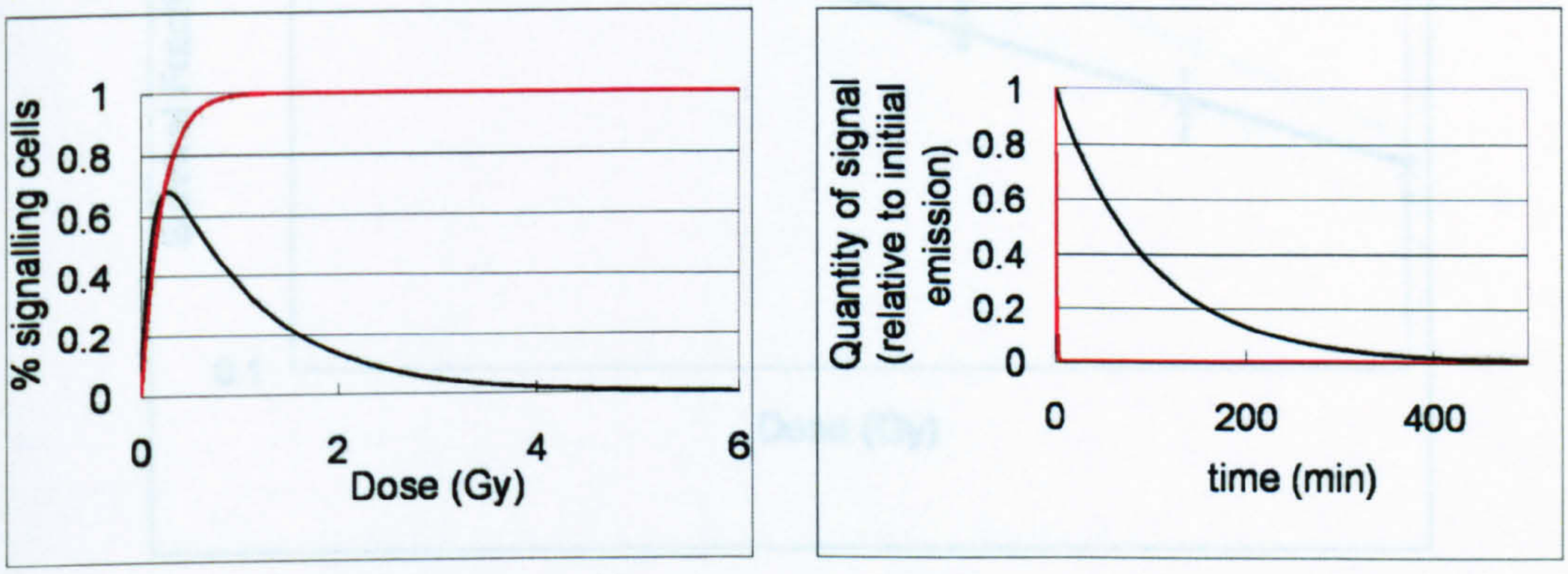

(a)

(b)

(c)

Figure 4.3: The Bystander Effect in V79: (a) Proportion of irradiated cells releasing the bystander signal for increasing dose (b) decay of the signal with time (c) proportion of G2 cells being killed by the signal for increasing signal quantity. The curves used in Model 1 are shown in black and the ones used in Model 2 in red.

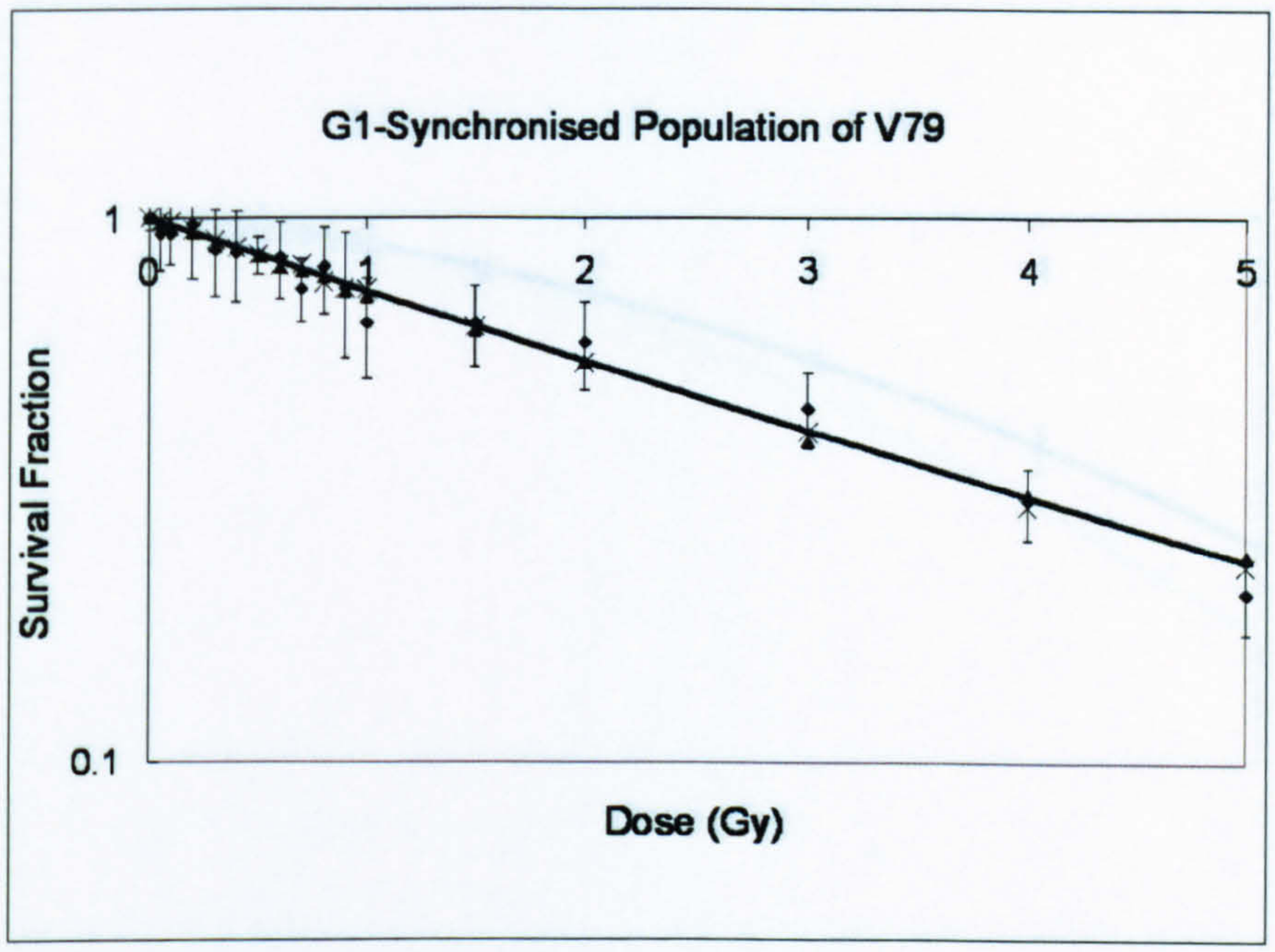

(a)

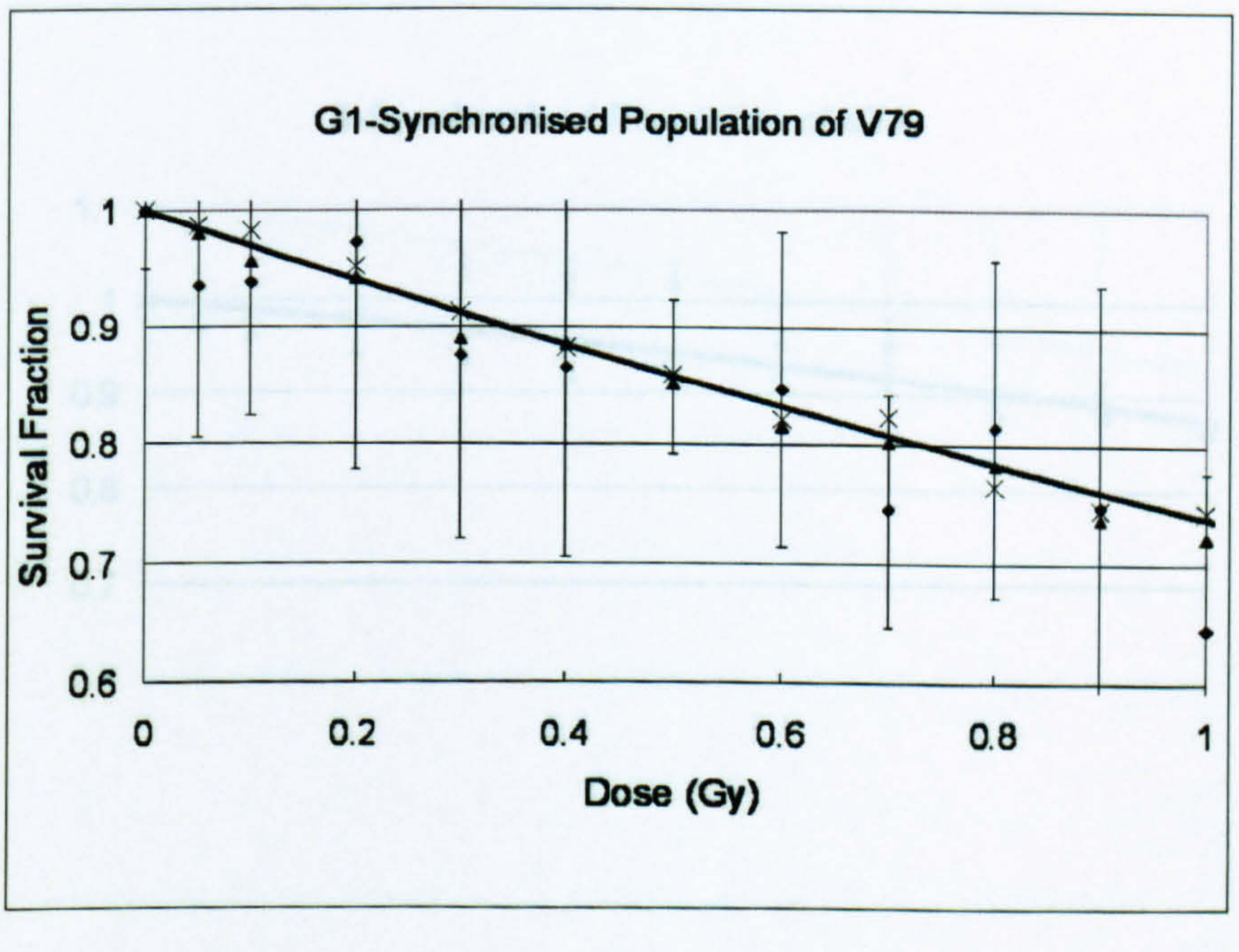

(b)

Figure 4.4: Survival Fraction of G1-Synchronised V79 Cells to 250 kVp X-rays: Dose domain (a) $[0, 5Gy]$ and (b) $[0, 1Gy]$. Diamonds are the experimental data, triangles are the simulations from Model 1, crosses are the simulations from Model 2 and the line is the LQ equation fitted to the high dose data (>1 Gy) only. Experimental error bars are shown.

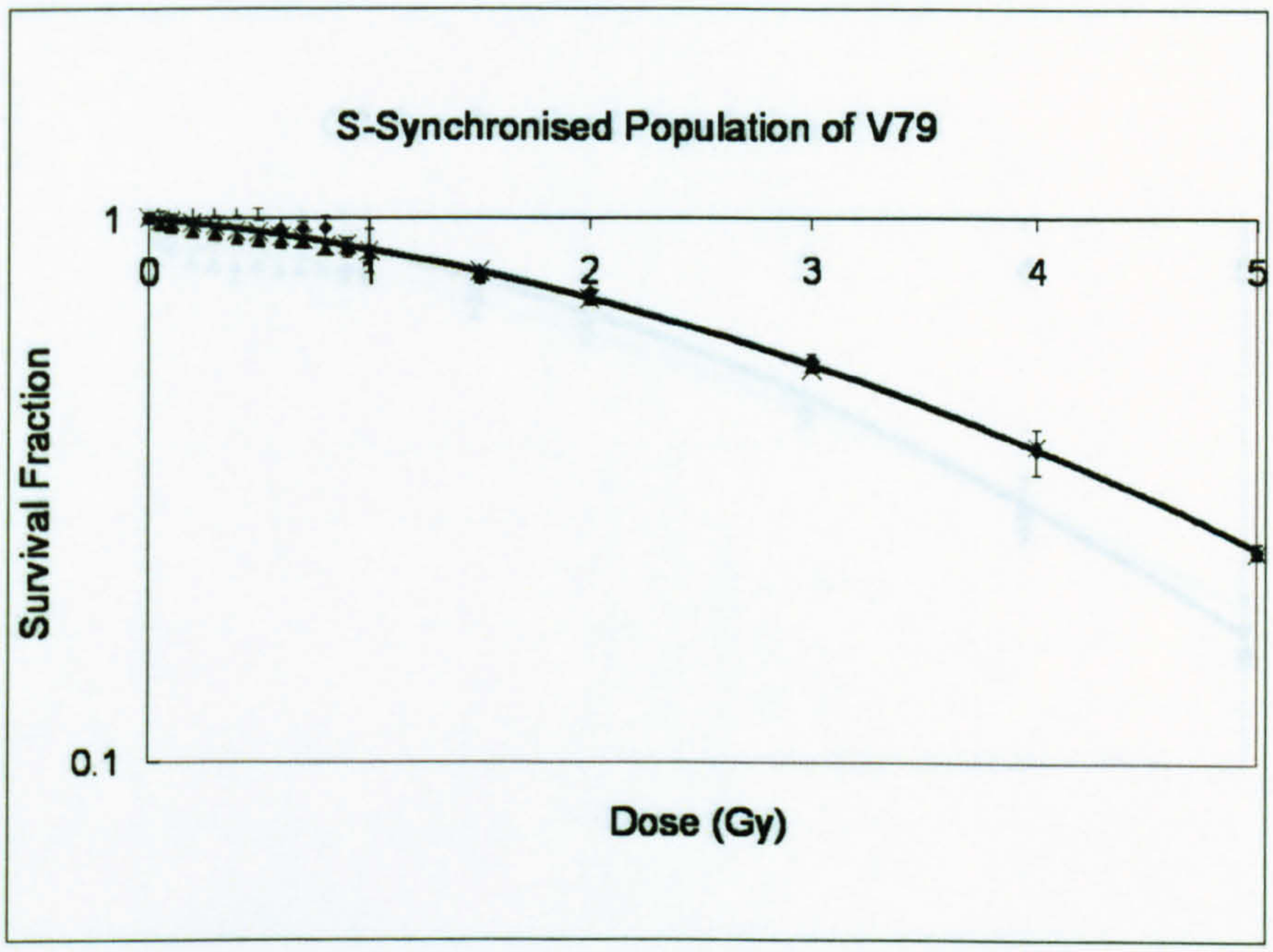

(a)

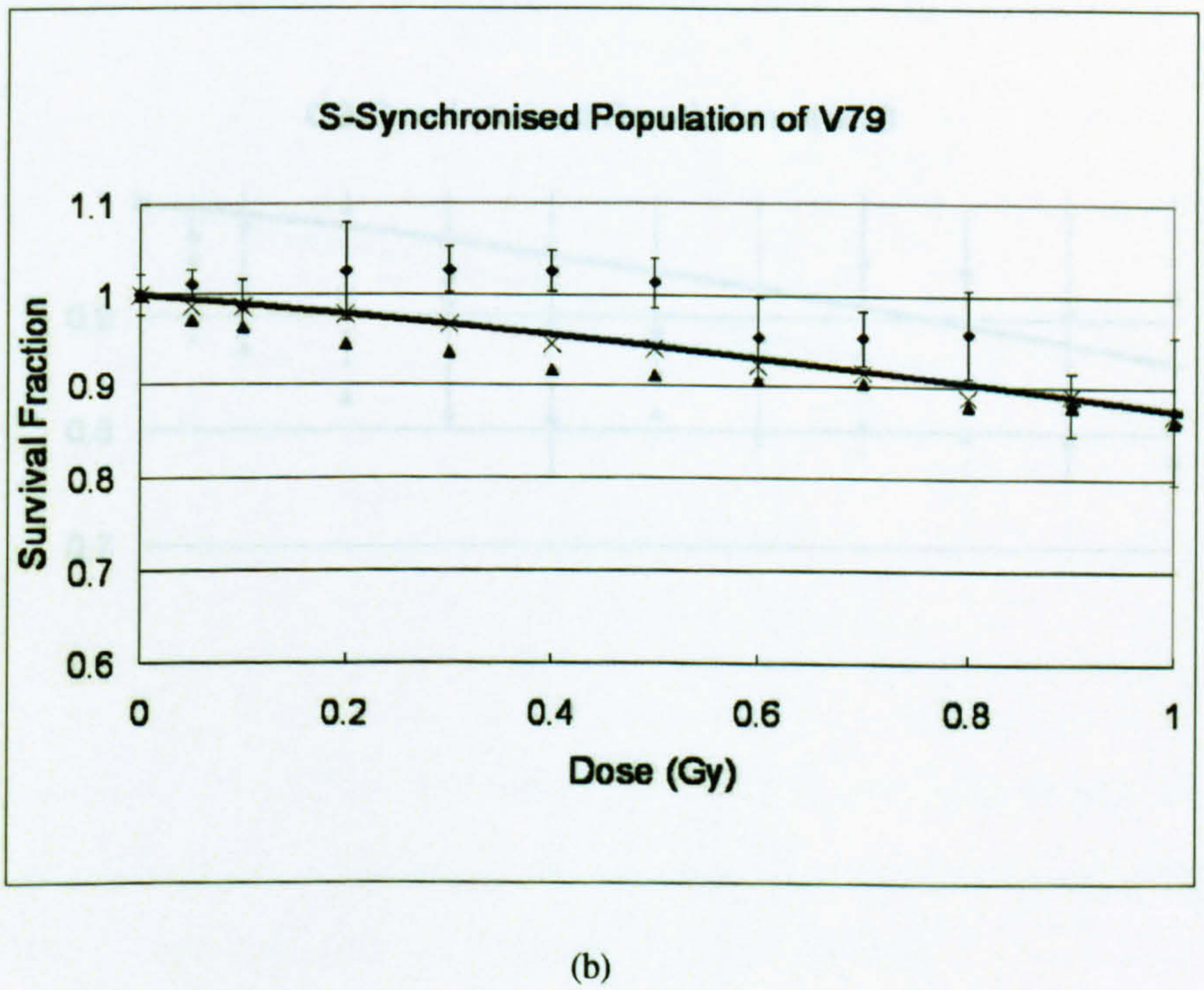

(b)

Figure 4.5: Survival Fraction of S-Synchronised V79 Cells to 250 kVp X-rays: Dose domain (a) $[0, 5Gy]$ and (b) $[0, 1Gy]$. Diamonds are the experimental data, triangles are the simulations from Model 1, crosses are the simulations from Model 2 and the line is the LQ equation fitted to the high dose data (>1 Gy) only. Experimental error bars are shown.

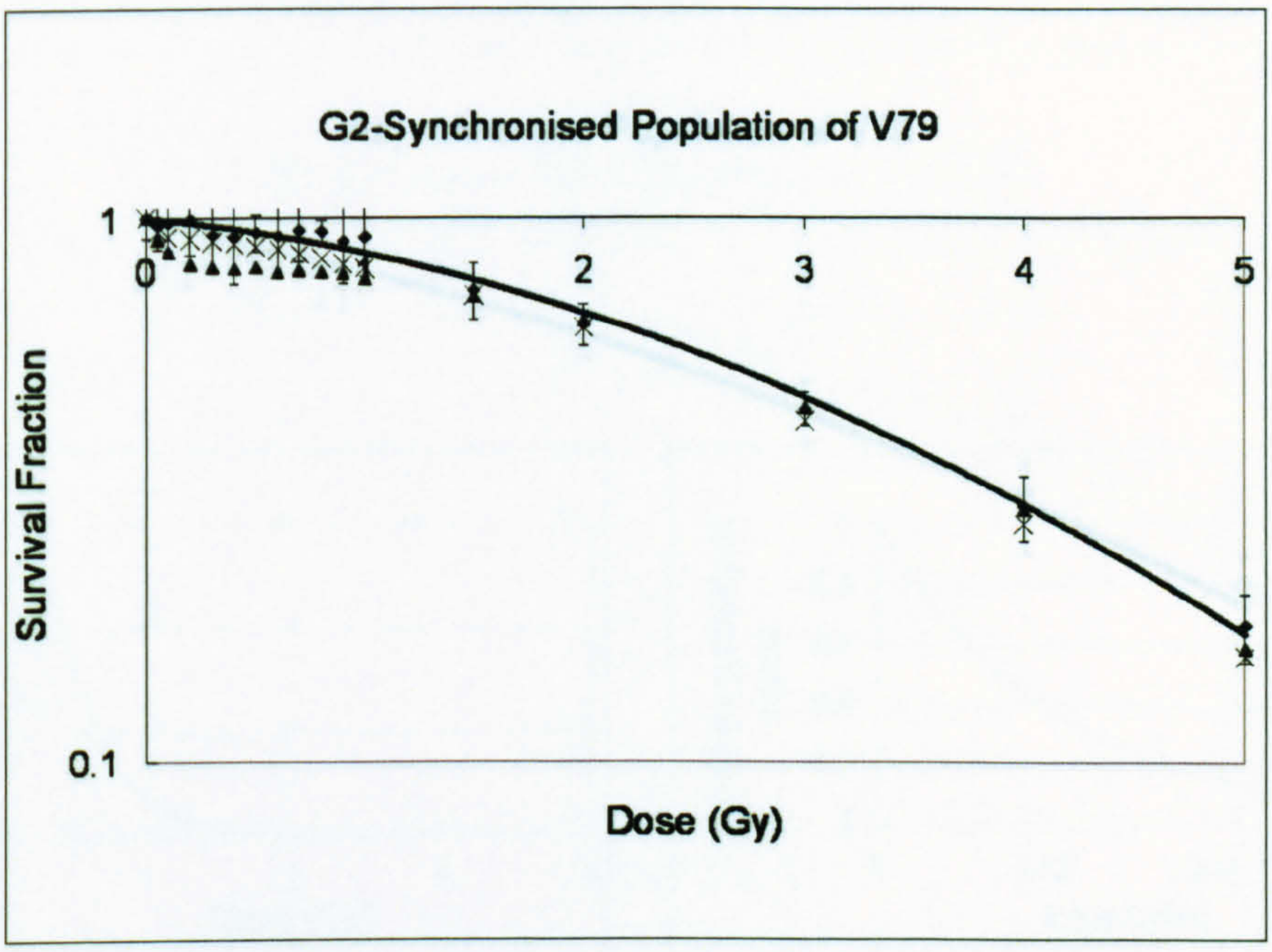

(a)

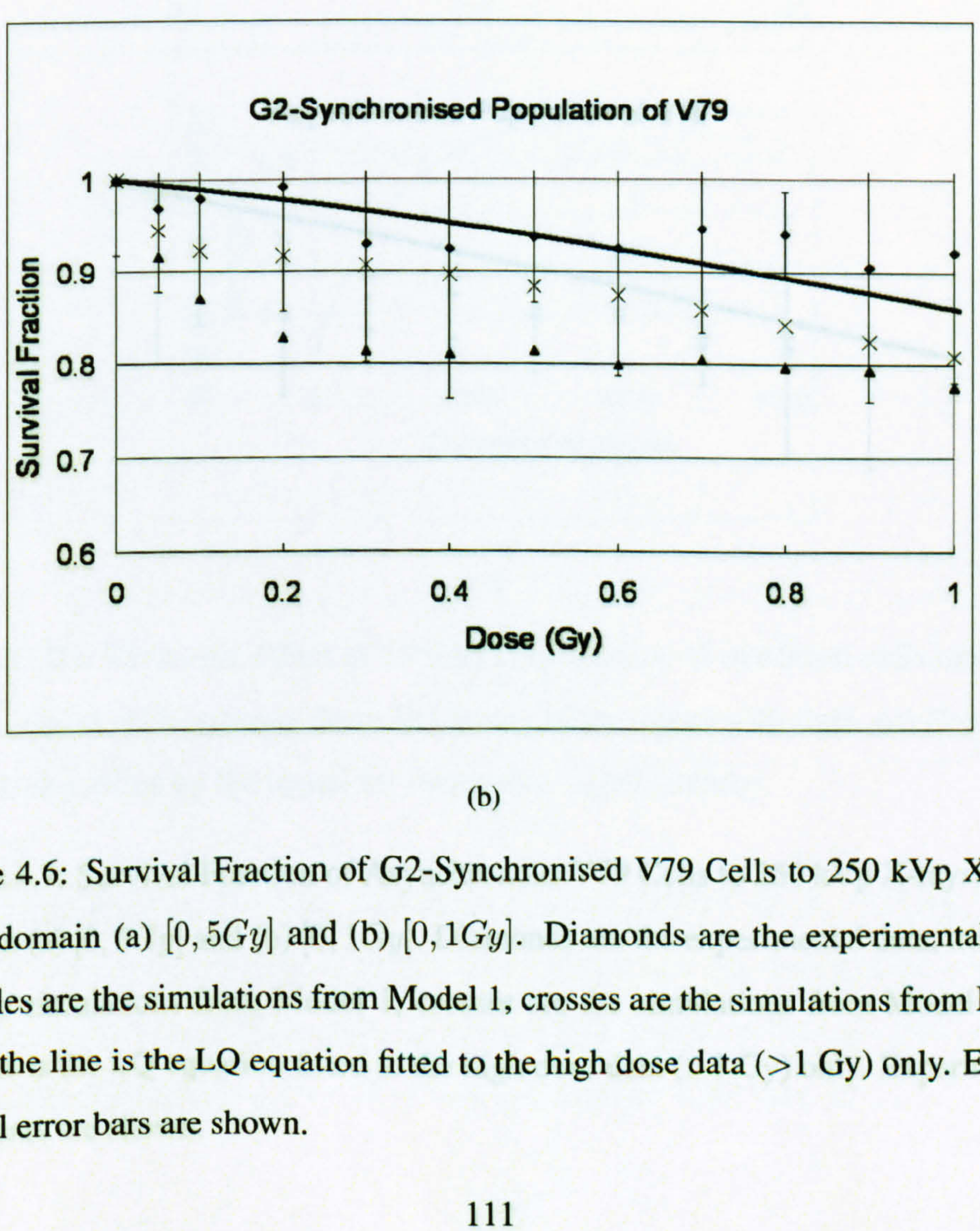

(b)

Figure 4.6: Survival Fraction of G2-Synchronised V79 Cells to 250 kVp X-rays: Dose domain (a) $[0, 5Gy]$ and (b) $[0, 1Gy]$. Diamonds are the experimental data, triangles are the simulations from Model 1, crosses are the simulations from Model 2 and the line is the LQ equation fitted to the high dose data ($>$1 Gy) only. Experimental error bars are shown.

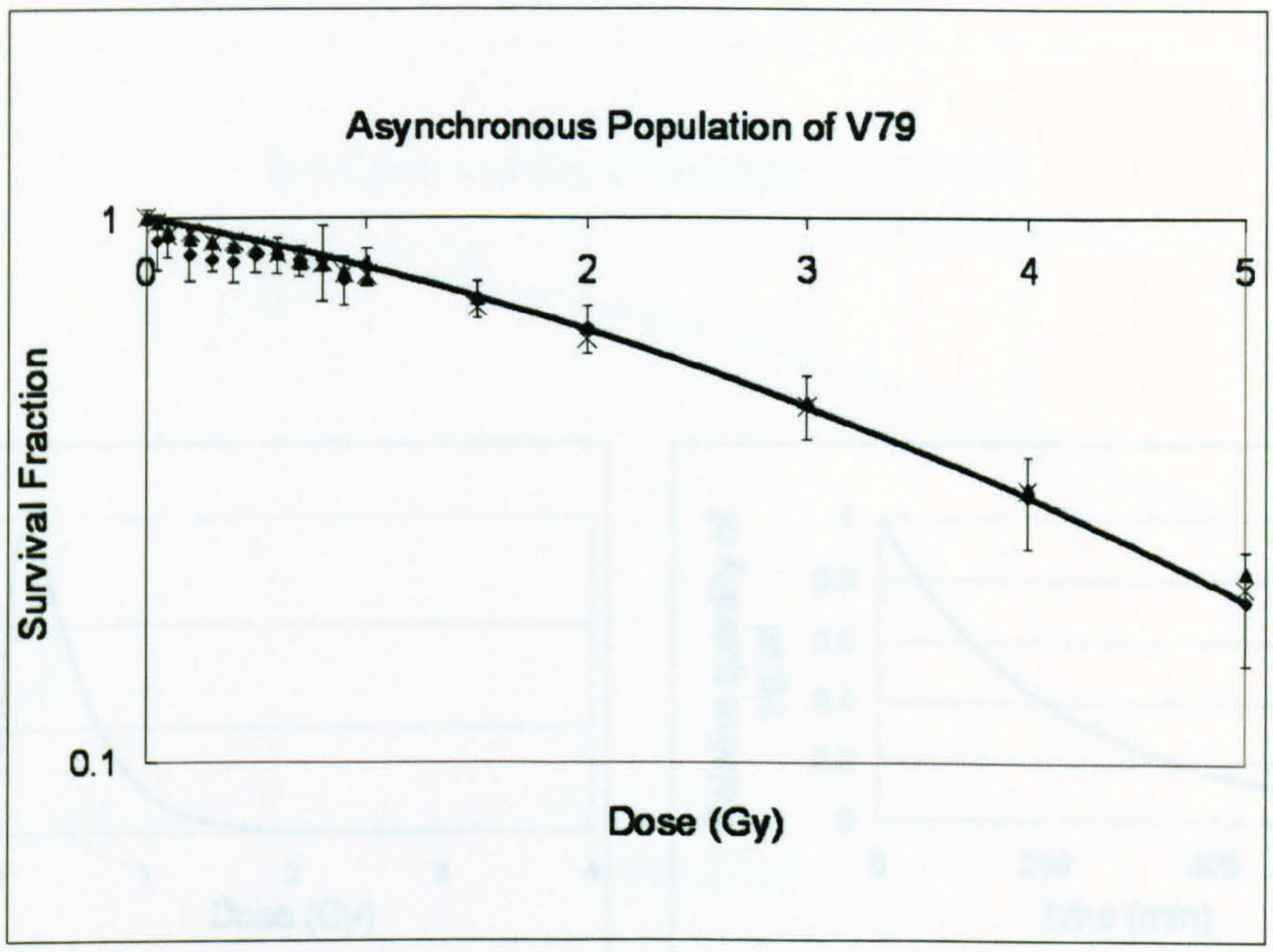

(a)

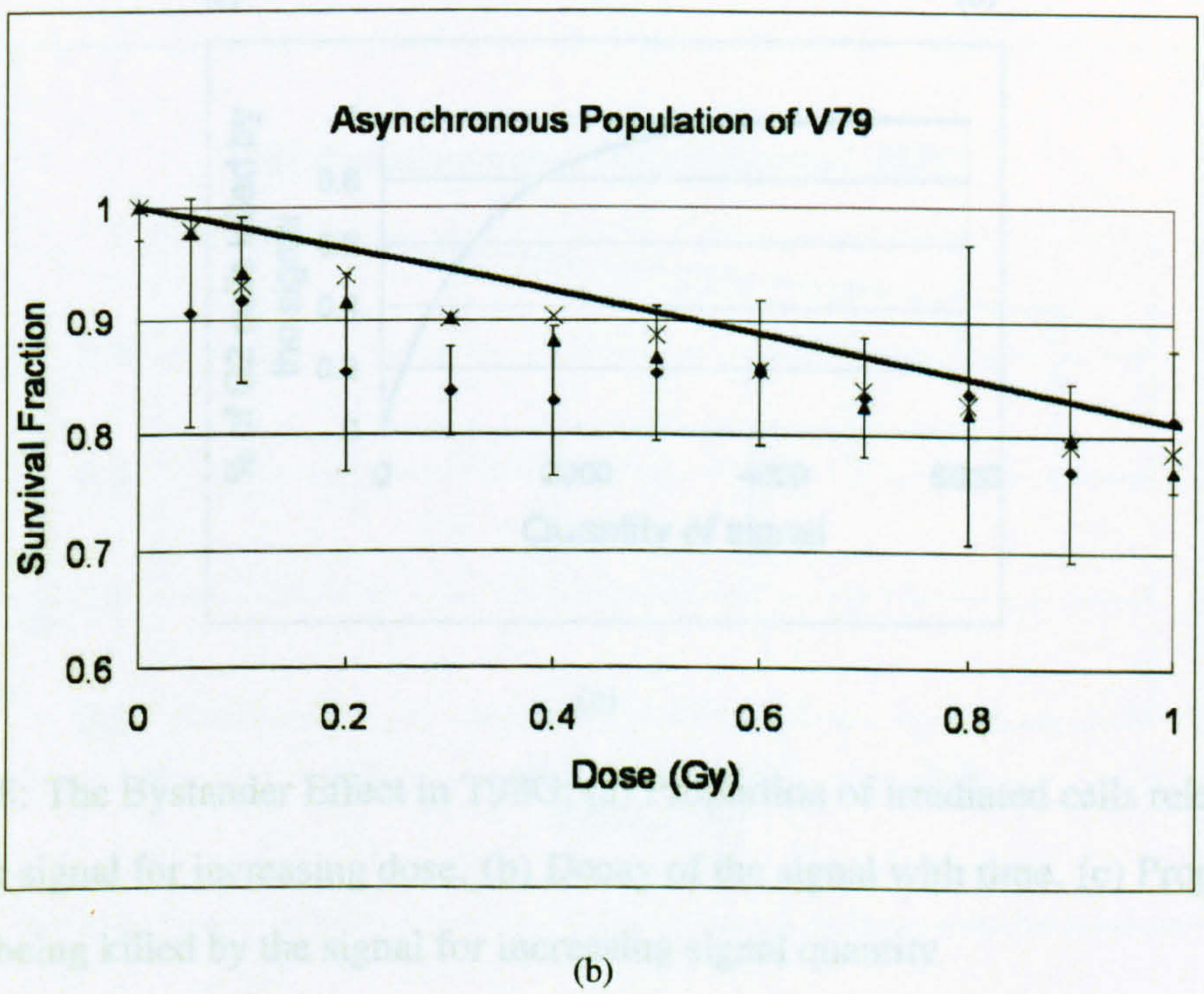

(b)

Figure 4.7: Survival Fraction of Asynchronous V79 Cells to 250 kVp X-rays: Dose domain (a) $[0, 5Gy]$ and (b) $[0, 1Gy]$. Diamonds are the experimental data, triangles are the simulations from Model 1, crosses are the simulations from Model 2 and the line is the LQ equation fitted to the high dose data (>1 Gy) only. Experimental error bars are shown.

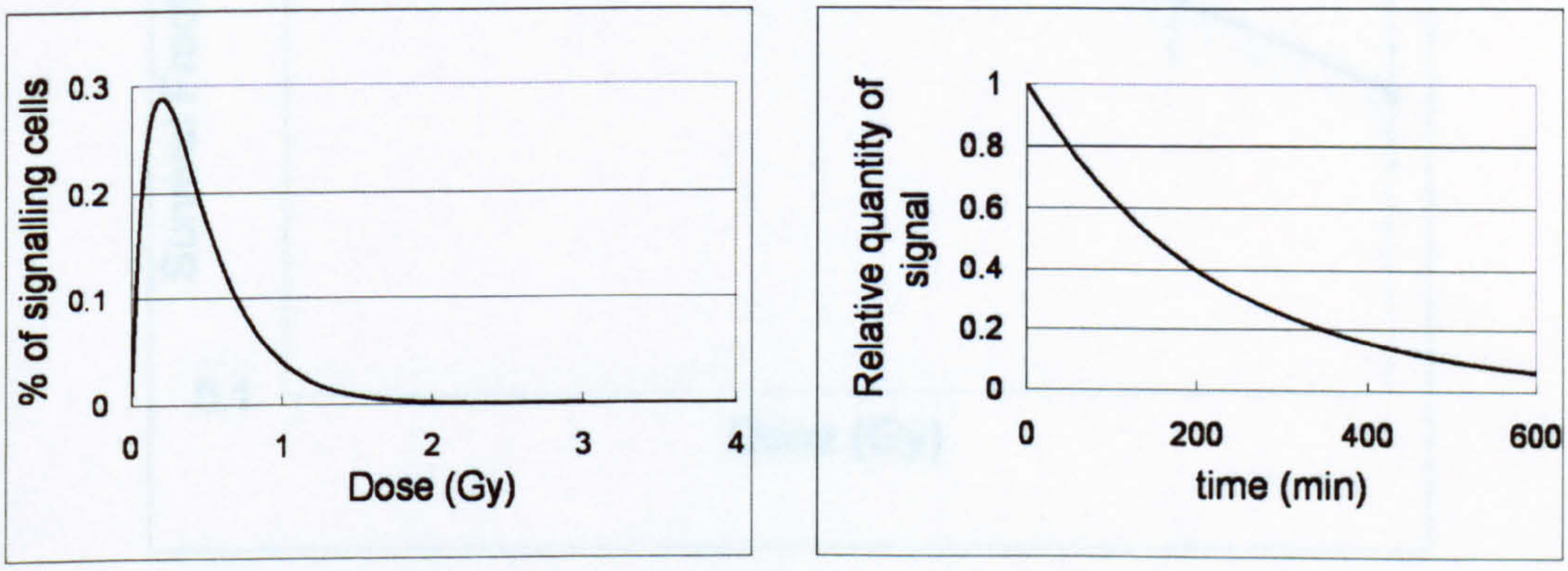

(a)

(b)

(c)

Figure 4.8: The Bystander Effect in T98G: (a) Proportion of irradiated cells releasing the bystander signal for increasing dose. (b) Decay of the signal with time. (c) Proportion of G2 cells being killed by the signal for increasing signal quantity.

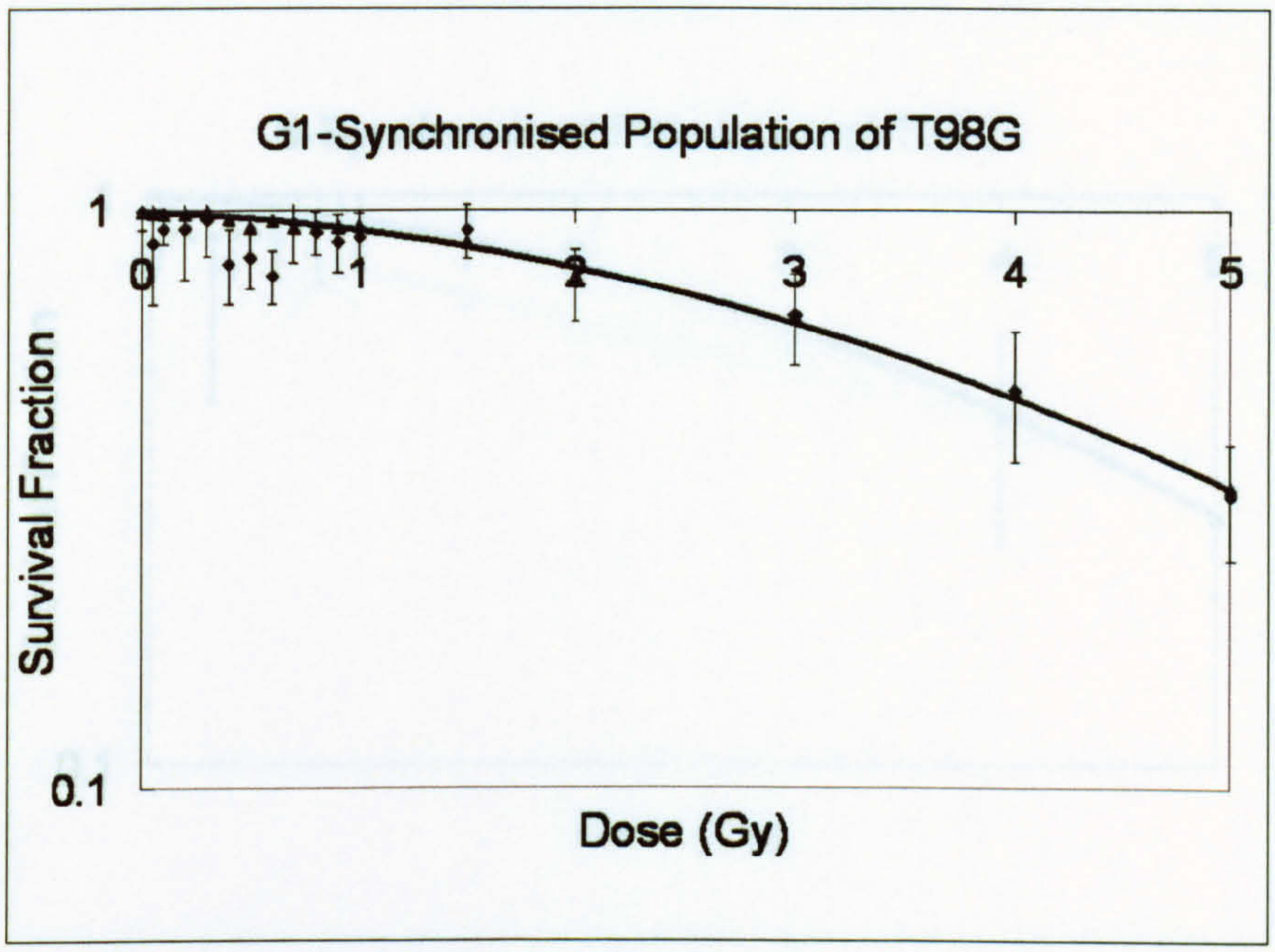

(a)

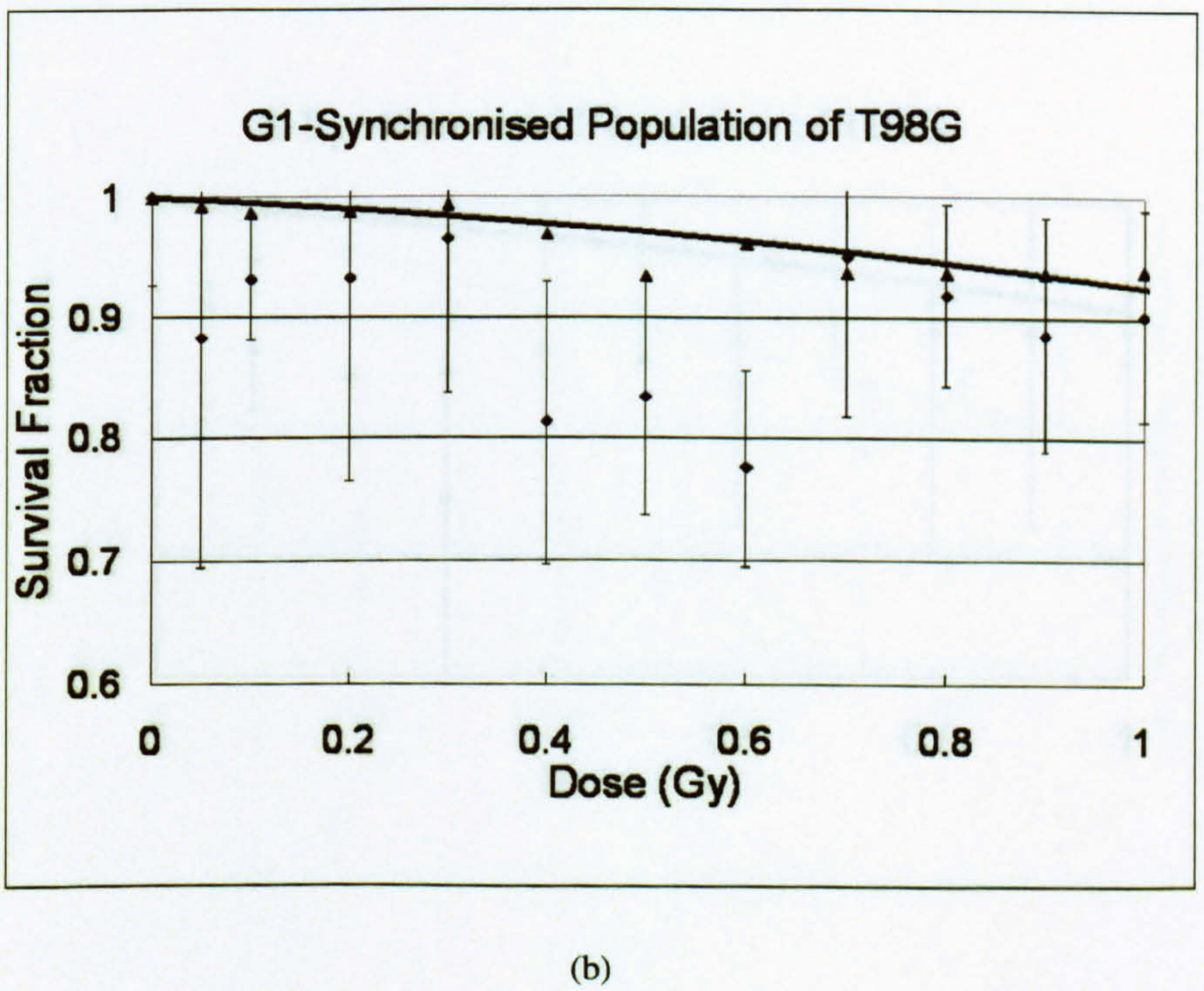

(b)

Figure 4.9: Survival Fraction of G1-Synchronised T98G Cells to 250 kVp X-rays: Dose domain (a) $[0, 5Gy]$ and (b) $[0, 1Gy]$. Diamonds are the experimental data, triangles are the simulations from the model, and the line is the LQ equation fitted to the high dose data (>1 Gy). Experimental standard errors are shown.

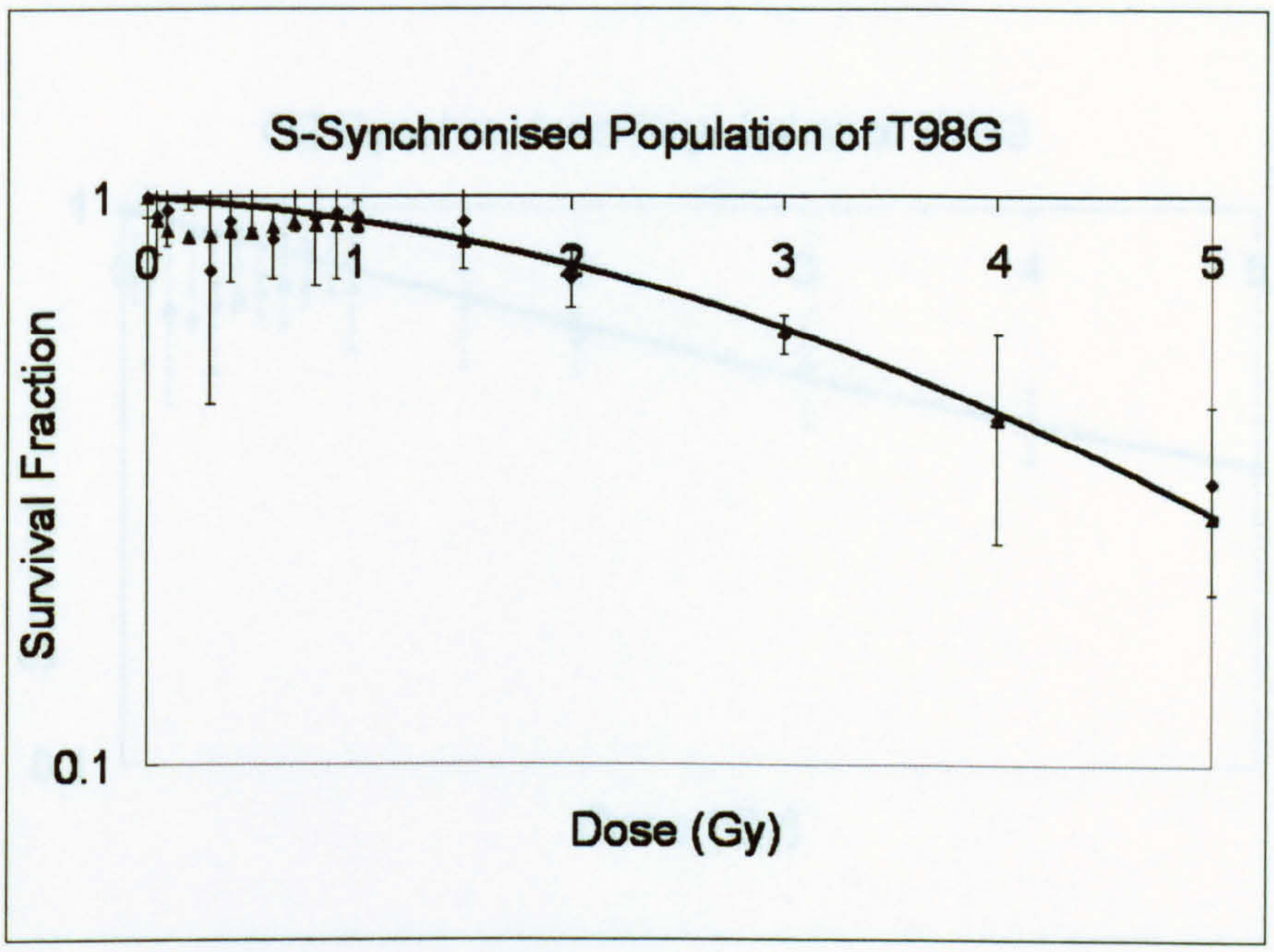

(a)

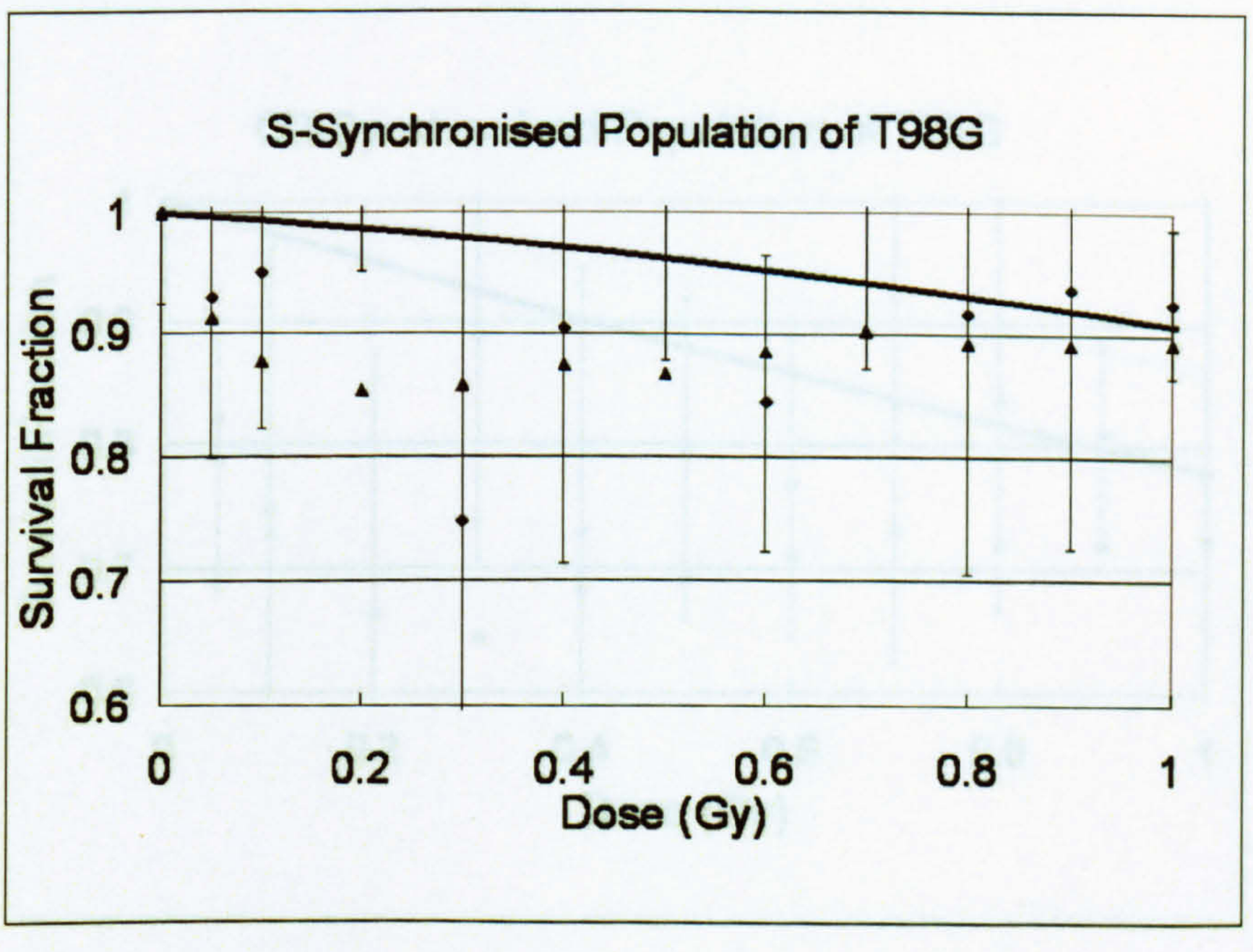

(b)

Figure 4.10: Survival Fraction of S-Synchronised T98G Cells to 250 kVp X-rays: Dose domain (a) $[0, 5Gy]$ and (b) $[0, 1Gy]$. Diamonds are the experimental data, triangles are the simulations from the model, and the line is the LQ equation fitted to the high dose data (>1 Gy). Experimental standard errors are shown.

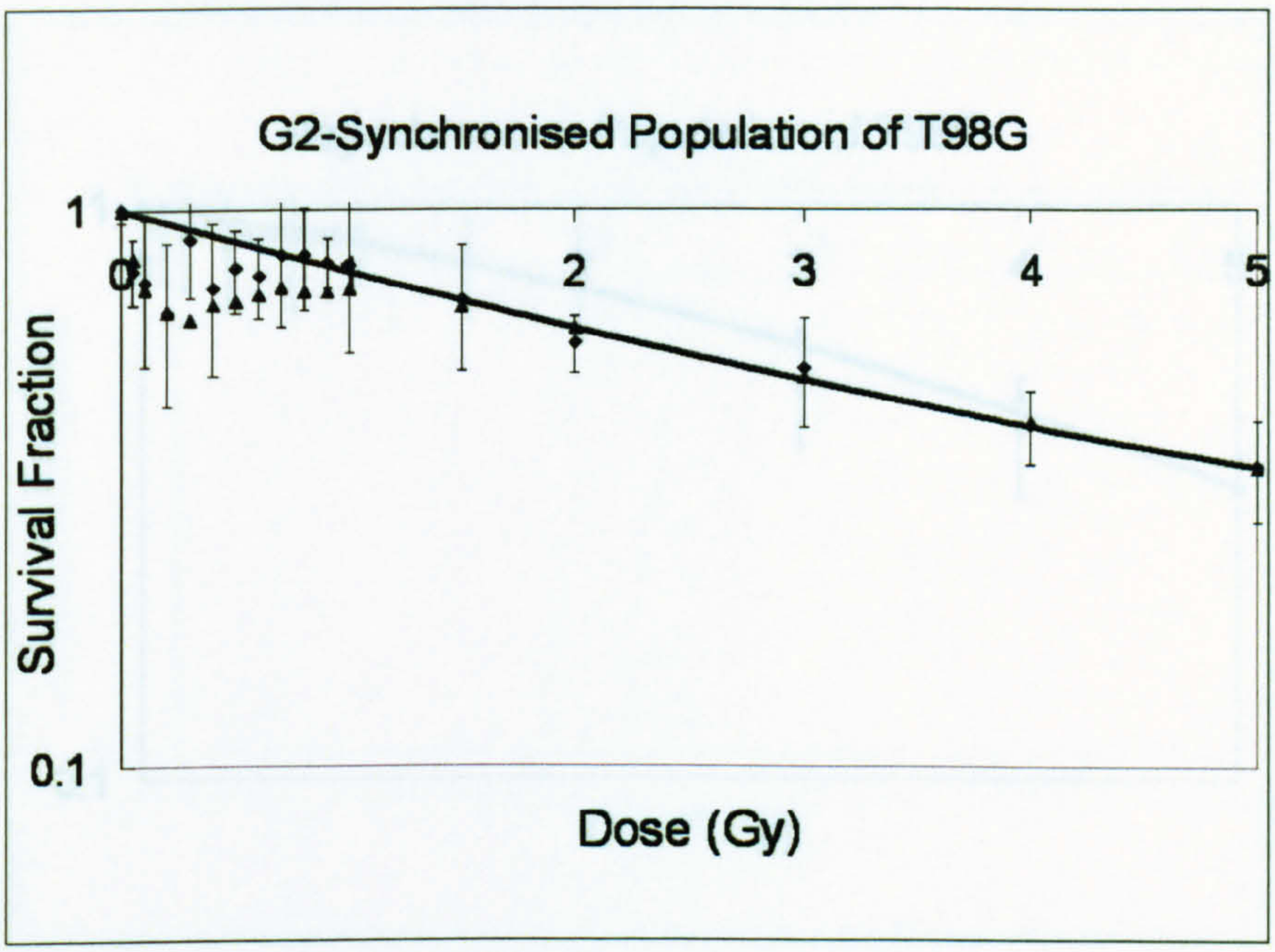

(a)

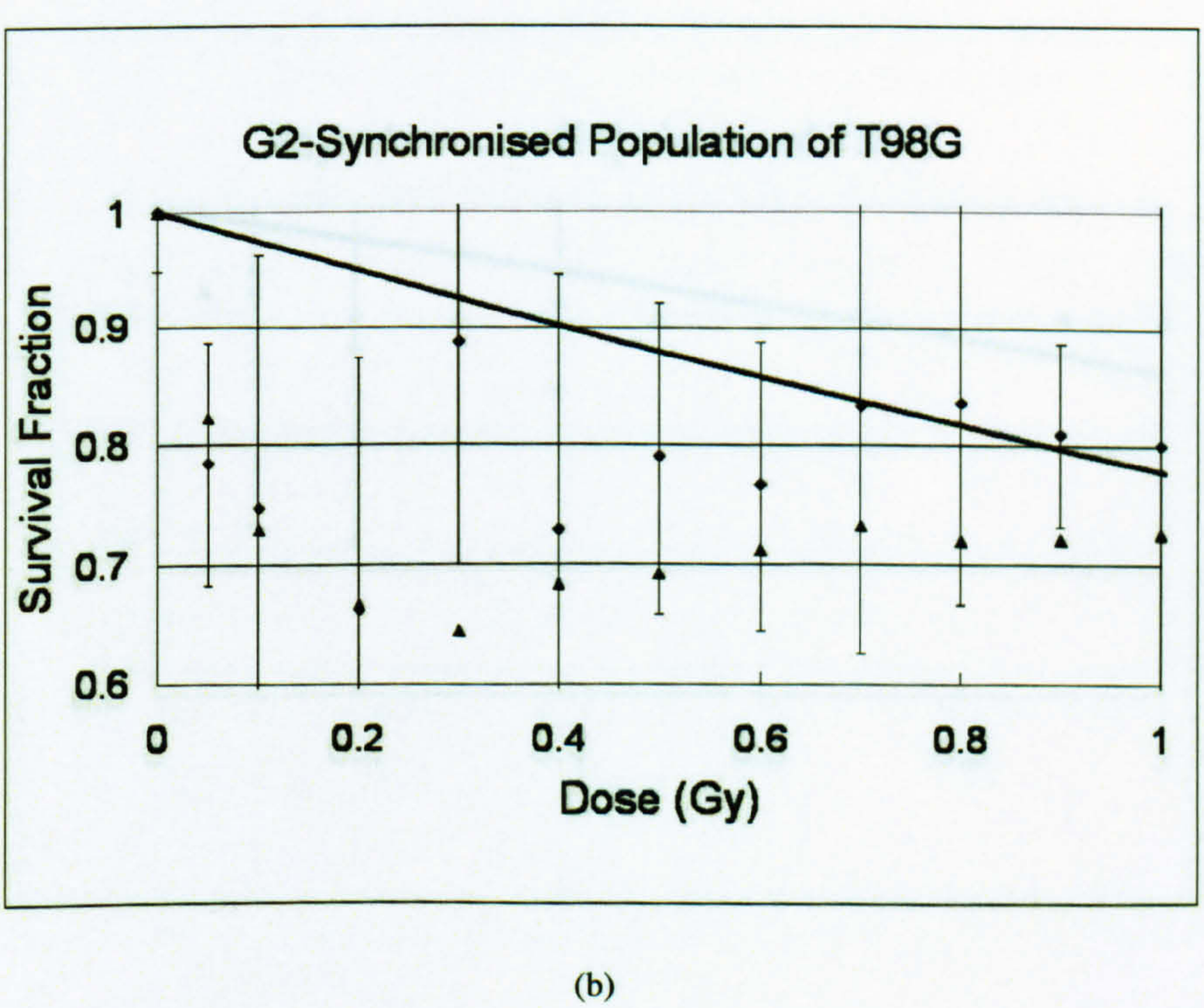

(b)

Figure 4.11: Survival Fraction of G2-Synchronised T98G Cells to 250 kVp X-rays: Dose domain (a) $[0, 5Gy]$ and (b) $[0, 1Gy]$. Diamonds are the experimental data, triangles are the simulations from the model, and the line is the LQ equation fitted to the high dose data (>1 Gy). Experimental standard errors are shown.

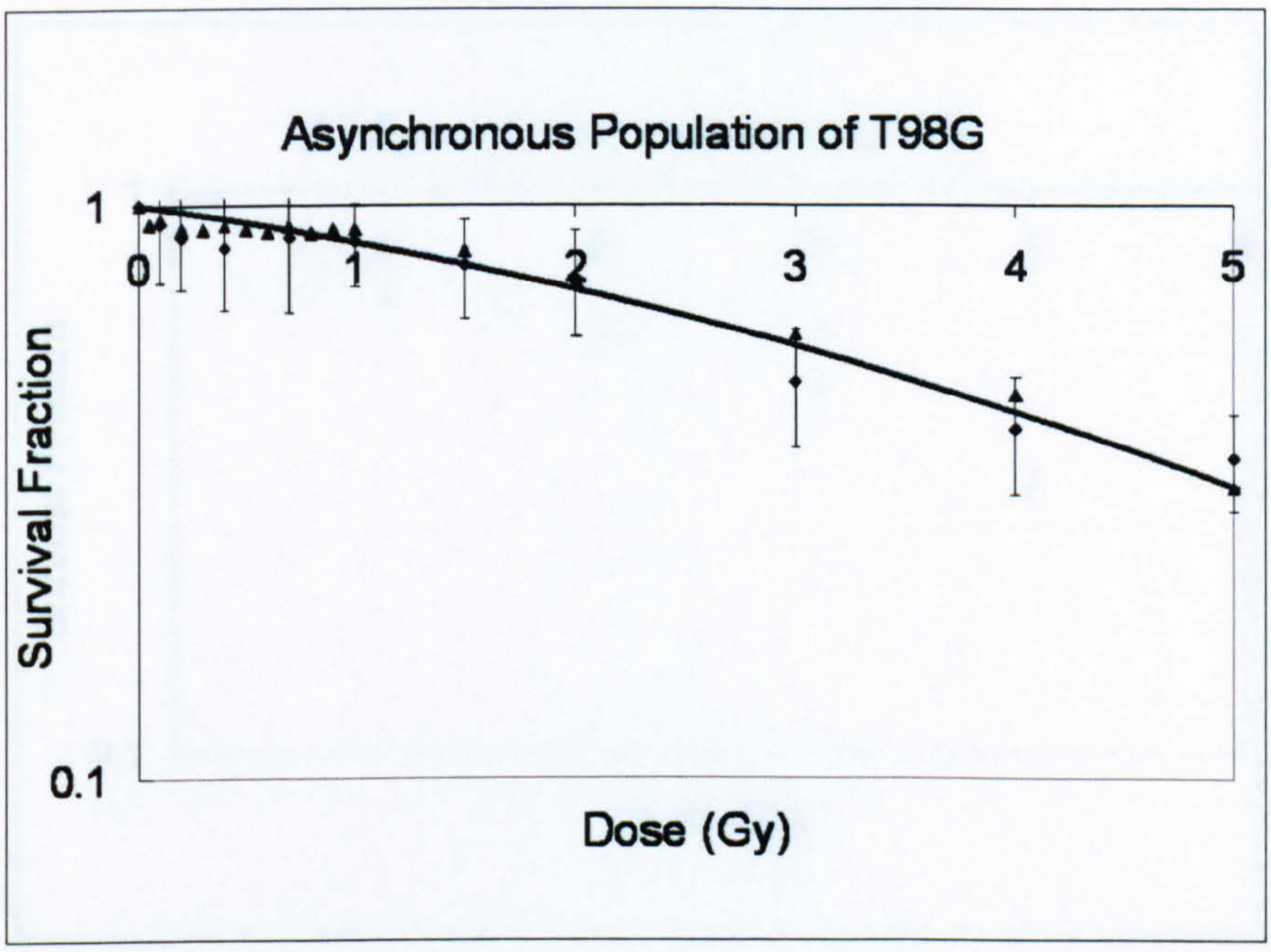

(a)

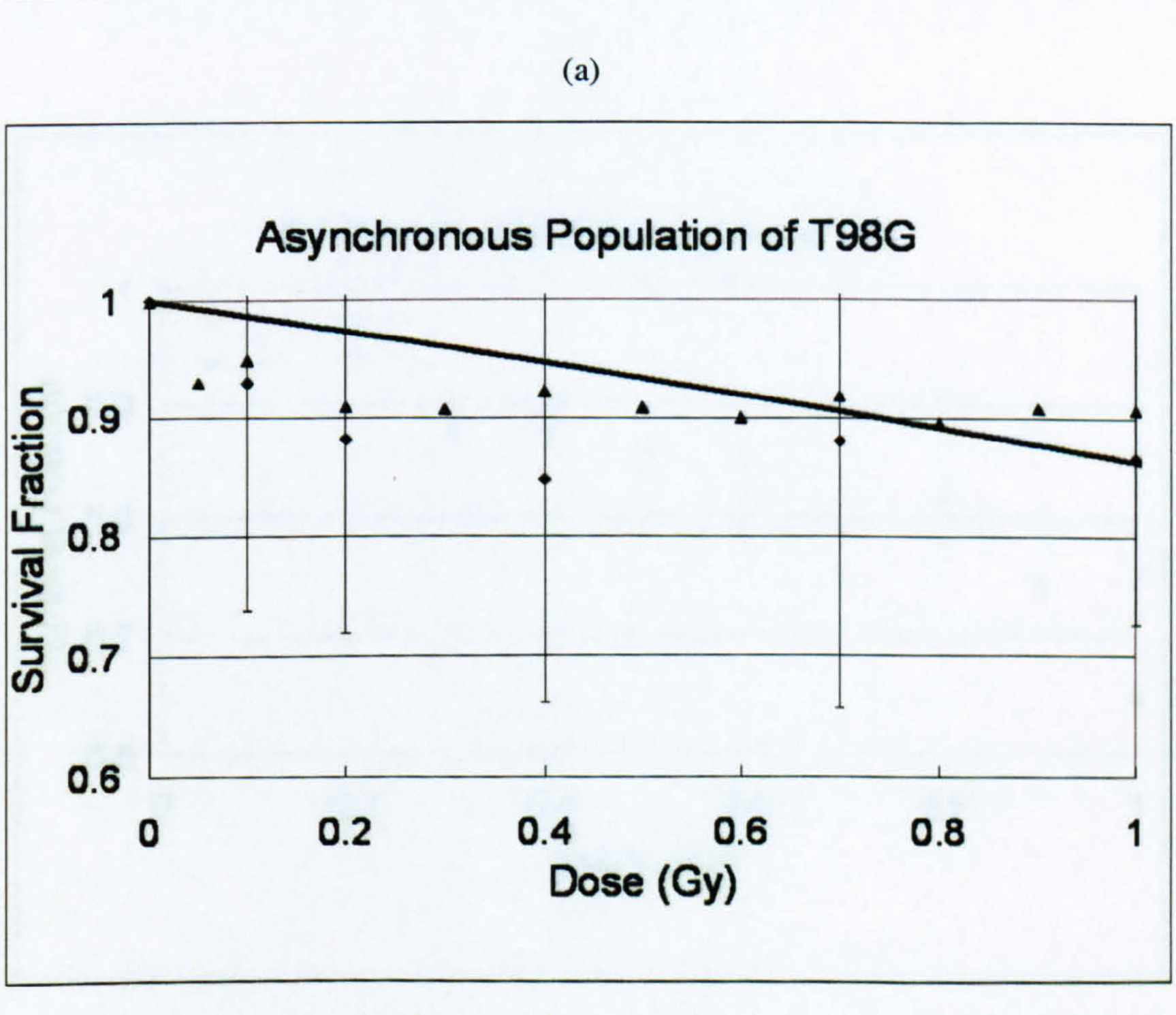

(b)

Figure 4.12: Survival Fraction of Asynchronous T98G cells to 250 kVp X-rays: Dose domain (a) $[0, 5Gy]$ and (b) $[0, 1Gy]$. Diamonds are the experimental data, triangles are the simulations from the model, and the line is the LQ equation fitted to the high dose data (>1 Gy). Experimental standard errors are shown.

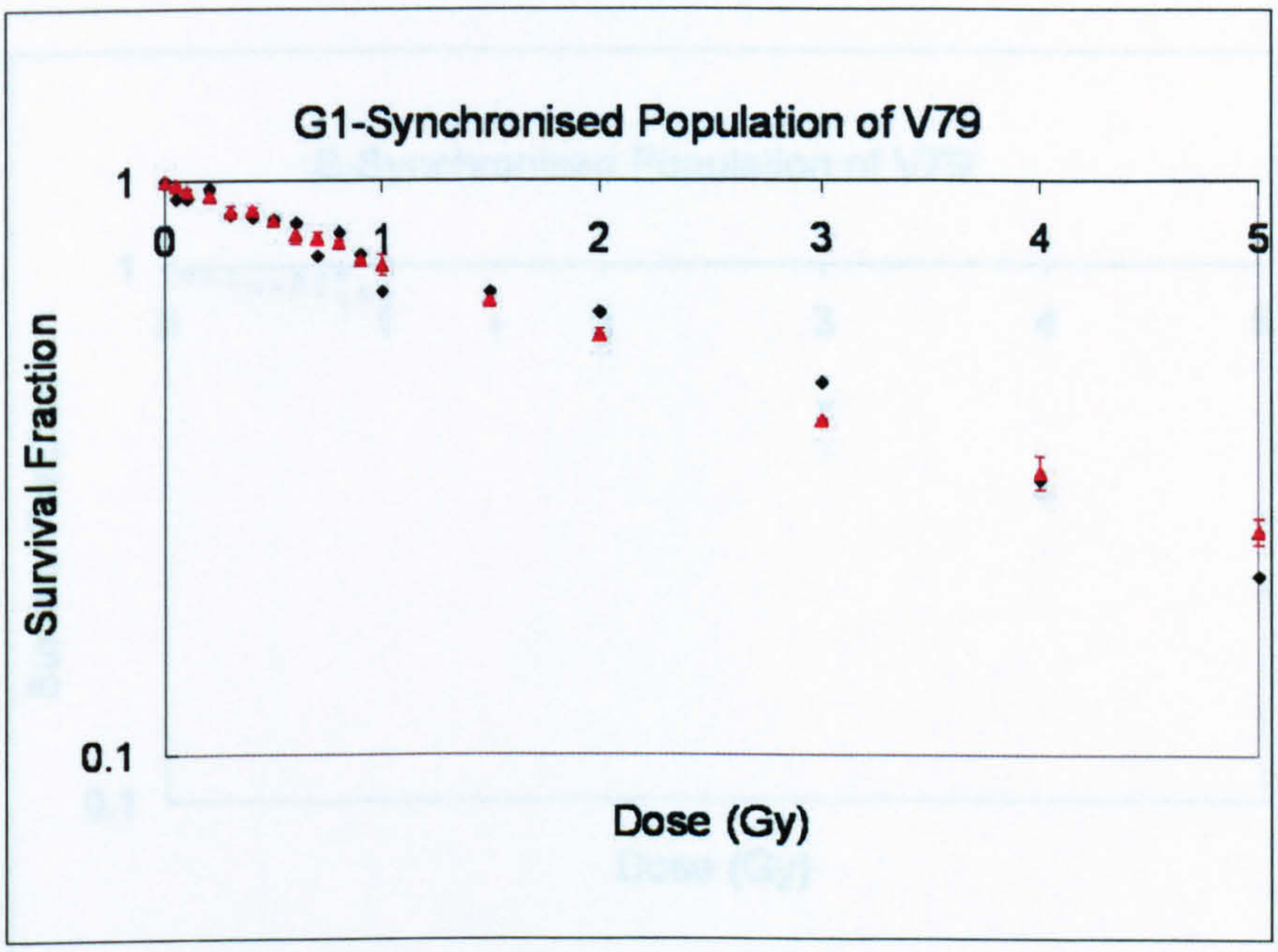

(a)

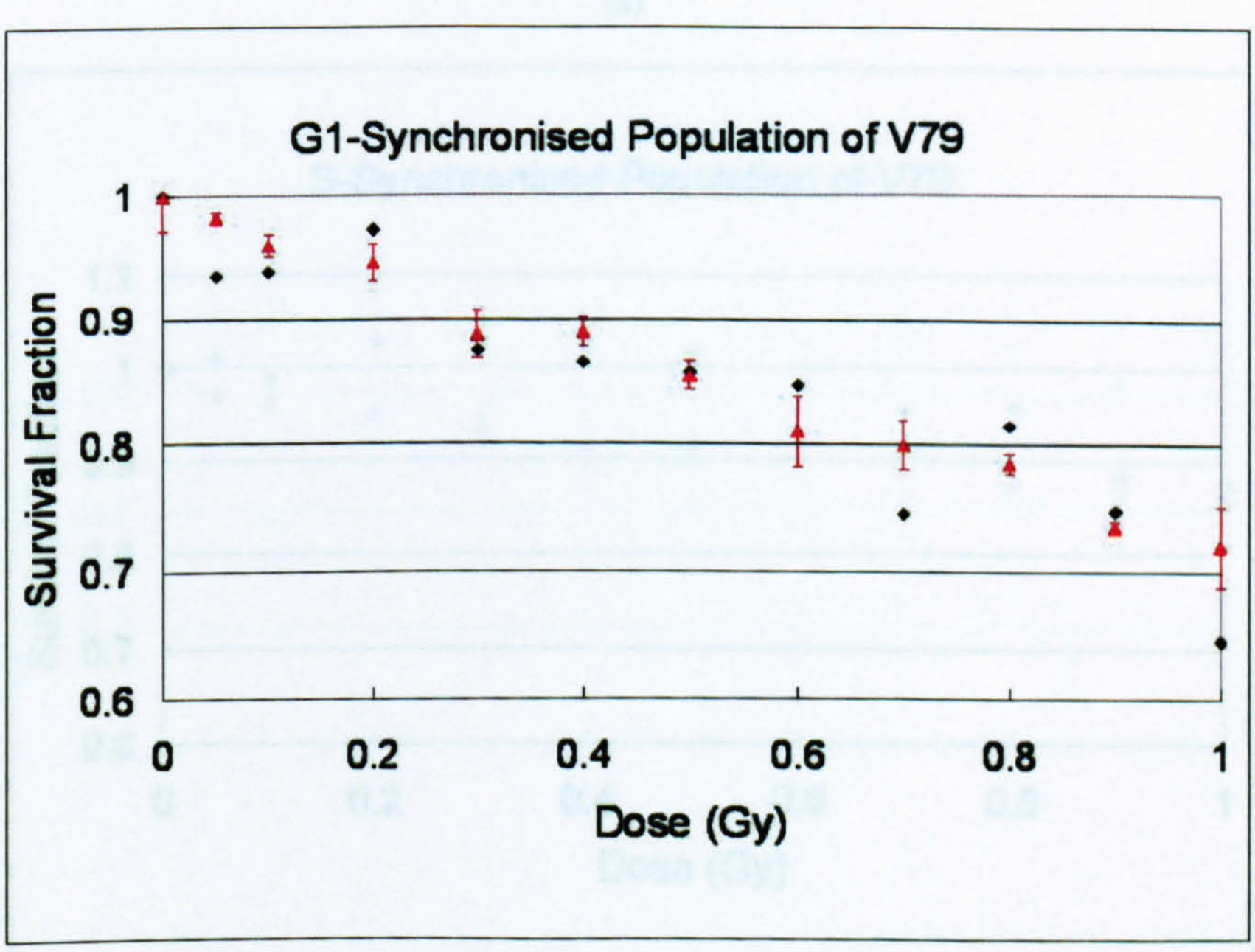

(b)

Figure 4.13: Standard Deviation of the Model on the G1 Population: Diamonds are the experimental data and red triangles are the model 1. The standard deviations shown are the ones of the model 1 (red bars). The low dose domain is shown on (b).

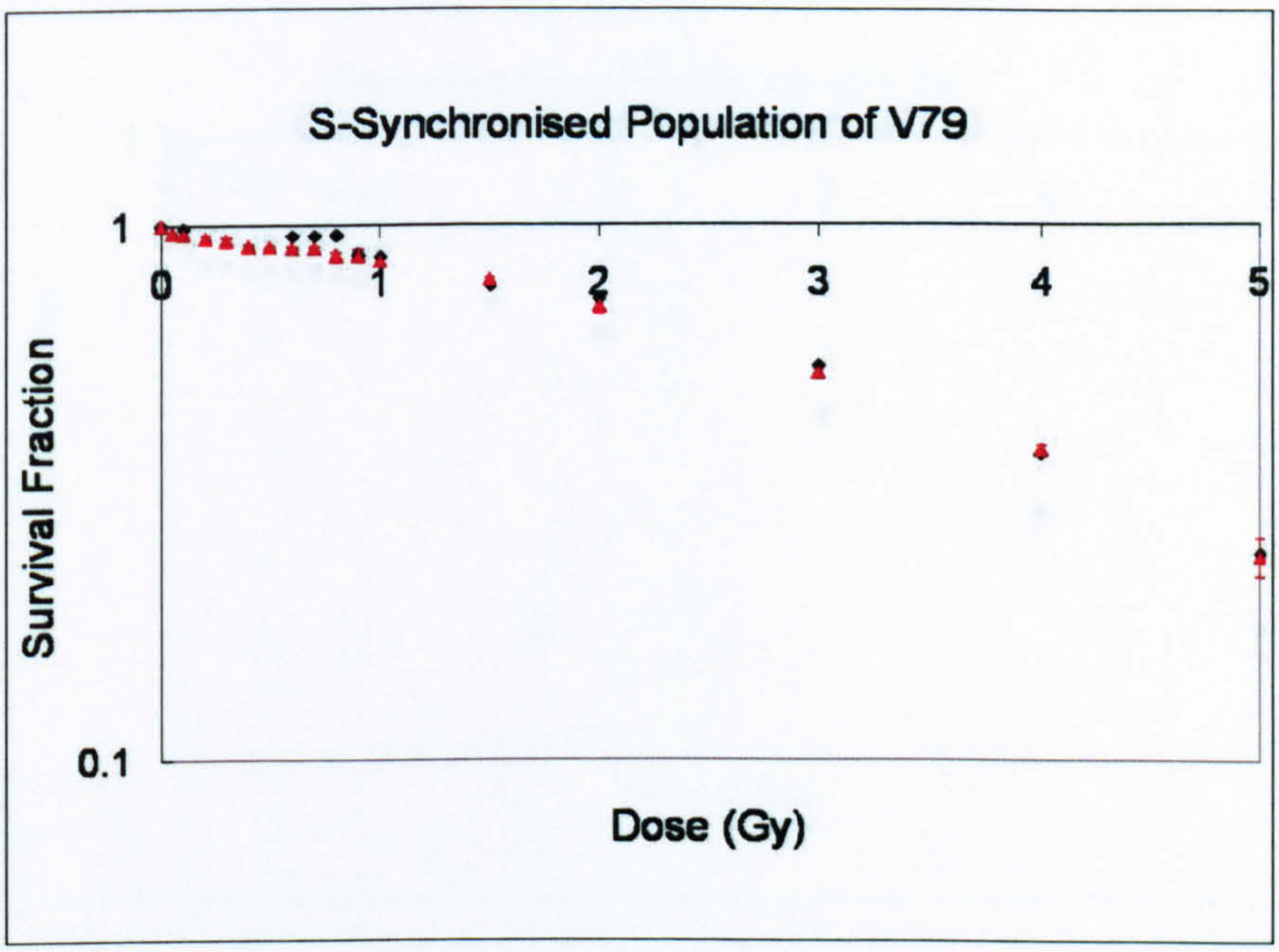

(a)

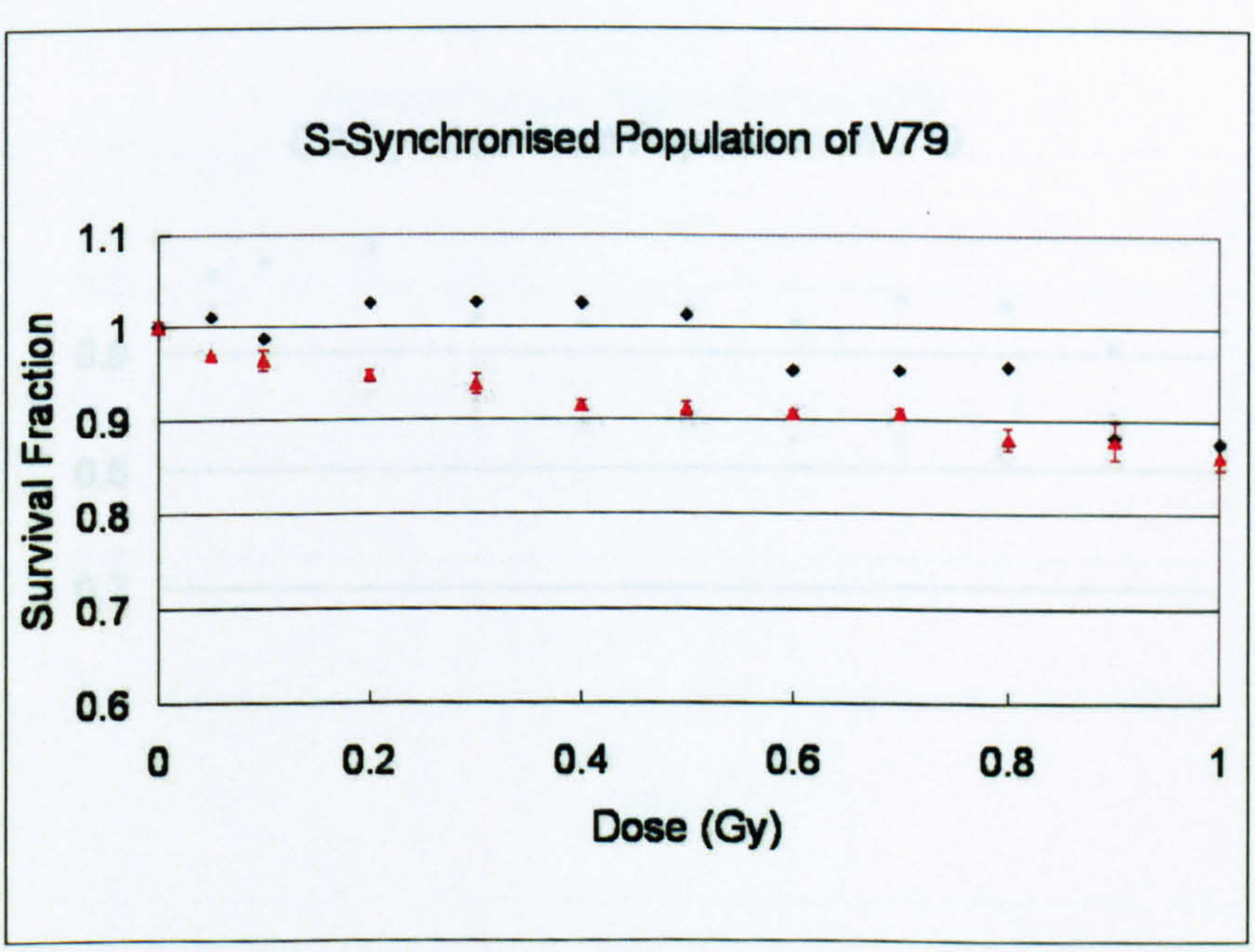

(b)

Figure 4.14: Standard Deviation of the Model on the S Population: Diamonds are the experimental data and red triangles are the model 1. The standard deviations shown are the ones of the model 1 (red bars). The low dose domain is shown on (b).

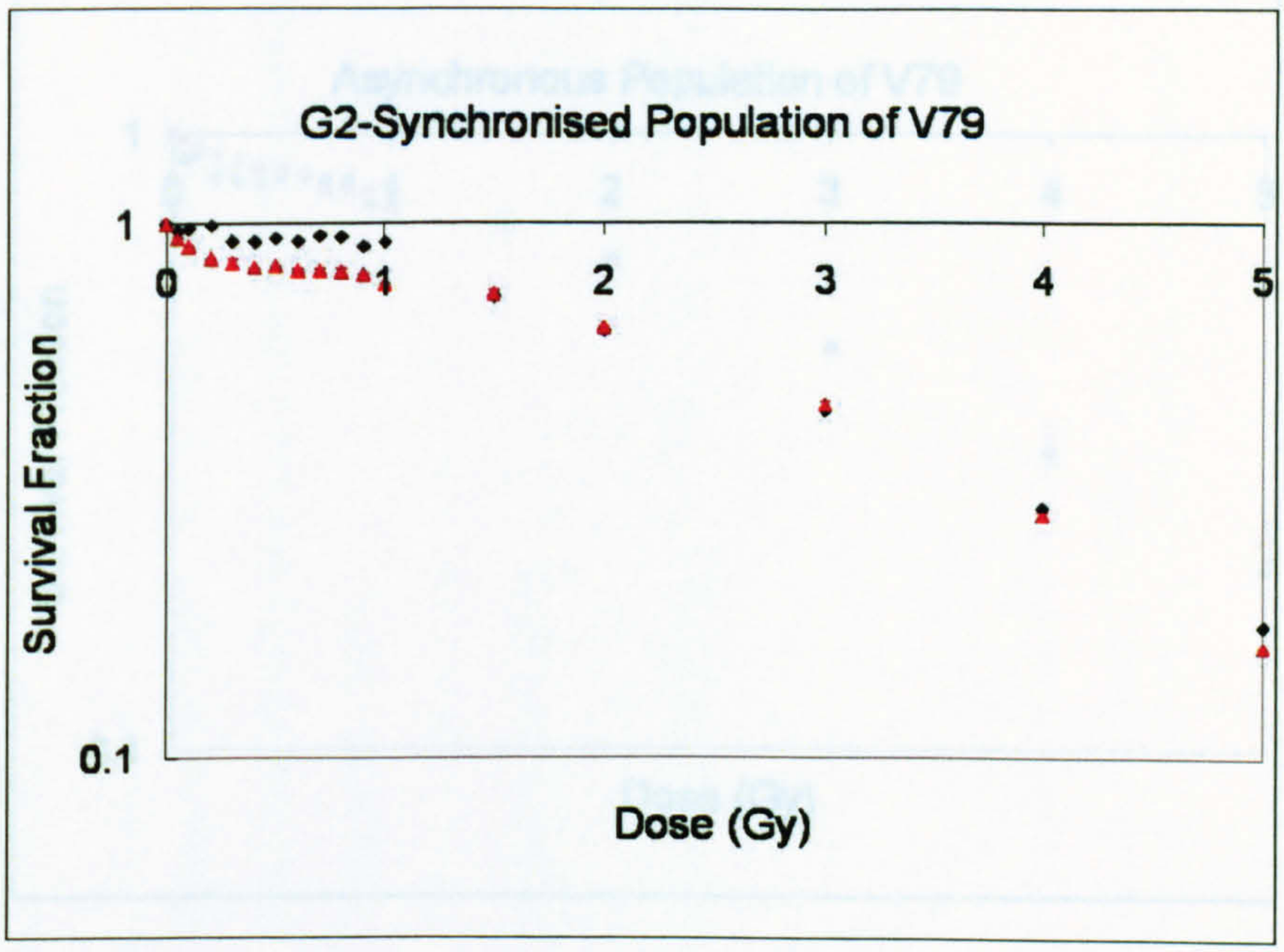

(a)

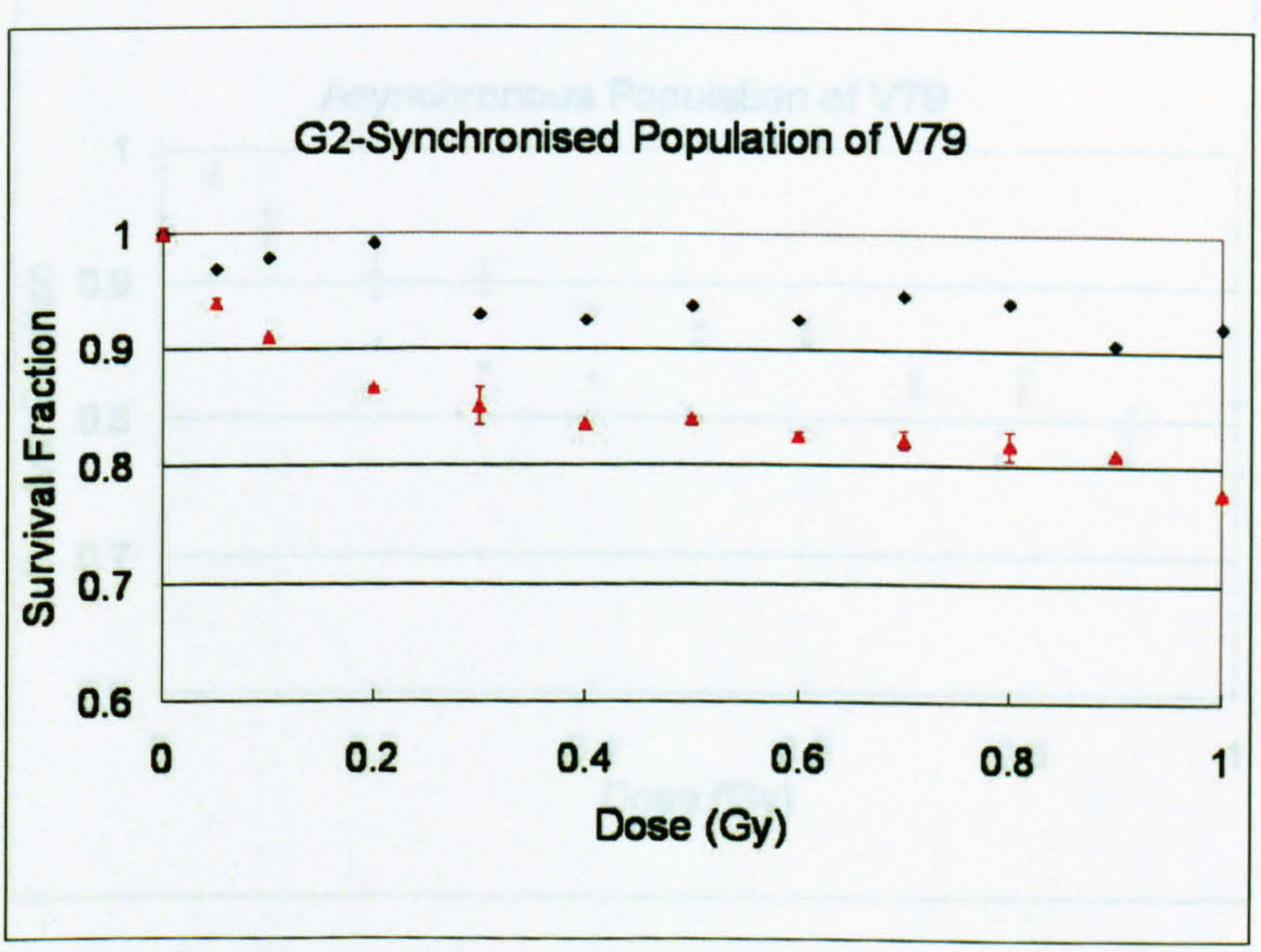

(b)

Figure 4.15: Standard Deviation of the Model on the G2 Population: Diamonds are the experimental data and red triangles are the model 1. The standard deviations shown are the ones of the model 1 (red bars). The low dose domain is shown on (b).

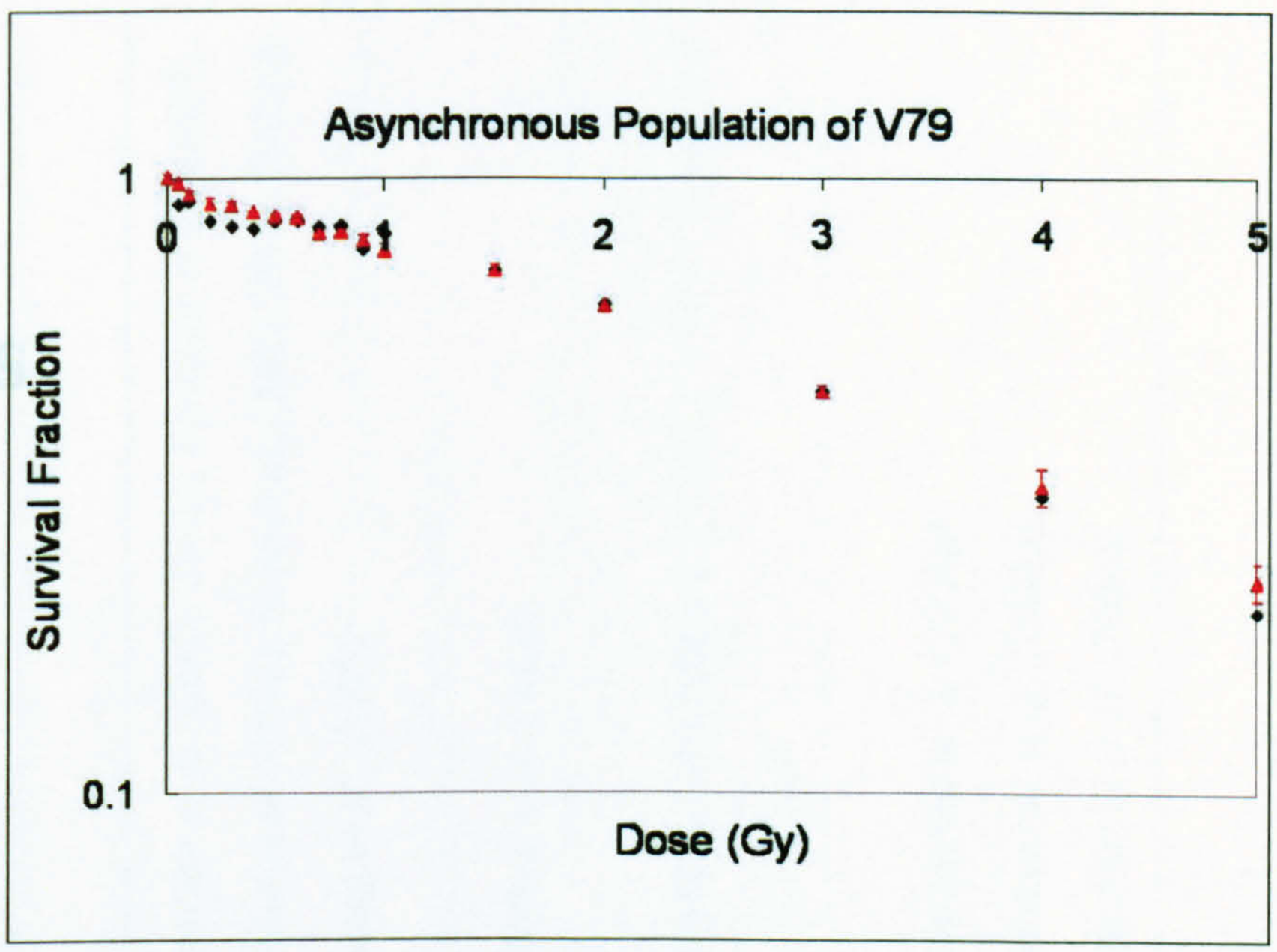

(a)

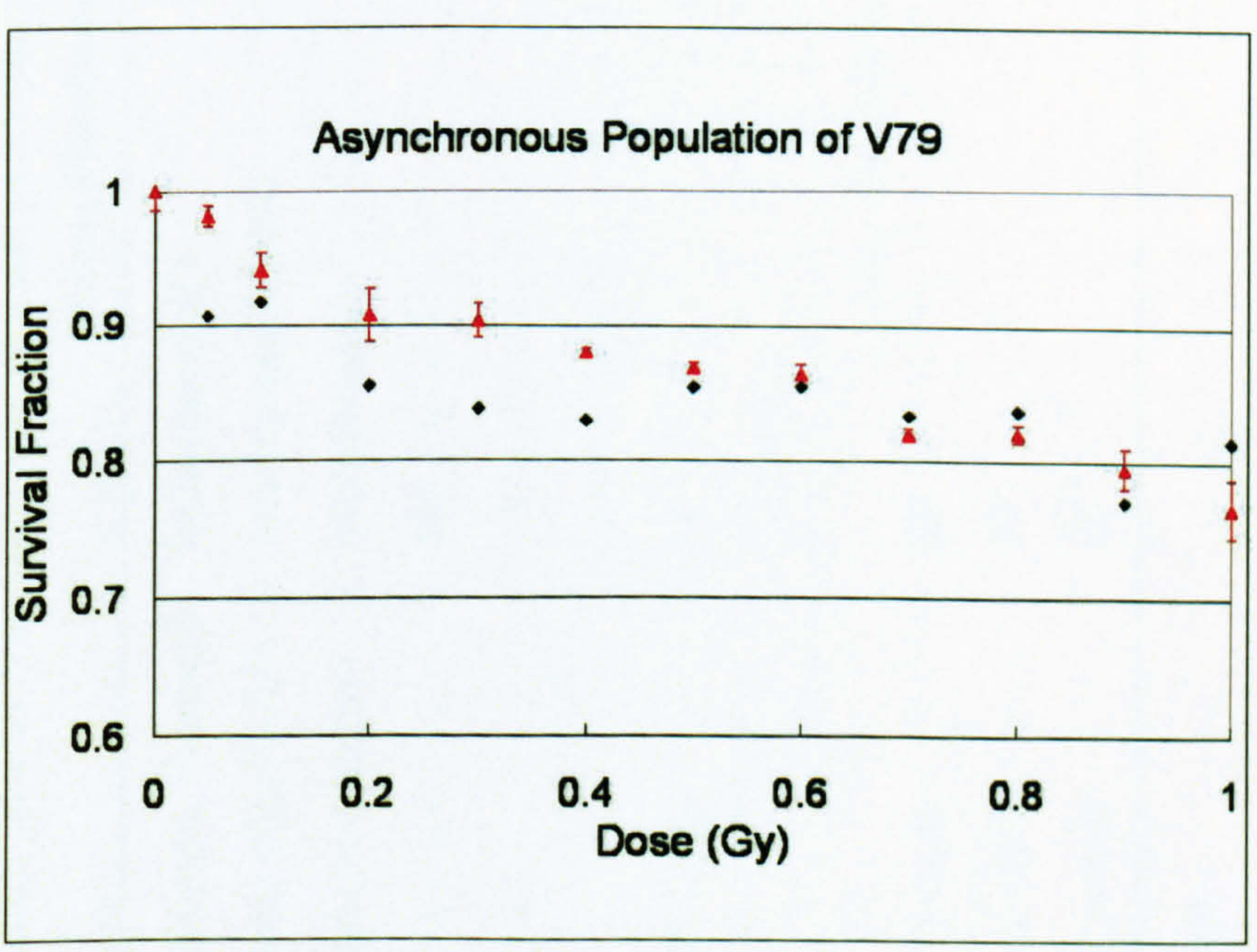

(b)

Figure 4.16: Standard Deviation of the Model on the Asynchronous Population: Diamonds are the experimental data and red triangles are the model 1. The standard deviations shown are the ones of the model 1 (red bars). The low dose domain is shown on (b).

Tables

Table 2.1: Summary of Cell Lines Studied in References Cited in the Dissertation

Name	BE	Endpoint[1]	HRS	References
		Human Fibroblasts		
AG0 1522	ICCM (X-rays, Uranium) microbeam (Ne, C, Ar[2]) low fluence α-particles	induction of p21 induction of CDKN1 MN[3] formation SF	×[4]	Azzam *et al.* (2001, 2002); Fournier *et al.* (2007); Prise *et al.* (1998); Shao *et al.* (2005, 2004, 2003b); Yang *et al.* (2005)
AT22IJE-TJ EBS7	×		✓	Wykes *et al.* (2006)
AT22IJE-TJ EBS7YZ5	×		✓	Wykes *et al.* (2006)
AT Br1	ICCM (γ-rays)	SF	×	Mothersill *et al.* (2004a)
180 Br	ICCM (γ-rays)	SF	×	Mothersill *et al.* (2004a)
1 Br 3	ICCM (γ-rays)	SF	×	Mothersill *et al.* (2004a)

Continued on Next Page...

[1]The column BE indicates the protocol(s) used, and the column Endpoint the endpoint used to quantify the BE
[2]Ne: Neon, C: Carbon and Ar: Argon
[3]MN: micronuclei
[4]the particular phenomenon has been (✓) or not (×) studied in the cell line

Table 2.1 – Continued

Name	BE	Endpoint	HRS	References
GS3	ICCM (γ-rays)	SF	✓	Mothersill *et al.* (2002)
GM 5758	microbeam (C)	induction of CDKN1A	×	Fournier *et al.* (2007)
GM 6419	low fluence α-particles	induction of p21 MN formation	×	Azzam *et al.* (2002)
HFL-1	ICCM (α-particles) low fluence α-particles	induction of sister chromatid exchange cell proliferation induction of p21	×	Azzam *et al.* (2001); Iyer and Lehnert (2000); Lehnert and Goodwin (1997)
MSU-1	ICCM (γ-rays)	SF apoptosis	✓	Mothersill and Seymour (1997, 1998); Mothersill *et al.* (2002)
		Human Keratinocytes		
HaCaT	ICCM (γ-rays)	SF apoptosis	✓	Mothersill and Seymour (1997, 1998); Mothersill *et al.* (2002)
HPV-G	ICCM (γ-rays)	SF apoptosis	✓	Lyng *et al.* (2000); Mothersill *et al.* (2002, 2004a, 2006)

Continued on Next Page...

Table 2.1 – Continued

Name	BE	Endpoint	HRS	References
		Human Salivary Gland		
HSG	ICCM (X-rays, C)	MN formation cell proliferation	×	Shao *et al.* (2002, 2001)
		Human Astrocyte		
NHA	ICCM (X-rays) micorbeam (α-particles)	induction of γ-H_2AX	×	Burdak-Rothkamm *et al.* (2006)
		Human Lymphoblast		
TK 6B	ICCM (X-rays)	SF GI	×	Moore *et al.* (2006)
		Human Glioma		
T98	ICCM (X-rays, γ-rays) microbeam (α-particles)	MN formation induction of γ-H_2AX	✓	Burdak-Rothkamm *et al.* (2006); Enns *et al.* (2004); Krause *et al.* (2005); Marples *et al.* (2003); Mitchell *et al.* (2002); Mitchell and Joiner (2002); Mothersill *et al.* (2002); Shao *et al.* (2005, 2003a, 2004); Short *et al.* (1999a, 2005, 1999b, 2003)

Continued on Next Page...

Table 2.1 – Continued

Name	BE	Endpoint	HRS	References
HLG21	ICCM (γ-rays)	SF	✓	Krause *et al.* (2005); Mothersill *et al.* (2002); Short *et al.* (1999b)
U373	ICCM (γ-rays)	SF	✓	Mitchell *et al.* (2002); Mothersill *et al.* (2002); Short *et al.* (2005, 1999b, 2003)
A7	×		✓	Krause *et al.* (2003); Mitchell *et al.* (2002); Short *et al.* (1999b)
U138	×		✓	Short *et al.* (1999b)
U87MG	×		✓	Short *et al.* (1999b)
M059J	×		✓	Wykes *et al.* (2006)
M059K	×		✓	Wykes *et al.* (2006)
		Human Carcinoma		
HT29	ICCM (γ-rays)	SF apoptosis	✓	Mothersill *et al.* (2004a, 2006); Wouters *et al.* (1996)
SW48	ICCM (γ-rays)	SF apoptosis	✓	Mothersill and Seymour (1997, 1998); Mothersill *et al.* (2002, 2004a)
RK036	ICCM (X-rays)	SF GI	×	Huang *et al.* (2007)

Continued on Next Page...

Table 2.1 – Continued

Name	BE	Endpoint	HRS	References
A 549	×		✓	Enns *et al.* (2004); Wouters *et al.* (1996)
MCF7	×		✓	Enns *et al.* (2004)
DU145	×		✓	Wouters *et al.* (1996)
SiHa	×		✓	Wouters *et al.* (1996)
PC-3	ICCM (γ-rays)	SF	✓	Mitchell *et al.* (2002); Mothersill and Seymour (1997); Mothersill *et al.* (2002)
		apoptosis		
RT-112	ICCM (γ-rays)	SF	✓	Mothersill *et al.* (2002)
		Human Lymphoma		
Raji TK^-	ICCM (γ-rays)	SF	×	Mothersill *et al.* (2006)
		apoptosis		
Raji 10	ICCM (γ-rays)	SF	×	Mothersill *et al.* (2004a, 2006)
		apoptosis		
Raji 9	ICCM (γ-rays)	SF	×	Mothersill *et al.* (2004a)
		Human Melanoma		
U1	×		✓	Wouters *et al.* (1996)

Continued on Next Page...

Table 2.1 – Continued

Name	BE	Endpoint	HRS	References
		HeLa Skin Fibroblast Hybrid		
CGL3	×		✓	Redpath *et al.* (2003)
		Human Hamster Hybrid		
A_L	ICCM (α-particles) microbeam (α-particles)	SF induction of mutation induction of chromatid fragments	×	Suzuki *et al.* (2004); Zhou *et al.* (2004, 2000, 2002a)
		Rodent Cell Lines		
V79	microbeam (C_K X-rays)	SF	✓	Bishayee *et al.* (1999); Bohrnsen *et al.* (2002); Marples and Joiner (1993, 1995); Marples and Skov (1996); Marples *et al.* (2003); Schettino *et al.* (2005, 2001, 2003); Skarsgard *et al.* (1994); Tsoulou *et al.* (2001)
C3H 10T1/2	microbeam (α-particles)	SF transformation frequency	×	Mitchell *et al.* (2004); Sawant *et al.* (2001a,b)

Continued on Next Page...

Table 2.1 – Continued

Name	BE	Endpoint	HRS	References
CHO	ICCM (X-rays) low fluence α-particles	Induction of sister chromatid exchange SF MN formation	×	Kashino *et al.* (2004); Nagasawa and Little (1992, 1st study of the BE)
Xrs-5	ICCM (X-rays and γ-rays)	SF MN formation	×	Kashino *et al.* (2004); Mothersill *et al.* (2004a)
CHO-K1	ICCM (γ-rays)	SF	✓	Bartkowiak *et al.* (2001); Mothersill *et al.* (2004a)
XR-1	ICCM (γ-rays)	SF	×	Mothersill *et al.* (2004a)
EM9	ICCM (X-rays)	SF MN formation	×	Kashino *et al.* (2004)
WB-F344	ICCM (γ-rays) low fluence α-particles	induction of p21 cell proliferation	×	Azzam *et al.* (2001); Gerashchenko and Howell (2003)
WM aB1	ICCM (γ-rays) low fluence α-particles	induction of p21 cell proliferation	×	Azzam *et al.* (2001); Gerashchenko and Howell (2003)
MR4	×		✓	Wykes *et al.* (2006)
3.7	×		✓	Wykes *et al.* (2006)

Parameter	V79	T98G
LX	100	100
LY	100	100
m	10	10
Cell_Init	2000	2000

Table 4.1: Parameters for the Cellular Automaton

Parameter	V79	T98G
Czero (μmol)	27.5	27.5
G1a (min)	30	320
S (min)	300	768
G2 (min)	90	132
M (min)	60	60
r (nmol/cell/min)	5×10^{-6}	5×10^{-6}
pf	1.7	1.7
G1b (min)	600	600
S_{max} (nmol/cell)	18×10^{-4}	18×10^{-4}

Table 4.2: Parameters for Cell Cycle and Glucose Consumption

V79 cells	α	β	Φ
G1	0.301	-0.004	1.32×10^{-2}
S	0.097	0.036	1.05×10^{-3}
G2	0.102	0.052	6.25×10^{-3}
Asynchronous	0.179	0.028	6.61×10^{-5}
T98G cells cells	α	β	Φ
G1	0.041	0.036	6.75×10^{-3}
S	0.056	0.040	7.47×10^{-3}
G2	0.261	-0.010	2.44×10^{-3}
Asynchronous	0.128	0.019	9.01×10^{-3}

Table 4.3: Parameters for the LQ Equations

Parameter	V79 (Model 1)	V79 (Model 2)	T98G
d_l	0.12	0.2	0.25
d_m	1	N/A	0.31
τ	$\frac{30}{\log(2)}$	$\frac{0.25}{\log(2)}$	$\frac{150}{\log(2)}$
D_{max}	1	0.1	1
Q_B	6000	1	1000

Table 4.4: Parameters for the Bystander Effect

Model	χ^2(G1)	χ^2(S)	χ^2(G2)	χ^2(As)
LQ (high doses only)	1.8	4.3	1.2	2.1×10^{-2}
LQ (all doses)	2.6	30.4	2.7	15.1
Model 1	4.09 (+/- 37%)	73.57 (+/- 7%)	22.93 (+/- 33%)	6.61 (+/- 34%)
Model 2	4.53 (+/- 75%)	38.92 (+/- 7%)	9.87 (+/- 16%)	7.80 (+/- 34%)

Table 4.5: χ^2 Values for the 3 models of V79 (LQ, Model 1 and Model 2): the χ^2 values are shown for the fit to the G1, S and G2 synchronised populations (χ^2(G1), χ^2(S) and χ^2(G2) respectively), as well as the χ^2 for the fit to the asynchronous population (χ^2(As)). The χ^2value for the LQ model is calculated when all data and when only data for doses above 1 Gy are taken into account.

Model	χ^2(G1)	χ^2(S)	χ^2(G2)	χ^2(As)
LQ (high doses only)	7.1×10^{-1}	9.1×10^{-1}	6.0×10^{-1}	8.8×10^{-1}
LQ (all doses)	12.7	3.0	8.9	1.6
Model	10.8	11.2	5.1	2.2

Table 4.6: χ^2 Values for T98G: the χ^2 values are shown for the fit to the G1, S and G2-synchronised populations (χ^2(G1), χ^2(S) and χ^2(G2) respectively), as well as the χ^2 for the fit to the asynchronous population (χ^2(As)), for the LQ model when all or high data only are taken into account, and for the cellular automaton model.

	Model 1	Q_B+5%	Q_B-5%	τ+5%	τ-5%	d_l+5%	d_l-5%	d_m+5%
χ^2	6.50	5.17	7.53	6.77	6.49	6.51	6.48	6.90
$\frac{\Delta(\chi^2)}{\chi^2}$		20%	16%	4%	0.08%	0.2%	0.3%	6%

	d_m-5%	G1+5%	G1-5%	S+5%	S-5%	G2+5%	G2-5%	M+5%
χ^2	6.19	9.49	5.07	5.96	6.72	8.13	9.02	4.01
$\frac{\Delta(\chi^2)}{\chi^2}$	5%	46%	22%	8%	3%	25%	39%	38%

	M-5%	Smax+5%	Smax-5%	G1b=357 min	α(G1)+5%	α(G1)-5%	β(G1)+5%	β(G1)-5%
χ^2	6.09	6.80	9.70	4.70	5.58	5.54	6.14	6.38
$\frac{\Delta(\chi^2)}{\chi^2}$	6%	4%	49%	28%	14%	15%	5%	2%

	α(S)+5%	α(S)-5%	β(S)+5%	β(S)-5%	α(G2)+5%	α(G2)-5%	β(G2)+5%	β(G2)-5%
χ^2	6.28	6.08	6.42	6.44	5.84	5.82	5.76	6.58
$\frac{\Delta(\chi^2)}{\chi^2}$	3%	6%	1%	0.9%	10%	10%	11%	1%

Table 4.7: Sensitivity Analysis of Model 1 for V79 Cells: the χ^2 are displayed for the fitting to the asynchronous population. The percentage of change in χ^2 corresponding to a small change (5%) in one parameter is calculated as follows: $\frac{\Delta(\chi^2)}{\chi^2} = \frac{\chi^2(\text{model 1}) - \chi^2(\text{modified model})}{\chi^2(\text{model 1})}$.

	Model 2	Q_B+5%	Q_B-5%	τ+5%	τ-5%	d_l+5%	d_l-5%
χ^2	10.75	8.19	10.75	10.56	10.75	10.75	10.75
$\frac{\Delta(\chi^2)}{\chi^2}$		24%	0%	2%	0%	0%	0%

Table 4.8: Sensitivity Analysis of Model 2 for V79 Cells: the χ^2 are displayed for the fitting to the asynchronous population, and the percentage of change in χ^2 corresponding to a small change (5%) in one parameter, compared to the model used; $\frac{\Delta(\chi^2)}{\chi^2} = \frac{\chi^2(\text{model 2}) - \chi^2(\text{modified model})}{\chi^2(\text{model 1})}$.

References

Alarcon, T., Byrne, H.M. and Maini, P.K. "A mathematical model of the effects of hypoxia on the cell- cycle of normal and cancer cells." *Journal Of Theoretical Biology*, 229(3):395–411, 2004

Antipas, V.P., Stamatakos, G.S., Uzunoglu, N.K., Dionysiou, D.D. and Dale, R.G. "A spatio-temporal simulation model of the response of solid tumours to radiotherapy in vivo: parametric validation concerning oxygen enhancement ratio and cell cycle duration." *Physics In Medicine And Biology*, 49(8):1485–1504, 2004

Azzam, E.I., de Toledo, S.M. and Little, J.B. "Direct evidence for the participation of gap junction-mediated intercellular communication in the transmission of damage signals from alpha -particle irradiated to nonirradiated cells." *Proceedings Of The National Academy Of Sciences Of The United States Of America*, 98(2):473–478, 2001

Azzam, E.I., de Toledo, S.M., Spitz, D.R. and Little, J.B. "Oxidative Metabolism Modulates Signal Transduction and Micronucleus Formation in Bystander Cells from alpha-Particle-irradiated Normal Human Fibroblast Cultures." *Cancer Res*, 62(19):5436–5442, 2002

Ballarini, F., Biaggi, M., Ottolenghi, A. and Sapora, O. "Cellular communication and bystander effects: a critical review for modelling low-dose radiation action." *Mutation Research-Fundamental And Molecular Mechanisms Of Mutagenesis*, 501(1-2):1–12, 2002

Bartkowiak, D., Hogner, S., Nothdurft, W. and Rottinger, E.M. "Cell cycle and growth response of CHO cells to X-irradiation: Threshold-free repair at low doses." *International Journal Of Radiation Oncology Biology Physics*, 50(1):221–227, 2001

Basse, B., Baguley, B.C., Marshall, E.S., Joseph, W.R., van Brunt, B., Wake, G. and Wall,

D.J.N. "A mathematical model for analysis of the cell cycle in cell lines derived from human tumors." *Journal Of Mathematical Biology*, 47(4):295–312, 2003

Basse, B., Baguley, B.C., Marshall, E.S., Wake, G.C. and Wall, D.J.N. "Modelling cell population growth with applications to cancer therapy in human tumour cell lines." *Progress In Biophysics & Molecular Biology*, 85(2-3):353–368, 2004

Belyakov, O.V., Mitchell, S.A., Parikh, D., Randers-Pehrson, G., Marino, S.A., Amundson, S.A., Geard, C.R. and Brenner, D.J. "Biological effects in unirradiated human tissue induced by radiation damage up to 1 mm away." *Proceedings Of The National Academy Of Sciences Of The United States Of America*, 102(40):14203–14208, 2005

Bishayee, A., Rao, D.V. and Howell, R.W. "Evidence for pronounced bystander effects caused by nonuniform distributions of radioactivity using a novel three-dimensional tissue culture model." *Radiation Research*, 152(1):88–97, 1999

Bohrnsen, G., Weber, K.J. and Scholz, M. "Low dose hypersensitivity and induced resistance of V79 cells after charged particle irradiation using 100 MeV/u carbon ions." *Radiation Protection Dosimetry*, 99(1-4):255–256, 2002

Borkenstein, K., Levegrun, S. and Peschke, P. "Modeling and computer simulations of tumor growth and tumor response to radiotherapy." *Radiation Research*, 162(1):71–83, 2004

Brenner, D.J., Little, J.B. and Sachs, R.K. "The bystander effect in radiation oncogenesis: II. A quantitative model." *Radiation Research*, 155(3):402–408, 2001

Burdak-Rothkamm, S., Short, S.C., Folkard, M., Rothkamm, K. and Prise, K.M. "ATR-dependent radiation-induced [gamma]H2AX foci in bystander primary human astrocytes and glioma cells." *Oncogene*, 2006

Burrows, R.C., Freeman, S.D., Charlop, A.W., Wiseman, R.W., Adamsen, T.C.H., Krohn, K.A. and Spence, A.M. "[F-18]-2-fluoro-2-deoxyglucose transport kinetics as a function of extracellular glucose concentration in malignant glioma, fibroblast and macrophage cells in vitro." *Nuclear Medicine And Biology*, 31(1):1–9, 2004

Chadwick, K.H. and Leenhout, H. "Molecular Theory Of Cell Survival." *Physics In Medicine And Biology*, 18(1):78–87, 1973

Dionysiou, D.D., Stamatakos, G.S., Uzunoglu, N.K., Nikita, K.S. and Marioli, A. "A four-dimensional simulation model of tumour response to radiotherapy in vivo: parametric validation considering radio sensitivity, genetic profile and fractionation." *Journal Of Theoretical Biology*, 230(1):1–20, 2004

Dionysiou, D.D., Stamatakos, G.S., Uzunoglu, N.K. and Nikita, K.S. "A computer simulation of in vivo tumour growth and response to radiotherapy: New algorithms and parametric results." *Computers in Biology and Medicine*, 36(5):448, 2006

Duchting, W., Ginsberg, T. and Ulmer, W. "Modeling Of Radiogenic Responses Induced By Fractionated-Irradiation In Malignant And Normal Tissue." *Stem Cells*, 13:301–306, 1995

Duchting, W. and Vogelsaenger, T. "Recent Progress In Modeling And Simulation Of 3-Dimensional Tumor-Growth And Treatment." *Biosystems*, 18(1):79–91, 1985

Enns, L., Bogen, K.T., Wizniak, J., Murtha, A.D. and Weinfeld, M. "Low-dose radiation hypersensitivity is associated with p53-dependent apoptosis." *Molecular Cancer Research*, 2(10):557–566, 2004

Faraday, D.B.F., Hayter, P. and Kirkby, N.F. "A mathematical model of the cell cycle of a hybridoma cell line." *Biochemical Engineering Journal*, 7(1):49–68, 2001

Fournier, C., Becker, D., Winter, M., Barberet, P., Heiss, M., Fischer, B., Topsch, J. and Taucher-Scholz, G. "Cell cycle-related bystander responses are not increased with LET after heavy-ion irradiation." *Radiation Research*, 167(2):194–206, 2007

Fuss, H., Dubitzky, W., Downes, C.S. and Kurth, M.J. "Mathematical models of cell cycle regulation." *Briefings In Bioinformatics*, 6(2):163–177, 2005

Gerashchenko, B.I. and Howell, R.W. "Cell proximity is a prerequisite for the proliferative response of bystander cells co-cultured with cells irradiated with gamma-rays." *Cytometry Part A*, 56A(2):71–80, 2003

Goodhead, D.T. "Initial Events In The Cellular Effects Of Ionizing-Radiations - Clustered Damage In Dna." *International Journal Of Radiation Biology*, 65(1):7–17, 1994

Goodhead, D.T., Thacker, J. and Cox, R. "Effects Of Radiations Of Different Qualities On Cells - Molecular Mechanisms Of Damage And Repair." *International Journal Of Radiation Biology*, 63(5):543–556, 1993

Hall, E. and Giaccia, A. *Radiobiology for the Radiologist.* Lippincott Williams & Wilkins, Philadelphia, 2006

Harney, J., Shah, N., Short, S., Daley, F., Groom, N., Wilson, G.D., Joiner, M.C. and Saunders, M.I. "The evaluation of low dose hyper-radiosensitivity in normal human skin." *Radiotherapy and Oncology*, 70(3):319–329, 2004a

Harney, J., Short, S.C., Shah, N., Joiner, M. and Saunders, M.I. "Low dose hyper-radiosensitivity in metastatic tumors." *International Journal of Radiation Oncology*Biology*Physics*, 59(4):1190–1195, 2004b

Hartwell, L.H. and Weinert, T.A. "Checkpoints - Controls That Ensure The Order Of Cell-Cycle Events." *Science*, 246(4930):629–634, 1989

Health Protection Agency website, Ionising Radiation Damage and Cancer. 2007. `http://www.hpa.org.uk/radiation/understand/radiation_topics/risks/damage.htm`

Health Protection Agency website, Radon. 2007. `http://www.hpa.org.uk/radiation/radon/index.htm`

Health Protection Agency website, The Estimation of Cancer Risk at Low Doses. 2007. `http://www.hpa.org.uk/radiation/understand/radiation_topics/risks/cancer_risk.htm`

Huang, L., Kim, P.M., Nickoloff, J.A. and Morgan, W.F. "Targeted and nontargeted effects of low-dose ionizing radiation on delayed genomic instability in human cells." *Cancer Research*, 67(3):1099–1104, 2007

Iyer, R. and Lehnert, B.E. "Factors underlying the cell growth-related bystander responses to alpha particles." *Cancer Research*, 60(5):1290–1298, 2000

Joiner, M., Marples, B., Lambin, P., Short, S. and Turesson, I. "Low-dose hypersensitivity: current status and posssible mechanisms." *International Journal of Radiation Oncology Biology and Physics*, 49(2):379–389, 2001

Jones, S.M. and Kazlauskas, A. "Growth factor-dependent signaling and cell cycle progression." *Febs Letters*, 490(3):110–116, 2001

Kadhim, M.A., Moore, S.R. and Goodwin, E.H. "Interrelationships amongst radiation-induced genomic instability, bystander effects, and the adaptive response." *Mutation Research-Fundamental And Molecular Mechanisms Of Mutagenesis*, 568(1):21–32, 2004

Kansal, A.R., Torquato, S., Harsh, G.R., Chiocca, E.A. and Deisboeck, T.S. "Simulated brain tumor growth dynamics using a three-dimensional cellular automaton." *Journal Of Theoretical Biology*, 203(4):367–382, 2000

Kashino, G., Prise, K.M., Schettino, G., Folkard, M., Vojnovic, B., Michael, B.D., Suzuki, K., Kodama, S. and Watanabe, M. "Evidence for induction of DNA double strand breaks in the bystander response to targeted soft X-rays in CHO cells." *Mutation Research/Fundamental and Molecular Mechanisms of Mutagenesis*, 556(1-2):209–215, 2004

Krause, M., Hessel, F., Wohlfarth, J., Zips, D., Hoinkis, C., Foest, H., Petersen, C., Short, S.C., Joiner, M.C. and Baumann, M. "Ultrafractionation in A7 human malignant glioma in nude mice." *International Journal Of Radiation Biology*, 79(6):377–383, 2003

Krause, M., Wohlfarth, J., Georgi, B., Pimentel, N., Dorner, D., Zips, D., Eicheler, W., Hessel, F., Short, S.C., Joiner, M.C. and Baumann, M. "Low-dose hyperradiosensitivity of human glioblastoma cell lines in vitro does not translate into improved outcome of ultrafractionated radiotherapy in vivo." *International Journal Of Radiation Biology*, 81(10):751–758, 2005

Lehnert, B.E. and Goodwin, E.H. "Extracellular factor(s) following exposure to alpha particles can cause sister chromatid exchanges in normal human cells." *Cancer Research*, 57(11):2164–2171, 1997

Little, J.B. "Cellular radiation effects and the bystander response." *Mutation Research-Fundamental And Molecular Mechanisms Of Mutagenesis*, 597(1-2):113–118, 2006

Little, J.B., Azzam, E.I., de Toledo, S.M. and Nagasawa, H. "Characteristics and mechanisms of the bystander response in monolayer cell cultures exposed to very low fluences of alpha particles." *Radiation Physics and Chemistry*, 72(2-3):307–313, 2005a

Little, J.B., Nagasawa, H., de Toledo, S.M. and Azzam, E. "Transmission of damage signals from irradiated to nonirradiated cells." *International Congress Series*, 1236:229, 2002

Little, M.P., Filipe, J.A.N., Prise, K.M., Folkard, M. and Belyakov, O.V. "A model for radiation-induced bystander effects, with allowance for spatial position and the effects of cell turnover." *Journal of Theoretical Biology*, 232(3):329–338, 2005b

Lyng, F.M., Seymour, C.B. and Mothersill, C. "Production of a signal by irradiated cells which leads to a response in unirradiated cells characteristic of initiation of apoptosis." *British Journal Of Cancer*, 83(9):1223–1230, 2000

Marples, B., Adomat, H., Koch, C.J. and Skov, K.A. "Response of V79 cells to low doses of X-rays and negative pi-mesons: Clonogenic survival and DNA strand breaks." *International Journal Of Radiation Biology*, 70(4):429–436, 1996

Marples, B. and Joiner, M.C. "The Response Of Chinese-Hamster V79 Cells To Low Radiation-Doses - Evidence Of Enhanced Sensitivity Of The Whole Cell- Population." *Radiation Research*, 133(1):41–51, 1993

Marples, B. and Joiner, M.C. "The Elimination Of Low-Dose Hypersensitivity In Chinese-Hamster V79-379a Cells By Pretreatment With X-Rays Or Hydrogen-Peroxide." *Radiation Research*, 141(2):160–169, 1995

Marples, B. and Skov, K.A. "Small doses of high-linear energy transfer radiation increase the radioresistance of Chinese hamster V79 cells to subsequent X irradiation." *Radiation Research*, 146(4):382–387, 1996

Marples, B., Wouters, B.G., Collis, S.J., Chalmers, A.J. and Joiner, M.C. "Low-dose hyper-radiosensitivity: A consequence of ineffective cell cycle arrest of radiation-damaged G(2)-phase cells." *Radiation Research*, 161(3):247–255, 2004

Marples, B., Wouters, B.G. and Joiner, M.C. "An association between the radiation-induced arrest of G(2)-phase cells and low-dose hyper-radiosensitivity: A plausible underlying mechanism?" *Radiation Research*, 160(1):38–45, 2003

Mitchell, C.R., Folkard, M. and Joiner, M.C. "Effects of exposure to low-dose-rate Co-60 gamma rays on human tumor cells in vitro." *Radiation Research*, 158(3):311–318, 2002

Mitchell, C.R. and Joiner, M.C. "Effect of subsequent acute-dose irradiation on cell survival in vitro following low dose-rate exposures." *International Journal Of Radiation Biology*, 78(11):981–990, 2002

Mitchell, S.A., Randers-Pehrson, G., Brenner, D.J. and Hall, E.J. "The bystander response in C3H 10T1/2 cells: The influence of cell-to-cell contact." *Radiation Research*, 161(4):397–401, 2004

Moore, S., Macdonald, D. and M.A., K. "The contribution of communication between irradiated cells and between bystander cells to clonogenic survival and genomic instability." *International Journal of Low Radiation*, 3(2-3):201–216, 2006

Morgan, W.F. "Non-targeted and delayed effects of exposure to ionizing radiation: I. Radiation-induced genomic instability and bystander effects in vitro." *Radiation Research*, 159(5):567–580, 2003

Mothersill, C., Harney, J., Lyng, F., Cottell, D., Parsons, K., Murphy, D.M. and Seymour, C.B. "Primary Explants Of Human Uroepithelium Show An Unusual Response To Low-Dose Irradiation With Co-60 Gamma-Rays." *Radiation Research*, 142(2):181–187, 1995

Mothersill, C. and Seymour, C. "Medium from irradiated human epithelial cells but not human fibroblasts reduces the clonogenic survival of unirradiated cells." *International Journal Of Radiation Biology*, 71(4):421–427, 1997

Mothersill, C. and Seymour, C. "Radiation-induced bystander effects: Past history and future directions." *Radiation Research*, 155(6):759–767, 2001

Mothersill, C. and Seymour, C.B. "Cell-cell contact during gamma irradiation is not required to induce a bystander effect in normal human keratinocytes: Evidence for release during irradi-

ation of a signal controlling survival into the medium." *Radiation Research*, 149(3):256–262, 1998

Mothersill, C. and Seymour, C.B. "Radiation-induced bystander effects - implications for cancer." *Nature Reviews Cancer*, 4(2):158–164, 2004a

Mothersill, C., Seymour, C.B. and Joiner, M.C. "Relationship between radiation-induced low-dose hypersensitivity and the bystander effect." *Radiation Research*, 157(5):526–532, 2002

Mothersill, C., Seymour, R.J. and Seymour, C.B. "Bystander effects in repair-deficient cell lines." *Radiation Research*, 161(3):256–263, 2004a

Mothersill, C., Seymour, R.J. and Seymour, C.B. "Increased radiosensitivity in cells of two human cell lines treated with bystander medium from irradiated repair-deficient cells." *Radiation Research*, 165(1):26–34, 2006

Mothersill, C.E., Moriarty, M.J. and Seymour, C.B. "Radiotherapy and the potential exploitation of bystander effects." *International Journal Of Radiation Oncology Biology Physics*, 58(2):575–579, 2004b

Mothersill, C. and Seymour, C. "Radiation-induced bystander effects and adaptive responses–the Yin and Yang of low dose radiobiology?" *Mutation Research/Fundamental and Molecular Mechanisms of Mutagenesis*, 568(1):121–128, 2004b

Murray, A. and Hunt, T. *The Cell Cycle an introduction*. Oxford University Press, Oxford, 1993

Murray, L.E., Singer, R.A., Fenwick, R.G. and Johnston, G.C. "The G1 Interval In The Mammalian-Cell Cycle - Dual Control By Mass Accumulation And Stage-Specific Activities." *Cell Proliferation*, 24(2):215–228, 1991

Nagasawa, H. and Little, J.B. "Induction Of Sister Chromatid Exchanges By Extremely Low-Doses Of Alpha-Particles." *Cancer Research*, 52(22):6394–6396, 1992

NASA website. 2007. `http://srag-nt.jsc.nasa.gov/SpaceRadiation/Why/Why.cfm`

National Cancer Institute website, Factsheet. 2007. `http://www.nci.nih.gov/cancertopics/factsheet/Therapy/radiation`

Neufeld, T.P. and Edgar, B.A. "Connections between growth and the cell cycle." *Current Opinion In Cell Biology*, 10(6):784–790, 1998

Nikjoo, H. and Khvostunov, I.K. "Biophysical model of the radiation-induced bystander effect." *International Journal Of Radiation Biology*, 79(1):43–52, 2003

Nikjoo, H., Uehara, S., Wilson, W.E., Hoshi, M. and Goodhead, D.T. "Track structure in radiation biology: theory and applications." *International Journal Of Radiation Biology*, 73(4):355–364, 1998

Nurse, P. "A long twentieth century of the cell cycle and beyond." *Cell*, 100(1):71–78, 2000

Pardee, A.B. "Restriction Point For Control Of Normal Animal-Cell Proliferation." *Proceedings Of The National Academy Of Sciences Of The United States Of America*, 71(4):1286–1290, 1974

Pathak, S.N. "G1 Variability Observed During Cell-Cycle Analyses Of Chinese-Hamster Cell Lines." *Nucleus*, 20(3):258–263, 1977

Press, W., Flannery, B., Teukolsky, S. and Vetterling, W. *Numerical Recipes in C The Art of Scientific Computing*. Cambridge University Press, New York, 1988

Prise, K.M., Belyakov, O.V., Folkard, M. and Michael, B.D. "Studies of bystander effects in human fibroblasts using a charged particle microbeam." *International Journal Of Radiation Biology*, 74(6):793–798, 1998

Prise, K.M., Folkard, M. and Michael, B.D. "Bystander responses induced by low LET radiation." *Oncogene*, 22(45):7043–7049, 2003

Prise, K.M., Schettino, G., Folkard, M. and Held, K.D. "New insights on cell death from radiation exposure." *Lancet Oncology*, 6(7):520–528, 2005

Puck, T.T. and Marcus, P.I. "A Rapid Method For Viable Cell Titration And Clone Production With Hela Cells In Tissue Culture - The Use Of X-Irradiated Cells To Supply Conditioning Factors." *Proceedings Of The National Academy Of Sciences Of The United States Of America*, 41(7):432–437, 1955

Redpath, J.L., Short, S.C., Woodcock, M. and Johnston, P.J. "Low-dose reduction in transformation frequency compared to unirradiated controls: The role of hyper-radiosensitivity to cell death." *Radiation Research*, 159(3):433–436, 2003

Sancar, A., Lindsey-Boltz, L.A., Unsal-Kacmaz, K. and Linn, S. "Molecular mechanisms of mammalian DNA repair and the DNA damage checkpoints." *Annual Review Of Biochemistry*, 73:39–85, 2004

Sawant, S.G., Randers-Pehrson, G., Geard, C.R., Brenner, D.J. and Hall, E.J. "The bystander effect in radiation oncogenesis: I. Transformation in C3H 10T(1)/(2) cells in vitro can be initiated in the unirradiated neighbors of irradiated cells." *Radiation Research*, 155(3):397–401, 2001a

Sawant, S.G., Randers-Pehrson, G., Metting, N.F. and Hall, E.J. "Adaptive response and the bystander effect induced by radiation in C3H 10T(1)/(2) cells in culture." *Radiation Research*, 156(2):177–180, 2001b

Schettino, G., Folkard, M., Michael, B.D. and Prise, K.M. "Low-dose binary behavior of bystander cell killing after microbeam irradiation of a single cell with focused C-K X rays." *Radiation Research*, 163(3):332–336, 2005

Schettino, G., Folkard, M., Prise, K.M., Vojnovic, B., Bowey, A.G. and Michael, B.D. "Low-dose hypersensitivity in Chinese hamster V79 cells targeted with counted protons using a charged-particle microbeam." *Radiation Research*, 156(5):526–534, 2001

Schettino, G., Folkard, M., Prise, K.M., Vojnovic, B., Held, K.D. and Michael, B.D. "Low-dose studies of bystander cell killing with targeted soft X rays." *Radiation Research*, 160(5):505–511, 2003

Seymour, C.B. and Mothersill, C. "Relative contribution of bystander and targeted cell killing to the low-dose region of the radiation dose-response curve." *Radiation Research*, 153(5):508–511, 2000

Shao, C., Folkard, M., Michael, B.D. and Prise, K.M. "Bystander signaling between glioma cells and fibroblasts targeted with counted particles." *International Journal Of Cancer*, 116(1):45–51, 2005

Shao, C., Furusawa, Y., Aoki, M., Matsumoto, H. and Ando, K. "Nitric oxide-mediated bystander effect induced by heavy-ions in human salivary gland tumour cells." *International Journal Of Radiation Biology*, 78(9):837–844, 2002

Shao, C., Stewart, V., Folkard, M., Michael, B.A. and Prise, K.M. "Nitric oxide-mediated signaling in the bystander response of individually targeted glioma cells." *Cancer Research*, 63(23):8437–8442, 2003a

Shao, C.L., Aoki, M. and Furusawa, Y. "Medium-mediated bystander effects on HSG cells co-cultivated with cells irradiated by X-rays or a 290 MeV/u carbon beam." *Journal Of Radiation Research*, 42(3):305–316, 2001

Shao, C.L., Folkard, M., Michael, B.D. and Prise, K.M. "Targeted cytoplasmic irradiation induces bystander responses." *Proceedings Of The National Academy Of Sciences Of The United States Of America*, 101(37):13495–13500, 2004

Shao, C.L., Furusawa, Y., Kobayashi, Y., Funayama, T. and Wada, S. "Bystander effect induced by counted high-LET particles in confluent human fibroblasts: a mechanistic study." *Faseb Journal*, 17(11):1422–1427, 2003b

Short, S., Mayes, C., Woodcock, M., Johns, H. and Joiner, M.C. "Low dose hypersensitivity in the T98G human glioblastoma cell line." *International Journal Of Radiation Biology*, 75(7):847–855, 1999a

Short, S.C., Bourne, S., Martindale, C., Woodcock, M. and Jackson, S.P. "DNA damage responses at low radiation doses." *Radiation Research*, 164(3):292–302, 2005

Short, S.C., Kelly, J., Mayes, C.R., Woodcock, M. and Joiner, M.C. "Low-dose hypersensitivity after fractionated low-dose irradiation in vitro." *International Journal Of Radiation Biology*, 77(6):655–664, 2001

Short, S.C., Mitchell, S.A., Boulton, P., Woodcock, M. and Joiner, M.C. "The response of human glioma cell lines to low-dose radiation exposure." *International Journal Of Radiation Biology*, 75(11):1341–1348, 1999b

Short, S.C., Woodcock, M., Marples, B. and Joiner, M.C. "Effects of cell cycle phase on low-dose hyper-radiosensitivity." *International Journal Of Radiation Biology*, 79(2):99–105, 2003

Skarsgard, L.D., Skwarchuk, M.W. and Wouters, B.G. "The Survival Of Asynchronous V79 Cells At Low Radiation-Doses - Modeling The Response Of Mixed Cell-Populations." *Radiation Research*, 138(1):S72–S75, 1994

Skarsgard, L.D., Skwarchuk, M.W., Wouters, B.G. and Durand, R.E. "Substructure in the radiation survival response at low dose in cells of human tumor cell lines." *Radiation Research*, 146(4):388–398, 1996

Skov, K.A. "Radioresponsiveness at low doses: hyper-radiosensitivity and increased radioresistance in mammalian cells." *Mutation Research/Fundamental and Molecular Mechanisms of Mutagenesis*, 430(2):241–253, 1999

Smith, L.G., Miller, R.C., Richards, M., Brenner, D.J. and Hall, E.J. "Investigation of hyper-sensitivity to fractionated low-dose radiation exposure." *International Journal of Radiation Oncology*Biology*Physics*, 45(1):187–191, 1999

Steel, G. *Basic Clinical Radiobiology.* Hodder Arnold, 2002

Suzuki, M., Zhou, H.N., Geard, C.R. and Hei, T.K. "Effect of medium on chromatin damage in bystander mammalian cells." *Radiation Research*, 162(3):264–269, 2004

Travis, J. "The Bad Seed: Rare stem cells appear to drive cancers." *Science News*, 165(12):184, 2004

Tsoulou, E., Baggio, L., Cherubini, R. and Kalfas, C.A. "Low-dose hypersensitivity of V79 cells under exposure to gamma-rays and He-4 ions of different energies: survival and chromosome aberrations." *International Journal Of Radiation Biology*, 77(11):1133–1139, 2001

Tyson, J.J. and Novak, B. "Regulation of the eukaryotic cell cycle: Molecular antagonism, hysteresis, and irreversible transitions." *Journal Of Theoretical Biology*, 210(2):249–263, 2001

Vermeulen, K., Van Bockstaele, D.R. and Berneman, Z.N. "The cell cycle: a review of regulation, deregulation and therapeutic targets in cancer." *Cell Proliferation*, 36(3):131–149, 2003

Vilenchik, M.M. and Knudson, A.G. "Inverse radiation dose-rate effects on somatic and germline mutations and DNA damage rates." *Proceedings Of The National Academy Of Sciences Of The United States Of America*, 97(10):5381–5386, 2000

Wilson, G.D. "Radiation and the cell cycle, revisited." *Cancer And Metastasis Reviews*, 23(3-4):209–225, 2004

Wolff, S. "Aspects of the adaptive response to very low doses of radiation and other agents." *Mutation Research/Fundamental and Molecular Mechanisms of Mutagenesis*, 358(2):135–142, 1996

World Health Organization website, Factsheet 297. 2006. `http://www.who.int/mediacentre/factsheets/fs297/en/`

World Health Organization website, Programmes and Projects. 2007. `http://www.who.int/ionizing_radiation/en/`

Wouters, B.G. and Skarsgard, L.D. "Low-dose radiation sensitivity and induced radioresistance to cell killing in HT-29 cells is distinct from the "adaptive response" and cannot be explained by a subpopulation of sensitive cells." *Radiation Research*, 148(5):435–442, 1997

Wouters, B.G., Sy, A.M. and Skarsgard, L.D. "Low-dose hypersensitivity and increased radioresistance in a panel of human tumor cell lines with different radiosensitivity." *Radiation Research*, 146(4):399–413, 1996

Wykes, S.M., Piasentin, E., Joiner, M.C., Wilson, G.D. and Marples, B. "Low-dose hyper-radiosensitivity is not caused by a failure to recognize DNA double-strand breaks." *Radiation Research*, 165(5):516–524, 2006

Xu, B., Kim, S.T., Lim, D.S. and Kastan, M.B. "Two molecularly distinct G(2)/M checkpoints are induced by ionizing irradiation." *Molecular And Cellular Biology*, 22(4):1049–1059, 2002

Yang, H.Y., Asaad, N. and Held, K.D. "Medium-mediated intercellular communication is involved in bystander responses of X-ray-irradiated normal human fibroblasts." *Oncogene*, 24(12):2096–2103, 2005

Zhou, B.B.S. and Elledge, S.J. "The DNA damage response: putting checkpoints in perspective." *Nature*, 408(6811):433–439, 2000

Zhou, H., Randers-Pehrson, G., Waldren, C.A. and Hei, T.K. "Radiation-induced bystander effect and adaptive response in mammalian cells." *Advances in Space Research*, 34(6):1368–1372, 2004

Zhou, H.N., Randers-Pehrson, G., Waldren, C.A., Vannais, D., Hall, E.J. and Hei, T.K. "Induction of a bystander mutagenic effect of alpha particles in mammalian cells." *Proceedings Of The National Academy Of Sciences Of The United States Of America*, 97(5):2099–2104, 2000

Zhou, H.N., Suzuki, M., Geard, C.R. and Hei, T.K. "Effects of irradiated medium with or without cells on bystander cell responses." *Mutation Research-Fundamental And Molecular Mechanisms Of Mutagenesis*, 499(2):135–141, 2002a

Zhou, H., Xu, A., Suzuki, M., Randers-Pehrson, G., Waldren, C.A., Hall, E.J. and Hei, T.K. "The Yin and Yan of bystander versus adaptive response: lessons from the microbeam studies." *International Congress Series*, 1236:241–247, 2002b

Appendix A

A Model of Low Dose Hyper-Radiosensitivity

A.1 Repair Processes Are Triggered

If the hyper-radiosensitivity is proved to happen as well *in vivo*, it represents a huge potential for improvement in radiotherapy treatment planning. A patient that would have a tumour which is hyper radio-sensitive at low doses could be treated efficiently with doses much lower than 2 Gy, which would spare the surrounding tissues.

However, the first step is to understand the mechanisms of HRS, to be able to fully control it. It has been suggested that HRS is due to a checkpoint in G2 phase that is not triggered when the cell is irradiated with doses smaller than 40 cGy (Marples *et al.*, 2004). Therefore a model was written based on this assumption.

The equation traditionally used to model the fraction of a population is the linear quadratic model (Equation 2.7, see Section 2.2). It was used as a base for the model of HRS.

A.1.1 Survival Probability of a Single-Cell

It was assumed that the sensitivity of a single cell changed at a given dose, named d_c. Two different models were used, depending on whether the irradiation dose was smaller or bigger

than d_c. The coefficient α of the LQ model used in the dose range $[0, d_c]$ was bigger than the corresponding coefficient of the LQ model used in the dose range $[d_c, \infty]$. Because the parameter β of the linear quadratic model was of the order of 10^{-2} Gy^{-2}, its effect was very small for doses below 1 Gy:

$$if \quad d < 1, \quad \exp(-\beta \times d^2) \approx 1 - \beta \times d^2 \tag{A.1}$$

Therefore, the same value of β was chosen for $d<d_c$ and $d\geq d_c$, with the survival fraction given by:

$$S_F = \begin{cases} \exp(-\alpha_s \times d - \beta \times d^2) & : \quad d < d_c \\ \exp(-\alpha_r \times d - \beta \times d^2) & : \quad d \geq d_c, \quad with \quad \alpha_r < \alpha_s \end{cases} \tag{A.2}$$

The survival probability of a single cell was therefore discontinuous (see figure A.1). The threshold d_c was supposed to be different for all cells of the population.

A.1.2 Survival Probability of a Population of Cells

The distribution of the threshold within the population was chosen to be a combination of two Gaussian distributions, so that the probability of having a 0 dose threshold was 0. The probability density function was given by the following equation:

$$p(d) = \frac{1}{2\sigma\sqrt{2}\pi \times erf(\frac{\bar{d}_c}{\sqrt{2}\sigma})} \cdot \left[\exp(-\frac{(d-\bar{d}_c)^2}{2\sigma^2}) - \exp(-\frac{(d+\bar{d}_c)^2}{2\sigma^2})\right] \tag{A.3}$$

In equation A.3, $\bar{d}_c$ and σ are respectively the mean and standard deviation of d_c. The average of the individual survival probability curves gave the curve of the survival fraction of the population (see Figure A.3 to Figure A.6).

A.2 Sensitivity to Radiation and Cell Cycle

It has been established for a long time that sensitivity to radiation varies across the cell cycle (Steel 2000); Short *et al.* (2003) also measured the variability of HRS with cell cycle for two glioblastoma cell lines (T98G and U373G). HRS is the strongest (i.e. α_r is the biggest) when

cells are in the G2 phase of the cell cycle at the time of irradiation. As a consequence, the model would have different values of the parameters $\alpha_r, \alpha_s, \beta$ and the distribution of d_c would have different means and standard deviations.

It was expected that cells irradiated in S-phase of the cell cycle would be the most resistant, and cells irradiated in the G2/M phase of the cell cycle would be the most radio-sensitive. Similarly, HRS was expected to be the strongest for cells irradiated in G2/M, and the weakest for cells irradiated in the S phase.

A.3 Model Implementation

The survival curve for a population of cells was generated by a Monte Carlo simulation, ran on 2000 individual cells. The parameters $\alpha_r, \alpha_s, \beta, \bar{d}_c$ and σ were optimised by random search, by minimizing the squared error between the model and experimental data from the Gray Cancer Institute, University of Oxford:

$$\phi = \sum_{d=0}^{N} (y(d) - m(d))^2 \tag{A.4}$$

In equation A.4, N is the number of experimental data, y the experimental value of survival fraction at a given dose d and m the corresponding calculated value.

A set of parameters were first best guessed from the parameters of the induced-repair model (Short *et al.*, 2003) and the shape of the survival curves; the squared error Φ was calculated. The following procedure was repeated until optimal values were found:

1. A set of new parameters $(\alpha_r^*, \alpha_s^*, \beta^*, \bar{d_c}^*, \sigma^*)$ in the range [0, 2] of the previous parameters were randomly chosen;

2. A Monte Carlo simulation was run to get the survival fraction at the different doses with this new set of parameters, and the corresponding squared error Φ^* was calculated;

3. If $\Phi^* < \Phi$, the best guessed parameters were changed to the new values $(\alpha_r^*, \alpha_s^*, \beta^*, \bar{d_c}^*, \sigma^*)$

4. else, the program generated another set of values $\left(\alpha_r^*, \alpha_s^*, \beta^*, \bar{d_c}^*, \sigma^* \right)$.

Once either a lower value of the squared error had been found or the process above had been repeated 1000 times, the searching interval was narrowed: each searching range was multiplied by 0.8. In each interval, all values are equi-probable. Moreover, the biggest interval was the initial searching interval around $\bar{d}_c$ and could be estimated to be at maximum $[0, 2]$, since HRS happens for doses below 1 Gy. Therefore values every $\frac{2}{1000} = 0.002$ Gy would be tested in average. The all process was repeated 20 times, so the size of the interval converged towards $10^{-2}\times$ the initial value of the parameter (see figure A.2 for a block diagram of the program).

The model has been run to fit the experimental survival fraction of T98G cells; the experimental data were obtained from Mr. Mick Woodcock, Gray Cancer Institute, UK. The parameters for the best fit to synchronised and asynchronous populations is shown in table A.1; the resulting curves, as well as the experimental data points are displayed on figures A.3 to A.6. The squared error obtained with the model are smaller than the error calculated for the induced-repair model (Short *et al.*, 2003, and see section 2.3).

The model does predict stronger values of α_r and α_s for cells in G2, which is in agreement with the fact that these cells are most sensitive to radiation are have the strongest HRS. The ratio $\frac{\alpha_r}{\alpha_s}$ is highest for the cells in S phase, indicating the smallest change in sensitivity, and therefore the smallest HRS; there is an strong induced radio-resistance, though, which contradicts the prediction of the induced-repair model.

This model can therefore simulate the low dose hyper-radiosensitivity. The problem stands in the standard deviations measured in the experimental data; there are big, and this questions the reality of the phenomenon. Moreover, the weakness of the model is that it assumes a discontinuity in the response of single cells to radiation; this is unrealistic. The interest of the model, though, compared to the induced repair model of Joiner et al. is that the survival of the population is built from the response of individuals.

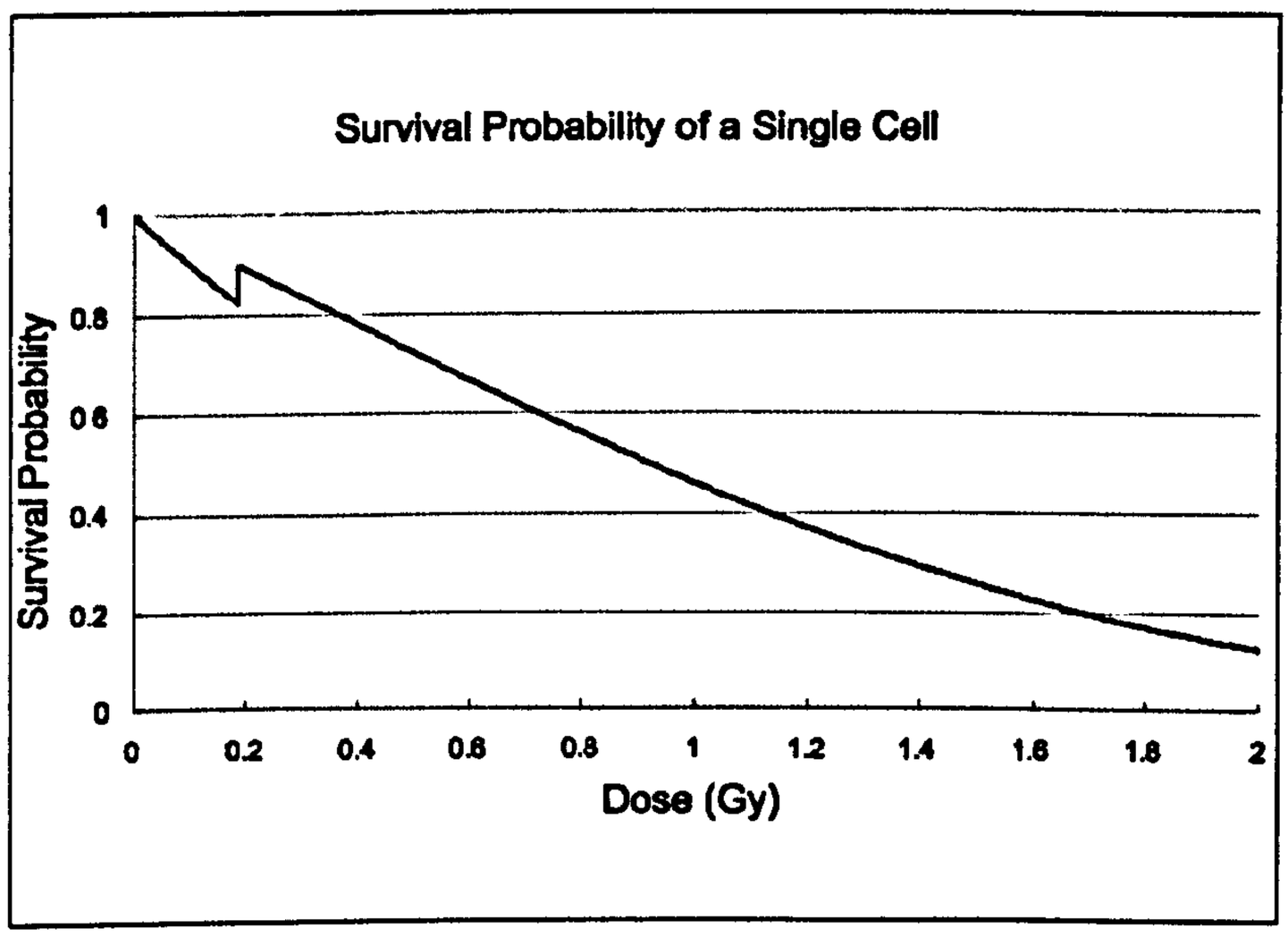

Figure A.1: Survival Probability of a Cell

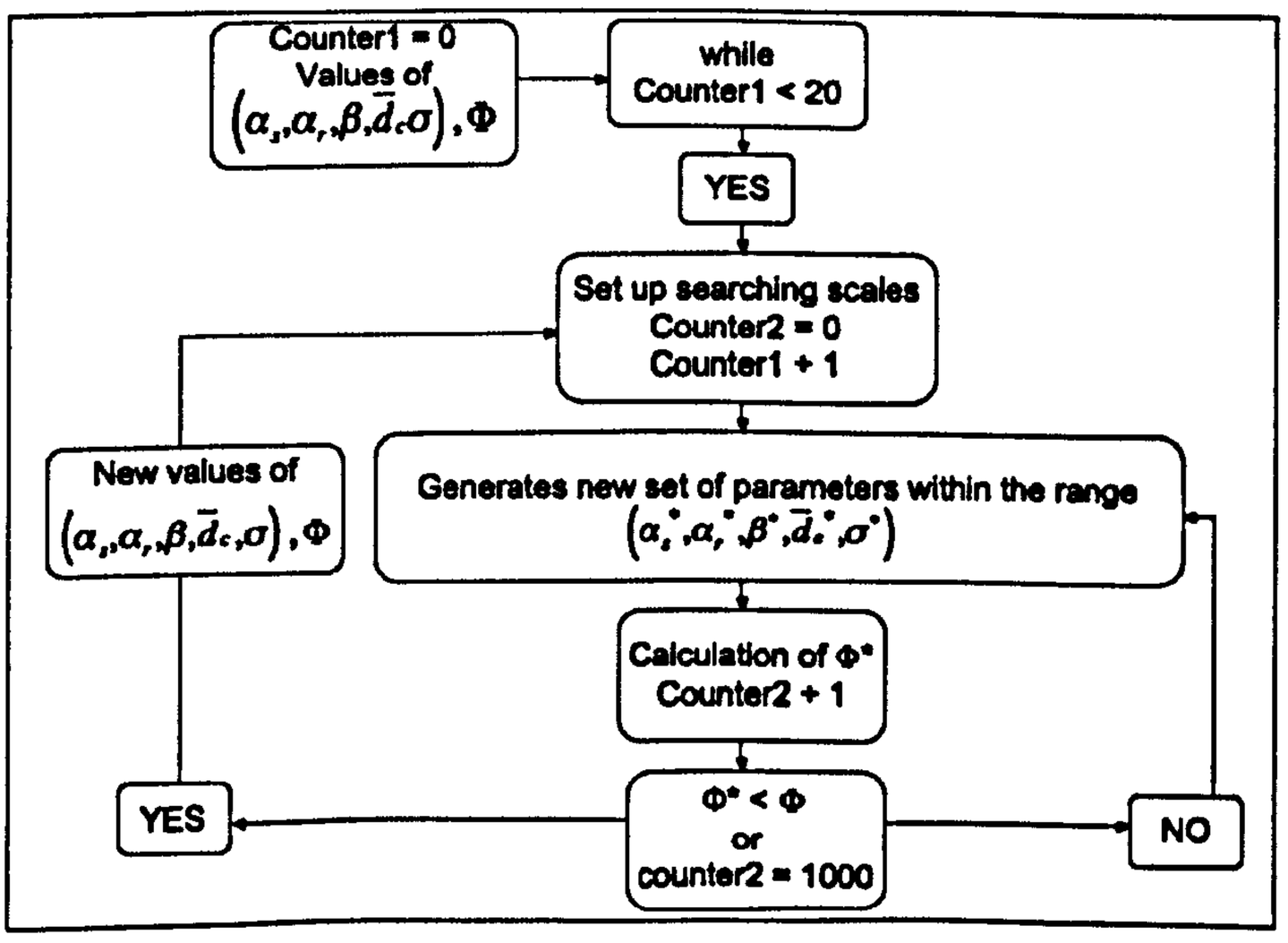

Figure A.2: Block Diagram of the Program for the Model of HRS: See main text for meaning of α_r, α_s, β, $\bar{d}_c$, σ , Φ, α_r^*, α_s^*, β^*, $\bar{d}_c^*$, σ^* and Φ^*.

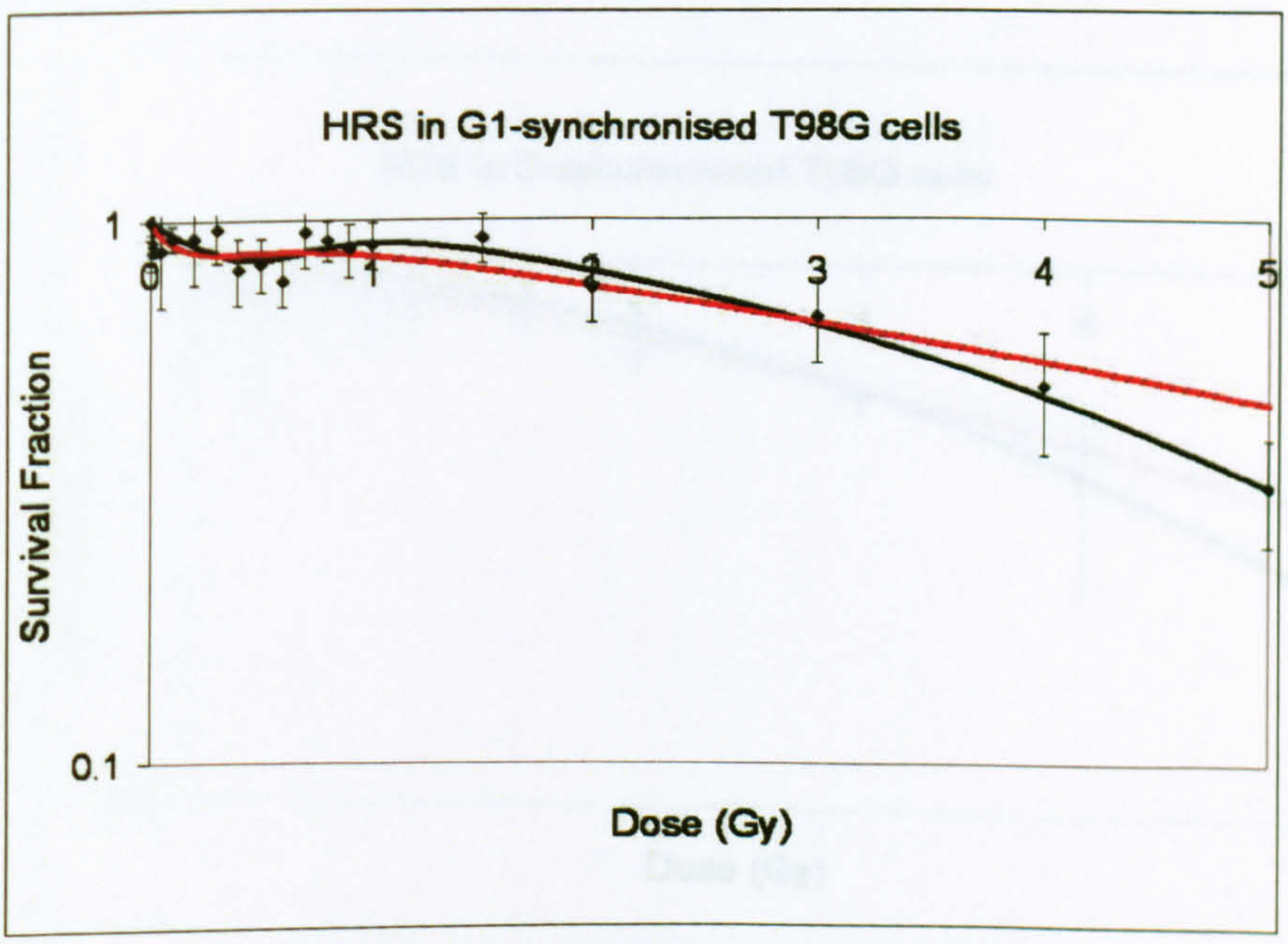

Figure A.3: Survival of G1-Synchronised T98G: cells are irradiated with 250 kVp X-rays. Black diamonds are the experimental data, the red line is the induced-repair model (Short *et al.*, 2003) and the black line is the fit obtained for the model of HRS. Experimental error bars are shown.

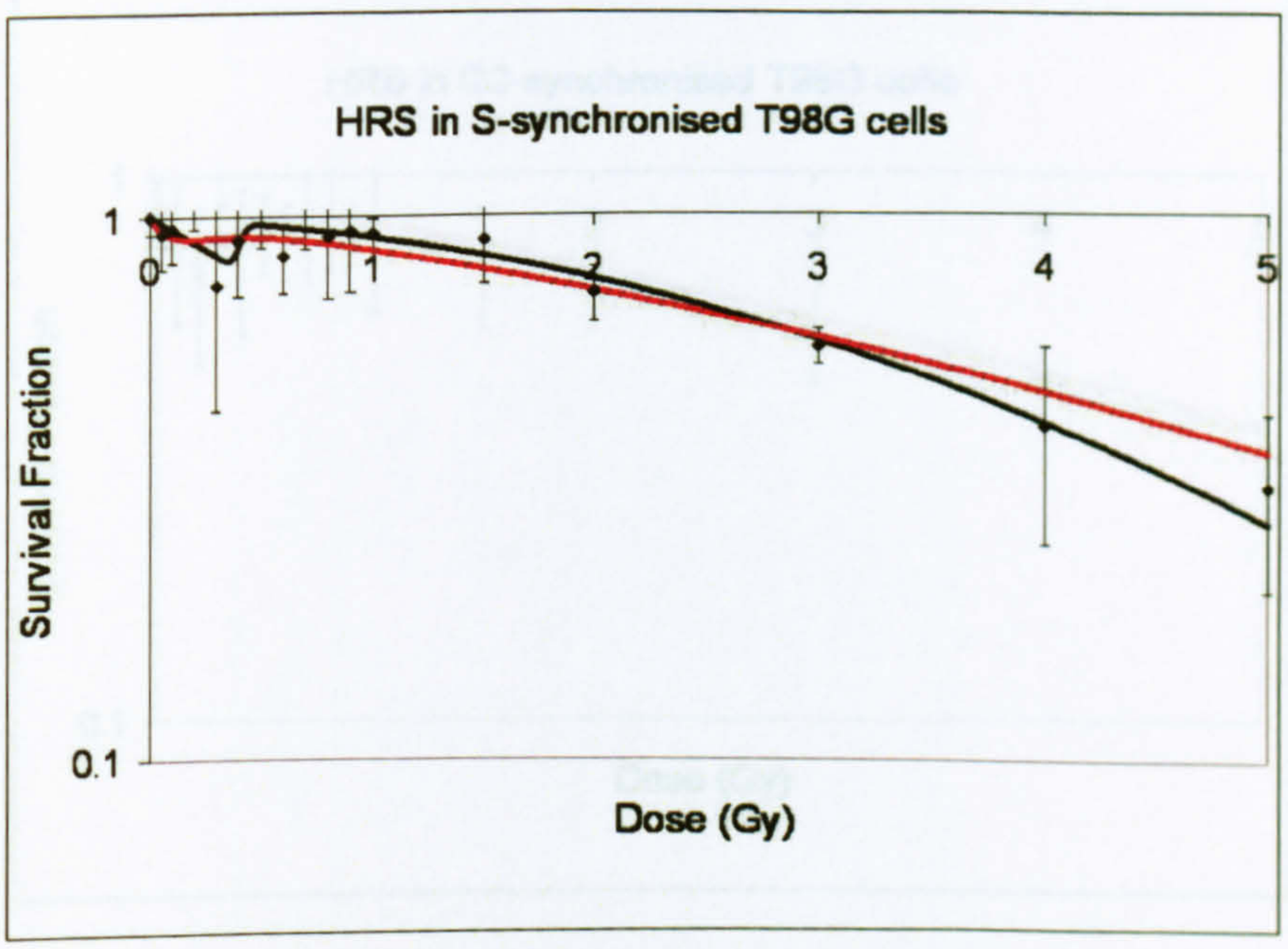

Figure A.4: Survival of S-Synchronised T98G: cells are irradiated with 250 kVp X-rays. Black diamonds are the experimental data, the red line is the induced-repair model (Short *et al.*, 2003) and the black line is the fit obtained for the model of HRS. Experimental error bars are shown.

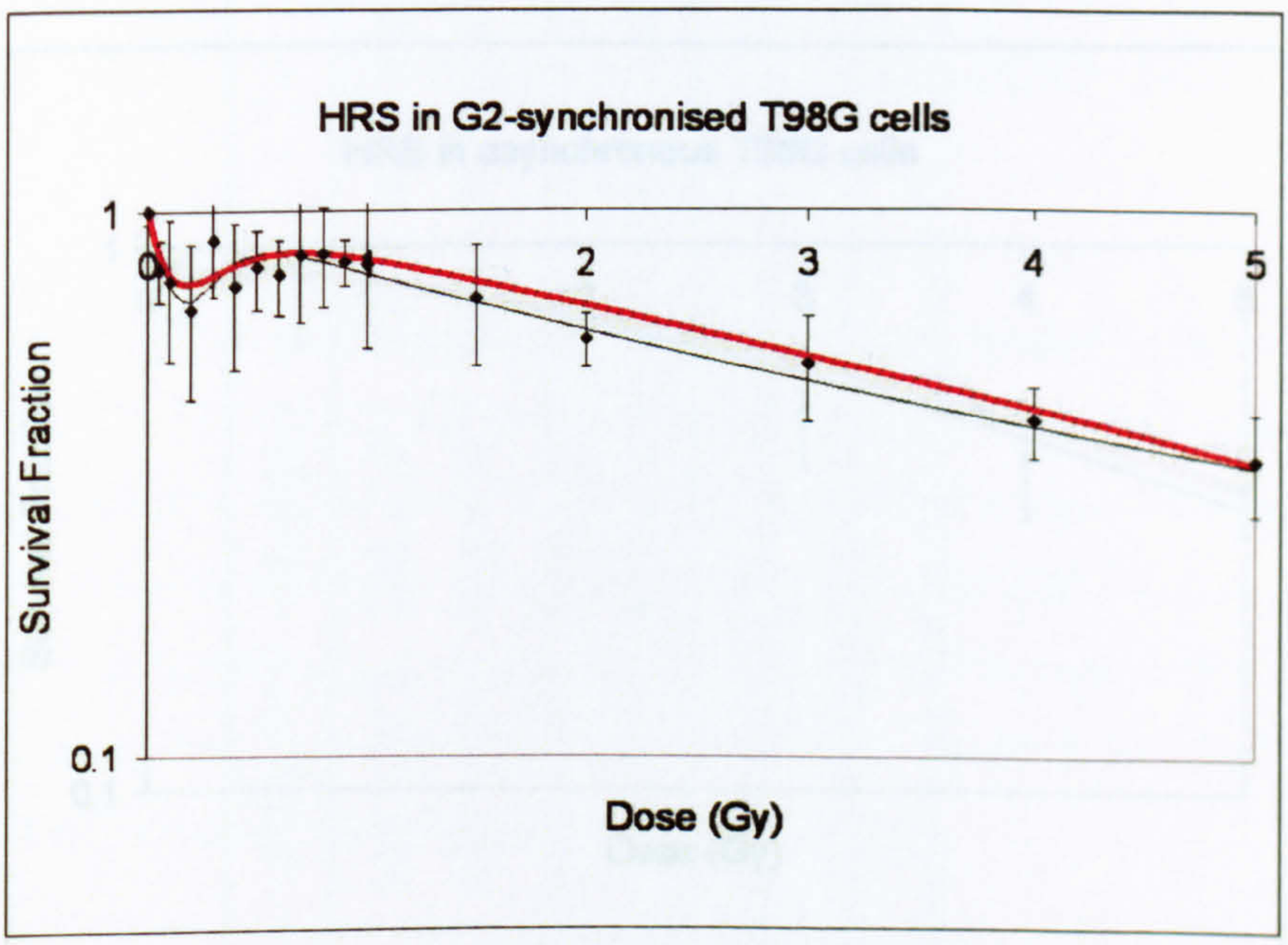

Figure A.5: Survival of G2-Synchronised T98G: cells are irradiated with 250 kVp X-rays. Black diamonds are the experimental data, the red line is the induced-repair model (Short *et al.*, 2003) and the black line is the fit obtained for the model of HRS. Experimental error bars are shown.

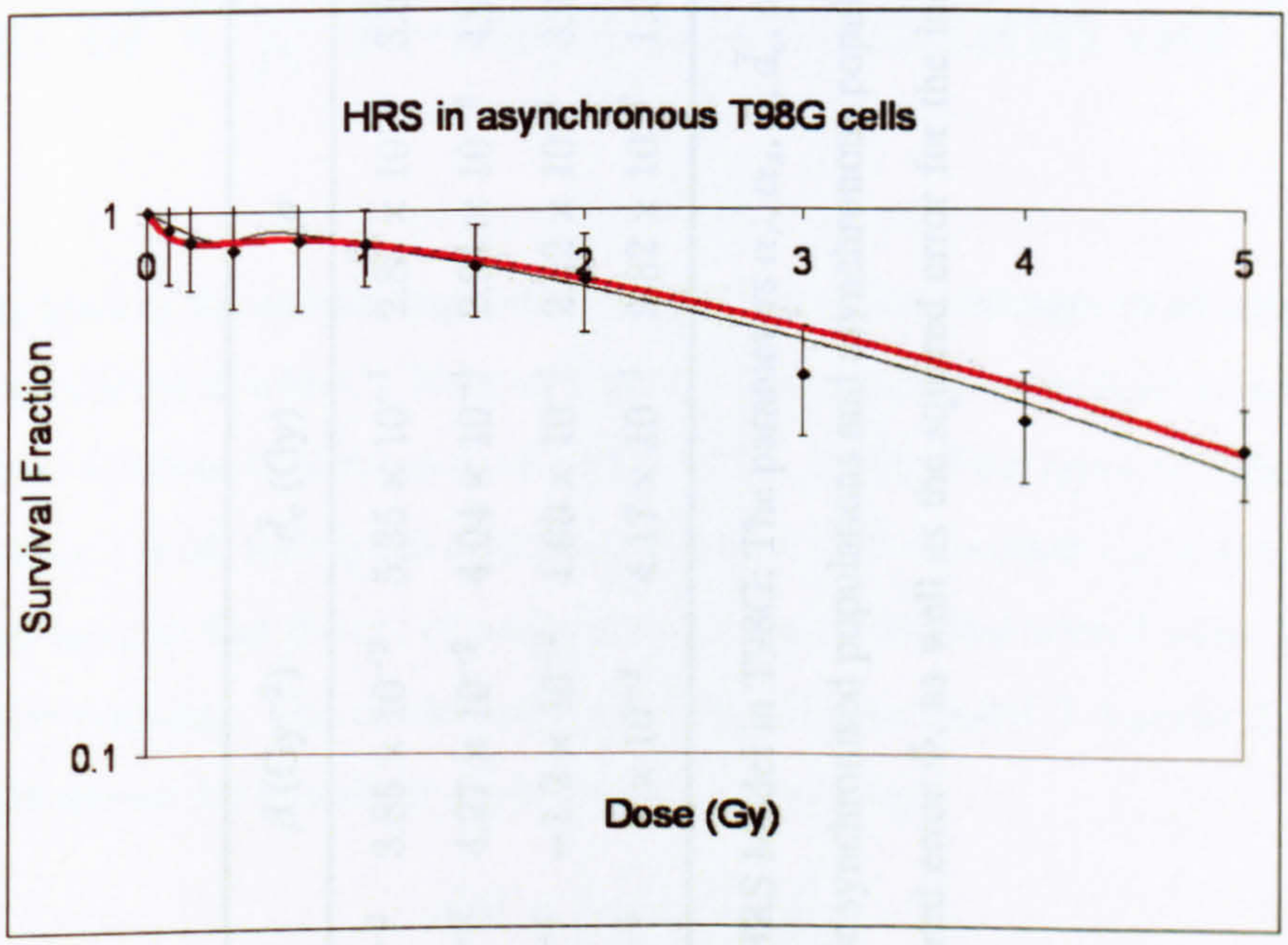

Figure A.6: Survival of Asynchronous T98G: cells are irradiated with 250 kVp X-rays. Black diamonds are the experimental data, the red line is the induced-repair model (Short *et al.*, 2003) and the black line is the fit obtained for the model of HRS. Experimental error bars are shown.

Phase	α_s (Gy)	α_r (Gy)	β (Gy^{-2})	$\bar{d}_c$ (Gy)	σ	Φ	Φ(IR)
G1	5.48×10^{-1}	3.22×10^{-2}	3.85×10^{-2}	5.35×10^{-1}	2.85×10^{-1}	3.83×10^{-2}	7.64×10^{-2}
S	5.36×10^{-1}	4.74×10^{-2}	4.27×10^{-2}	4.04×10^{-1}	2.91×10^{-2}	4.99×10^{-2}	8.90×10^{-2}
G2	3.67	2.75×10^{-1}	-1.2×10^{-2}	1.00×10^{-1}	2.12×10^{-1}	3.71×10^{-2}	4.63×10^{-2}
Asynchronous	4.58×10^{-1}	1.22×10^{-1}	2×10^{-2}	4.17×10^{-1}	9.82×10^{-2}	1.06×10^{-2}	1.81×10^{-2}

Table A.1: Parameters of the HRS Model in T98G: The parameters α_r, α_s, β, $\bar{d}_c$, σ fitted to the experimental data are given for synchronised populations and asynchronous populations. Also given is the value of the squared error Φ, as well as the squared error for the induced-repair model Φ(IR).

Appendix B

Effects of C_K X-rays irradiation on V79

Further simulations of the cellular automaton model were run to attempt modelling the survival of V79 cells to irradiation with C_K X-rays. The experimental data came from experiments led at the Gray Cancer Institute (Schettino *et al.*, 2005, 2001, 2003). Two types of experiments were conducted: either 1 or all individual cells were targeted with a focused C_K X-rays microbeam. The objectives were to find the set of parameters of the model that would allow fitting to both sets of experimental data. The model used was based on the model 2 described in Chapter 4. Any cell could release the bystander signal, with a probability:

$$p(d) = 1 - \exp(-\frac{d}{0.2}) \tag{B.1}$$

The concentration of the signal in the dish was dimensionless and was equal to the number of emitting cells. This concentration decreased with time according to:

$$Q(t) = Q_0 \times \exp(\frac{t \times \ln(2)}{30}) \tag{B.2}$$

The proportion of G2 cells killed by the signal depended on the quantity of signal in the dish; two equations were used:

$$D_B(Q) = 0.26 \times (1 - \exp(-C(t))) \tag{B.3}$$

or:

$$D_B(Q) = 0.26 \times (1 - \exp(-Q(t) \times 10)) \tag{B.4}$$

The probability for irradiated cells to survive was calculated either with the traditional LQ equation or with the multi-target model (see equation 2.6). The best fit to the experimental data

for doses ≥ 1 Gy was obtained using the program described in Chapter 4 for the LQ parameters, and using the Microsoft Excel program for the multi-target model.

$$S_F = \exp(-0.2012 \times d - 0.4049 \times d^2) \quad \text{(B.5)}$$
$$\Phi = 4.4110^{-3}$$

$$S_F = 1 - (1 - \exp(-d \times 2.1837))^{8.4267} \quad \text{(B.6)}$$
$$\text{correlation coefficient} = 0.9702$$

In the absence of experimental data on synchronized cells, the same equation was used for calculating the survival probability of any cell to direct irradiation.

The multi-target model was used because it may allow for the direct effect to be nearly null at low doses, while the LQ model predicts a linear increase. With the multi-target model:

$$\begin{aligned} S_F(d) &= 1 - (1 - exp(-\frac{d}{d_0}))^n \\ \frac{dS_F(d)}{dd} &= -n(\frac{1}{d_0})\exp(-\frac{d}{d_0}))(1 - exp(-\frac{d}{d_0}))^{n-1} \\ \text{If } n > 1, \frac{dS_F(d)}{dd}|_{d=0} &= 0 \\ \text{If } n = 1, \frac{dS_F(d)}{dd}|_{d=0} &= -\frac{1}{d_0} \end{aligned} \quad \text{(B.7)}$$

With the linear quadratic model:

$$\begin{aligned} S_F(d) &= \exp(-\alpha \times d - \beta \times d^2) \\ \frac{dS_F(d)}{dd} &= -(\alpha + 2\beta \times d) \times \exp(-\alpha \times d - \beta \times d^2) \\ \frac{dS_F(d)}{dd}|_{d=0} &= -\alpha \end{aligned} \quad \text{(B.8)}$$

In the case of the LQ model, the gradient is not zero at low doses, while the gradient is zero at dose 0 for the MT target model, and can be approximated as zero for doses $d \ll d_0$, provided that the exponent is not 1.

Three situations were examined: either the LQ model with the equation B.3 or the equation B.4, or the multi-target model with the equation B.4 were used. The use of the equation B.4

predicts better the response of a population where only 1 cell has been irradiated (see figure B.2); however, the best prediction when all cells are irradiated is obtained with the use of the LQ model and the equation B.3. The difference of fit to the data on populations entirely irradiated between these 3 models comes from the low dose domain (below 1 Gy, see figure B.1); with the use of the LQ model and the equation B.4 and the use of the multi-target model and equation B.4, the survival fraction is slightly under-predicts.

This short study suggests that the LQ model is not appropriate for modelling the direct effect of radiation at low doses, when the bystander effect is taken into account as well. Indeed, the BE here is best predicted by the equation B.4, but then if it is used in combination with the LQ model, the survival at low doses is significantly under-predicts. Better simulations can be obtained by using the multi-target model. The multi-target model has stopped being used in radiotherapy; this however shows that the LQ model might need to be re-thought.

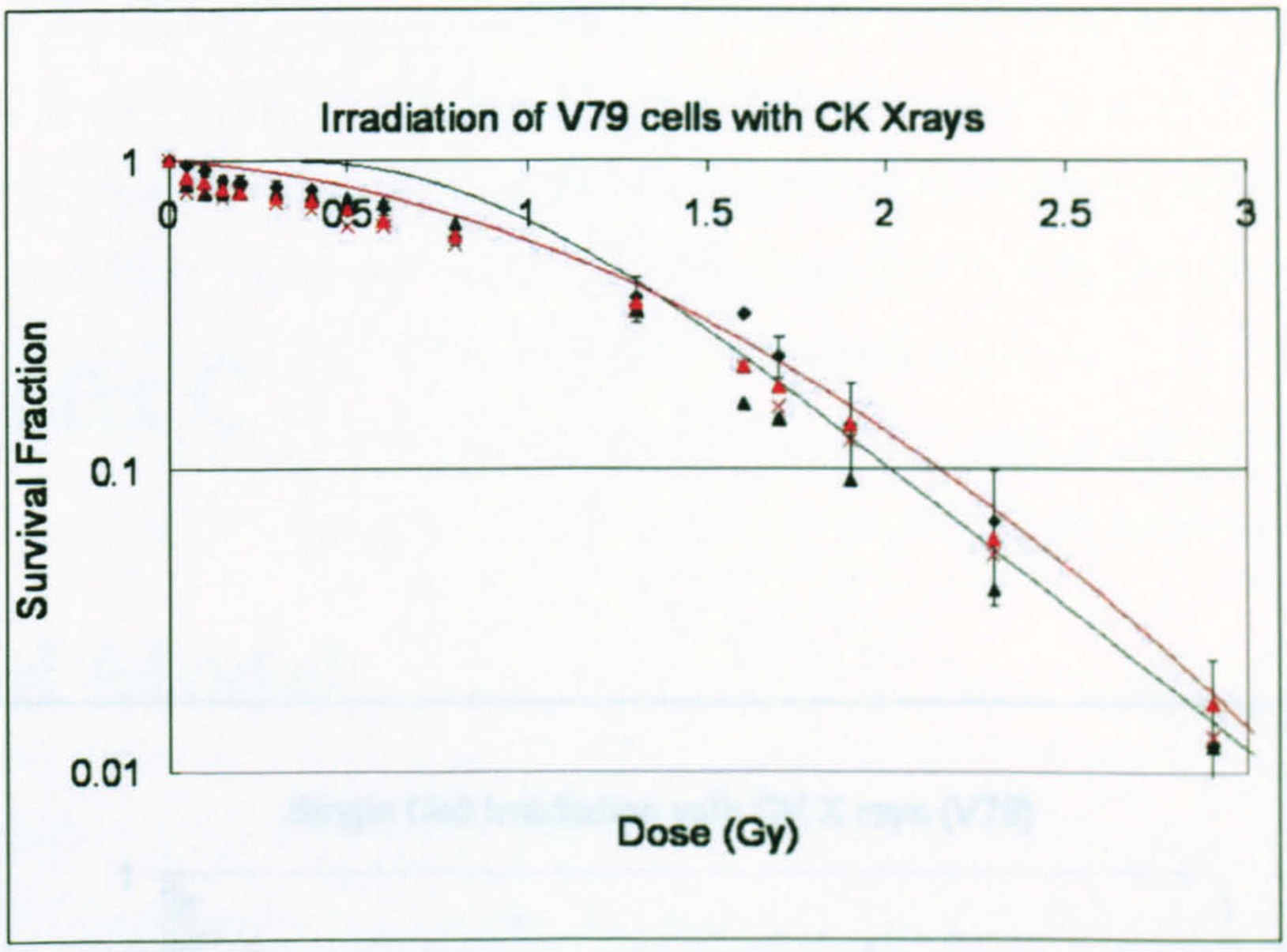

(a)

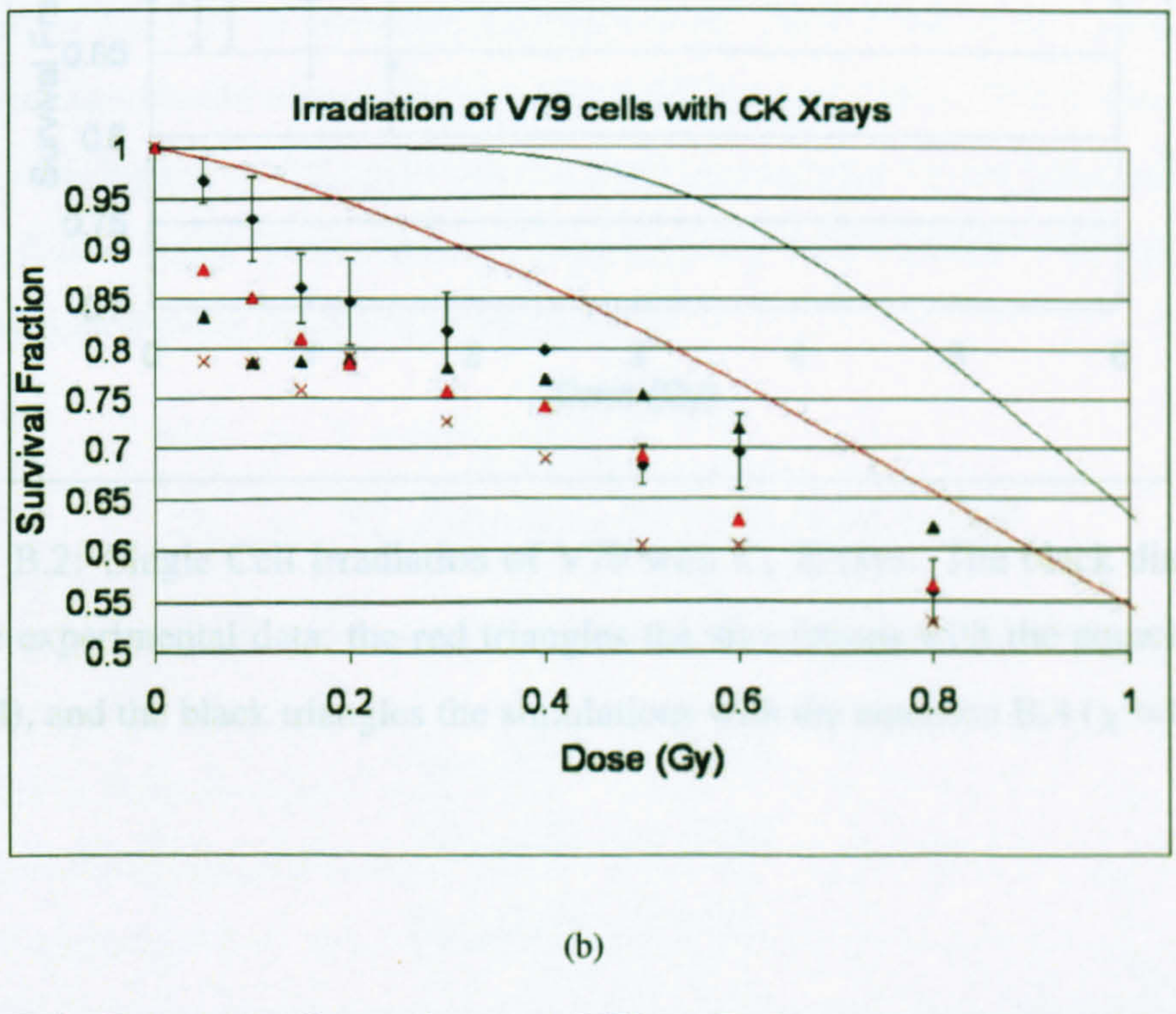

(b)

Figure B.1: Response of asynchronous V79 to C_k X-rays: all cells are irradiated (a) all dose domain and (b) low dose domain. Diamonds are experimental data, the red line is the LQ model and the black line the multi-target model. The red triangles and crosses are two simulations with the LQ model and the equations B.3 and B.4 respectively (χ^2=32 and 122). The black triangles are the simulation with the multi-target model (χ^2=81).

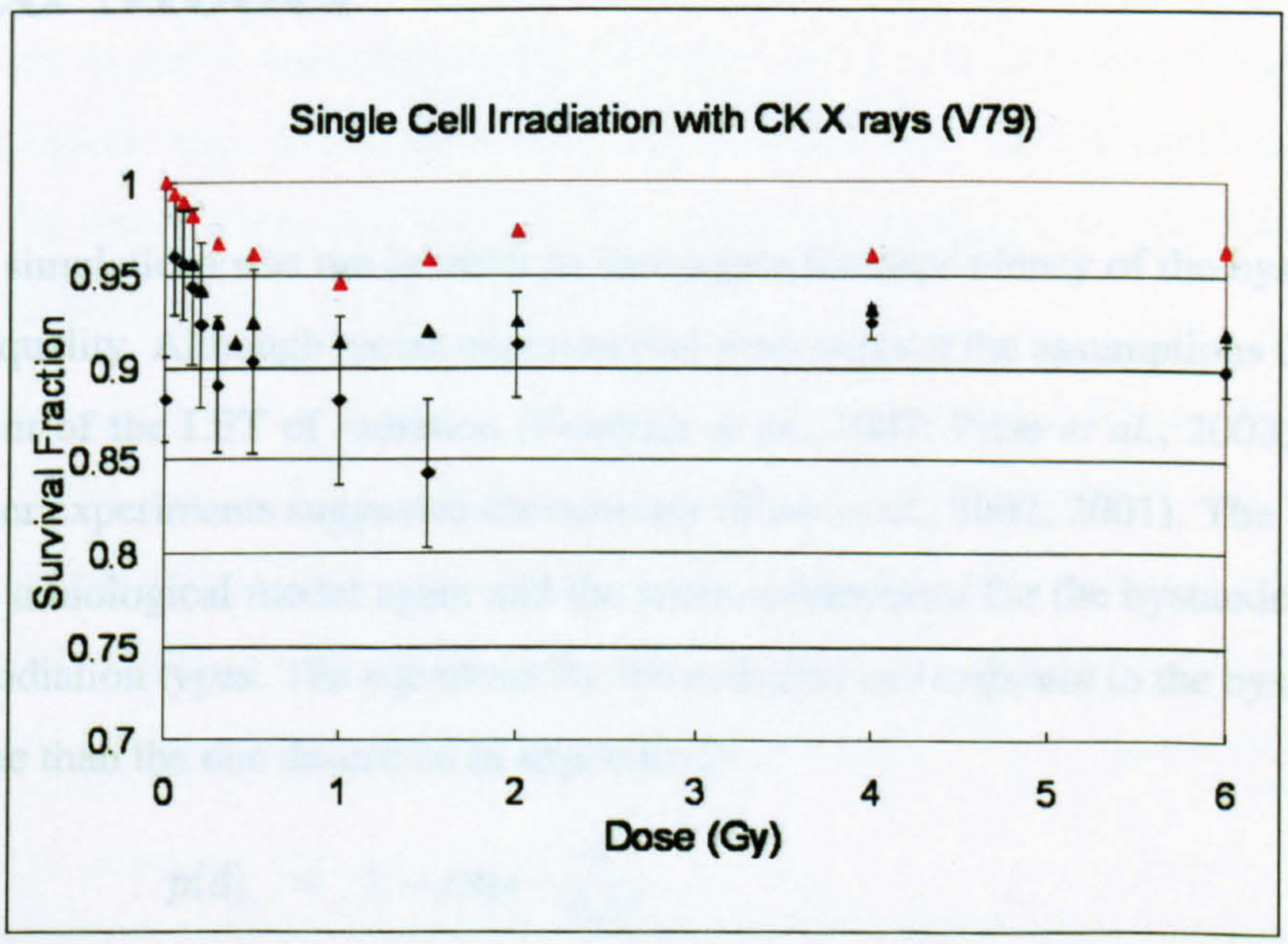

Figure B.2: Single Cell Irradiation of V79 with C_k X-rays: The black diamonds are the experimental data, the red triangles the simulations with the equation B.3 (χ^2=64), and the black triangles the simulations with the equation B.4 (χ^2=14).

Appendix C

Unified Model

A last set of simulations was run in order to investigate the dependency of the bystander effect on radiation quality. Although recent experimental work support the assumptions that the effect is independent of the LET of radiation (Fournier *et al.*, 2007; Prise *et al.*, 2003; Shao *et al.*, 2003b), earlier experiments suggested the contrary (Shao *et al.*, 2002, 2001). The V79 cell line was taken as a biological model again and the same assumptions for the bystander effect were used for all radiation types. The equations for the emission and response to the bystander signal were the same than the one described in appendix B:

$$p(d) = 1 - \exp(-\frac{d}{0.2}) \quad \text{(C.1)}$$

$$D_B = D_{max}(phase) \times (1 - \exp(-Q(t) \times 10)) \quad \text{(C.2)}$$

In this case, however, all cells were sensitive to the signal, although with different intensities:

$$D_{max}(G1) = 0.006$$

$$D_{max}(S) = 0.001$$

$$D_{max}(G2) = 0.13$$

Cells that survived the signal all got resistant to it for their entire cell cycle, and their resistance was lost at division. In fact, therefore, cells in S and G2 phase present at the time of radiation only would be killed by the signal; the progeny of those cells dies or gets resistant in G1 phase always. Cells that were not emitting but were exposed to the signal could become secondary emitters. This assumptions has been made by several groups (Burdak-Rothkamm *et al.*, 2006;

Moore *et al.*, 2006; Schettino *et al.*, 2003) because on the one hand, the very short lived reactive species are likely to be involved in the bystander effect, and on the other hand, there seems to be little space and time limitation to it. In the absence of knowledge about how and how much the possible secondary emitters would emit, the same equation C.1 was used than the primary sources. In this model, the signal was considered not to decrease concentration for the time of the experiments. Therefore, no equation was introduced for the life time of the signal. As in the model described in appendix B, the direct effect was calculated with the multi-target model:

$$S_F = 1 - (1 - \exp(-\frac{d}{d_0}))^n \tag{C.3}$$

The parameters d_0 and n depended on the radiation quality, and were the only differences between the radiation types. Those parameters were fitted to experimental survivals for doses > 1 Gy, using the Excel Microsoft program. The different parameters for C_K X-rays, 250 kVp X-rays and 3.2 MeV protons are shown on table C.1.

In this case, no cell cycle consideration was taken into account for the direct effect and a single multi-target model was used for all cells after irradiation with 250 kVp X-rays. Four experiments were simulated and compared with experiments: single cell irradiation with C_K X-rays (Schettino *et al.*, 2005), all cells irradiation with C_K X-rays (Schettino *et al.*, 2003), all cells irradiation with 250 kVp X-rays and all cells irradiation with 3.2 MeV protons (Schettino *et al.*, 2001).

The results of the simulations are shown with the experimental data and the multi-target models on figures C.1 to C.4. The bystander effect calculated by the model is stronger than the one measured (see figure C.1) for dose between 0.5 and 1.5 Gy; however, the steepness at doses below 0.3 Gy are similar. Moreover, the model also shows a significant decrease in the survival of the population, even though only one cell is irradiated. Also, the experimental data when all cells are irradiated can all be simulated with the same assumptions on the bystander effect. For all the experiments where all cells were irradiated, the simulations indicate a survival fraction significantly lower than the one predicted by the multi-target model at low doses, while they agree at higher doses. The induced radio-resistance, with a flat response of cells to radiation around 1 Gy could not be seen with the simulations, though. This suggests that additional mechanisms induce this behaviour.

Therefore, those early results support the theory that some mechanisms of cellular response

to radiation, and probably the bystander effect, may be independent of LET. The direct effect, however, differs for different radiation quality, as demonstrated by the parameters of the multi-target model (see table C.1). Furthermore, the bystander effect only cannot explain the shape of the survival response at low doses, with the assumptions taken here. There must be additional mechanisms that induce a flat response around 1 Gy.

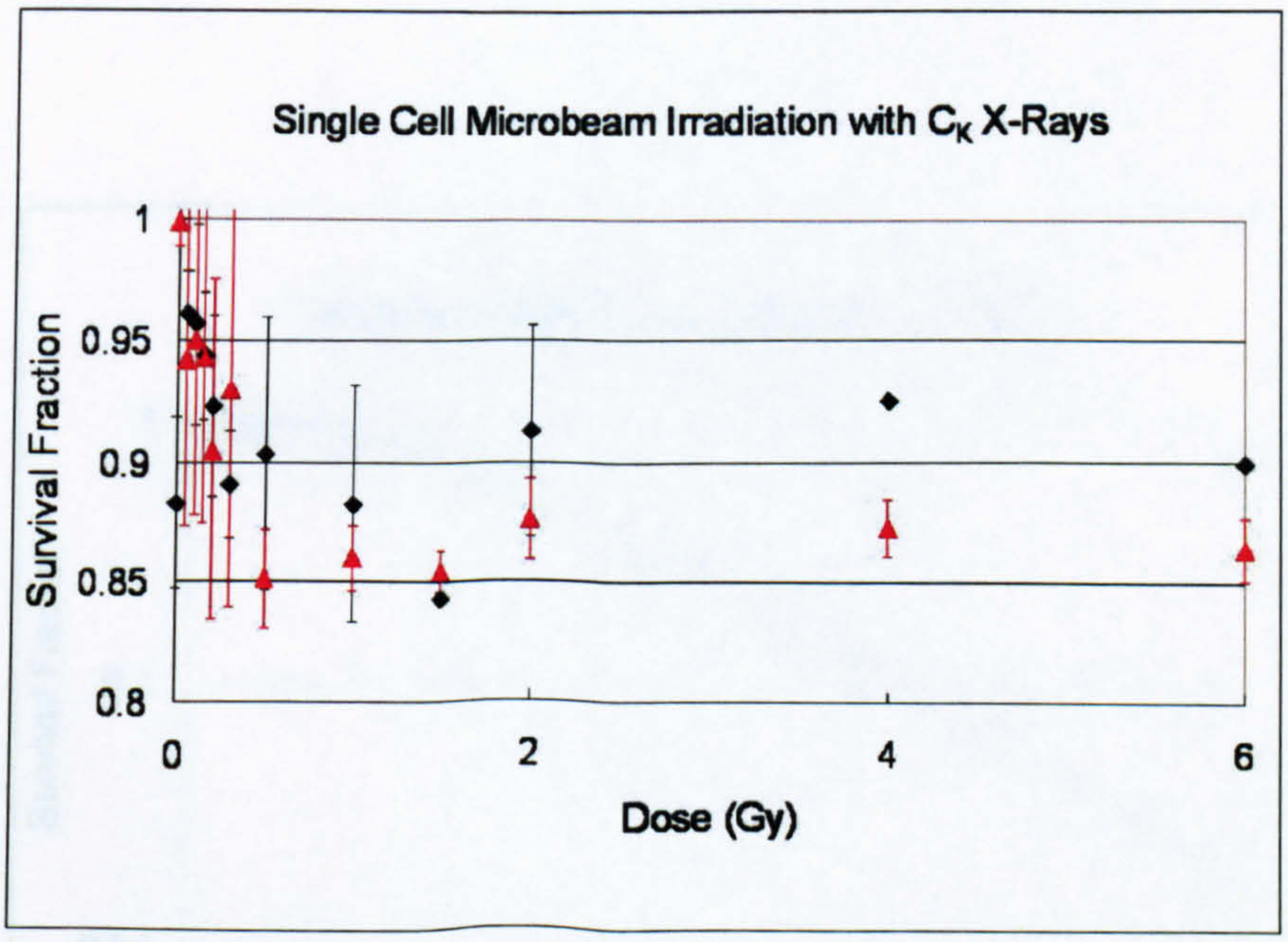

Figure C.1: Single Cell Irradiation: 1 cell was randomly irradiated with C_K X-rays in the dish and the survival of the population simulated. Black diamonds are the experimental data, and red squares are the results of the simulation. Experimental error bars are shown. Parameters are shown on Table C.1.

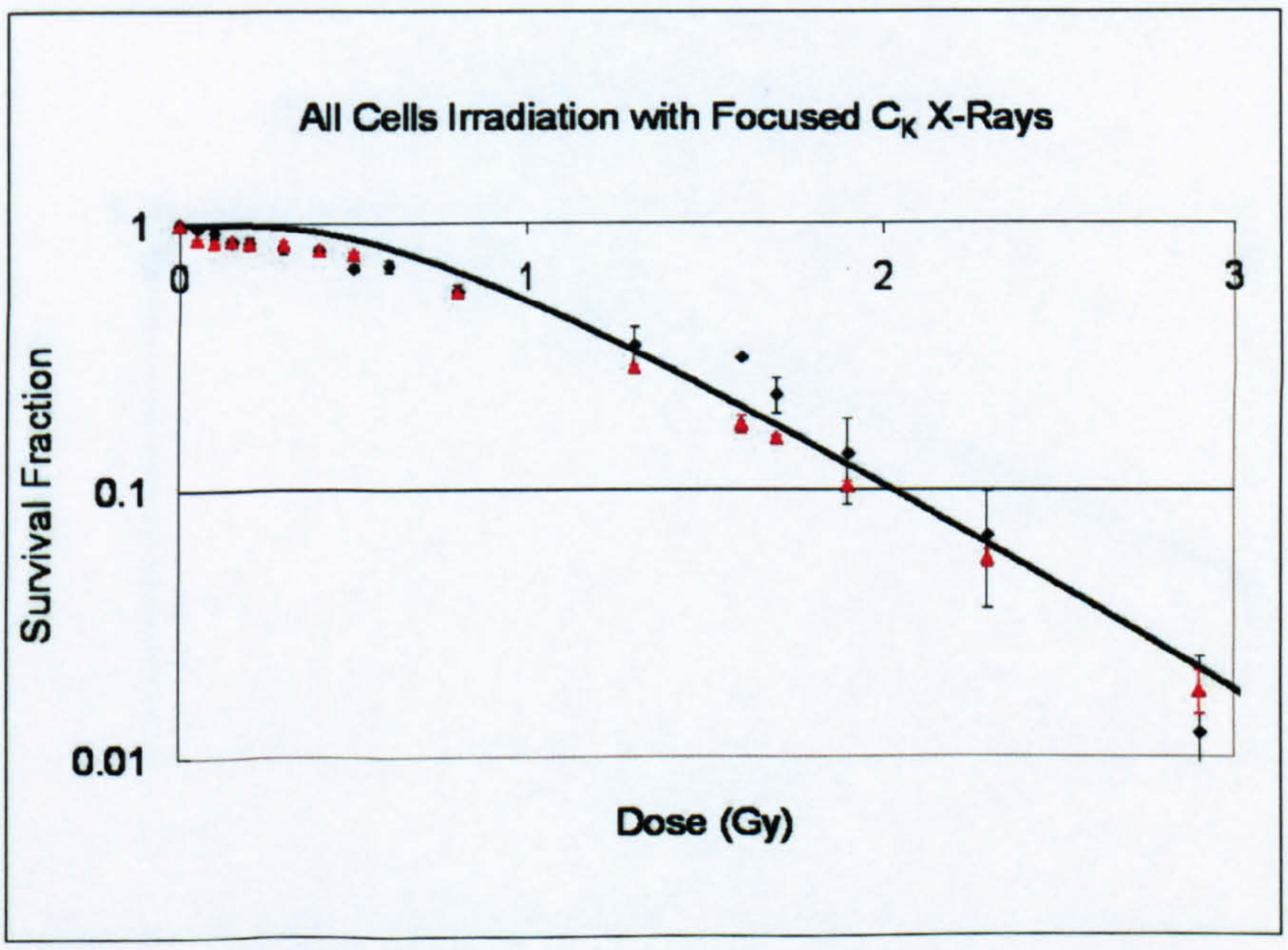

Figure C.2: Irradiation of All Cells: with C_K X-rays. Black diamonds are the experimental data, red squares are the results of the simulation and the line represents the multi-target model. Experimental error bars are shown. Parameters are shown on Table C.1.

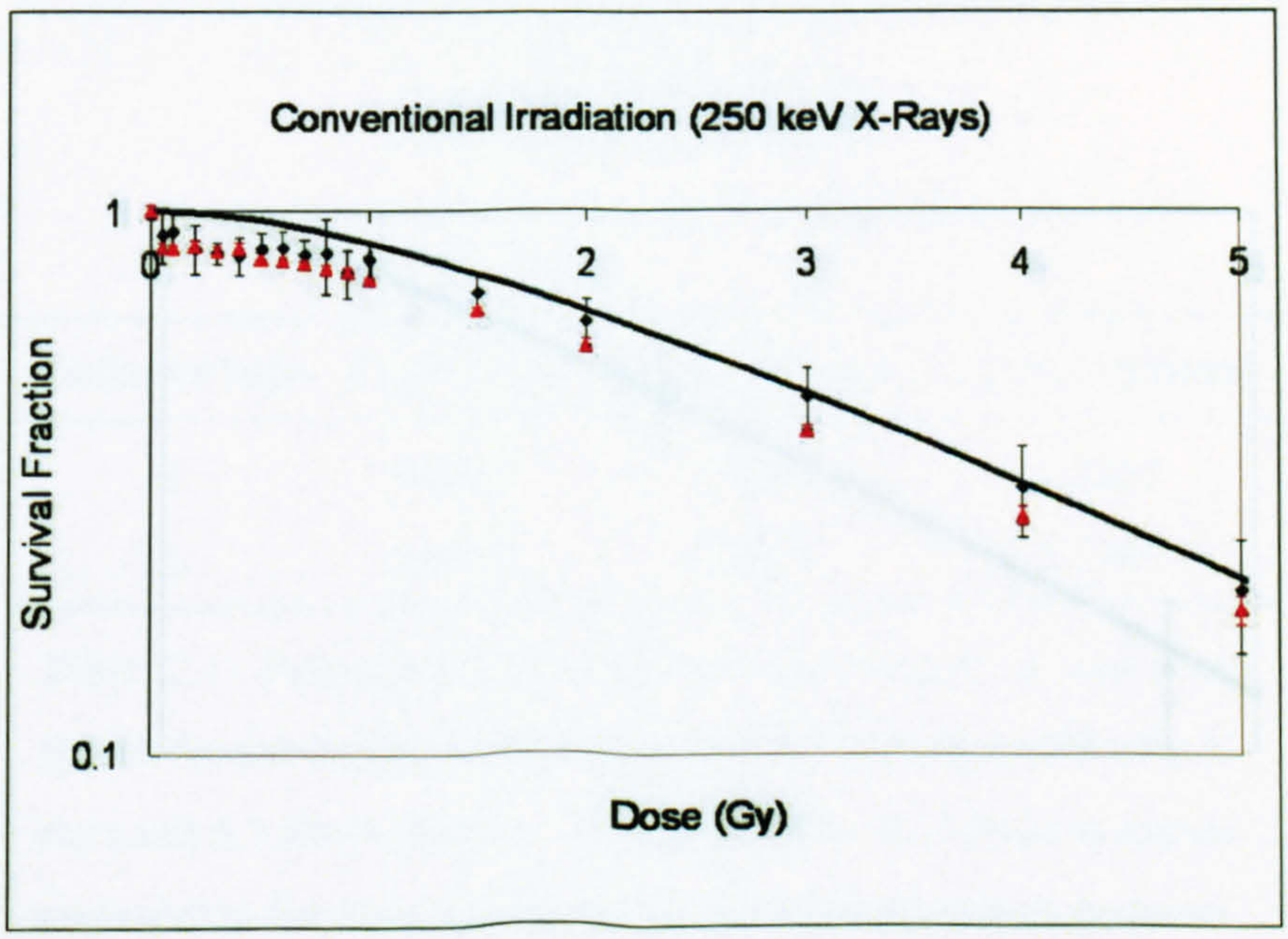

Figure C.3: Conventional Irradiation: cells are irradiated with 250 kVp X-rays. Black diamonds are the experimental data, red squares are the results of the simulation and the line represents the multi-target model. Experimental error bars are shown. Parameters are shown on Table C.1.

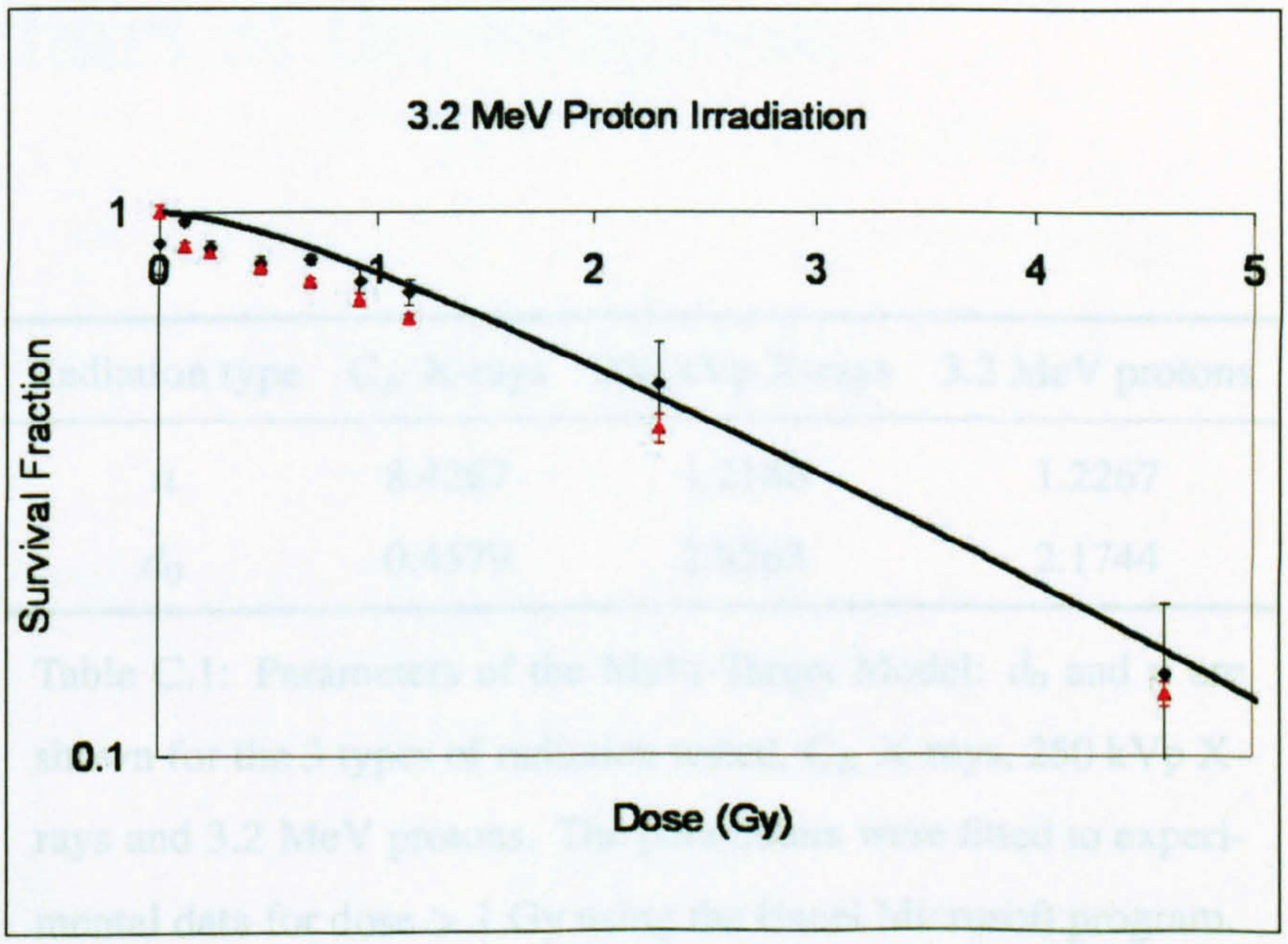

Figure C.4: Ion Irradiation: cells are irradiated with 3.2 MeV protons. Black diamonds are the experimental data, red squares are the results of the simulation, and the black line represents the multi-target model. Experimental error bars are shown. Parameters are shown on Table C.1.

Radiation type	C_K X-rays	250 kVp X-rays	3.2 MeV protons
n	8.4267	1.2186	1.2267
d_0	0.4579	2.8563	2.1744

Table C.1: Parameters of the Multi-Target Model: d_0 and n are shown for the 3 types of radiation tested, C_K X-rays, 250 kVp X-rays and 3.2 MeV protons. The parameters were fitted to experimental data for dose > 1 Gy using the Excel Microsoft program.

Appendix D

Flowchart of the Program

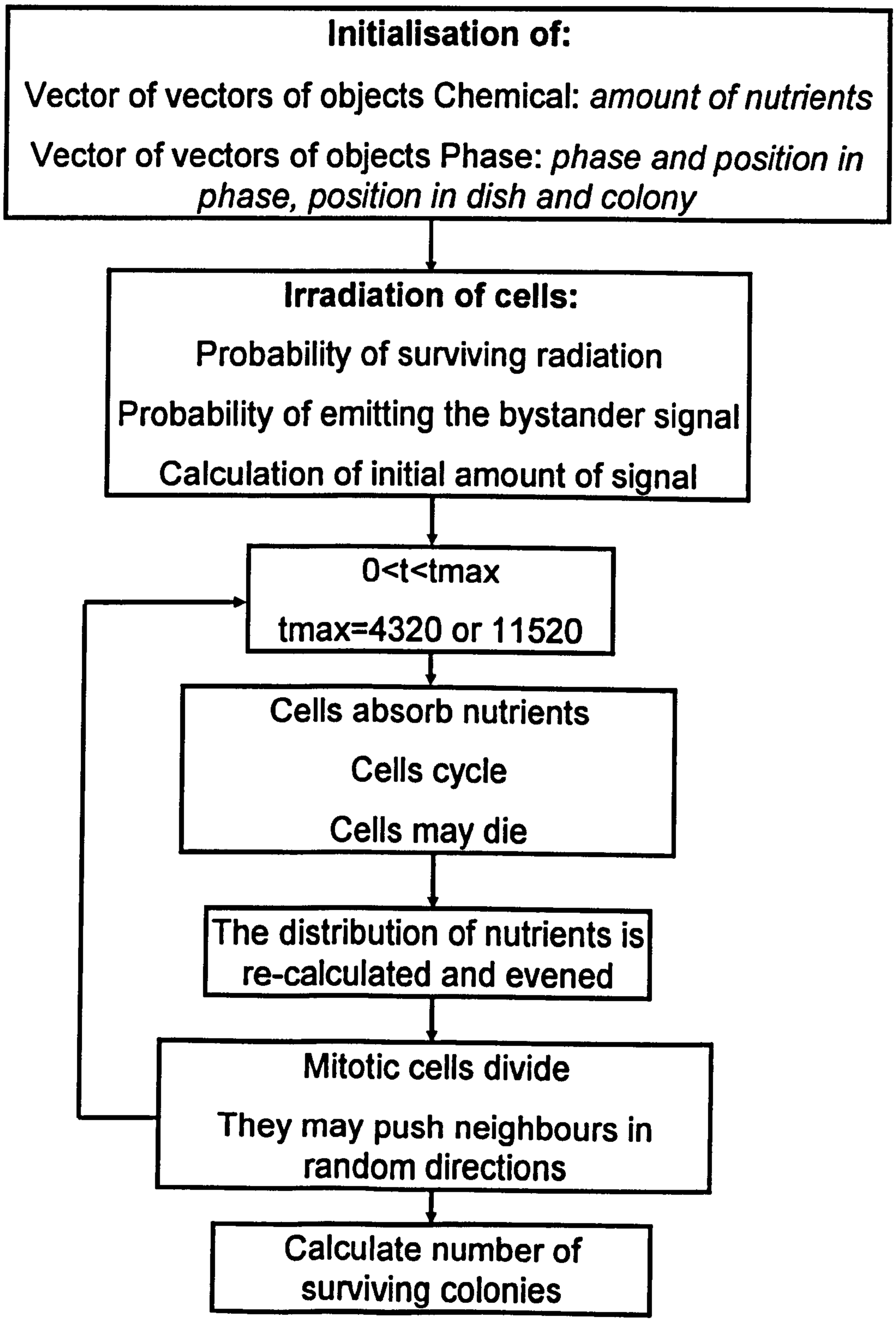
Initialisation of:
Vector of vectors of objects Chemical: amount of nutrients
Vector of vectors of objects Phase: phase and position in phase, position in dish and colony
Irradiation of cells:
Probability of surviving radiation
Probability of emitting the bystander signal
Calculation of initial amount of signal
0<t<tmax
tmax=4320 or 11520
Cells absorb nutrients
Cells cycle
Cells may die
The distribution of nutrients is re-calculated and evened
Mitotic cells divide
They may push neighbours in random directions
Calculate number of surviving colonies

Appendix E

Main Program

The files of the main program can be found on the attached CD.

Main Text	Program
Q_0	BS _Conc
τ	BS_LIFE
D_{max}	BS_SF

Table E.1: Parameters of the Model in the Main Program.

THESIS CONTAINS CD ROM